NASA TECHNICAL NOTE

NASA TN D-6826

NASA TN D-6826

WIND-TUNNEL INVESTIGATION AT LOW SPEEDS OF A MODEL OF THE KESTREL (XV-6A) VECTORED-THRUST V/STOL AIRPLANE

by Richard J. Margason, Raymond D. Vogler, and Matthew M. Winston

Langley Research Center
Hampton, Va. 23365

NATIONAL AERONAUTICS AND SPACE ADMINISTRATION • WASHINGTON, D. C. • JULY 1972

WIND-TUNNEL INVESTIGATION AT LOW SPEEDS OF A MODEL OF THE KESTREL (XV-6A) VECTORED-THRUST V/STOL AIRPLANE

By Richard J. Margason, Raymond D. Vogler,
and Matthew M. Winston
Langley Research Center

SUMMARY

An investigation was made in the 5.18-meter (17-foot) test section of the Langley 300-MPH 7- by 10-foot tunnel to determine the longitudinal and lateral characteristics of a 1/6-scale model of the Kestrel (XV-6A) vectored-thrust V/STOL airplane at low-speed cruise and transition conditions. Data were obtained out of and in ground effect over a moving ground plane for a range of model angles of attack and sideslip at various thrust coefficients by using compressed air ejecting from nozzles in the fuselage.

In the cruise configuration, the model is longitudinally stable, but in transition, model instability is increased as power is increased, and the flaps and horizontal tail have little effect at high thrust coefficients (low forward speeds). At high thrust conditions in transition, the model is unstable in roll and yaw at small sideslip angles. Jet-free-stream interference generally results in an increase in drag and noseup pitching moments and a reduction in lift. Ground proximity generally reduces the interference effects on lift and pitching moment but has little effect on drag. Deflected thrust at speeds above transition produces increments of lift and large deceleration forces useful in maneuvering flight, but with a reduction in stability.

INTRODUCTION

The National Aeronautics and Space Administration has provided a large body of detailed information on various vertical take-off and landing (VTOL) concepts and has recently emphasized the importance of continued development in this area of aeronautics. Detailed aerodynamic data have been obtained for several configurations such as the ducted propeller (ref. 1), tilt wing (refs. 2 and 3), lift jet (ref. 4), and lift fan (ref. 5), some of which have evolved into flight vehicles.

One V/STOL airplane now operational is the Harrier (AV-8A) vectored-thrust fighter. The present paper supplements previous investigations on the prototype Hawker

(P-1127) version of this airplane, first flown in the early 1960's. The previous works include the results of flight tests of a 1/6-scale model (ref. 6) and the results of static-force tests at high subsonic speeds (refs. 7 and 8). The present investigation utilizes a 1/6-scale model of the Kestrel (XV-6A) version of this airplane. This version was used by the United Kingdom (U.K.), Federal Republic of Germany (F.R.G.), and United States (U.S.) in tripartite evaluations conducted during the mid-1960's. Since those evaluations, two of these Kestrels were loaned to NASA Langley Research Center for flight tests (ref. 9). Completing the evolution of this vectored-thrust V/STOL fighter to operational status is the Harrier (AV-8A), the third version of this airplane which is currently being flown by both the U.K. and U.S. military forces.

Both the Kestrel and Harrier were developed largely through modifications of earlier versions of this airplane. As a result, very few wind-tunnel data are available on either airplane. The present investigation of the Kestrel (XV-6A) was undertaken to provide static longitudinal and lateral characteristics with a wind-tunnel model to complement the flight-test results obtained by both the NASA and the USAF (ref. 10). The principal purpose of these flight tests has been the determination of the V/STOL transition-flight characteristics between hover and wingborne flight. Correspondingly, most data herein pertain to this speed regime.

These tests were made through angle-of-attack and angle-of-sideslip ranges at several thrust conditions, flap deflections, and nozzle deflections. Also included are results of tests made for several heights above a moving ground plane to determine the effects of ground proximity in transition flight. Interference effects between the jets and the free stream are also presented.

Recently considerable interest (ref. 11) has been expressed regarding the use of deflected thrust for situations not related to take-off or landing. One area of interest is its use to increase airplane maneuverability. Some of the recent flight tests conducted at Langley with the Kestrel (XV-6A) airplane have used deflected thrust at an altitude of approximately 4572 meters (15 000 feet). To complement this flight experience, some wind-tunnel data are included herein to describe the static aerodynamic characteristics of the plane in these maneuvers.

SYMBOLS

The longitudinal force and moment data are referred to the stability-axis system. The lateral-directional data are referred to the body-axis system. The coefficients include jet and inlet momentum effects. For all data, the origin is located at the moment center shown in figure 1. The units of measurement used in this paper are given in both the International System of Units (SI) (ref. 12) and U.S. Customary Units. The measurements and calculations were made in U.S. Customary Units.

b	wing span, m (ft)
C_D	drag coefficient, $\frac{D}{q_\infty S}$
C_L	lift coefficient, $\frac{L}{q_\infty S}$
C_l	rolling-moment coefficient, $\frac{\text{Rolling moment}}{q_\infty Sb}$
C_m	pitching-moment coefficient, $\frac{M_Y}{q_\infty S\bar{c}}$
C_n	yawing-moment coefficient, $\frac{\text{Yawing moment}}{q_\infty Sb}$
C_T	thrust coefficient, $\frac{T}{q_\infty S}$
C_Y	side-force coefficient, $\frac{\text{Side force}}{q_\infty S}$
$\bar{c}$	mean aerodynamic chord, m (ft)
D	drag, N (lbf)
D_e	equivalent diameter (diameter of nozzle equivalent in area to total area of four model nozzles), 0.193 m (0.633 ft)
h	height of moment center above ground plane, m (ft)
i_t	tail incidence angle, positive when trailing edge is down, deg
L	lift, N (lbf)
M_Y	pitching moment, m-N (ft-lbf)
M_∞	free-stream Mach number
p_{ref}	total pressure in ejector plenum, N/mm^2 (lbf/in^2)
q_∞	free-stream dynamic pressure, N/m^2 (lbf/ft^2)

S	wing area, m^2 (ft^2)
T	thrust at static conditions, N (lbf)
V_e	effective-velocity ratio, $\sqrt{\frac{\text{Free-stream dynamic pressure}}{\text{Nozzle-exit dynamic pressure}}}$
V_∞	free-stream velocity (true airspeed), knots
w_i	ejector-inlet weight flow, N/sec (lbf/sec)
α	fuselage angle of attack (wing incidence, 1.75^o), deg
β	angle of sideslip, deg
$\Delta L, \Delta D, \Delta M_Y$	increments of lift, drag, and pitching moment, respectively, due to interference
δ_a	aileron-deflection angle (sum of right (up) and left (down) deflections), deg
δ_f	flap-deflection angle, deg
δ_n	nozzle-deflection angle, measured downward from plane containing fuselage reference line and perpendicular to plane of symmetry, deg
δ_r	rudder deflections, positive when trailing edge is deflected toward left, deg
C_{l_β}	effective-dihedral parameter
C_{n_β}	directional-stability parameter
C_{Y_β}	side-force parameter
$\partial C_l / \partial \delta_a$	rolling moment per degree of aileron deflection
$\partial C_m / \partial i_t$	pitching moment per degree of tail deflection
$\partial C_n / \partial \delta_r$	yawing moment per degree of rudder deflection

MODEL AND APPARATUS

A three-view drawing of the model with dimensions is given in figure 1, and photographs of the model are given in figure 2. The model was a 1/6-scale representation of the Kestrel (XV-6A) vectored-thrust jet V/STOL airplane. It was constructed of aluminum and wood covered with fiber glass. The flaps and ailerons could be fixed at various deflection angles. The empennage includes a variable-incidence horizontal tail and adjustable rudder. Landing-gear provision was made to simulate both the landing and the cruise conditions.

The model was mounted on a six-component strain-gage balance attached to a support sting which enclosed the air line to the model powerplant (fig. 1(b)). The sting was fixed to a vertical strut which had provisions for varying the angle of attack, angle of sideslip, and height above a movable ground plane. The movable ground plane was a fabric belt over two spanwise rollers driven by an electric motor (ref. 13).

The model was powered by four cold-air ejectors (ref. 14) each exhausting through swiveling nozzles along the fuselage and supplied by a compressed-air line enclosed in the support sting. The nozzles were individually adjustable to give jet deflection angles between 0° and 95° with respect to the model horizontal plane. Power variations were obtained by varying the ejector air-supply pressure. Ejector operating variables were determined from calibrations based on the reference pressures measured in the ejector plenum chambers by electrical pressure transducers. Angles of attack were measured by an electronic inclinometer mounted in the fuselage, and sideslip angles were determined from a calibrated gearing arrangement on the model support strut. The foregoing measurements together with tunnel operating variables and forces and moments were recorded on magnetic tape.

TESTS AND CORRECTIONS

The investigation was conducted in the 5.18-meter (17-foot) test section of the Langley 300-MPH 7- by 10-foot tunnel. The maximum free-stream dynamic pressure was 527 N/m^2 (11.0 lbf/ft^2) or a maximum free-stream velocity of 29.3 m/sec (96.1 ft/sec) resulting in a Reynolds number based on $\bar{c}$ of about 0.88×10^6.

Data were obtained through a range of angles of attack from -4° to 24° and a range of sideslip angles generally from -12° to 12° (or -6° to 24° in some cases) at various thrust coefficients or effective free-stream—to—jet velocity ratios. Model variations investigated at fixed thrust coefficients and nozzle deflections were tail incidence, rudder deflection, flap deflection, aileron deflection, and height above the ground plane. In addition to the study of the transition configuration ($\delta_f = 60^{\circ}$, $\delta_n = 65^{\circ}$, 85°, and 95°, and landing gear down), the normal-cruise configuration ($\delta_f = 0^{\circ}$, $\delta_n = 0^{\circ}$, and landing gear

retracted) was investigated with and without power to determine horizontal-tail, rudder, and aileron effectiveness in cruise.

Attachment of the air-supply line to the model affects the sensitivity of the strain-gage balance. Variations in air-line pressure also produce forces and moments on the balance. Both of these nonaerodynamic effects are consistently repeatable. Calibrations were made to determine these effects for which corrections were made on the balance readings. No blockage or wall corrections have been applied as they are believed to be small for a model of the present size in the 5.18-meter (17-foot) test section (ref. 15).

ENGINE SIMULATION

Simulator Calibration

The Pegasus 5 turbofan engine of the Kestrel (XV-6A) was simulated by using four cold-air-powered ejectors (ref. 14) exhausting through swiveling nozzles. Figure 3 presents the variation of inlet weight flow and thrust for each ejector as functions of the reference pressure measured in the ejector plenum chambers. The inlet weight flow was determined by using a calibrated bellmouthed entrance. The thrust was the total resultant force measured statically by the strain-gage balance; as a result, the thrust in this paper corresponds to the airplane gross thrust. The model thrust used to compute thrust coefficient during this investigation was determined from these calibration curves as a function of the reference pressure.

The swiveling nozzles were modeled to represent the Pegasus 5 turbofan engine. In this investigation, there were some variations in individual nozzle deflections for a given nominal total-thrust deflection angle. For example, for a nominal setting of 85°, individual nozzle deflections were 89°, 82°, 88°, and 88°, or a total-thrust deflection of 86° based on measured axial and normal forces. This investigation also used nominal nozzle deflections of 0°, 45°, 65°, and 95°. For these nominal deflections, the actual deflections, based on measured axial and normal forces, were -3°, 45°, 66°, and 96°.

Effective-Velocity-Ratio Simulation

The relationship between effective velocity ratio V_e and thrust coefficient C_T for this investigation is given in figure 4. The velocity ratios were obtained by varying both the jet thrust T and the tunnel dynamic pressure q_∞. A series of runs were made to determine whether the force- and moment-thrust ratios for a given velocity ratio V_e were independent of the magnitude of the dynamic pressures involved. Runs were made at several tunnel dynamic pressures while varying the jet thrust. This procedure gave force- and moment-thrust ratios at some equivalent velocity ratios but at different dynamic pressures. The data are presented in figure 5(a) for the 0° nozzle deflection

and in figure 5(b) for the 85° nozzle deflection. The curves do not always coalesce and this indicates that force and moment ratios for a given velocity ratio are not entirely independent of the dynamic pressures used in obtaining that velocity ratio. However, examination of these data generally indicates that the major differences in the curves occur at conditions where both the lower values of tunnel dynamic pressure $q_\infty < 191.5$ N/m^2 (4 lbf/ft^2) and the lower values of thrust $T < 133.4$ N (30 lbf) are involved. In these cases, small errors in force measurements and in calculated thrust may noticeably affect ratios of small values. From these results, a combination of q_∞ and T was established for variation of the effective-velocity ratio through the transition-speed range. The maximum thrust was used for $V_e < 0.20$ while q_∞ was varied from 0 to 527 N/m^2 (11 lbf/ft^2). For V_e between 0.20 and 0.50, the maximum q_∞ was used while thrust was varied from the maximum value 645 N (145 lbf) to approximately 146 N (33 lbf). Unfortunately, it was necessary to use very low values of T at the maximum tunnel dynamic pressure (527 N/m^2 (11 lbf/ft^2)) to obtain values of V_e greater than 0.50; as a result, the accuracy of these data may not be as good as the transition ($V_e < 0.50$) data.

PRESENTATION OF RESULTS

The data figures are presented in the following table. The out-of-ground-effect data were obtained near the center line of the tunnel, or approximately two wing spans above the ground plane. When in-ground-effect data are presented, the fact is noted in the figures.

Data description	δ_f, deg	δ_n, deg	C_T or V_e	Figure
Longitudinal				
Model-component contributions	0	0	0	6
Effect of horizontal-tail incidence	0	0	Range	7
Effect of horizontal-tail incidence	60	65	Range	8
Effect of horizontal-tail and interference increments	60	65	Range	9
Effect of horizontal-tail incidence	60	85	Range	10
Effect of horizontal-tail and interference increments	60	85	Range	11
Effect of flap deflection	Range	85	Range	12
Effect of flap and interference increments	Range	85	Range	13
Effect of nozzle deflection	60	Range	Range	14
Effect of nozzle deflection and interference increments	60	Range	Range	15
Interference increments and effect of ground, tail off	60	65	Range	16
Interference increments and effect of ground, tail off	60	85	Range	17
Interference increments and effect of ground, tail on	60	65	Range	18
Interference increments and effect of ground, tail on	60	85	Range	19

Data description	δ_f, deg	δ_n, deg	C_T or V_e	Figure
Lateral				
Model-component contributions in sideslip	0	0	Range	20
Model-component contributions in sideslip	60	85	Range	21
Lateral-stability parameters	0, 60	0, 85	Range	22
Effect of rudder deflection	60	85	Range	23
Effect of aileron deflection	60	85	Range	24
Effect of aileron deflection at high angles of attack	60	85	Range	25
Effect of combined angles of attack and sideslip	60	85	Range	26
Rudder effectiveness in cruise	0	0	Range	27
Effect of aileron deflection in cruise	0	0	Range	28
Effect of aileron deflection at high angles of attack in cruise	0	0	Range	29
Special figures				
Control-surface effectiveness	0, 60	0, 65	Range	30
Effective-velocity ratio with Mach number	-----	-------	-----	31
Free-stream velocity with effective-velocity ratio	-----	-------	-----	32
Effect of nozzle deflection in cruise, tail off	0	0, 65, 95	0.2	33
Effect of nozzle deflection in cruise, tail off	0	Range	Range	34
Effect of nozzle deflection in cruise, tail on	0	0, 65, 95	0.2	35
Effect of nozzle deflection in cruise, tail on	0	Range	Range	36
Effect of horizontal-tail incidence in cruise	0	0, 65, 95	0.2	37

RESULTS AND DISCUSSION

Longitudinal Aerodynamic Characteristics

Model-component contributions.- The power-off longitudinal characteristics of the major components of the model are shown in figure 6. The usual instability of an elongated body is accentuated in the present model by the increased diameter of the forward end of the fuselage made to accommodate the engine inlets. The addition of the wing with flaps undeflected neutralizes the unstable body moments, and the addition of the tail gives a stable configuration.

Effect of horizontal tail.- In the cruise configuration (fig. 7), small deflections of the horizontal tail are sufficient to trim the model for the thrust range shown. Thrust produces positive pitching moments as indicated by the tail-off curves, but it also increases the trimming capability of the horizontal tail owing to the increased dynamic pressure at the tail. The longitudinal characteristics of the transition configurations $\left(\delta_n = 65^\circ \text{ and } 85^\circ,\ \delta_f = 60^\circ\right)$ are shown in figures 8 to 11. Without power, the model is

stable, and small tail deflections are adequate to trim the diving moments produced by the wing with flaps deflected. As power is introduced, the model becomes unstable and large positive out-of-trim pitching moments occur for all tail incidences tested (figs. 8, 10(b), 10(c), and 10(d)). These changes with power result from several factors. Static tests on the model showed that positive pitching moments were produced by jet thrust. The inlet drag with power on also produces positive pitching moments (ref. 16) which increase with angle of attack and produce instability. As the thrust coefficient is increased, more of the lift is obtained from the jet thrust, and the influence of the wing and flaps on pitching moments is reduced. The increased thrust of the deflected jets combined with the reduction in forward speed increases the downwash and reduces the dynamic pressure at the tail, thus rendering the tail less effective as a control and trim device. The full-scale airplane uses jet-reaction nozzles located in the wing tips and front and rear of the fuselage for control at low speeds and in hovering.

Effect of flaps.- The increments of lift owing to deflection of the partial-span flaps are rather small (figs. 12 and 13) even at zero and low thrust conditions or the higher forward speeds. At high thrust $\left(C_T = 6\right)$, the jet lift is so much greater than the aerodynamic lift at the low free-stream dynamic pressure that the flap deflection has little noticeable lift effect. The deflected flaps do reduce the magnitude of the out-of-trim positive pitching moments of the model with flaps undeflected.

Effect of nozzle deflection.- The nozzle deflections shown in figures 14 and 15 may be considered typical deflections for forward transition $\left(\delta_f = 65^o\right)$, hovering $\left(\delta_f = 85^o\right)$, and deceleration $\left(\delta_f = 95^o\right)$. Without power, nozzle-deflection effects are negligible except for the drag. The drag is affected by the amount of turning the nozzle produces on the free-stream air that flows through the nozzles. With power at low forward speeds, the force and moment characteristics of the model depend primarily on the jet force, and the large variations in lift and drag with nozzle deflection are the direct results of jet axis inclination and jet thrust.

Ground-plane and interference effects.- The data showing the effects of ground-plane proximity are shown in figures 16 to 19. The closest position to the ground plane is indicated by $h/D_e = 2.04$. At this height the bottom of the model nose wheel was 5.08 cm (2 inches) above the ground plane. The measured data are presented as ratios of forces and moments to thrust, and the interference effects between jet and free stream are presented as ratios of incremental forces and moments to thrust. These ratios are equivalent to conventional aerodynamic force and moment coefficients divided by the thrust coefficient; for example, $L/T = C_L/C_T$. The effect of increased velocity ratio is indicated by the large increase in lift-thrust ratios, especially for the data at $\alpha = 9^o$. Ground proximity increases the lift-thrust ratios and decreases the pitching-moment ratios at the higher velocity ratios, but has little effect on the drag ratios. Addition of the horizontal tail $\left(i_t = 0^o\right)$ to the model (figs. 18 and 19) results in positive pitching moments and a

reduction of the lift-thrust ratios except when the tail is nearest the ground plane at a model angle of attack of 9°. This reduction in download on the tail results from reduced downwash as the tail gets nearer the ground plane.

The measured total force and moments on the model are composed of the jet forces, the aerodynamic forces, and the forces due to the mutual interference effects of the jet, model, and free stream; for example

$$L = T \sin\left(\delta_n + \alpha\right) + C_L q_\infty S + \Delta L$$

From this and similar equations for drag and pitching moment, the interference increments shown in figures 9, 11, 13, 15, 16, 17, 18, and 19 were obtained. Interference generally results in an increase in drag and positive pitching moments and a reduction in lift. In previous investigations, similar results were obtained with lift engines in pods adjacent to the fuselage (ref. 16) and in models similar to the present one (ref. 17). As expected, the pitching-moment interference effects increase considerably when the horizontal tail is added to the model (compare figs. 16 and 18; 17 and 19). Ground proximity generally reduces the interference effects on the lift and pitching moment when the effects are significant but has little effect on the drag.

Lateral Aerodynamic Characteristics

Model components.- The lateral characteristics of major model components are presented in figure 20 for the cruise configuration and in figure 21 with flaps and nozzles deflected.

In general, the wing-body combination (fig. 21), with $\delta_f = 60^{\circ}$, $\delta_n = 85^{\circ}$, and $\alpha = 0^{\circ}$, was directionally unstable and laterally stable over the angle-of-sideslip and thrust-coefficient ranges tested except for small angles of sideslip at the high thrust coefficient where the model was unstable in roll. The addition of the vertical tail increased the lateral stability and caused the model to become directionally stable except at the high thrust coefficient where instability in yaw and roll occurred at small sideslip angles. These results (fig. 21(d)) are consistent with Langley flight tests in which rolling instability was exhibited by the airplane at low speeds (high thrust) at small angles of sideslip. The directional and lateral characteristics of the complete model were about the same as those of the wing-body-vertical tail combination. In general, there was no effect of angle of sideslip on the longitudinal characteristics except for a pitchup at the high thrust coefficient.

These results are summarized in figure 22 which presents the variation of lateral-directional stability parameters with thrust coefficient for $C_T < 2.2$. With flaps and noz-

zles deflected, the model shows a little less directional stability and more effective dihedral ($\approx 10^{\circ}$) than with flaps and nozzles undeflected.

Control-surface characteristics in transition.- The effect of rudder deflection on the characteristics of the model in sideslip is shown in figure 23. With power off, the lateral forces and moments vary linearly with sideslip angle, and the yawing moments are proportional to rudder deflection. At high thrust conditions, all moment curves show nonlinearities at small sideslip angles with or without rudder deflection. For the sideslip range shown, the yawing moments increase little when rudder deflection is increased from 5° to 10°, but effectiveness is regained at a deflection of 15°.

Aileron deflection of 18° (9° up and down) generally gives constant increments of rolling and favorable yawing moments through the sideslip range (fig. 24). Model characteristics through an angle-of-attack range with larger aileron deflections are shown in figure 25. Without power, the ailerons lose effectiveness at model angles of attack above 12°, but with power, the ailerons have almost constant incremental effects with angle of attack up to 24° except at the highest thrust coefficient.

The characteristics of the model at combined angles of attack and angles of sideslip without aileron deflection are shown in figure 26. Except for the yawing moments at the highest angle of attack, the lateral force and moment coefficients change little with angle of attack and increase almost linearly with sideslip angle for the power-off condition. With power, an increase in angle of attack increases the effective dihedral and the directional stability of the model with flaps deflected (fig. 26). At the highest thrust coefficient, scatter in the data produced by unsteady forces and moments is emphasized when these forces and moments are nondimensionalized by the low dynamic pressure and expressed as coefficients.

Control-surface characteristics in cruise.- The aerodynamic characteristics of the model for the cruise condition in sideslip are presented in figures 27 and 28. The data show that the forces and moments produced by rudder or aileron deflection are linear with sideslip angle as was the case at low thrust conditions with flaps deflected. The ailerons show little loss in effectiveness with angle of attack up to a model angle of attack of about 14° (fig. 29). The variation of control-surface effectiveness with thrust coefficient per degree of deflection, including the horizontal tail, is shown in figure 30. The rudder and aileron show little variation in effectiveness with thrust coefficient or model configuration. The effectiveness of the horizontal tail increases with thrust coefficient owing to the increased dynamic pressure at the tail with the nozzles undeflected for the cruise condition.

Effect of Deflected Thrust Above Transition Speeds

Wind-tunnel tests were conducted with the present model to determine the effect of deflected thrust at conditions which represent velocities above transition speeds. Note that these tests were conducted at a dynamic pressure of 527 N/m^2 (11.0 lbf/ft^2); therefore, compressibility effects present at high subsonic speeds are not represented by these data.

The estimated engine thrust with the engine operating at 0.90 of the maximum low-pressure fan speed at the altitude of the Langley flight tests (4572 meters (15 000 feet)) was used to compute the effective-velocity ratio V_e as a function of Mach number (fig. 31), and the free-stream velocity as a function of effective-velocity ratio (fig. 32). From these figures, it can be seen that an effective velocity ratio of 1.1 represents a Mach number of 0.58 and a velocity of approximately 350 knots at an altitude of 4572 meters (15 000 feet). This represents approximately the upper limit of the equivalent speed simulated in the present wind-tunnel data.

The results presented in figures 33 to 37 show effects which are similar in character to those found in the upper-speed range of the transition-flight regime. Of course, the thrust contribution to the lift and drag is less than it is at the lower speed (that is, higher thrust conditions). There is a loss in lift and an increase in drag owing to interference as indicated by comparing the undeflected jet data for $C_T = 0.2$ (fig. 33(a)) with the power-off data of figure 7(a). At small angles of attack, deflecting the jets does not significantly change the interference loss since the increment of lift due to jet deflection (fig. 33) is approximately equal to the lift component of the jet. The decelerative force on an airplane in level flight without special drag devices, such as dive brakes, is the drag of the airframe with power off. The power-off drag coefficient of the present model is about 0.06 (fig. 7(a)), but with the nozzle deflected 95^o, figure 33(a) shows a drag coefficient of 0.185 at low angles of attack and $C_T = 0.2$, or about three times the drag of the model with power off. These results are consistent with the results of flight tests which show that deflected thrust on the Kestrel (XV-6A) at high subsonic speeds produces large decelerative forces which are especially useful in evasive turns.

The effect of horizontal-tail incidence on the longitudinal characteristics of the model at speeds above transition with the jets deflected is shown in figure 37. The stability of the model with jets undeflected is reduced to near neutral stability for a jet deflection of 65^o and to instability at moderate angles of attack for a jet deflection of 95^o. Jet deflection also causes small trim changes requiring 3^o to 5^o of positive tail incidence for correction.

SUMMARY OF RESULTS

An investigation was made to determine the longitudinal and lateral characteristics of a 1/6-scale model of the Kestrel (XV-6A) vectored-thrust V/STOL airplane at low-speed cruise and transition conditions. Data were obtained out of and in ground effect over a moving ground plane for a range of model angles of attack and sideslip at various thrust coefficients by using compressed air ejecting from nozzles in the fuselage.

Some results are as follows:

1. In the cruise configuration, the model is longitudinally stable, but in transition, model longitudinal instability is increased as power is increased. The flaps and horizontal tail have little effect in transition at high thrust coefficients.

2. Jet and free-stream interference generally results in an increase in drag and noseup pitching moments and a reduction in lift.

3. Ground proximity generally reduces the interference effects on lift and pitching moment but has little effect on the drag. Ground proximity increases the lift-thrust ratios and reduces the positive pitching-moment ratios at the higher velocity ratios.

4. At high thrust coefficients in transition, the model was unstable in roll and yaw at small sideslip angles.

5. The effectiveness of the control surfaces with the exception of the horizontal tail varies little with flight configuration or thrust coefficient in the low thrust range.

6. Deflected thrust at speeds above transition produce increments of lift and large deceleration forces useful in maneuvering flight, but with a reduction in stability.

Langley Research Center,
National Aeronautics and Space Administration,
Hampton, Va., June 8, 1972.

REFERENCES

1. Spreemann, Kenneth P.: Wind-Tunnel Investigation of Longitudinal Aerodynamic Characteristics of a Powered Four-Duct-Propeller VTOL Model in Transition. NASA TN D-3192, 1966.

2. Goodson, Kenneth W.: Effect of Ground Proximity on the Longitudinal, Lateral, and Control Aerodynamic Characteristics of a Tilt-Wing Four-Propeller V/STOL Model. NASA TN D-4237, 1967.

3. Newson, William A., Jr.; and Kirby, Robert H.: Flight Investigation of Stability and Control Characteristics of a 1/9-Scale Model of a Four-Propeller Tilt-Wing V/STOL Transport. NASA TN D-2443, 1964.

4. Winston, Matthew M.: Induced Interference Effects on the Aerodynamic Characteristics of a 0.16-Scale Six-Jet V/STOL Model in Transition. NASA TN D-5257, 1970.

5. Kirk, Jerry V.; Hickey, David H.; and Hall, Leo P.: Aerodynamic Characteristics of a Full-Scale Fan-In-Wing Model Including Results in Ground Effect With Nose-Fan Pitch Control. NASA TN D-2368, 1964.

6. Smith, Charles C., Jr.: Flight Tests of a 1/6-Scale Model of the Hawker P 1127 Jet VTOL Airplane. NASA TM SX-531, U.S. Air Force, 1961.

7. Schmeer, James W.; Cassetti, Marlowe D.; and Simonson, Albert J.: Transonic Aerodynamic Characteristics of a Model of a Single-Engine Four-Jet V/STOL Airplane. NASA TM SX-528, U.S. Air Force, 1961.

8. Schmeer, James W.; and Runckel, Jack F.: Jet Interference Effects on a Model of a Single-Engine Four-Jet V/STOL Airplane at Mach Numbers From 0.60 to 1.00. NASA TM SX-685, U.S. Air Force, 1962.

9. Morello, Samuel A.; Person, Lee H., Jr.; Shanks, Robert E.; and Culpepper, Richard G.: A Flight Evaluation of a Vectored-Thrust-Jet V/STOL Airplane During Simulated Instrument Approaches Using the Kestrel (XV-6A) Airplane. NASA TN D-6791, 1972.

10. McKinzie, Gordon A.; Ludwig, John H.; Bradfield, Edward N., Jr.; and Casey, William R.: P-1127 (XV-6A) VSTOL Handling Qualities Evaluation. FTC-TR-68-10, U.S. Air Force, Aug. 1968.

11. Attinello, J.: Supermaneuverability of Fighter Aircraft. Res. Paper P-520, Systems Evaluation Div., Inst. Def. Anal., Oct. 1969.

12. Mechtly, E. A.: The International System of Units – Physical Constants and Conversion Factors (Revised). NASA SP-7012, 1969.

13. Turner, Thomas R.: A Moving-Belt Ground Plane for Wind-Tunnel Ground Simulation and Results for Two Jet-Flap Configurations. NASA TN D-4228, 1967.

14. Margason, Richard J.; and Gentry, Garl L.: Static Calibration of an Ejector Unit for Simulation of Jet Engines in Small-Scale Wind-Tunnel Models. NASA TN D-3867, 1967.

15. Staff of Powered-Lift Aerodynamics Section, NASA Langley Research Center: Wall Effects and Scale Effects in V/STOL Model Testing. AIAA Aerodynamic Testing Conference, Mar. 1964, pp. 8-16.

16. Vogler, Raymond D.: Wind-Tunnel Investigation of a VTOL Jet-Transport Model With Powered Lift Engines in Pods at Wing Midspan or Inboard. NASA TN D-5770, 1970.

17. Vogler, Raymond D.; and Kuhn, Richard E.: Longitudinal and Lateral Stability Characteristics of Two Four-Jet VTOL Models in the Transition Speed Range. NASA TM X-1092, 1965.

Geometric characteristics

	Wing	Horizontal tail	Vertical tail
Span, cm (in.)	116.38 (45.82)	70.73 (27.85)	28.57 (11.25)
Root, cm (in.)	59.27 (23.33)	28.53 (11.23)	36.80 (14.49)
Tip chord, cm (in.)	23.71 (9.33)	7.55 (2.97)	9.86 (3.88)
Mean aerodynamic chord, cm (in.)	44.02 (17.33)	20.07 (7.90)	25.92 (10.20)
Area, m^2 (ft^2)	0.4810 (5.18)	0.1226 (1.32)	0.066 (0.72)
Taper ratio	0.40	0.26	0.27
Aspect ratio	2.81	4.08	1.23
Sweep, deg:			
Leading edge	40.01	38.72	47.37
Quarter-chord line	34.00	32.89	40.37
Dihedral, deg	-12.00	-15.84	
Thickness-chord ratio:			
Root	0.10	0.07	0.08
Tip	0.05	0.07	0.07
Tail length (moment center to quarter-chord of tail), cm (in.)		90.88 (35.78)	87.68 (34.52)
Wing incidence, deg	1.75		

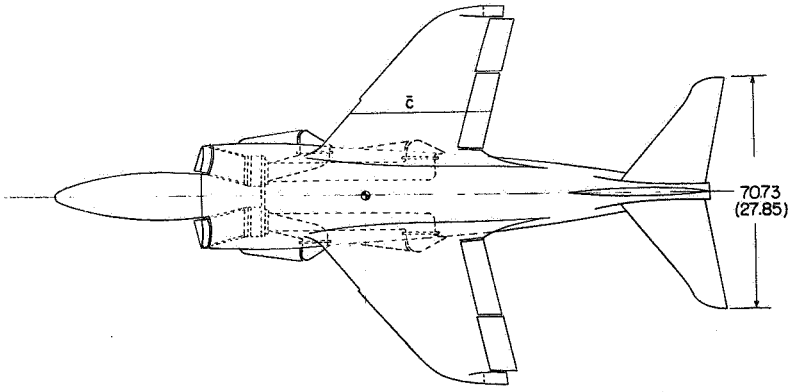

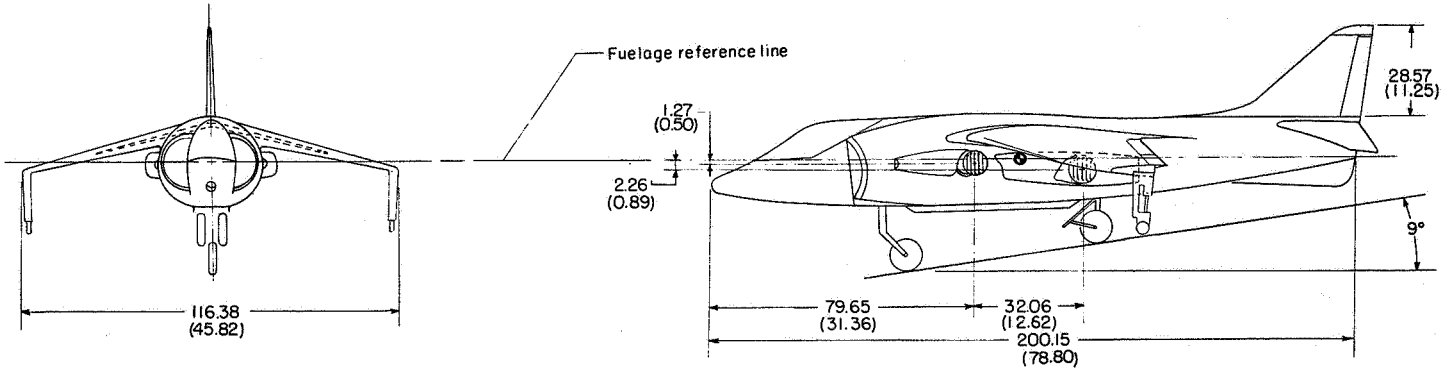

(a) Three-view drawing of model.

Figure 1.- Three-view drawing of model and air supply system. Dimensions in cm (inches).

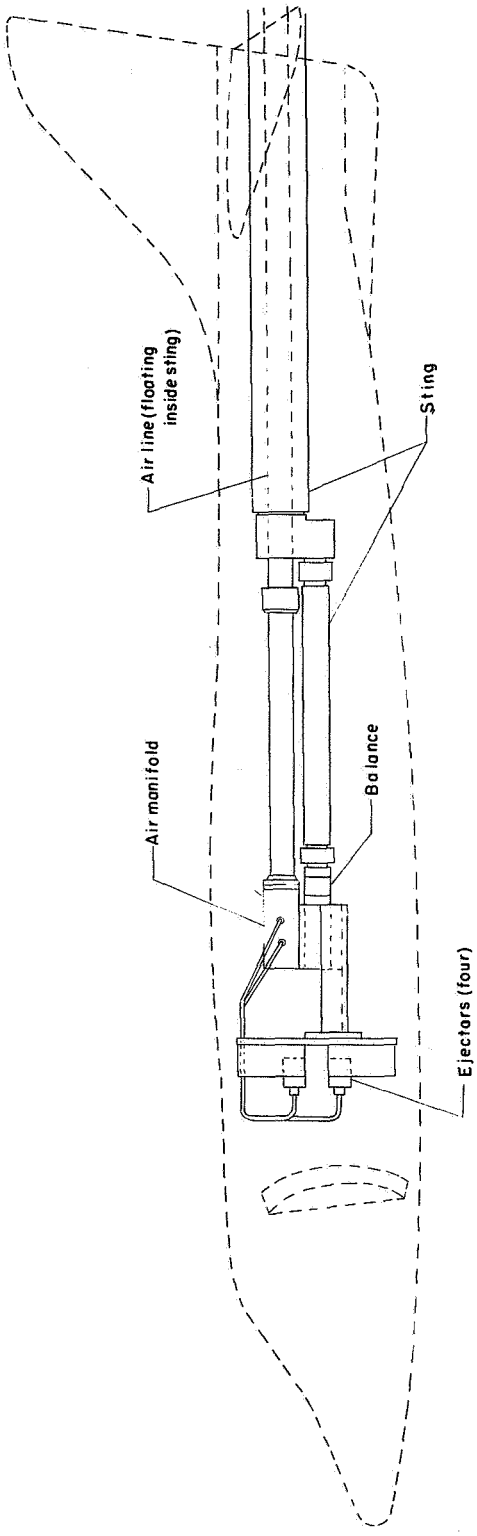

(b) Details of air lines to ejectors.

Figure 1.- Concluded.

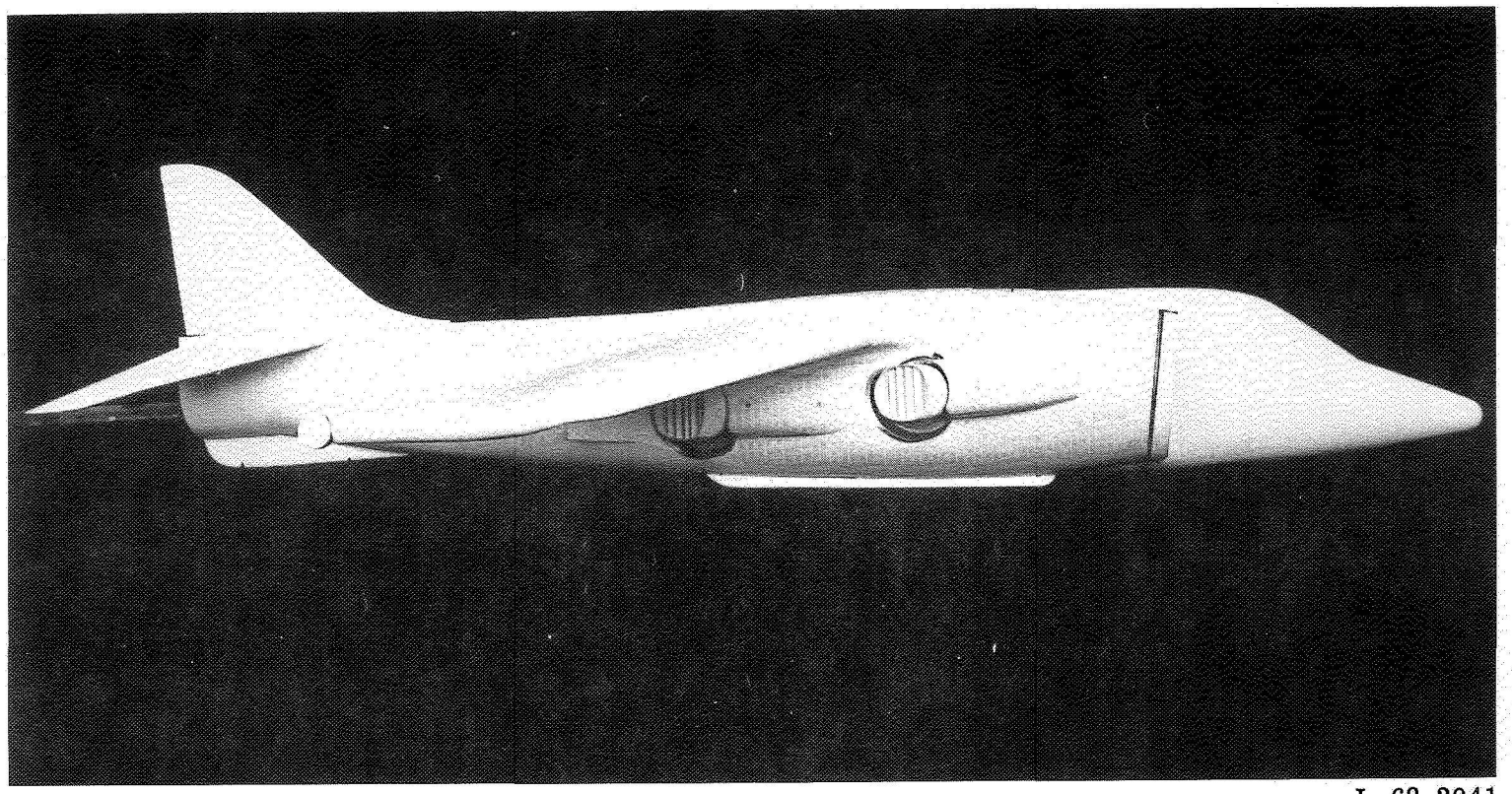

L-68-2041

(a) Landing gear up.

Figure 2.- Side view of model.

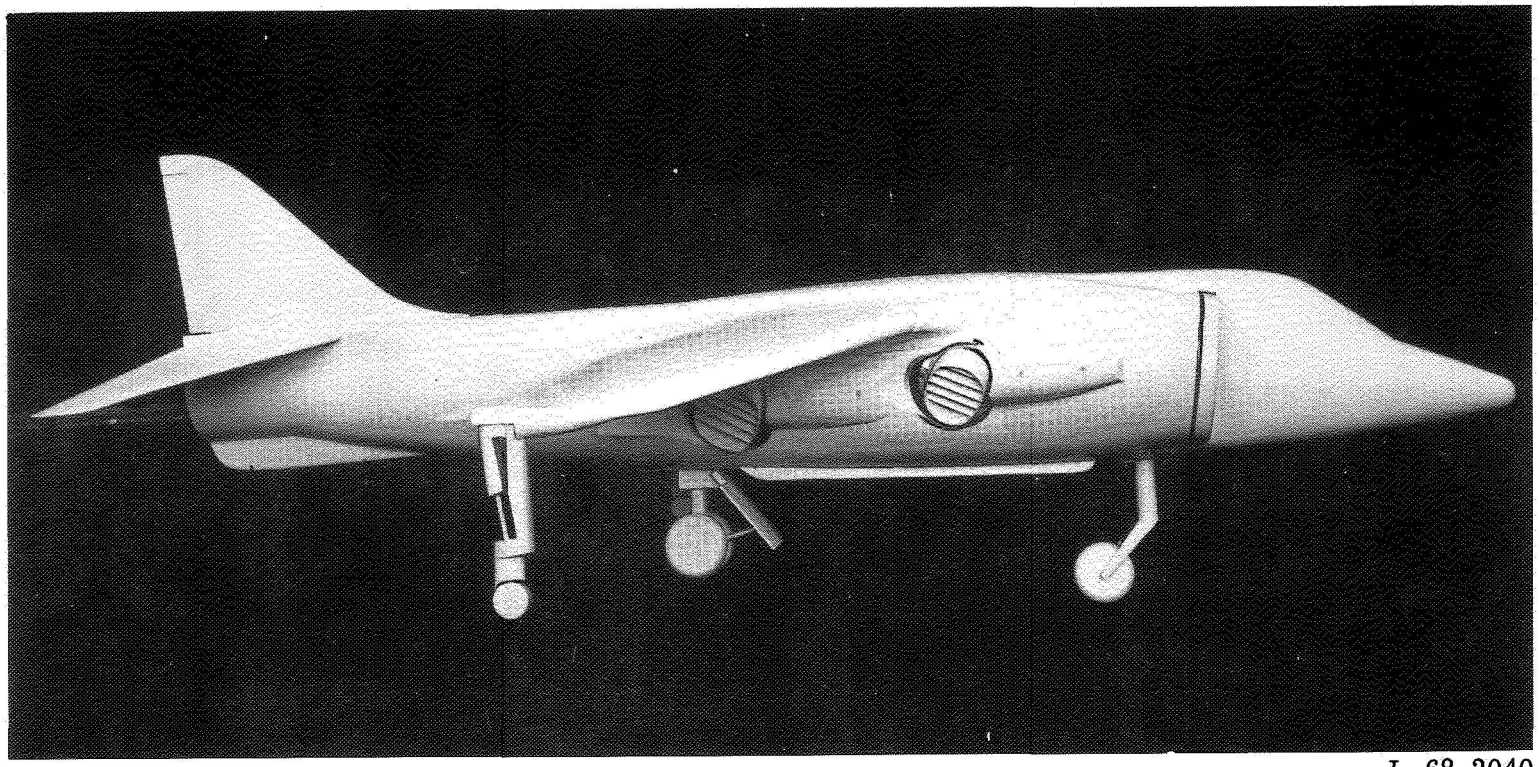

L-68-2040

(b) Landing gear down.

Figure 2.- Concluded.

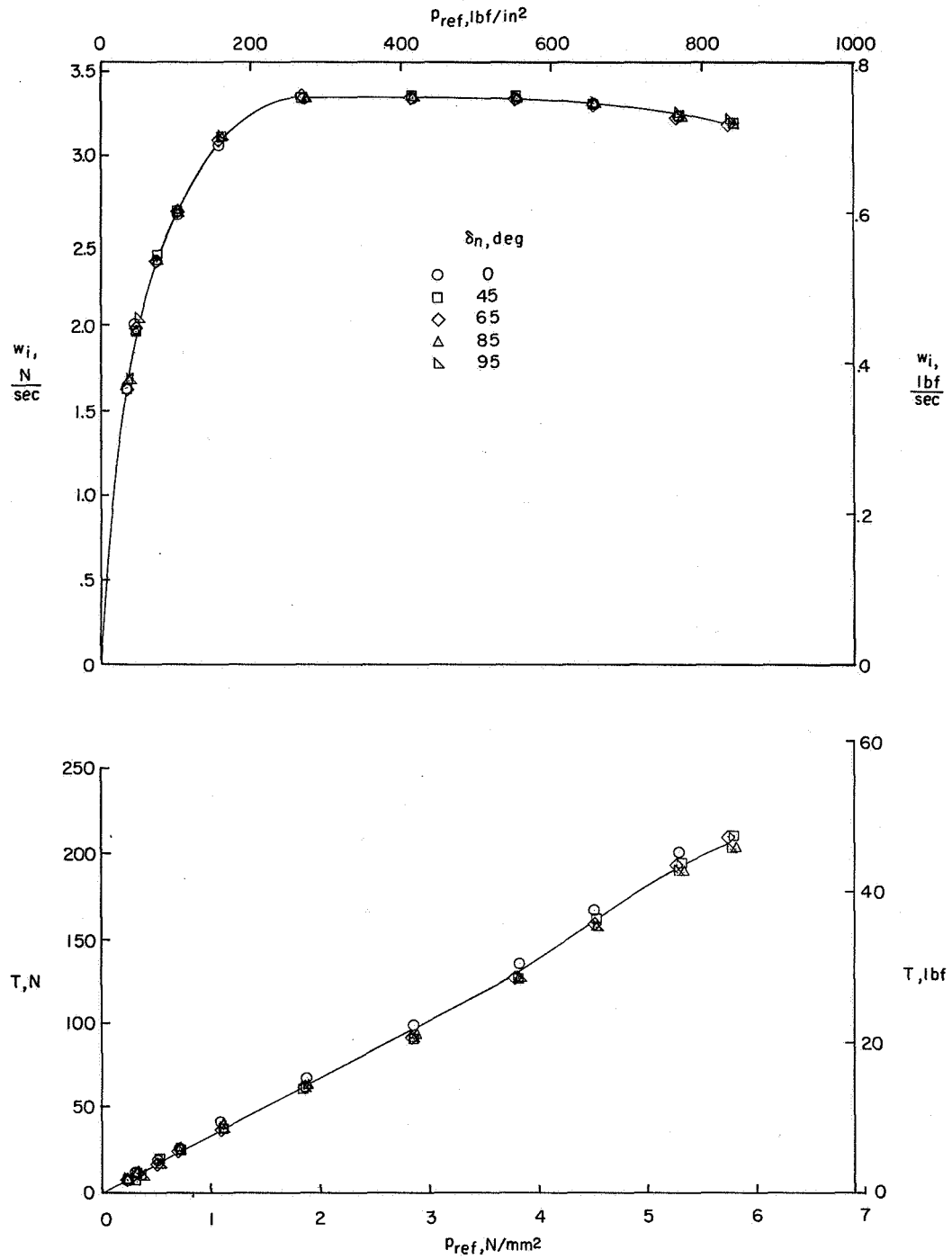

(a) Left front.

Figure 3.- Model ejector characteristics.

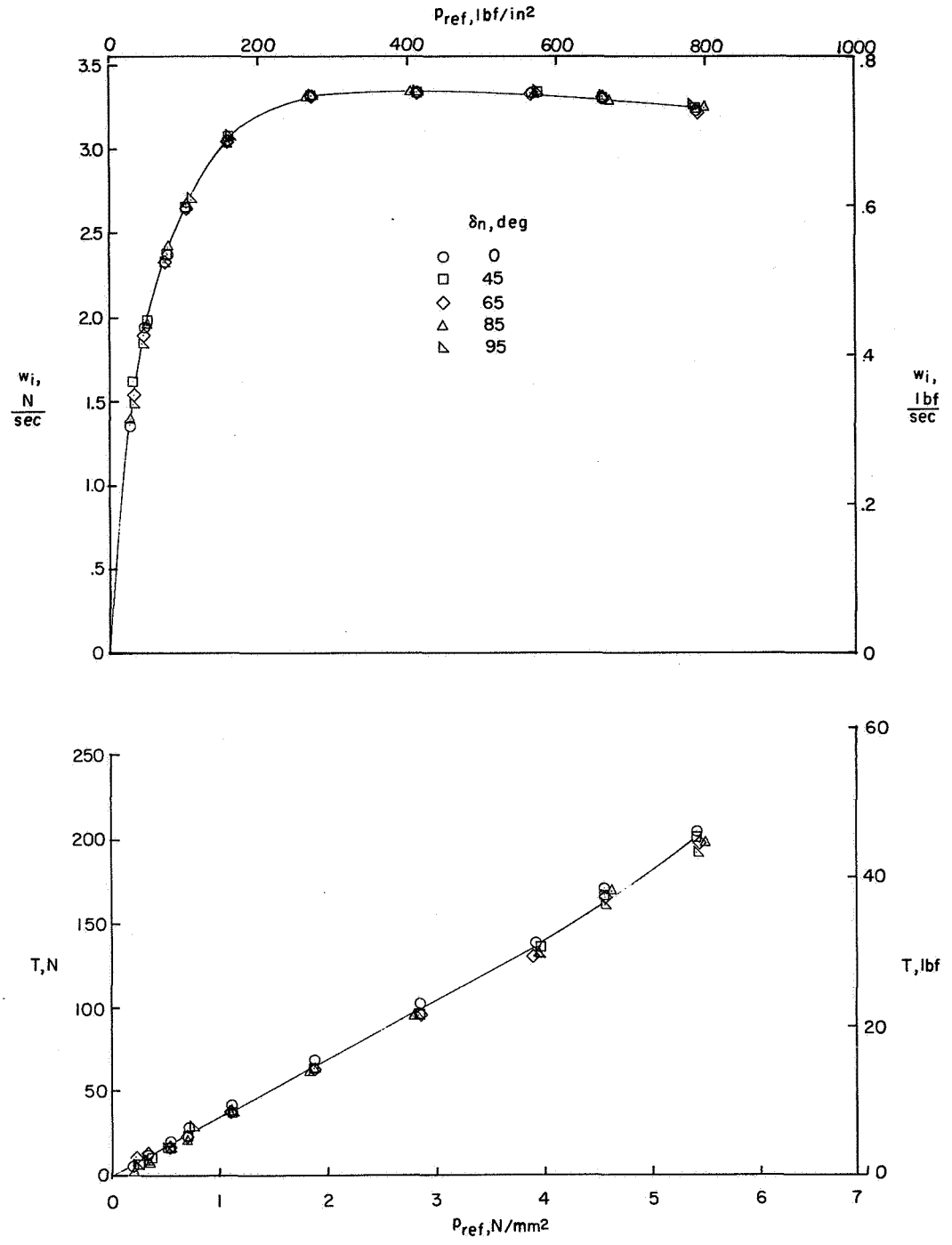

(b) Right front.

Figure 3.- Continued.

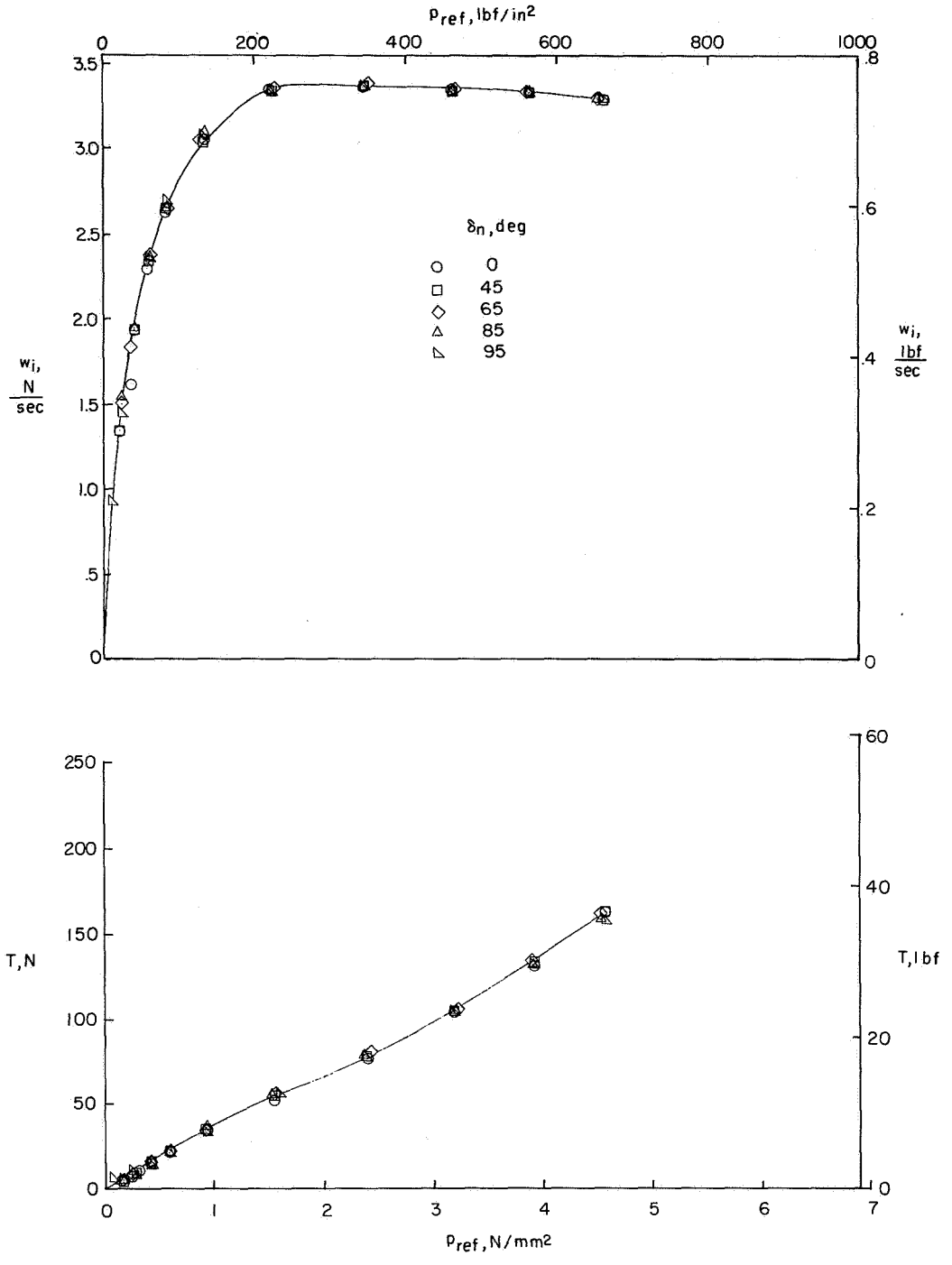

(c) Left rear.

Figure 3.- Continued.

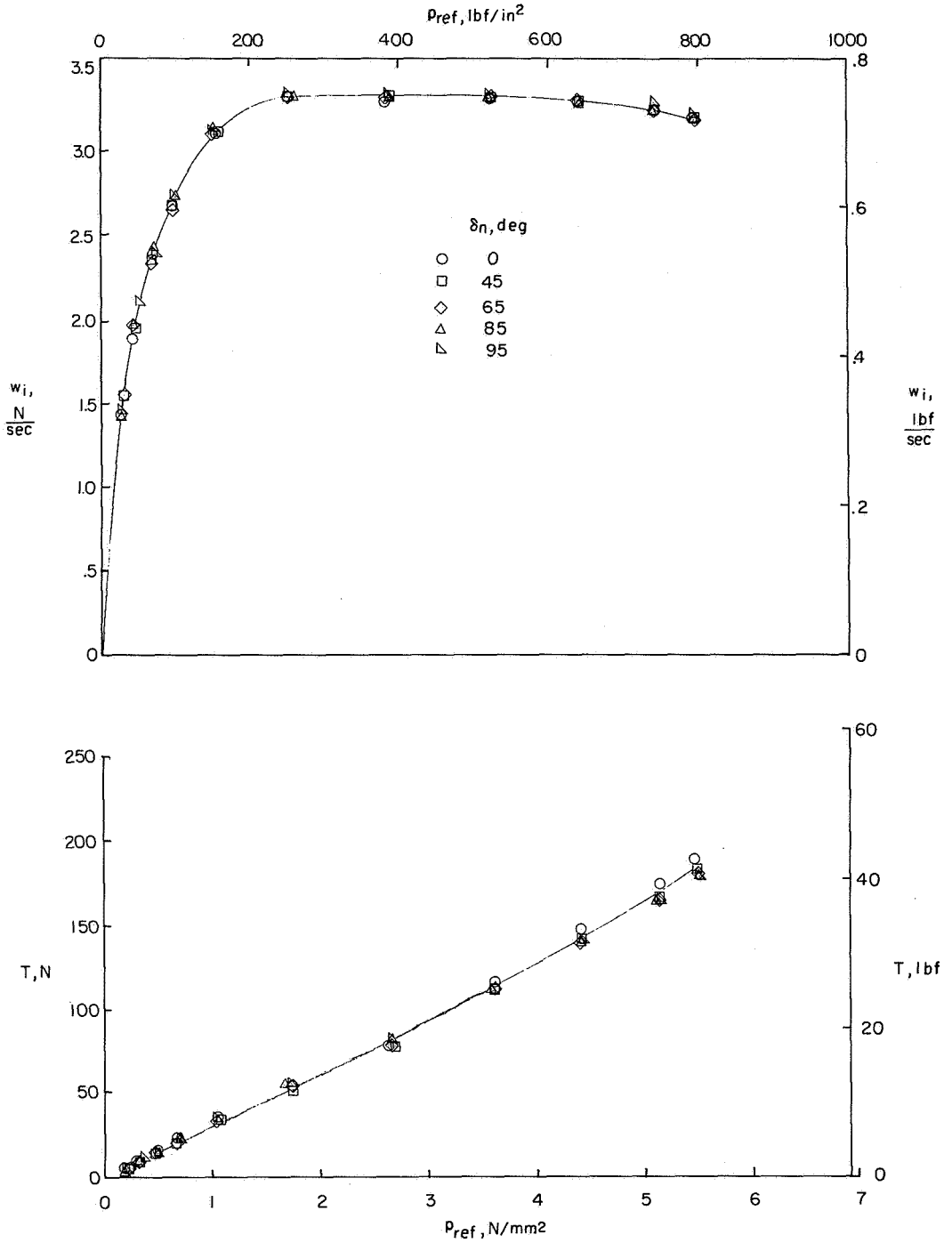

(d) Right rear.

Figure 3.- Concluded.

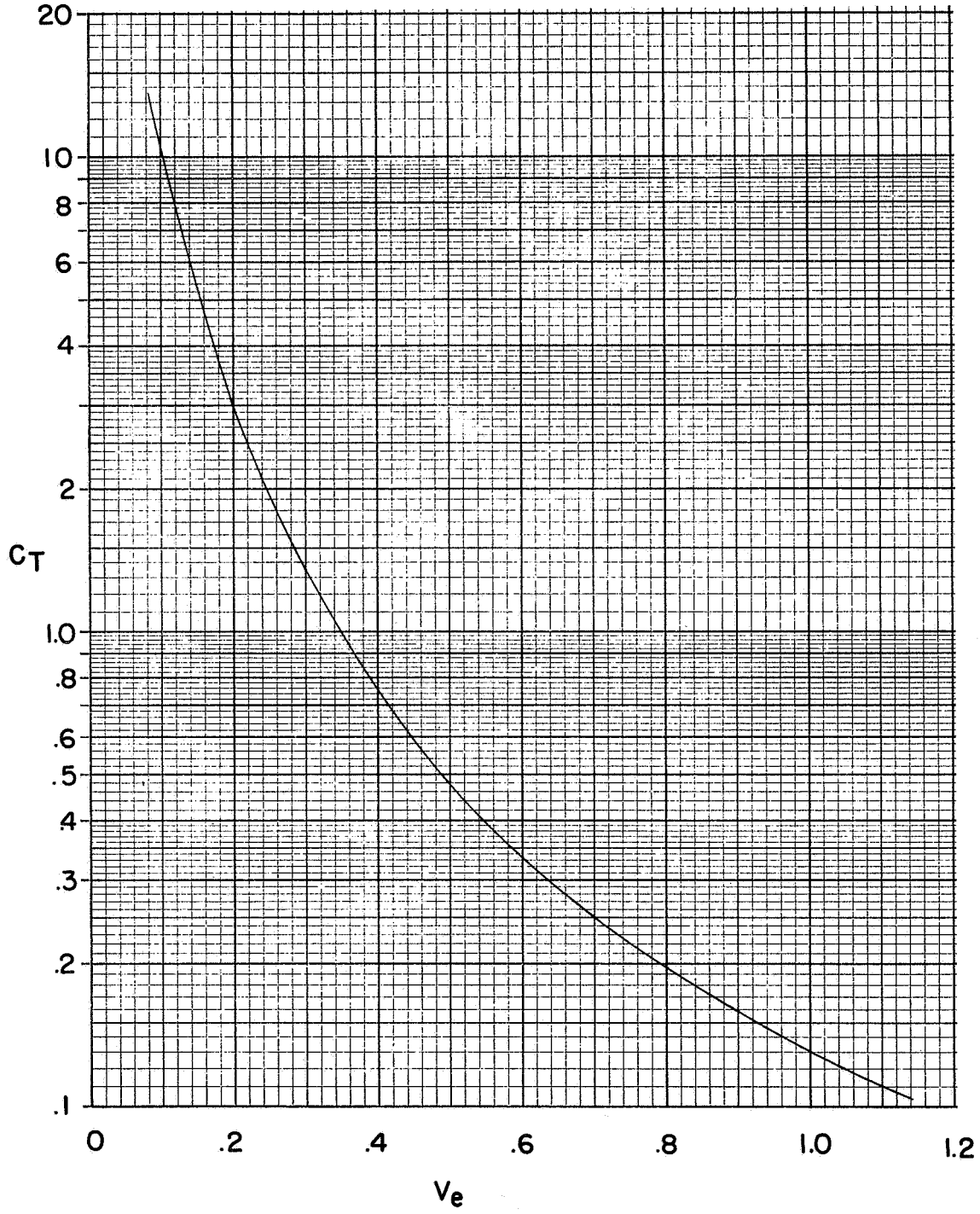

Figure 4.- Variation of thrust coefficient with effective-velocity ratio.

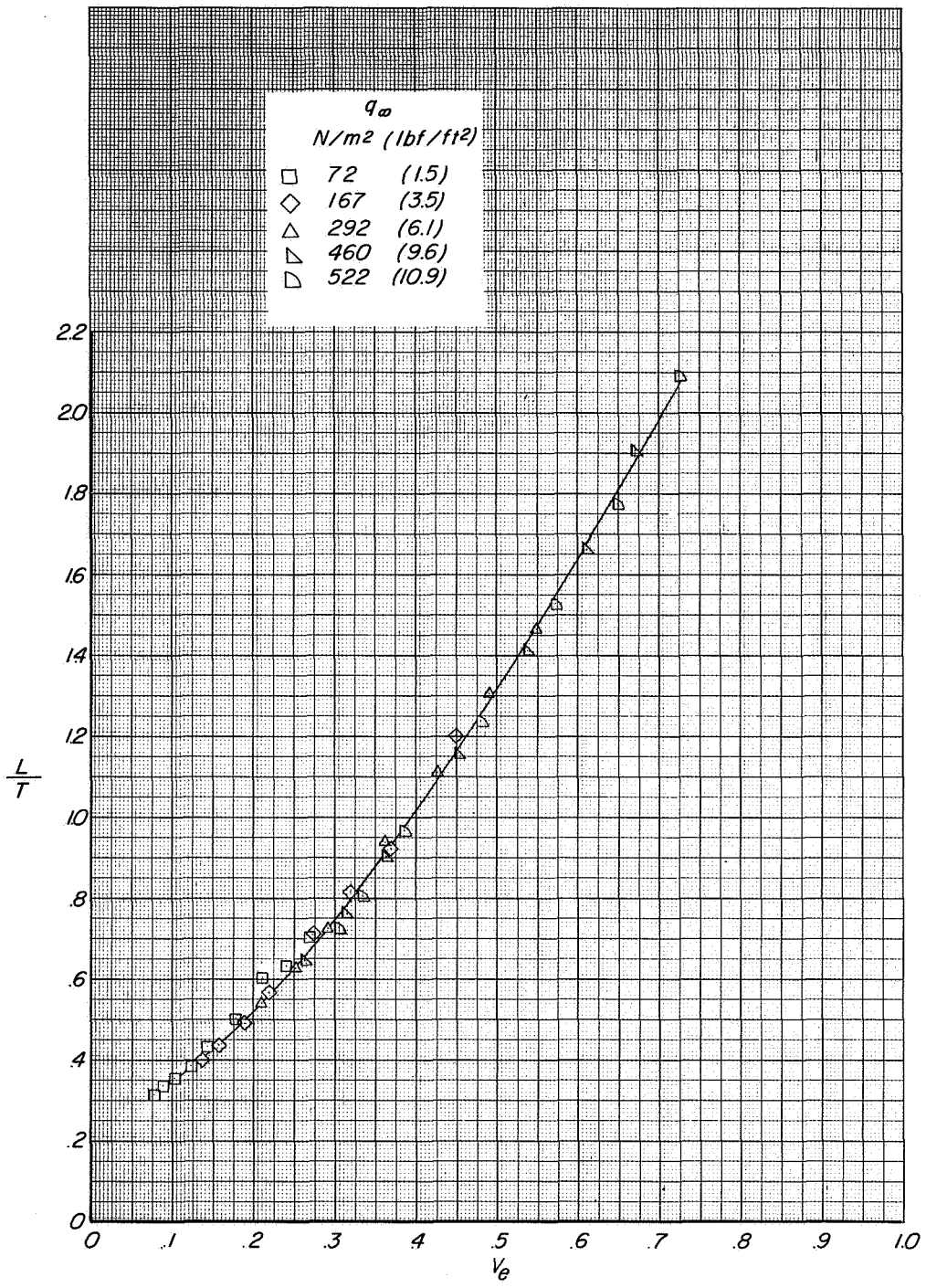

(a) $\delta_n = 0^o$.

Figure 5.- Force- and moment-thrust ratio variation with velocity ratio obtained by various combinations of thrust and tunnel dynamic pressures.

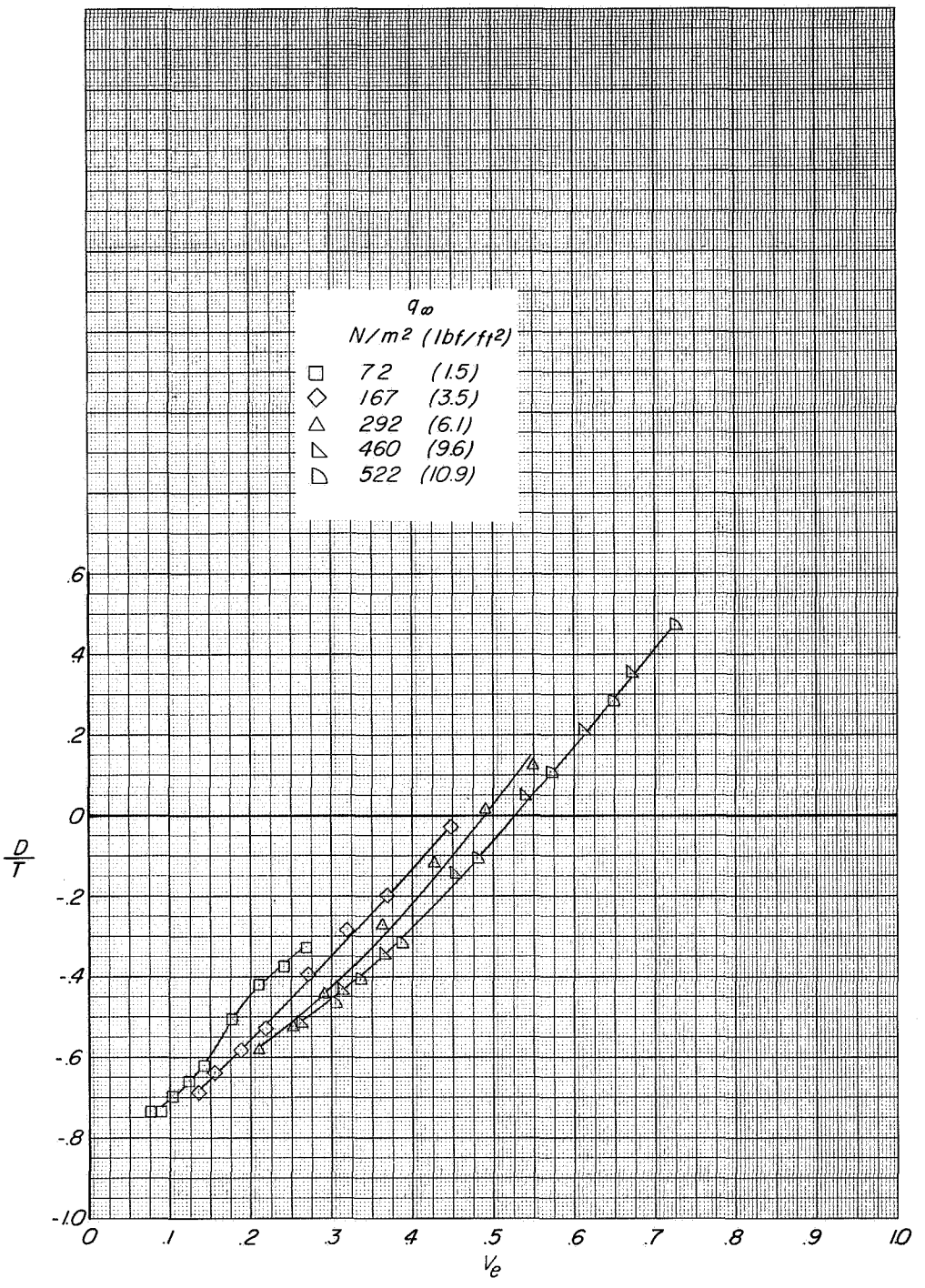

(a) Continued.

Figure 5.- Continued.

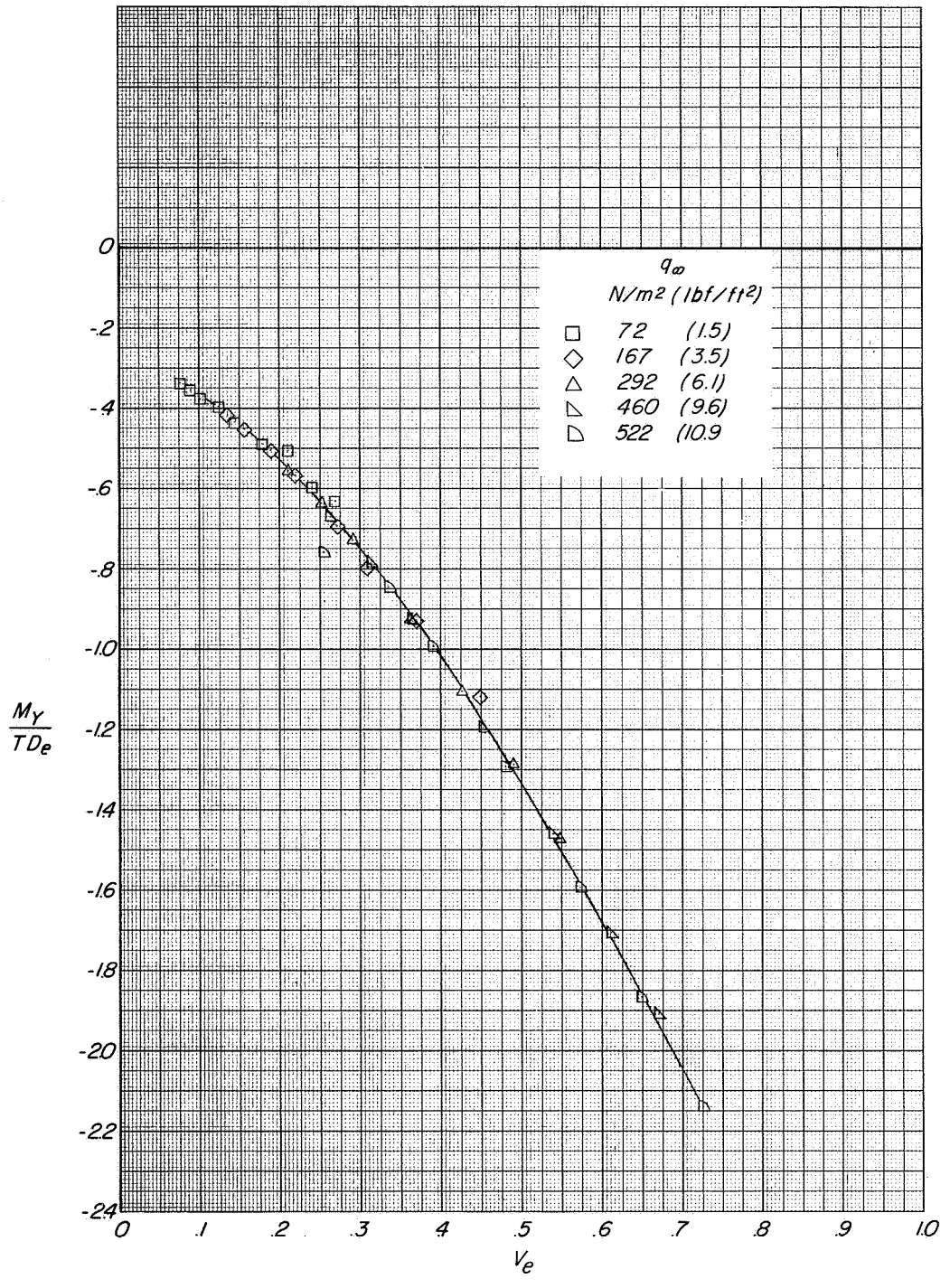

(a) Concluded.

Figure 5.- Continued.

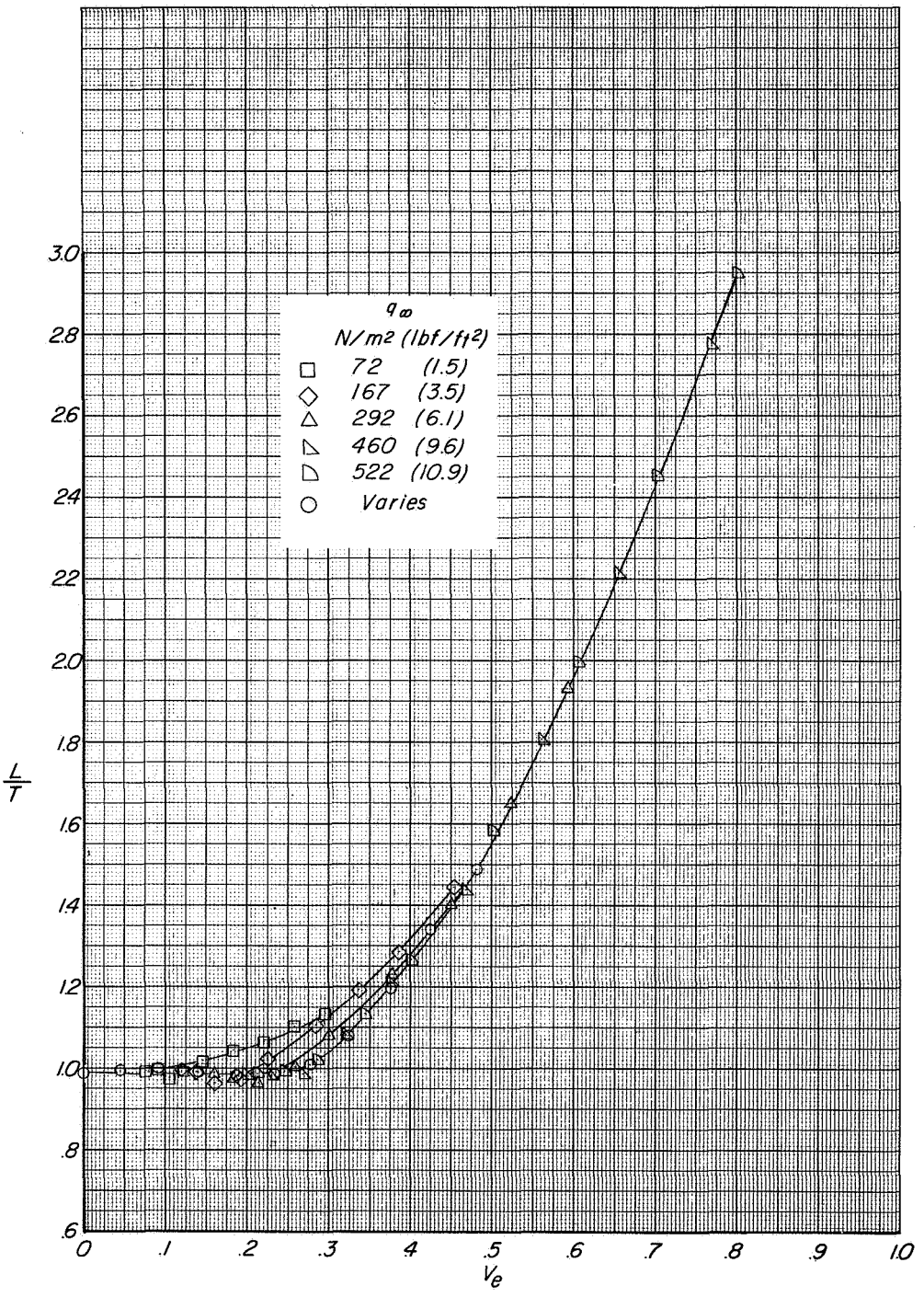

(b) $\delta_n = 85^o$.

Figure 5.- Continued.

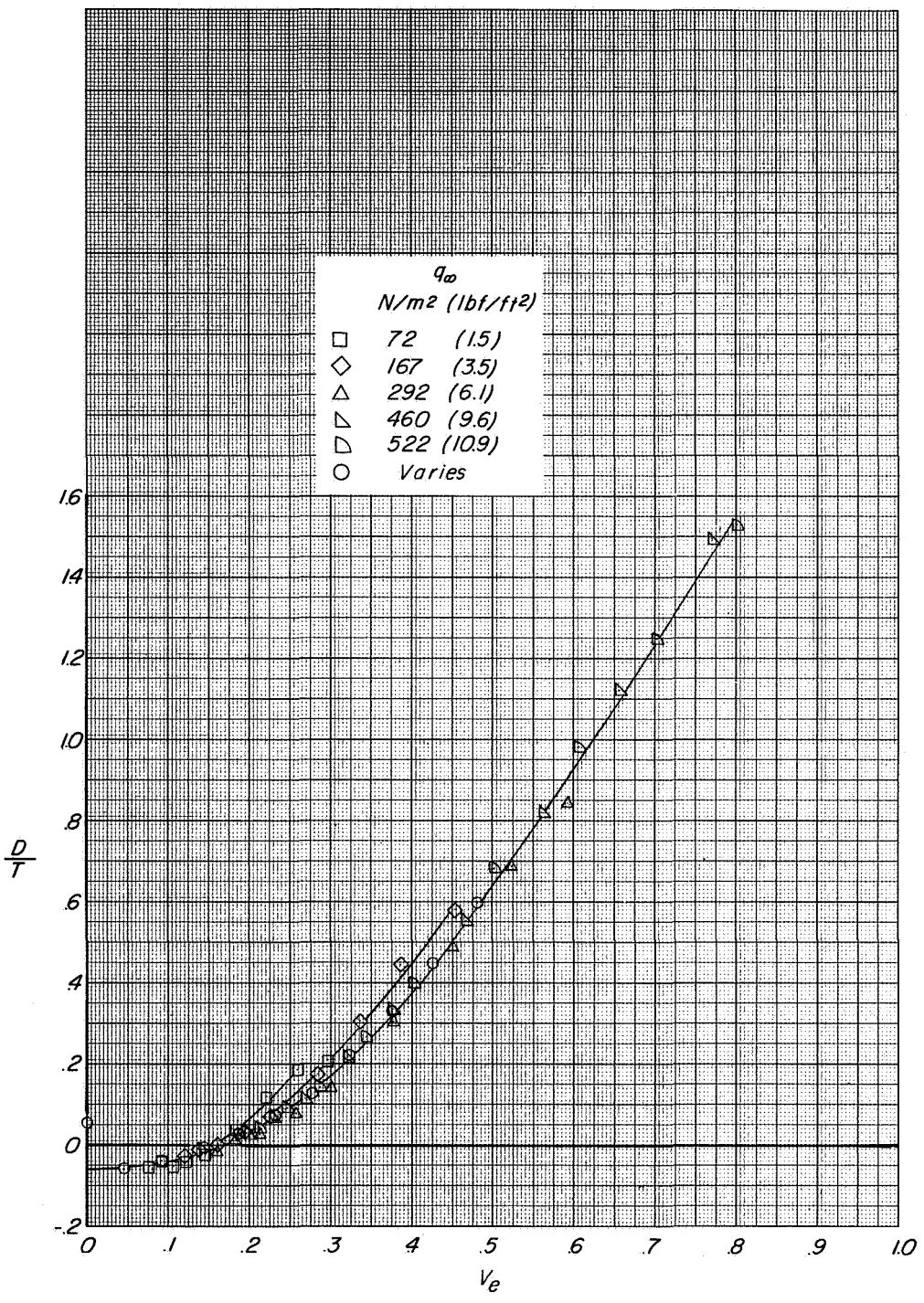

(b) Continued.

Figure 5.- Continued.

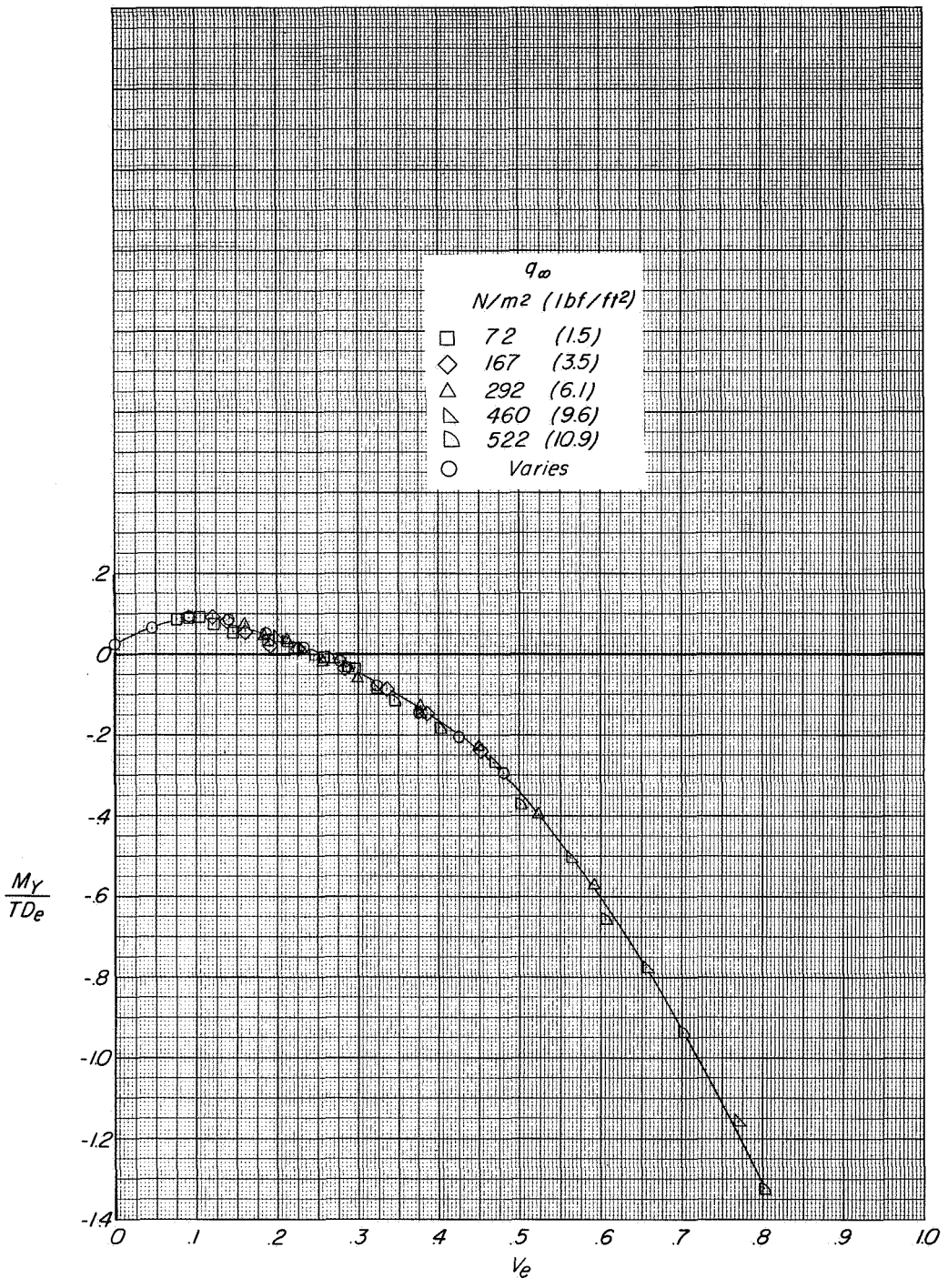

(b) Concluded.

Figure 5.- Concluded.

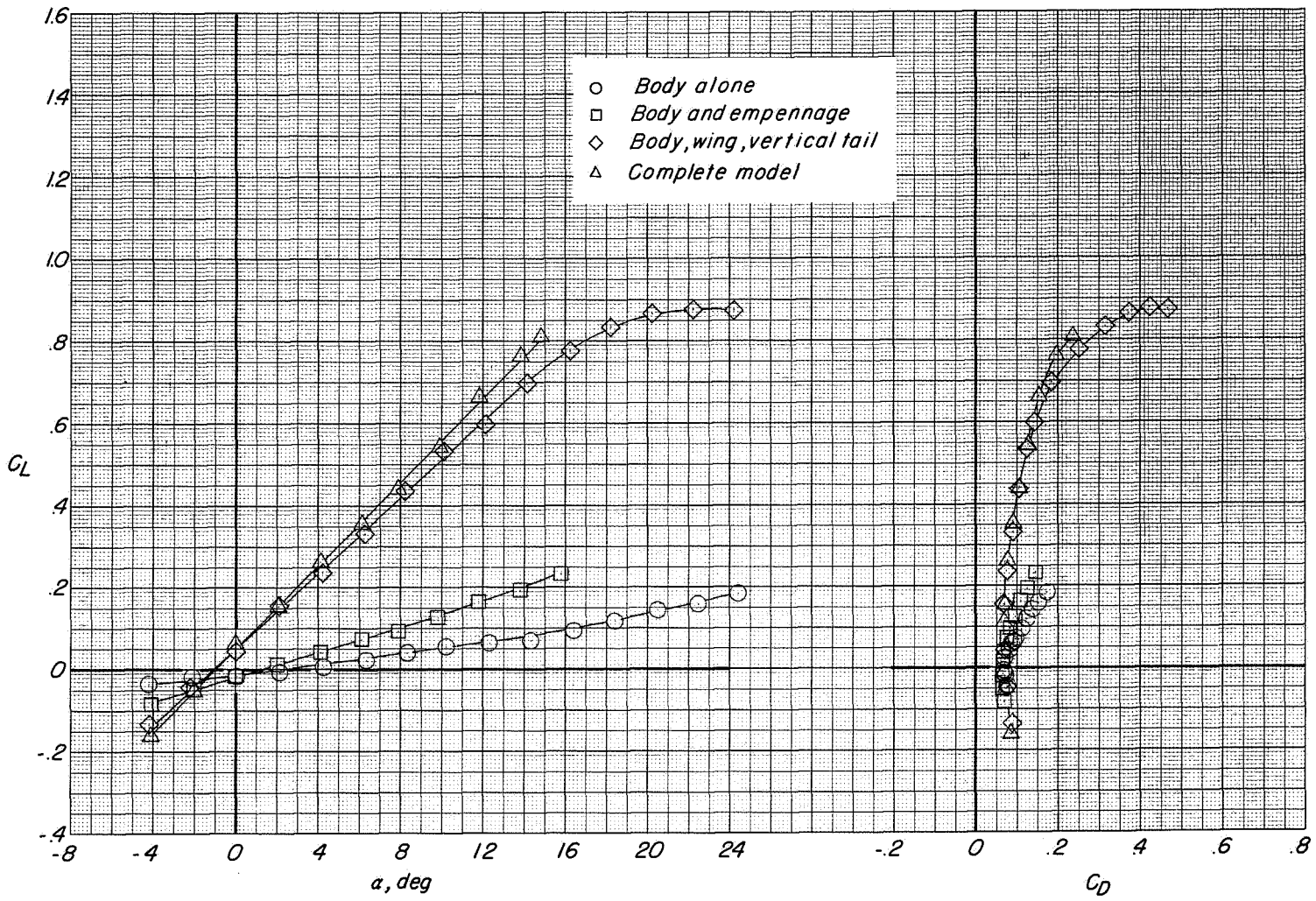

(a) Variation of C_L with α and C_D.

Figure 6.- Longitudinal aerodynamic characteristics of model showing contributions of major components. Power off; $\delta_f = 0^o$; $i_t = 0^o$ when tail is on model.

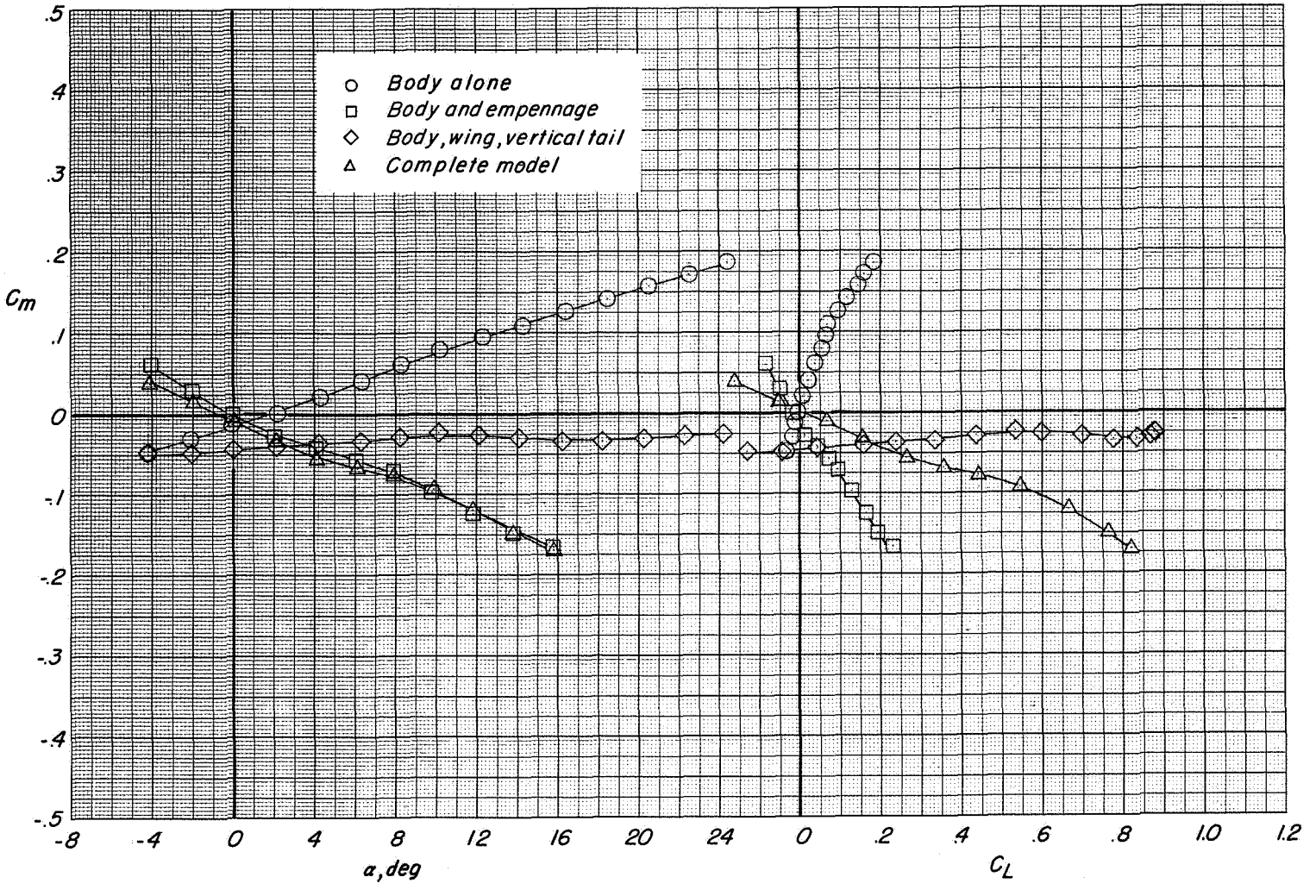

(b) Variation of C_m with α and C_L.

Figure 6.- Concluded.

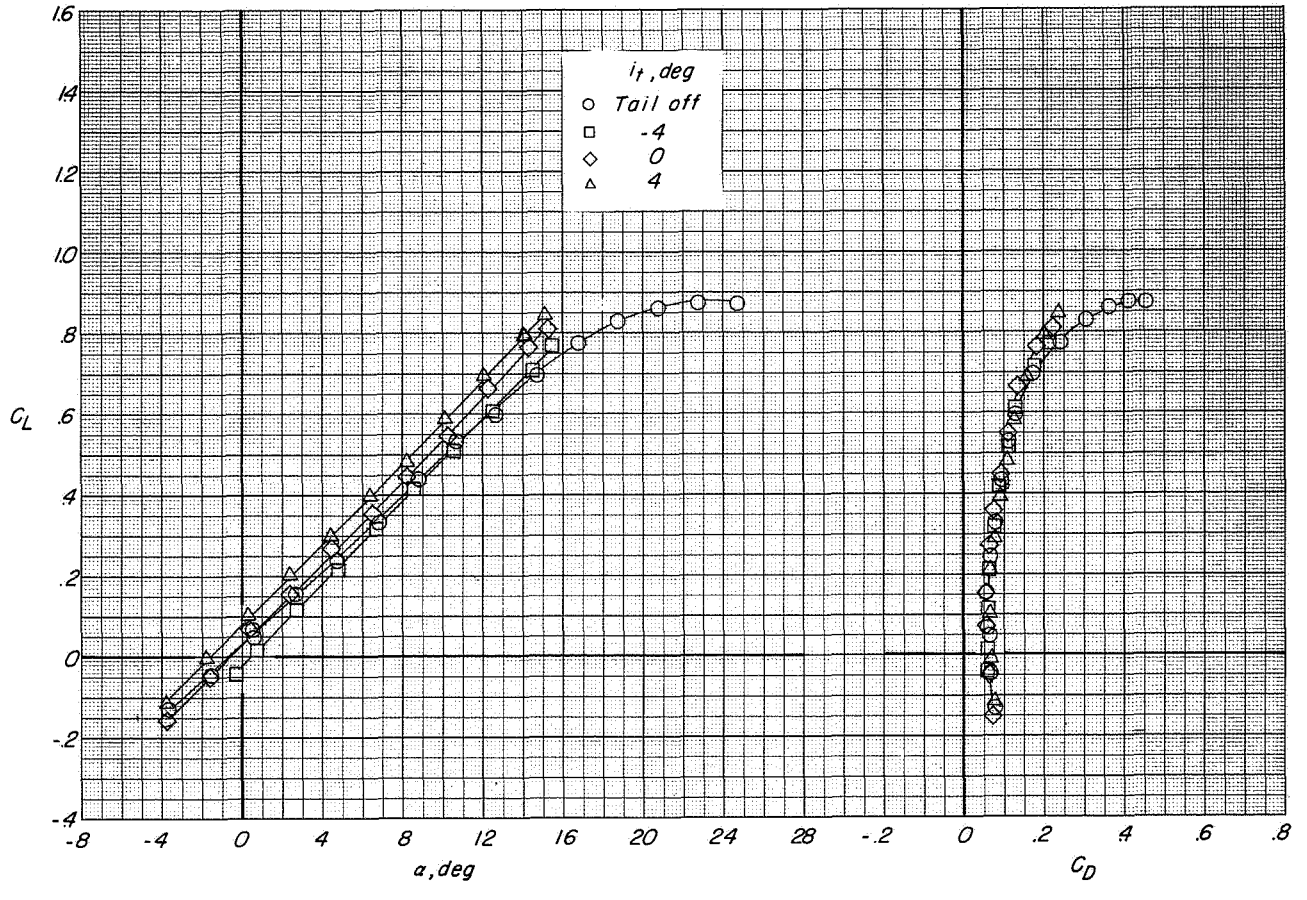

(a) $C_T = 0$.

Figure 7.- Longitudinal aerodynamic characteristics of cruise configuration showing effect of horizontal-tail incidence. $\delta_n = 0^o$; $\delta_f = 0^o$; landing gear up.

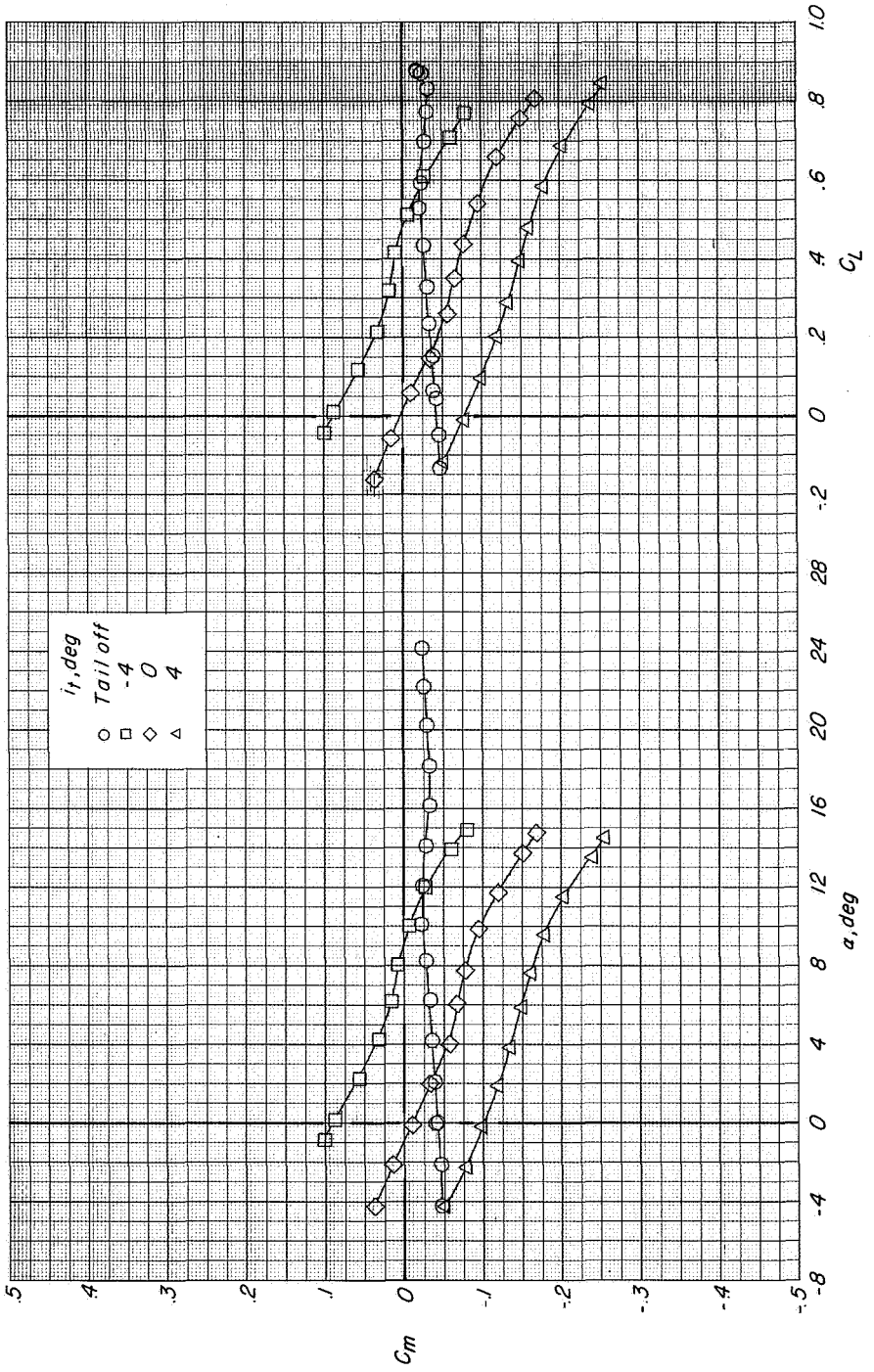

(a) Concluded.

Figure 7.- Continued.

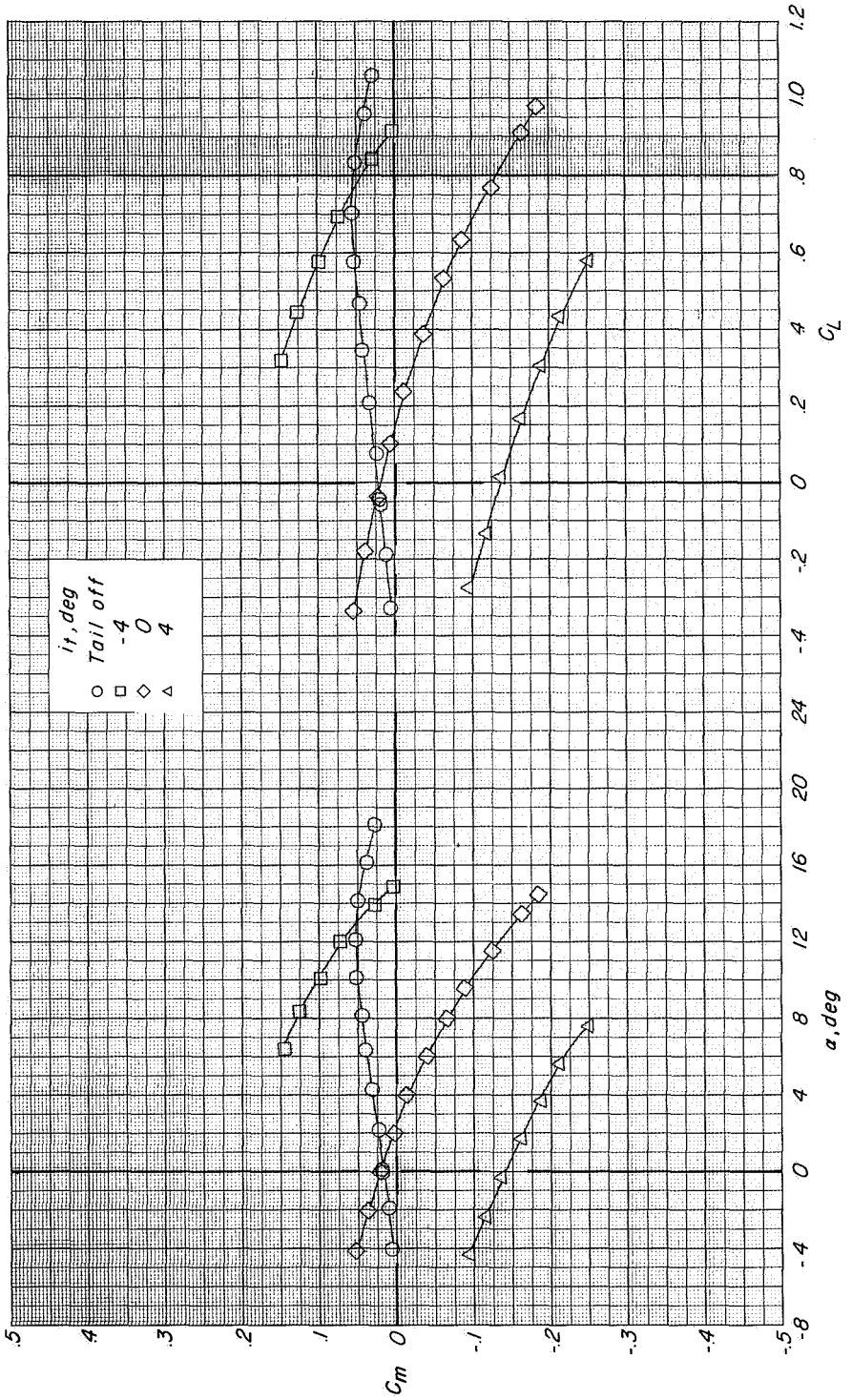

(b) $C_T = 0.6$.

Figure 7.- Continued.

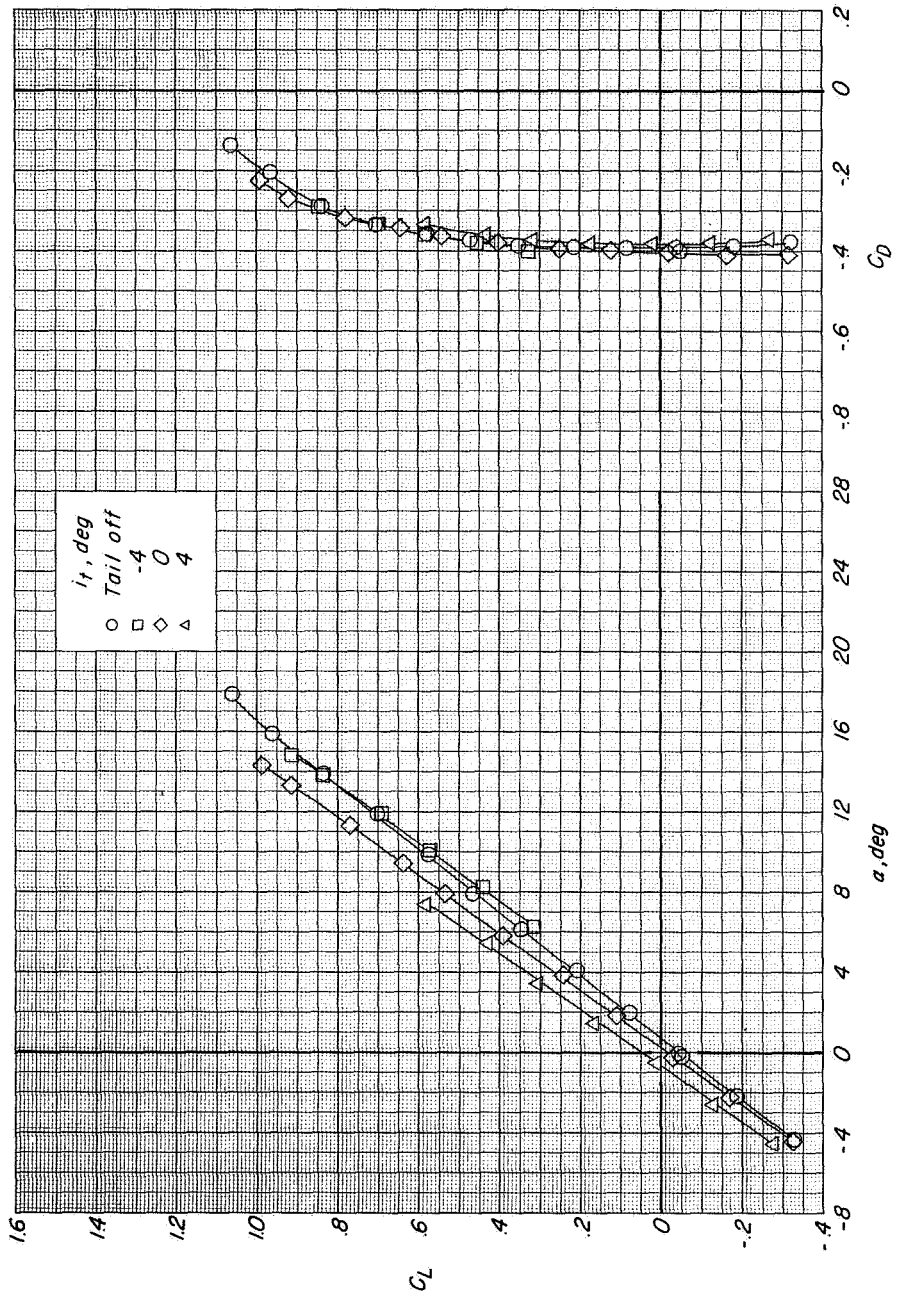

(b) Concluded.

Figure 7.- Continued.

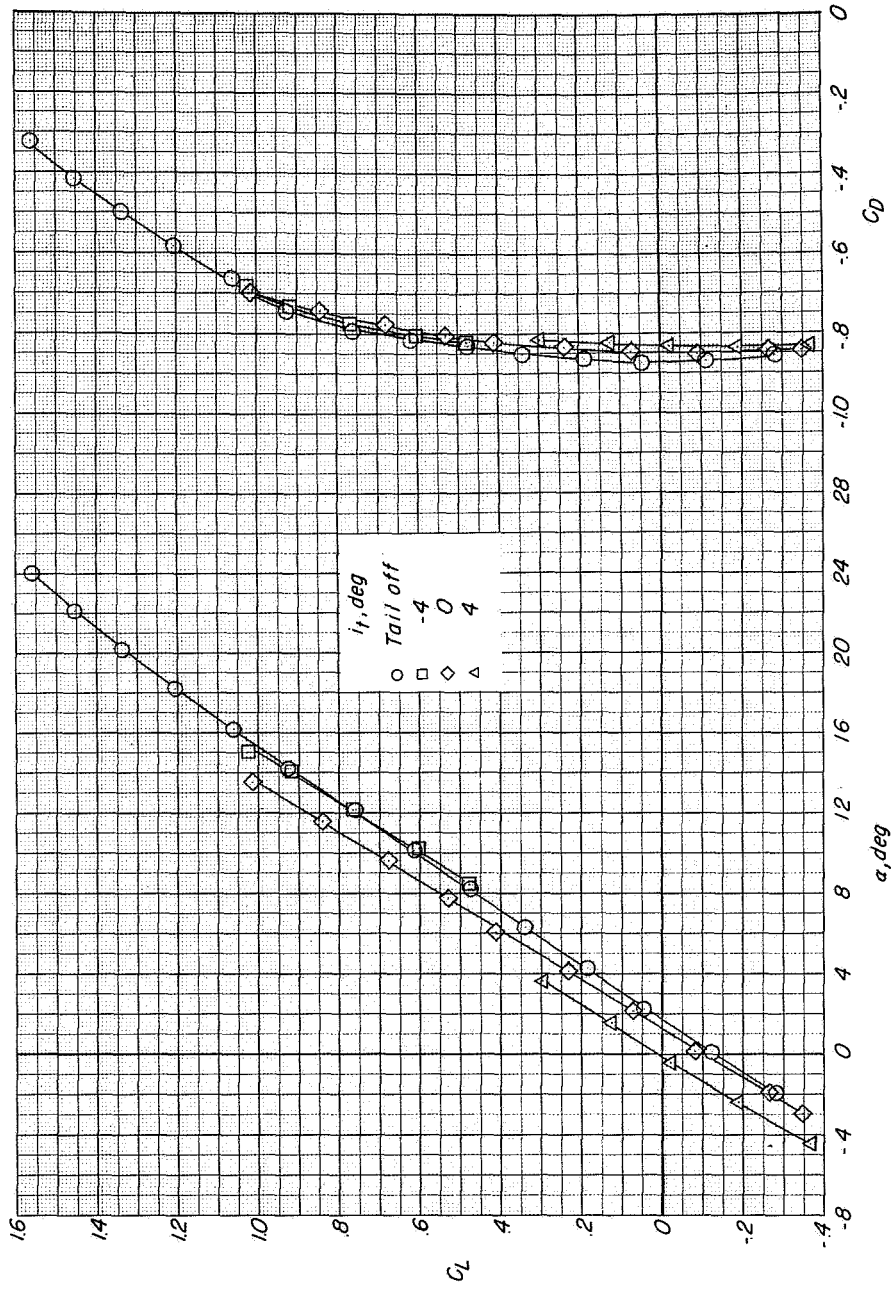

(c) $C_T = 1.1$.

Figure 7.- Continued.

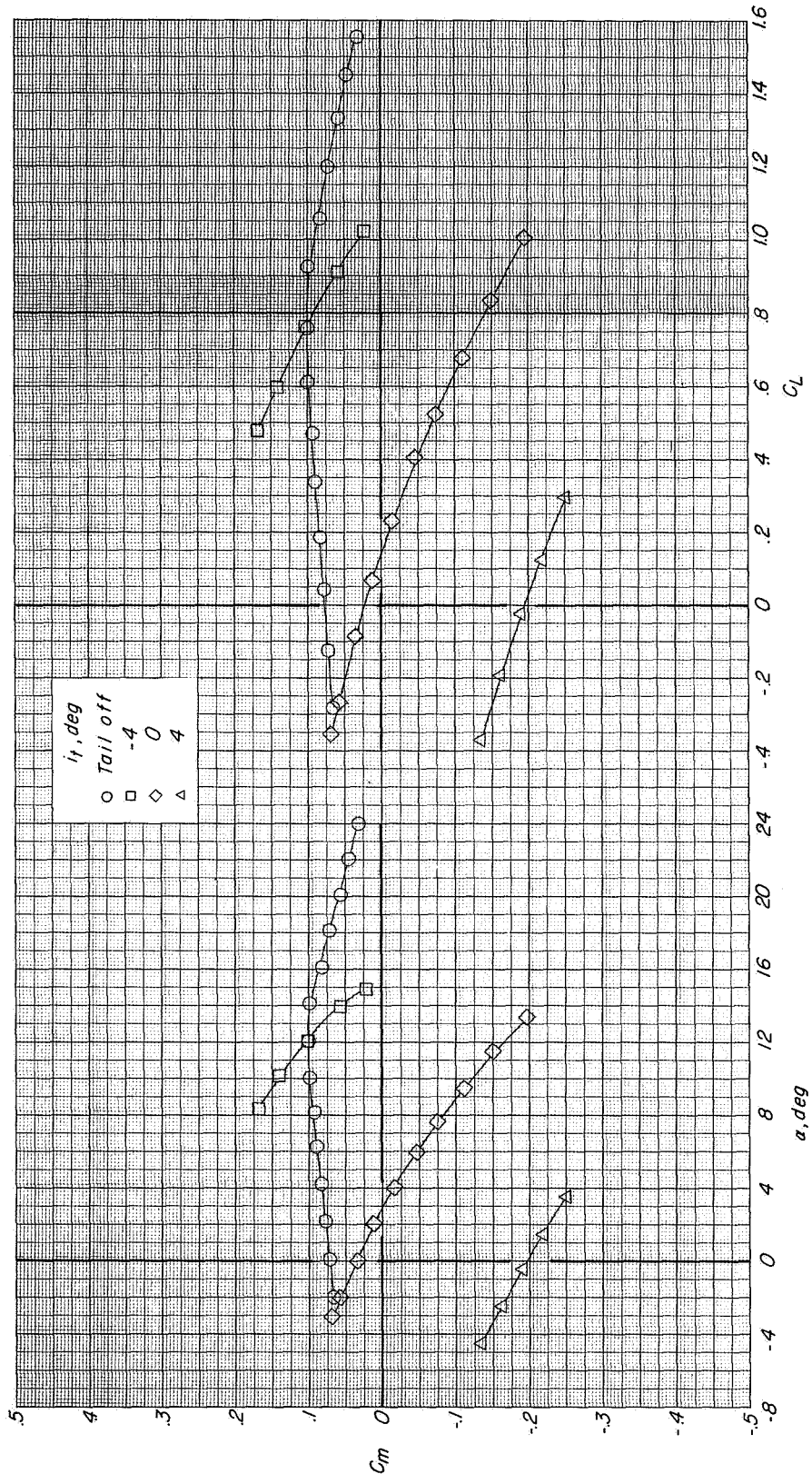

(c) Concluded.

Figure 7.- Concluded.

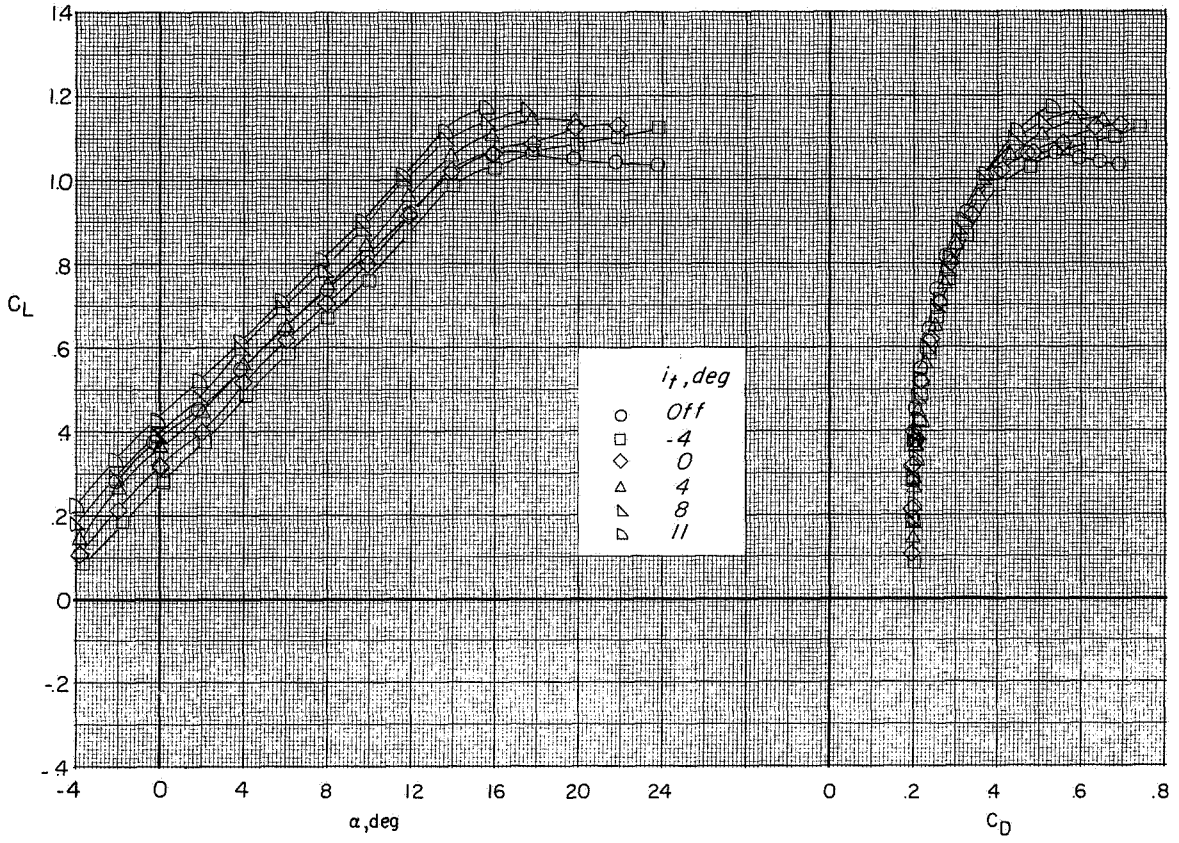

(a) $C_T = 0$.

Figure 8.- Longitudinal aerodynamic characteristics showing effect of horizontal-tail incidence. $\delta_n = 65^o$; $\delta_f = 60^o$.

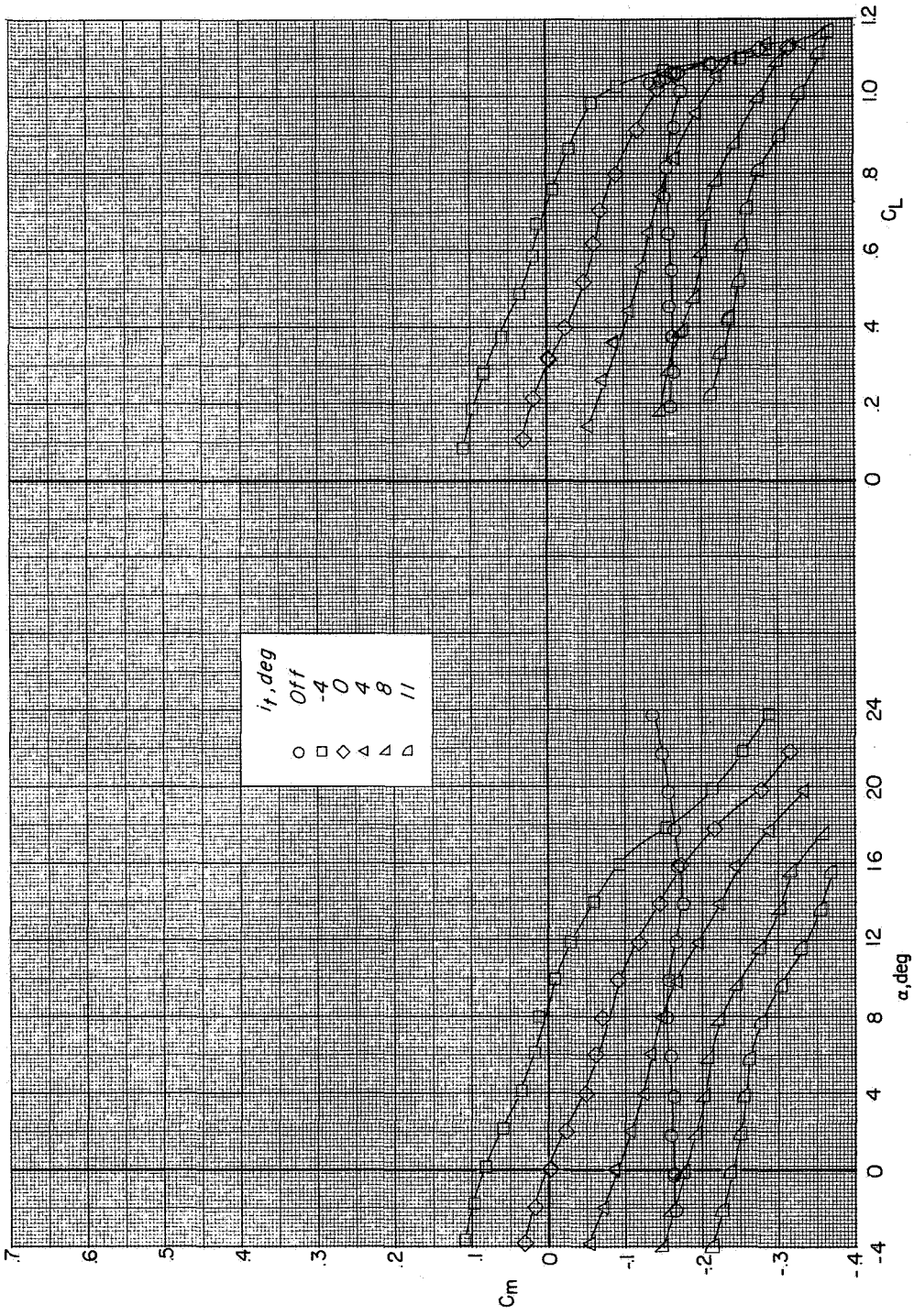

(a) Concluded.

Figure 8.- Continued.

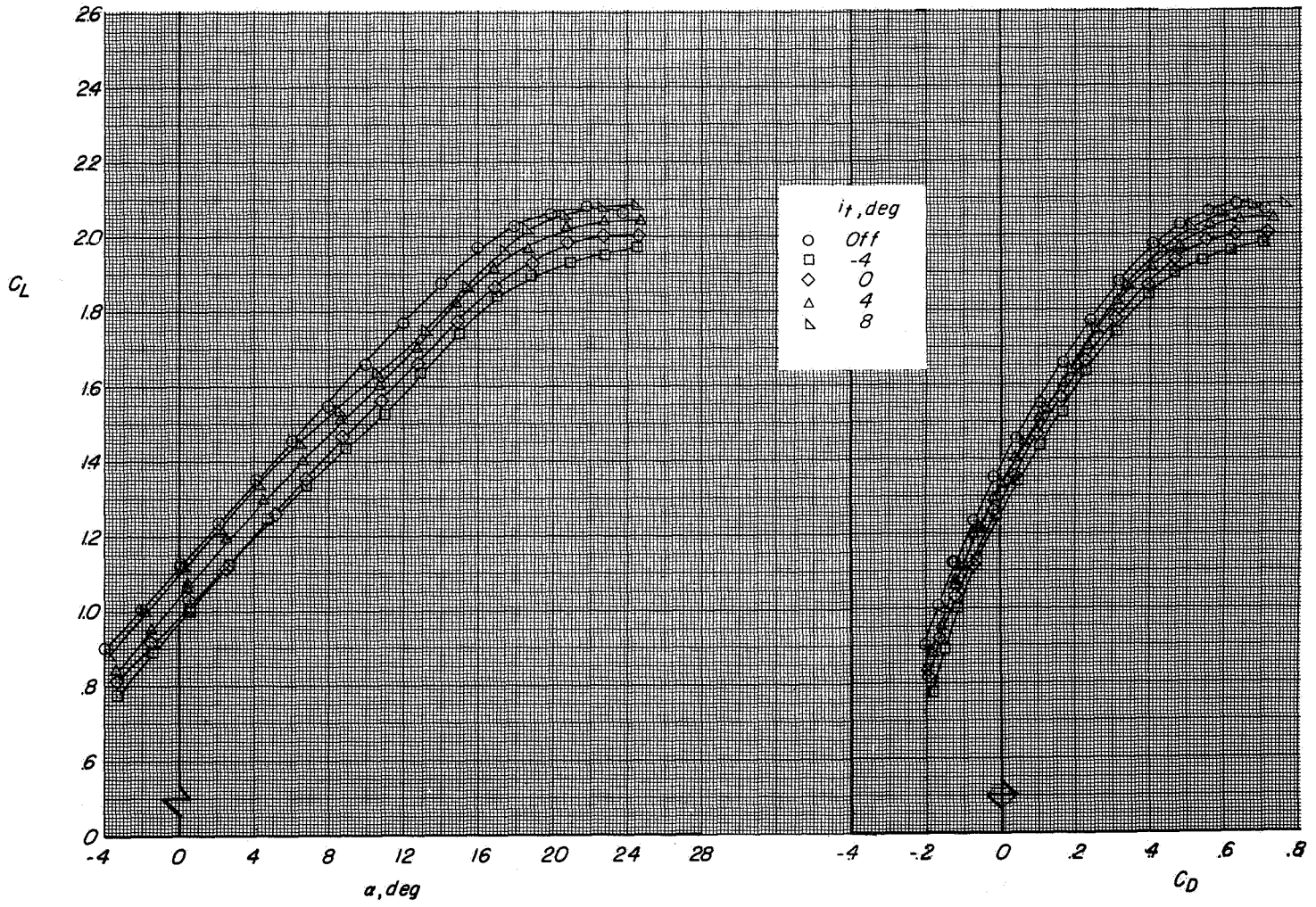

(b) $C_T = 1.1$.

Figure 8.- Continued.

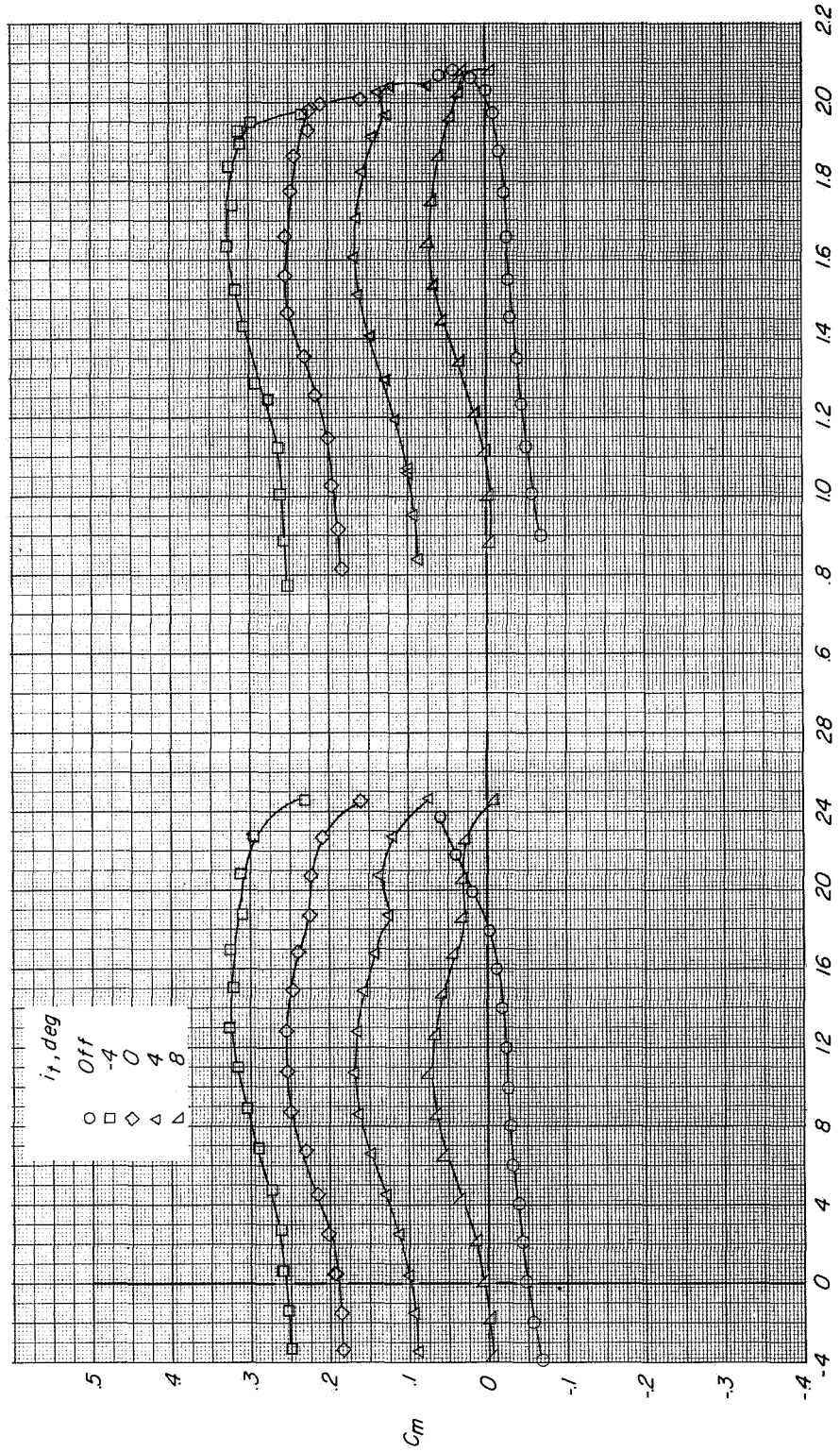

(b) Concluded.

Figure 8.- Continued.

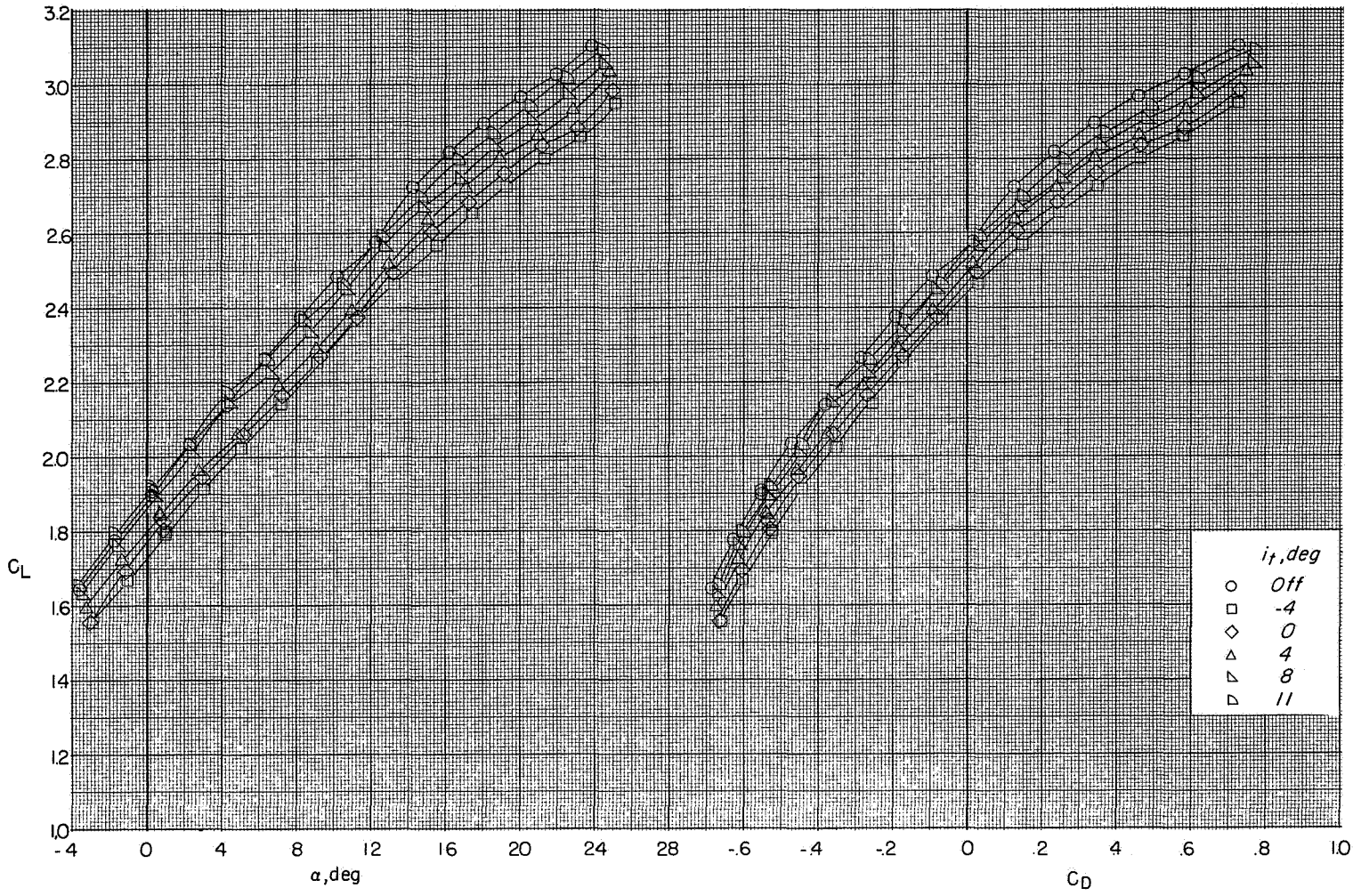

(c) $C_T = 2.0$.

Figure 8.- Continued.

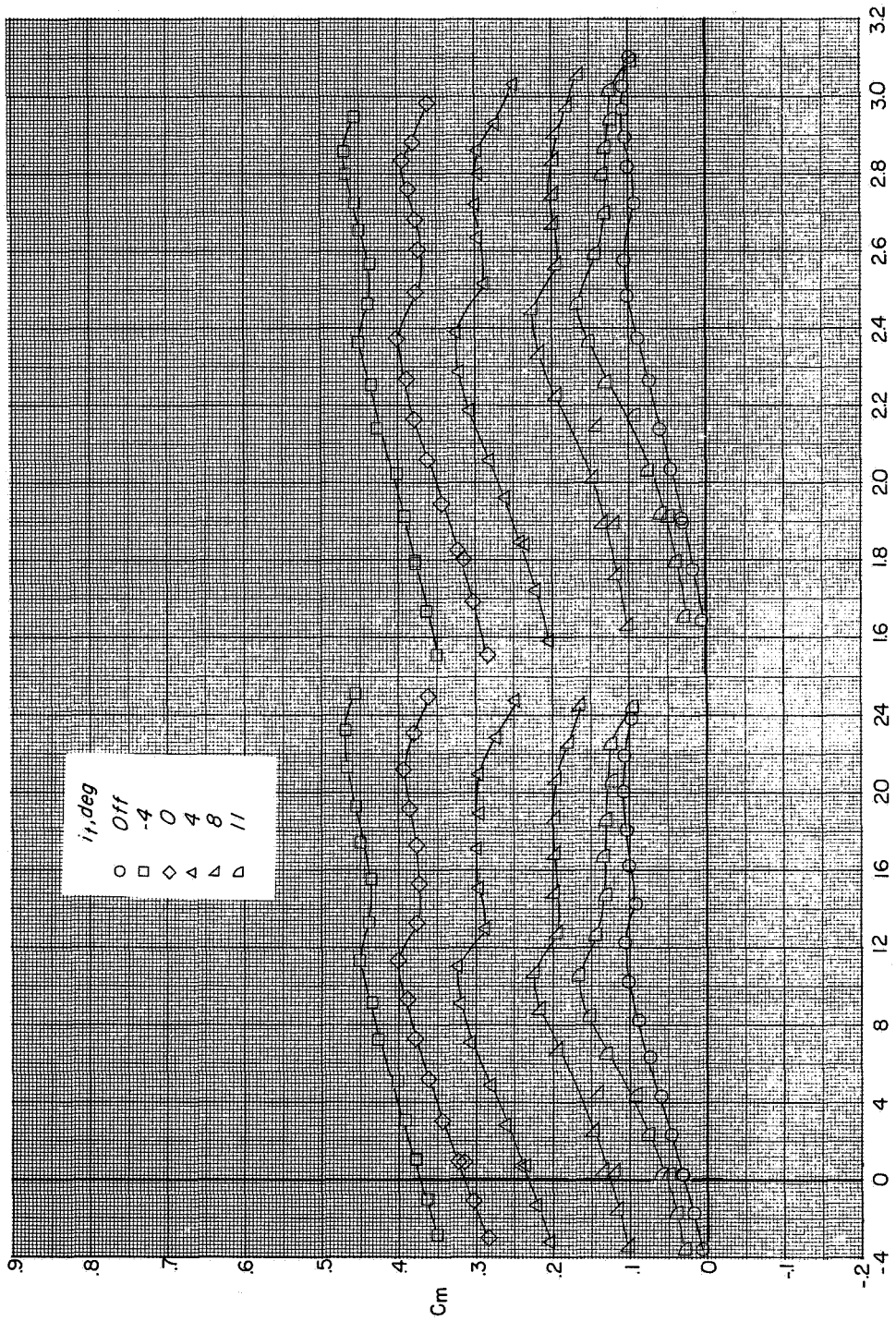

(c) Concluded.

Figure 8.- Continued.

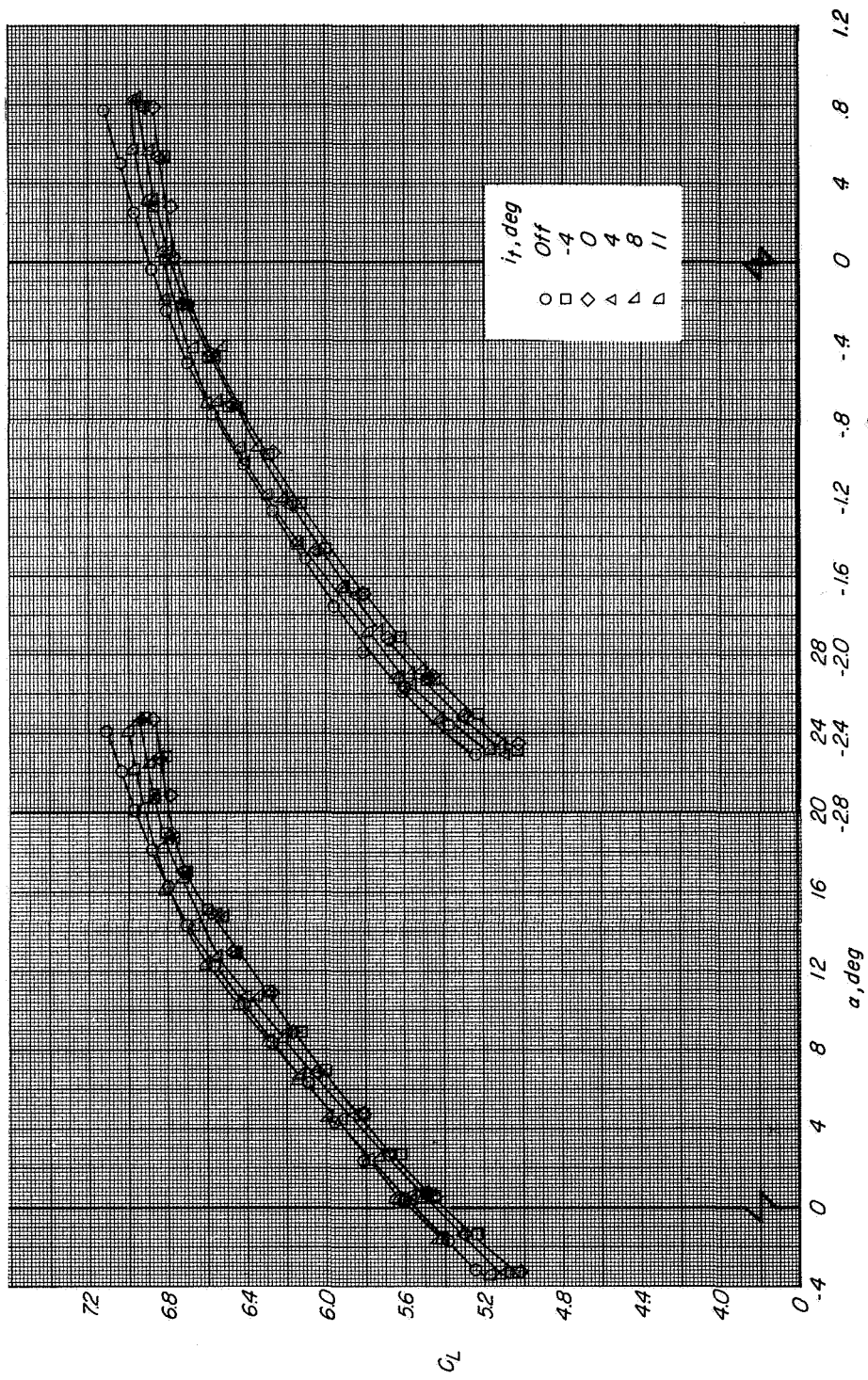

(d) $C_T = 6.0$.

Figure 8.- Continued.

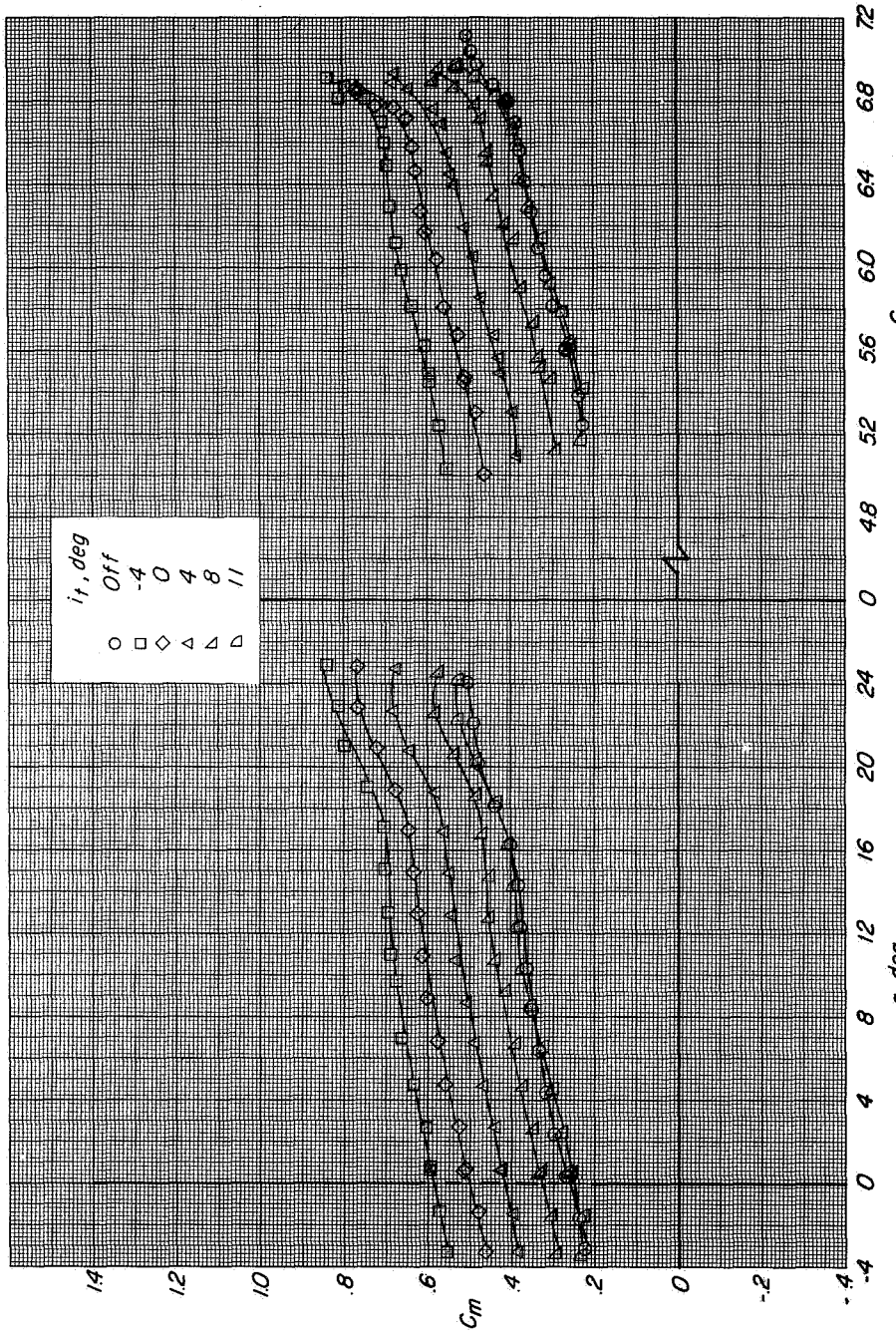

(d) Concluded.

Figure 8.- Concluded.

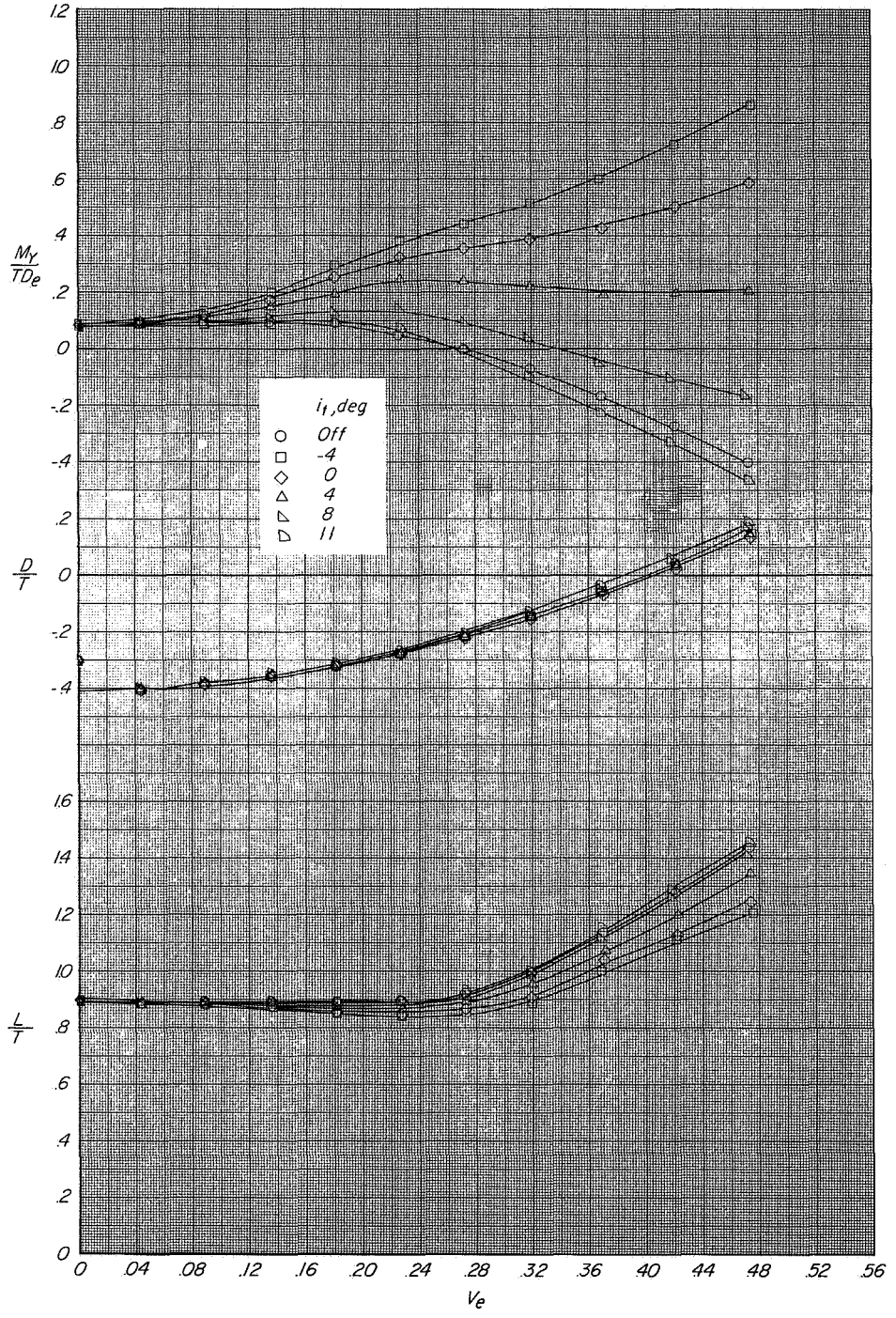

(a) Measured characteristics at $\alpha = 0^{o}$.

Figure 9.- Variation of longitudinal characteristics and interference increments with effective-velocity ratio showing effects of horizontal-tail incidence. $\delta_n = 65^{o}$; $\delta_f = 60^{o}$.

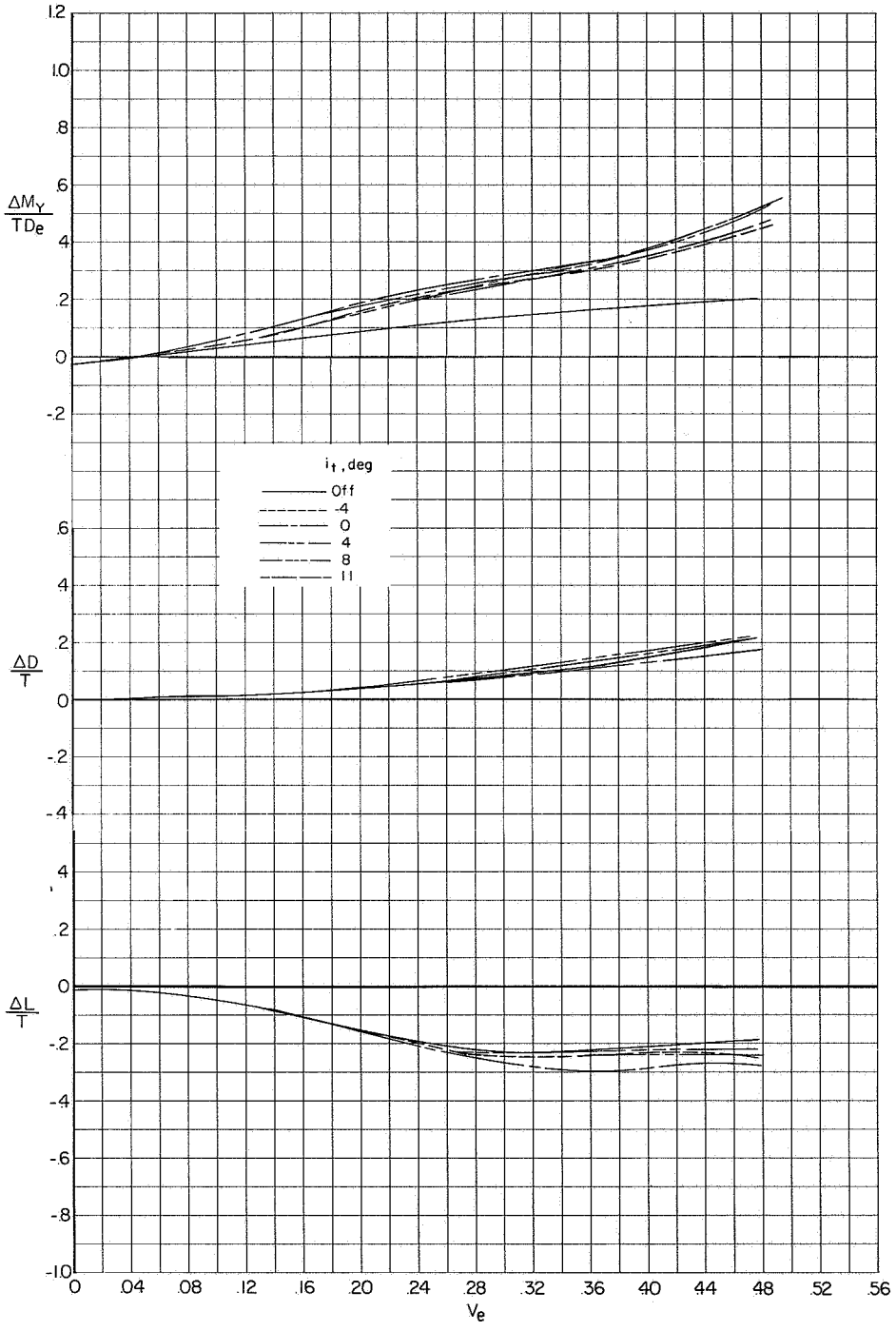

(b) Interference increments at $\alpha = 0^{o}$.

Figure 9.- Continued.

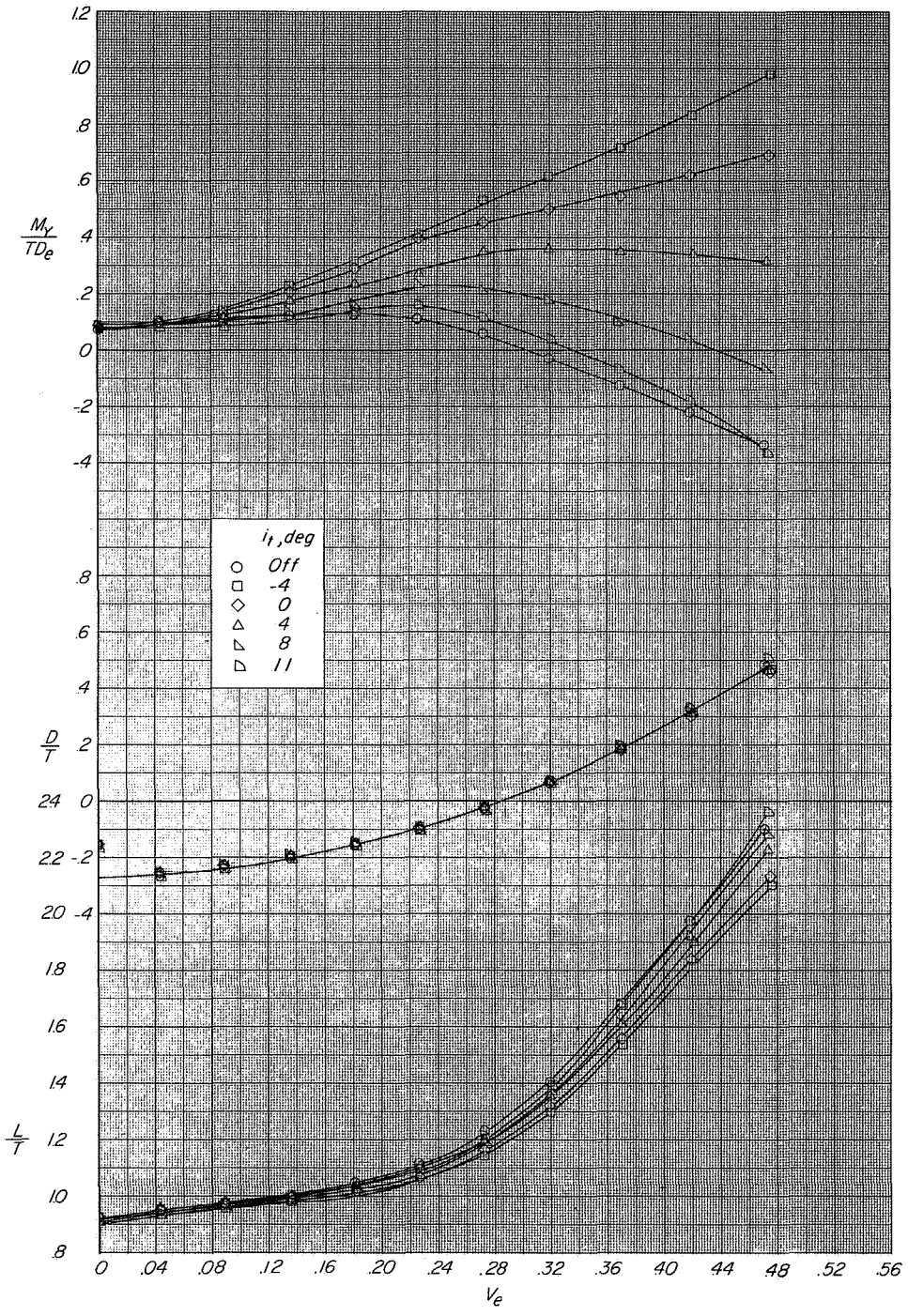

(c) Measured characteristics at $\alpha = 9^{\circ}$.

Figure 9.- Continued.

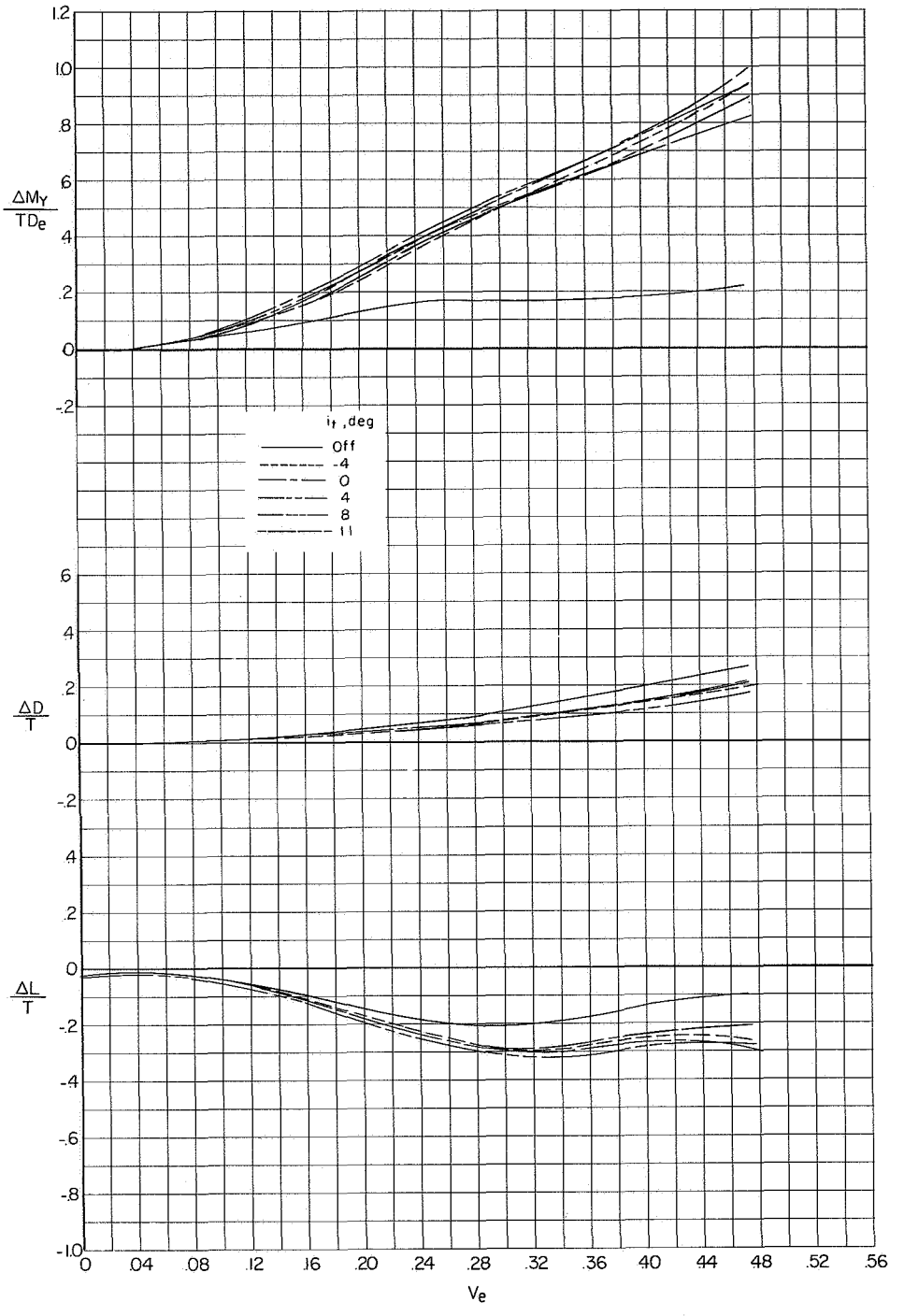

(d) Interference increments at $\alpha = 9^{o}$.

Figure 9.- Concluded.

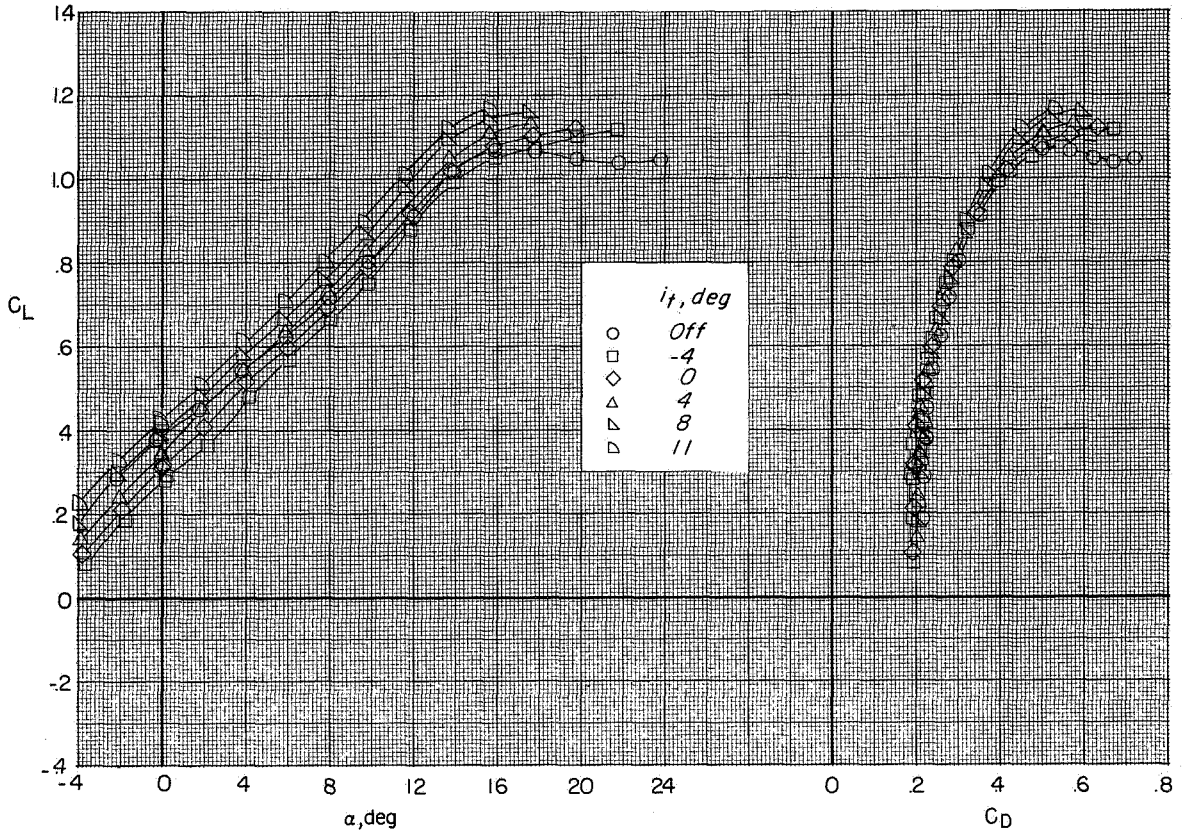

(a) $C_T = 0$.

Figure 10.- Longitudinal aerodynamic characteristics showing effect of horizontal-tail incidence. $\delta_n = 85^o$; $\delta_f = 60^o$.

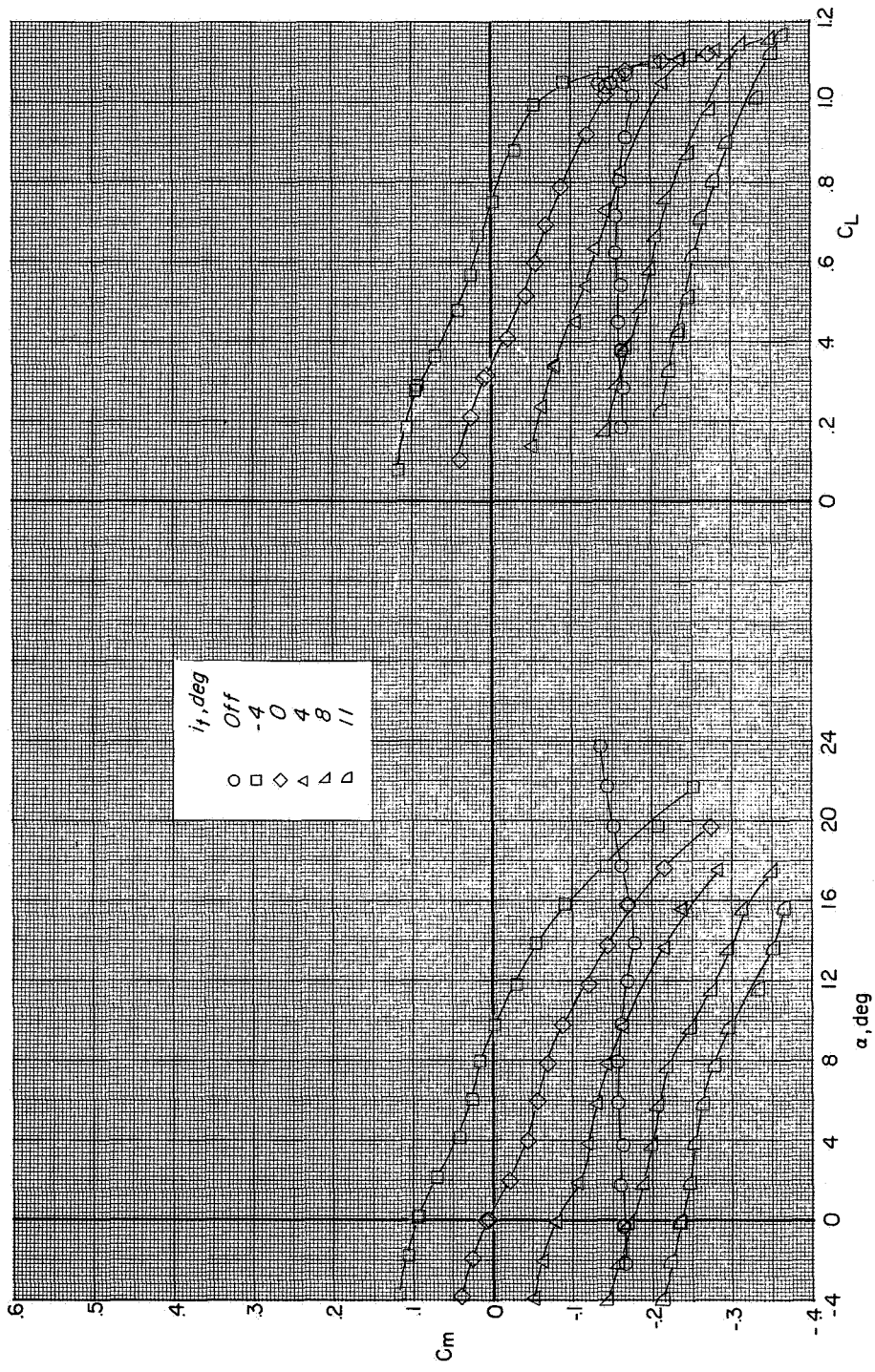

(a) Concluded.

Figure 10.- Continued.

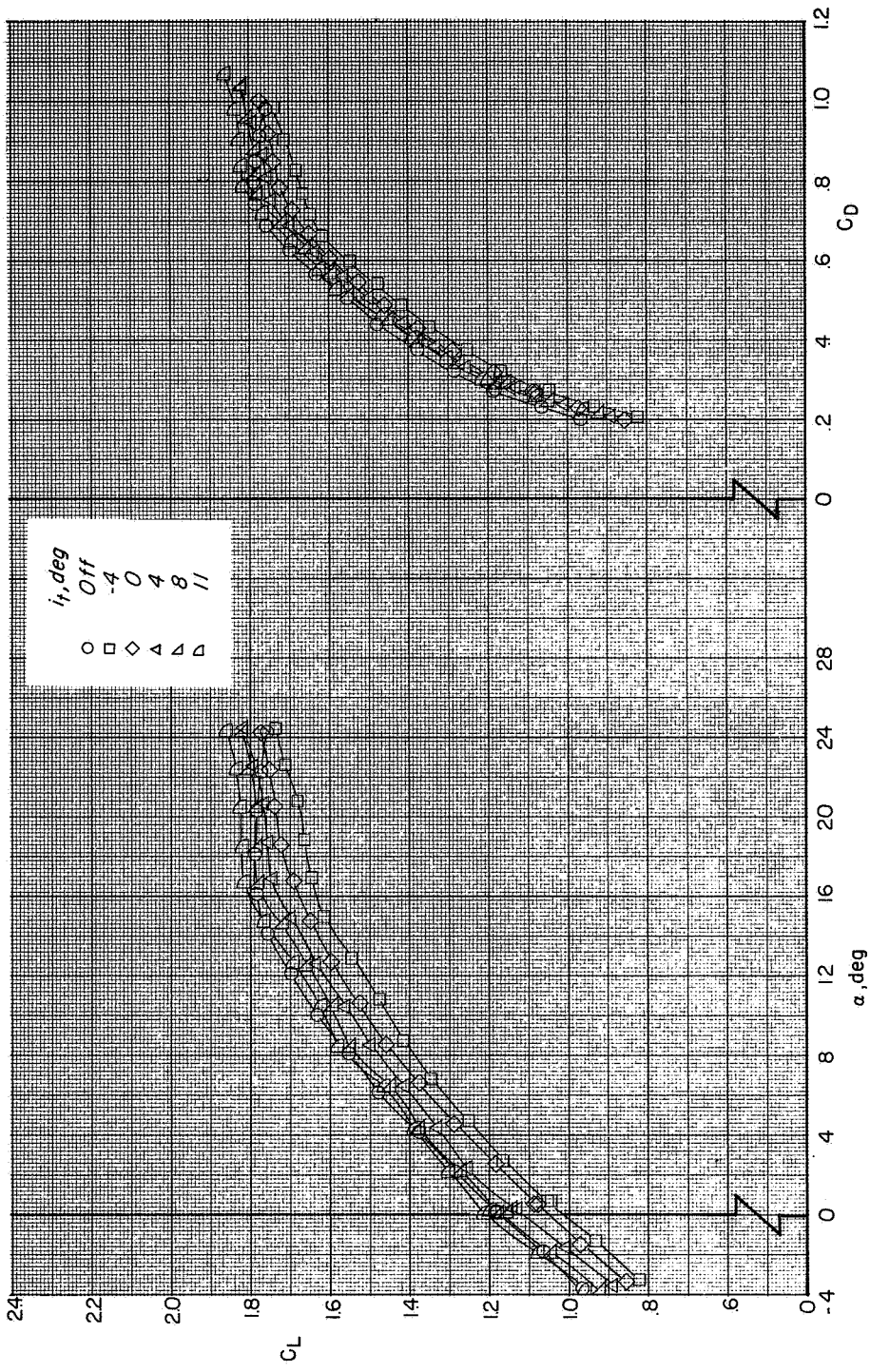

(b) $C_T = 1.1$.

Figure 10.- Continued.

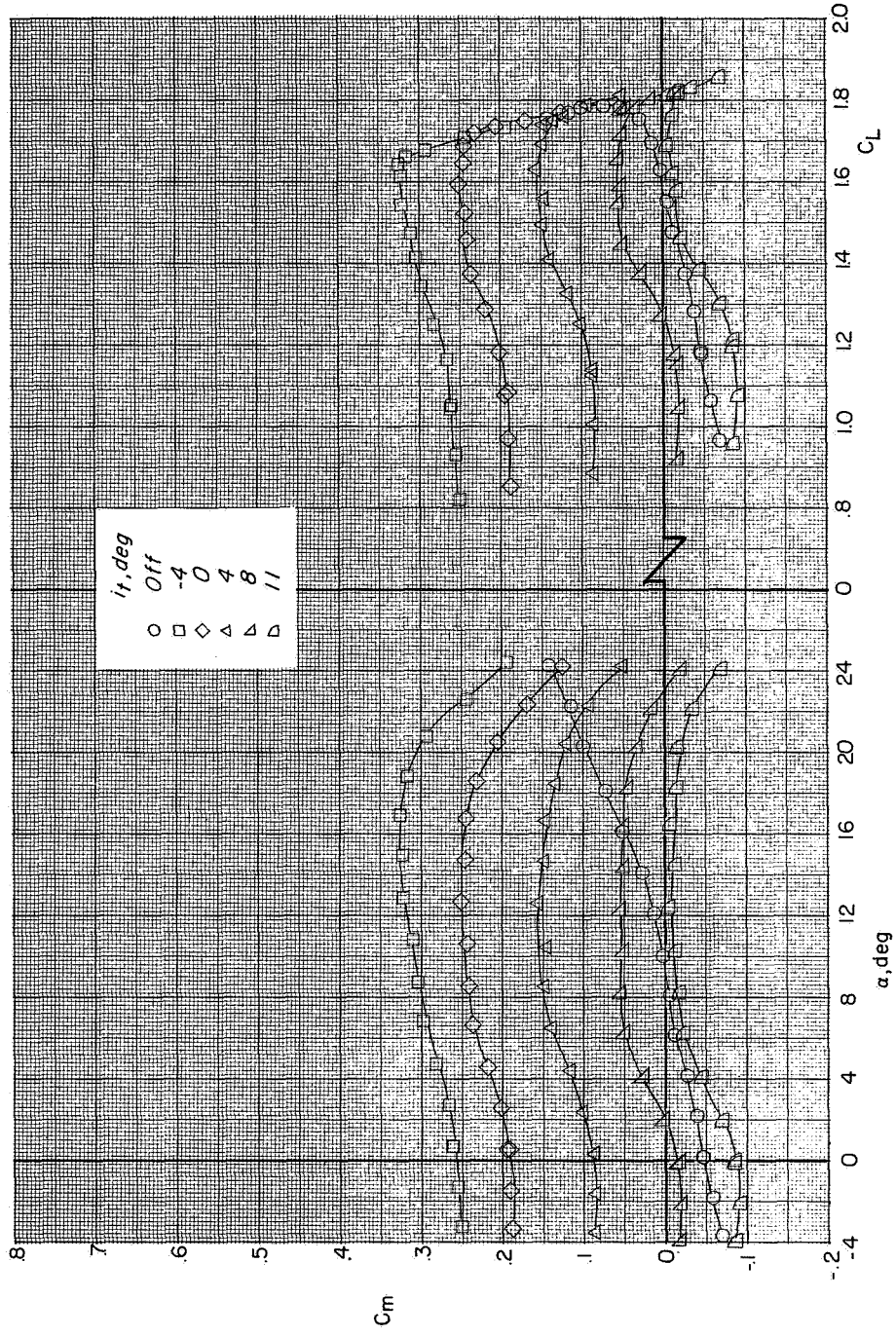

(b) Concluded.

Figure 10.- Continued.

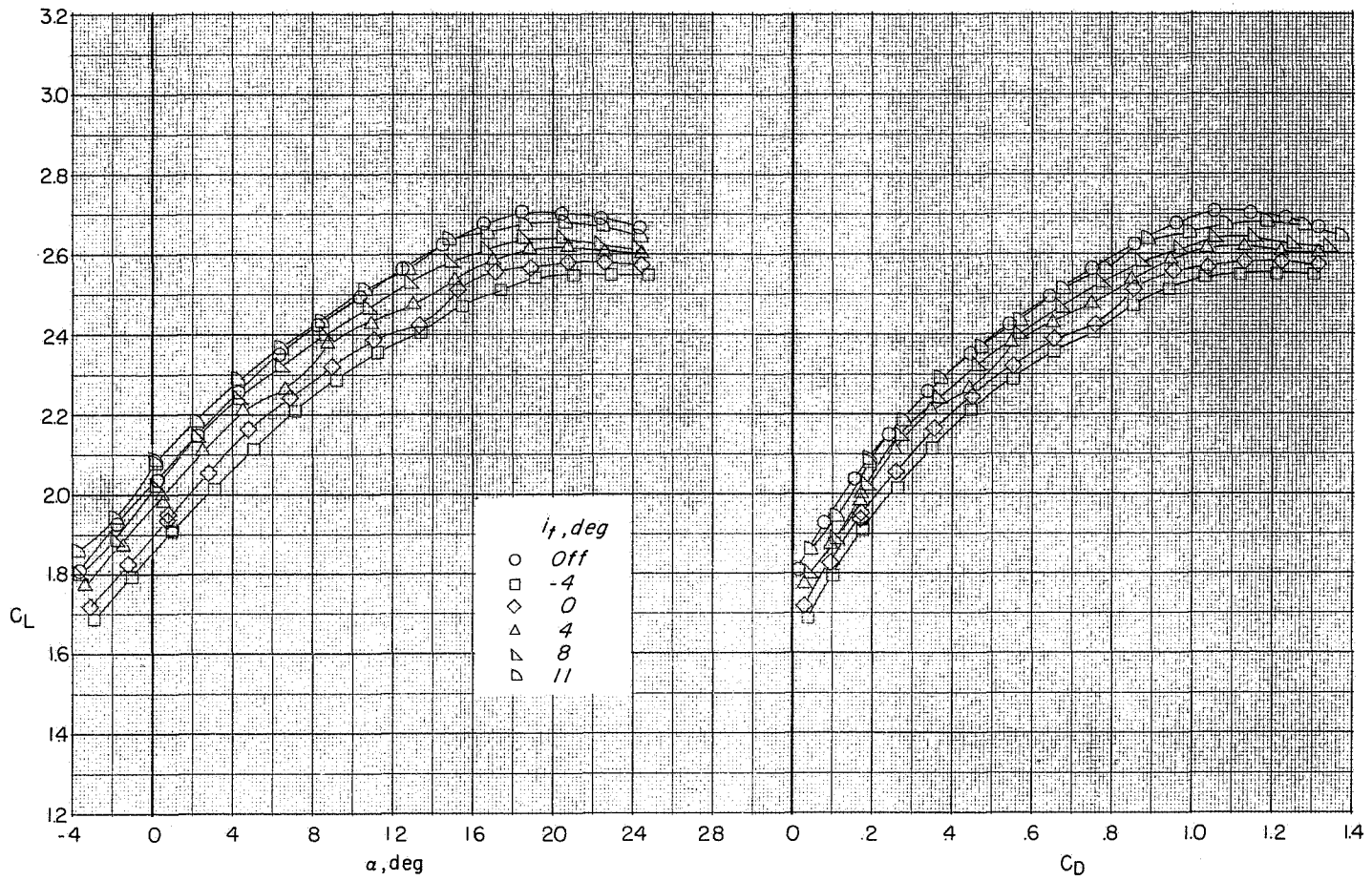

(c) $C_T = 2.0$.

Figure 10.- Continued.

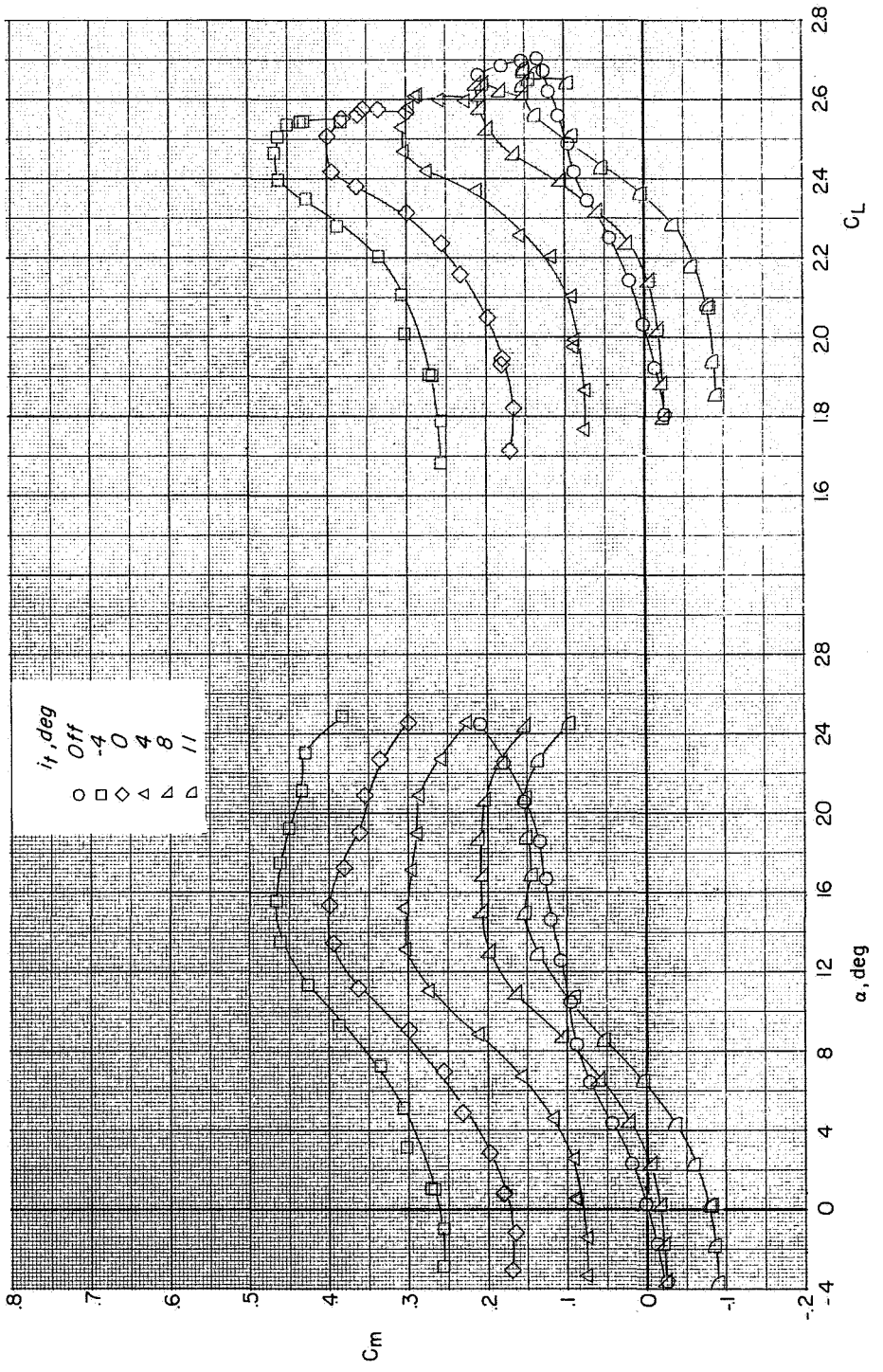

(c) Concluded.

Figure 10.- Continued.

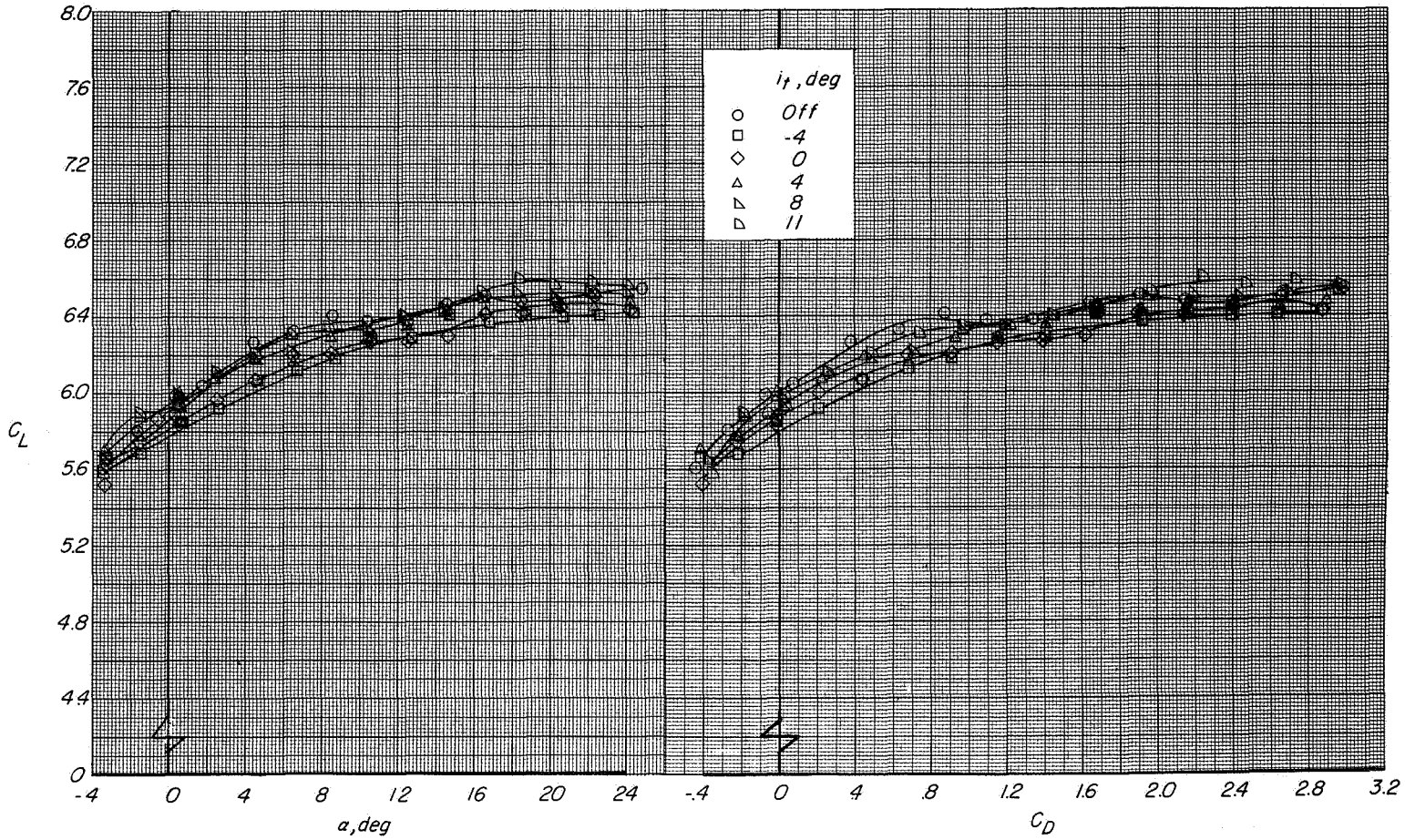

(d) $C_T = 6.0$.

Figure 10.- Continued.

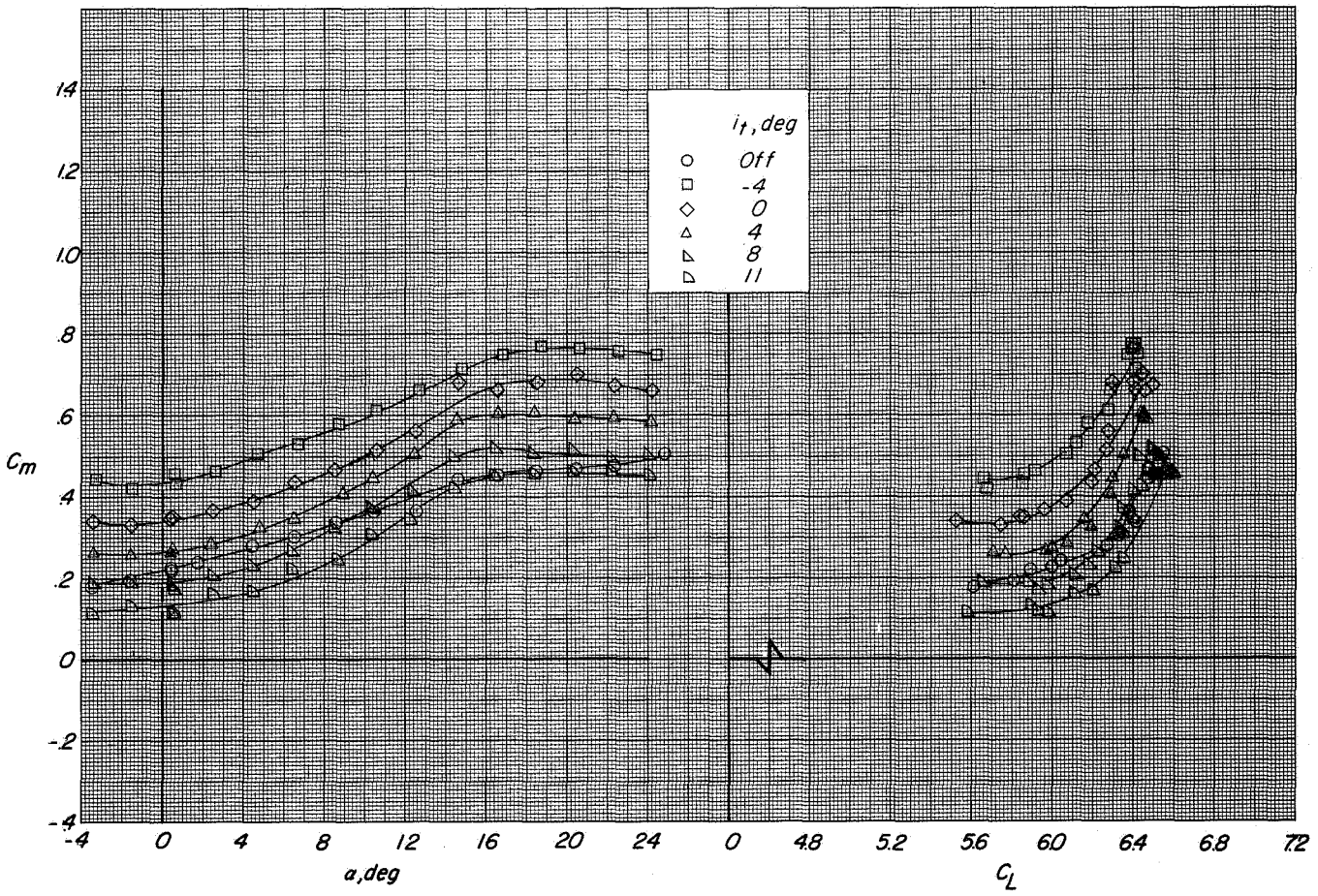

(d) Concluded.

Figure 10.- Concluded.

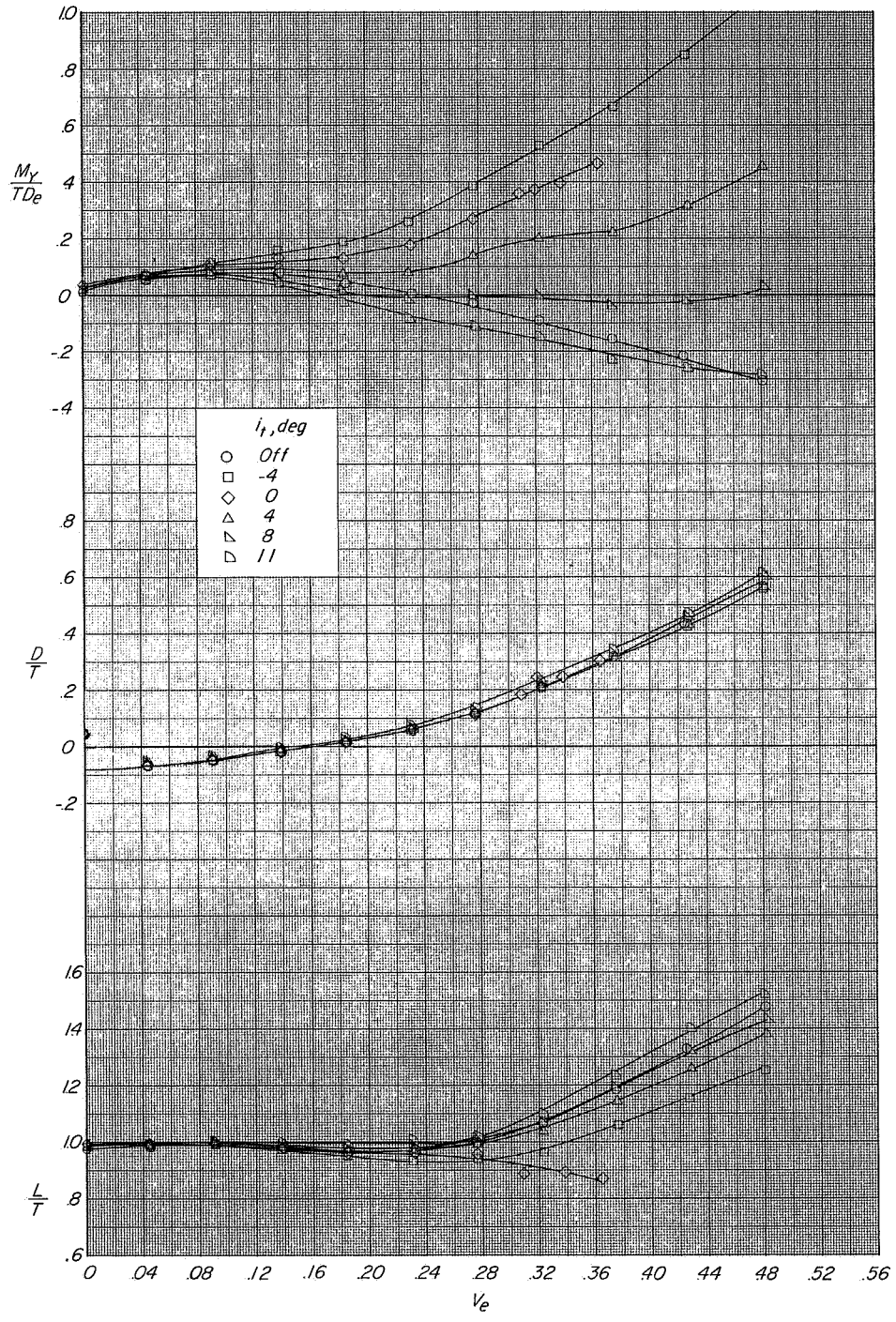

(a) Measured characteristics at $\alpha = 0^{\circ}$.

Figure 11.- Variation of longitudinal characteristics and interference increments with effective-velocity ratio showing effects of horizontal-tail incidence. $\delta_n = 85^{\circ}$; $\delta_f = 60^{\circ}$.

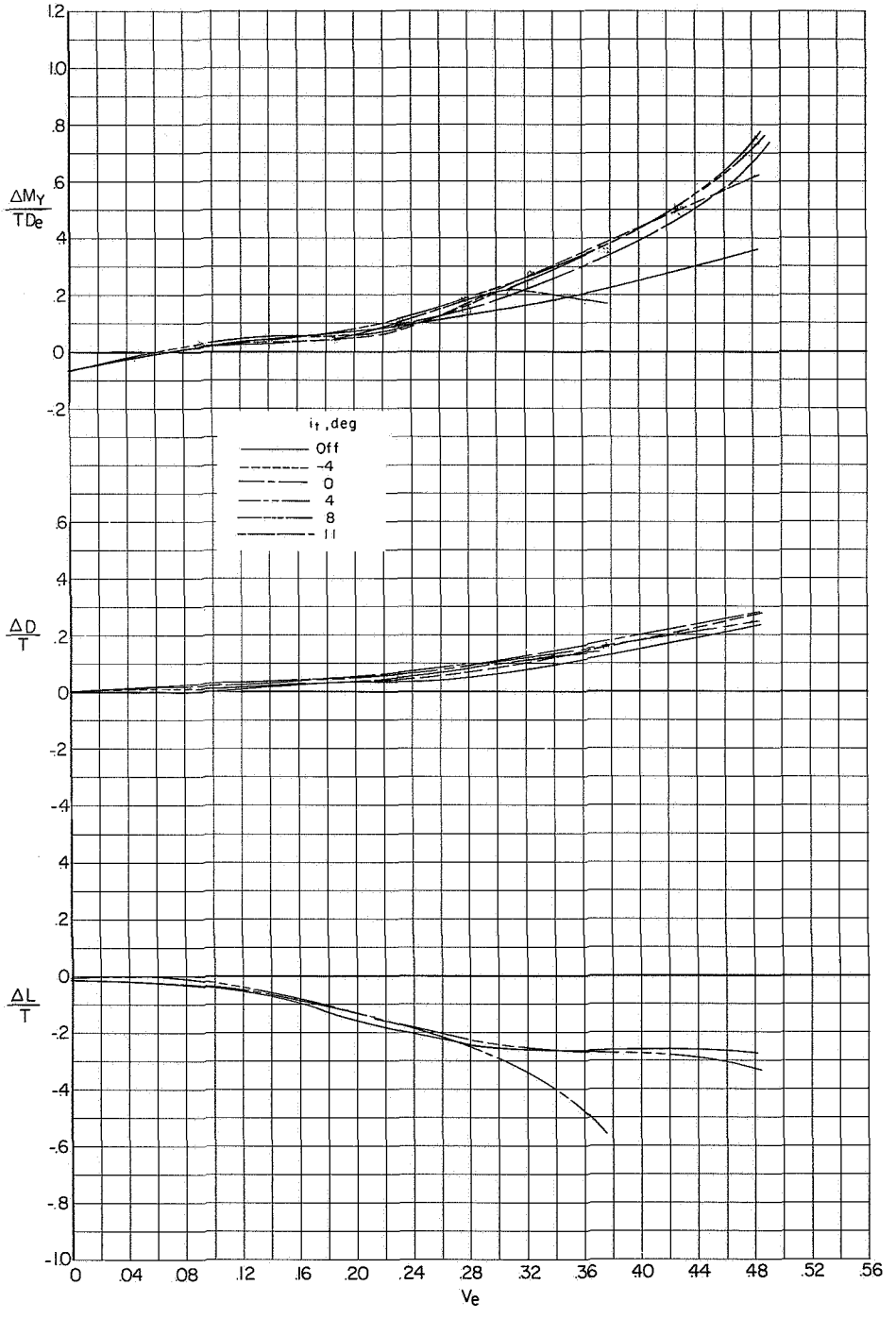

(b) Interference increments at $\alpha = 0^{o}$.

Figure 11.- Continued.

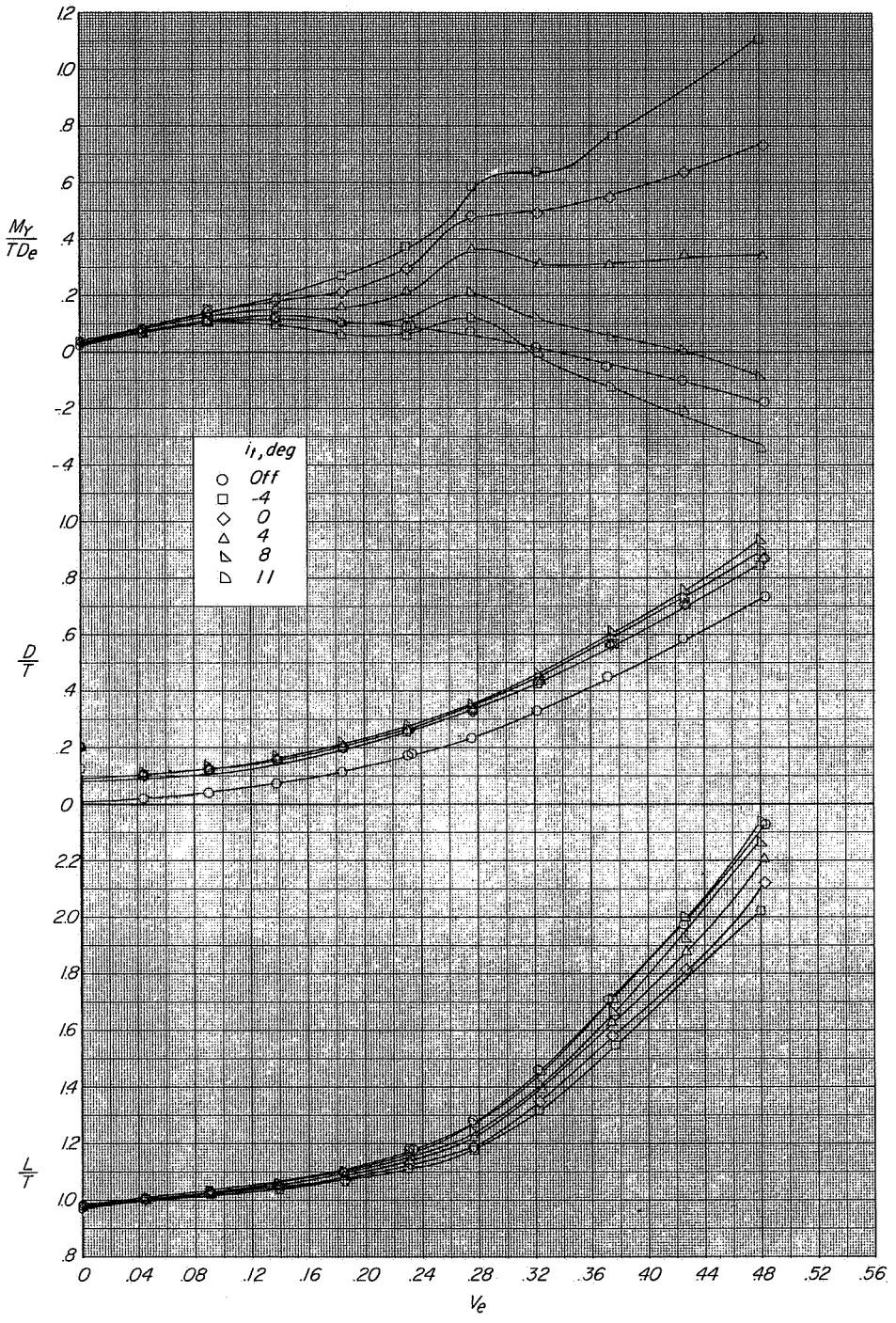

(c) Measured characteristics at $\alpha = 9^{\circ}$.

Figure 11.- Continued.

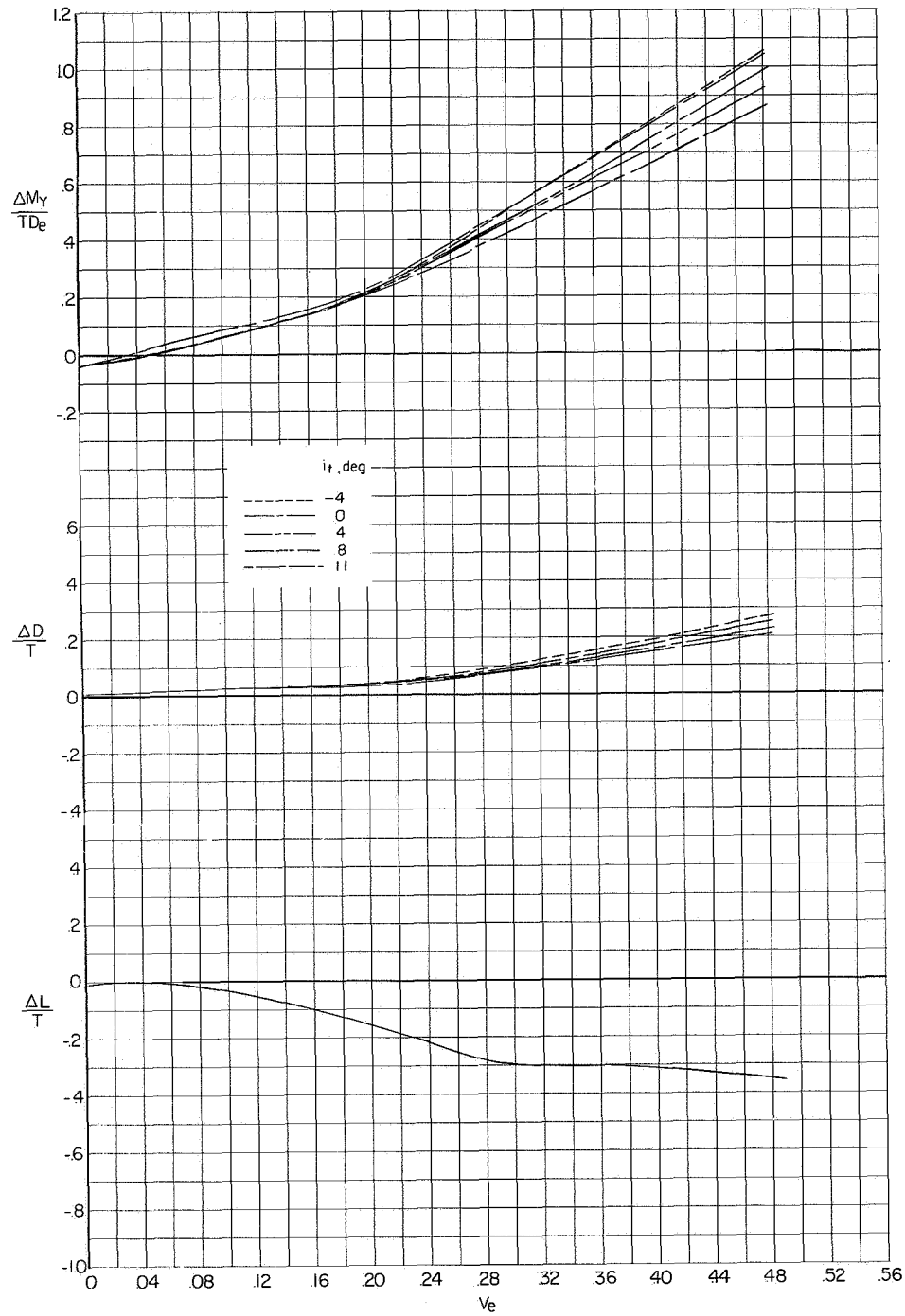

(d) Interference increments at $\alpha = 9^{o}$.

Figure 11.- Concluded.

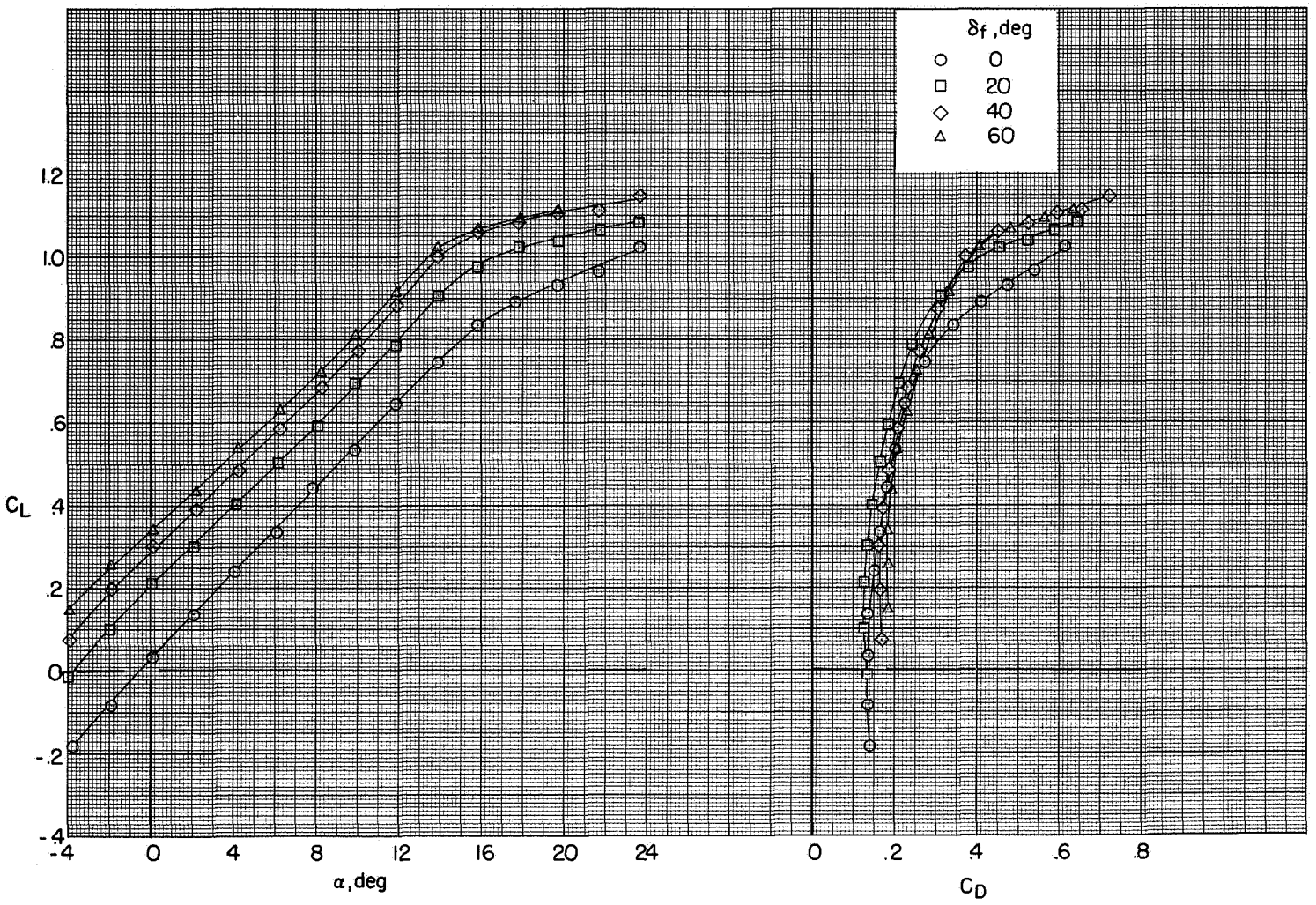

(a) $C_T = 0$.

Figure 12.- Longitudinal aerodynamic characteristics showing flap effectiveness. $\delta_n = 85^o$; $i_t = 0^o$.

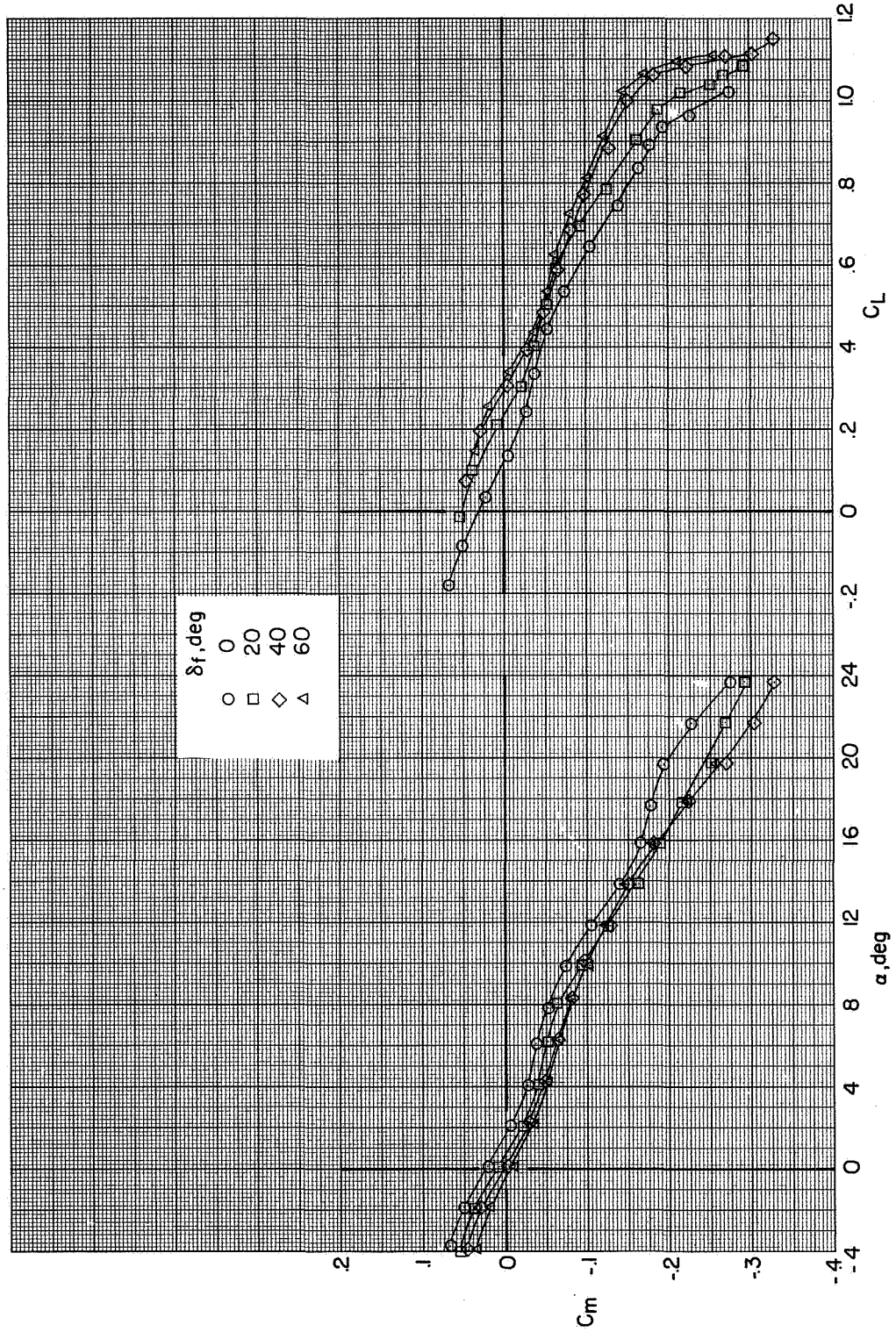

(a) Concluded.

Figure 12.- Continued.

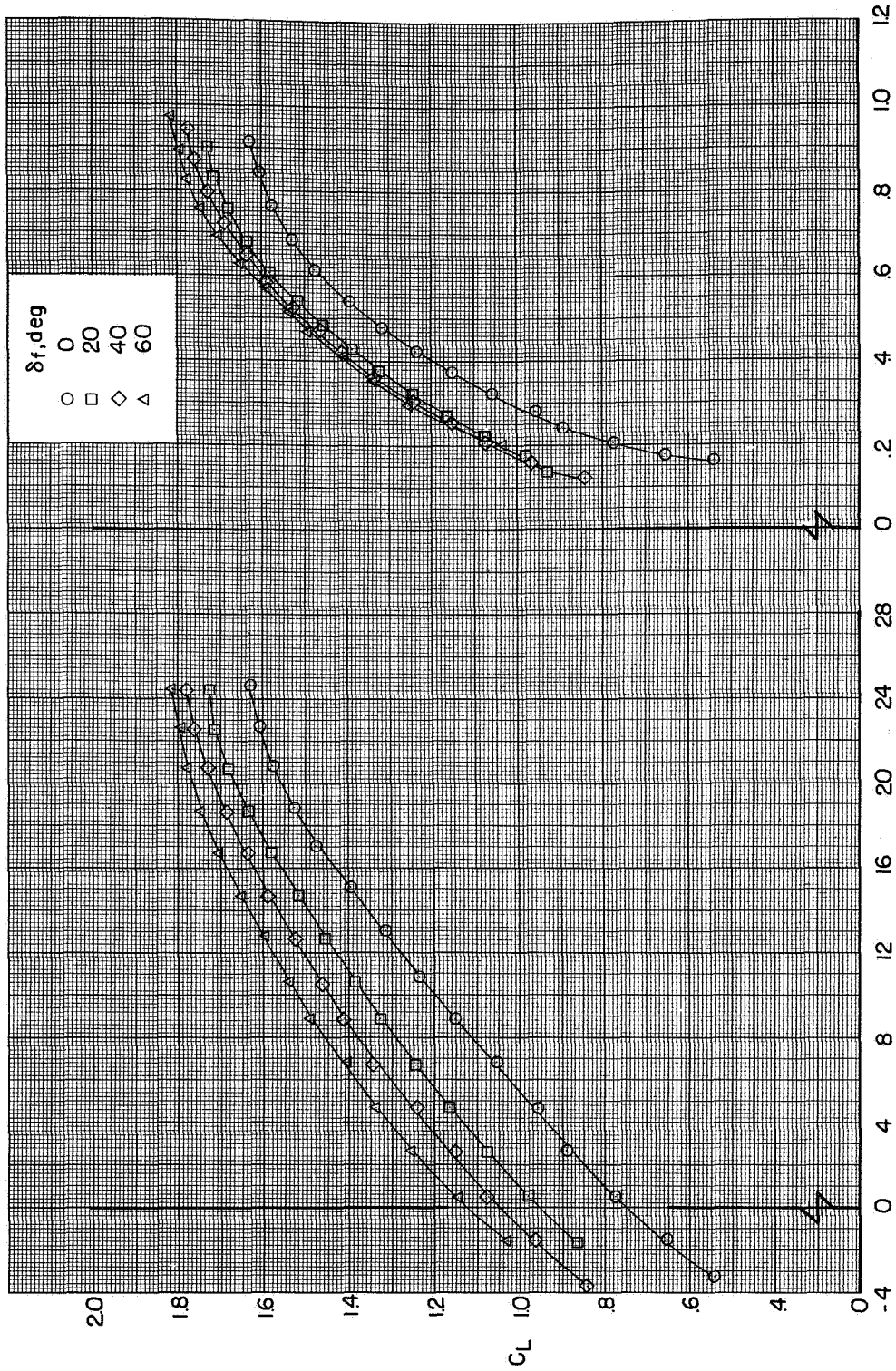

(b) $C_T = 1.0$.

Figure 12.- Continued.

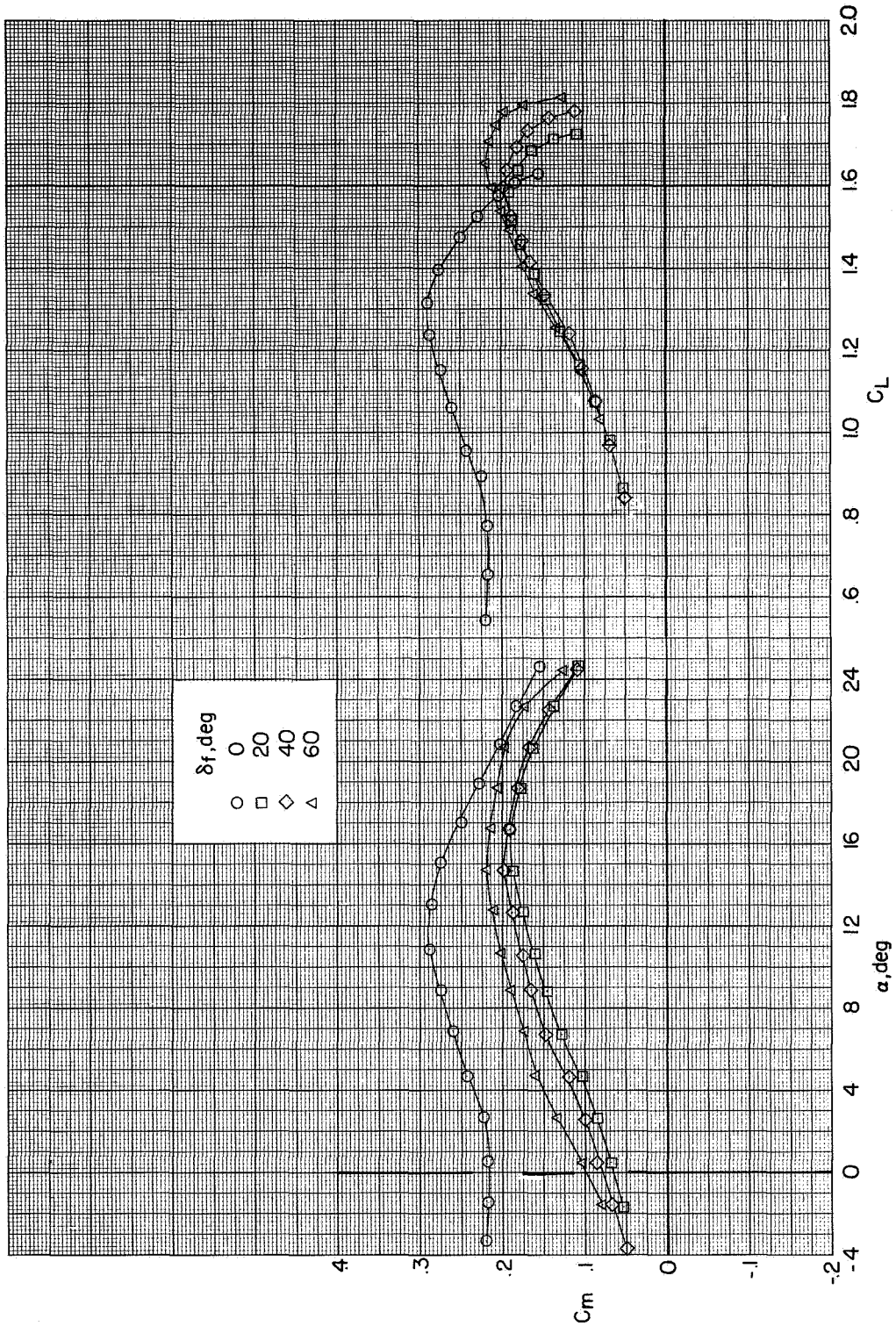

(b) Concluded.

Figure 12.- Continued.

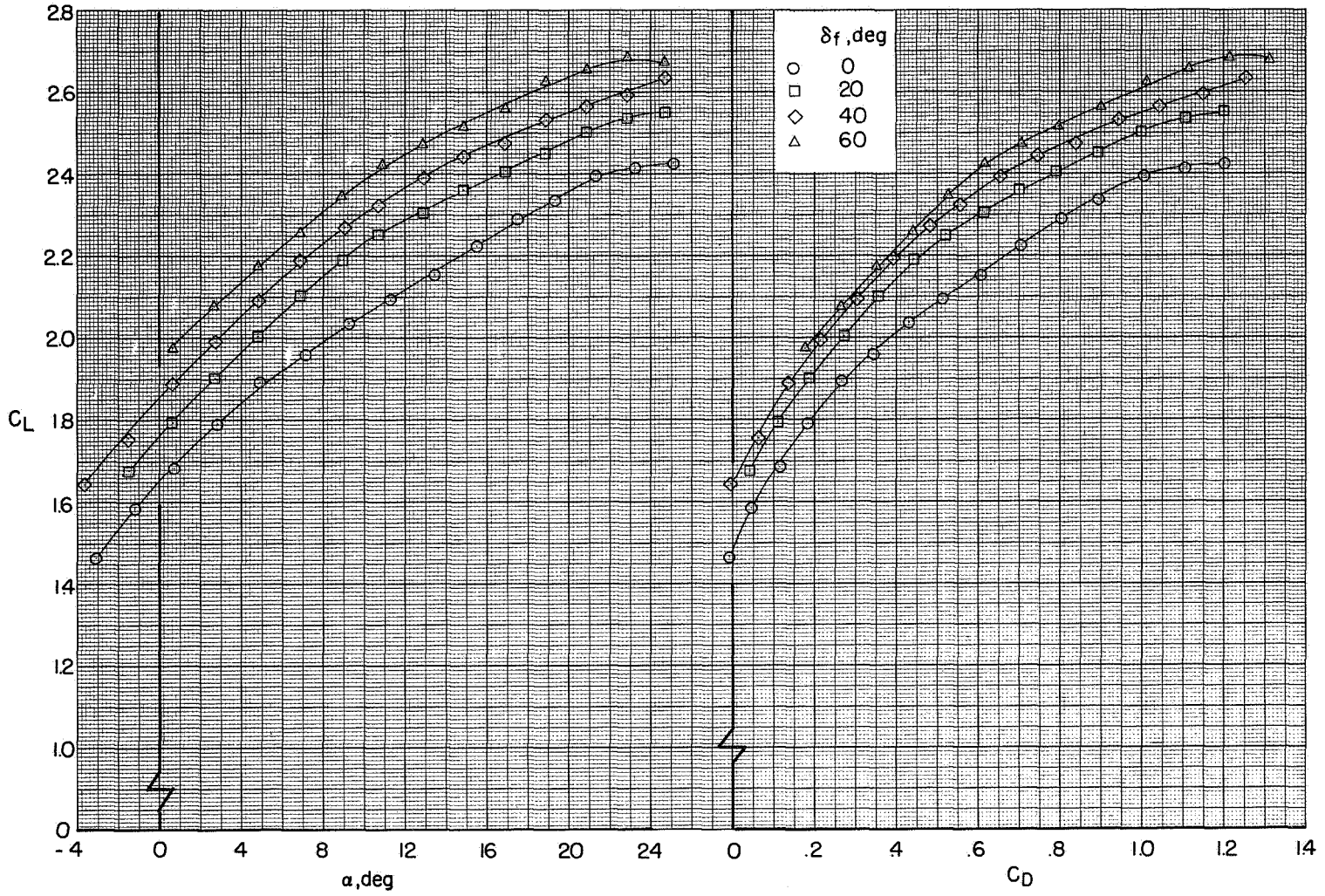

(c) $C_T = 2.0$.

Figure 12.- Continued.

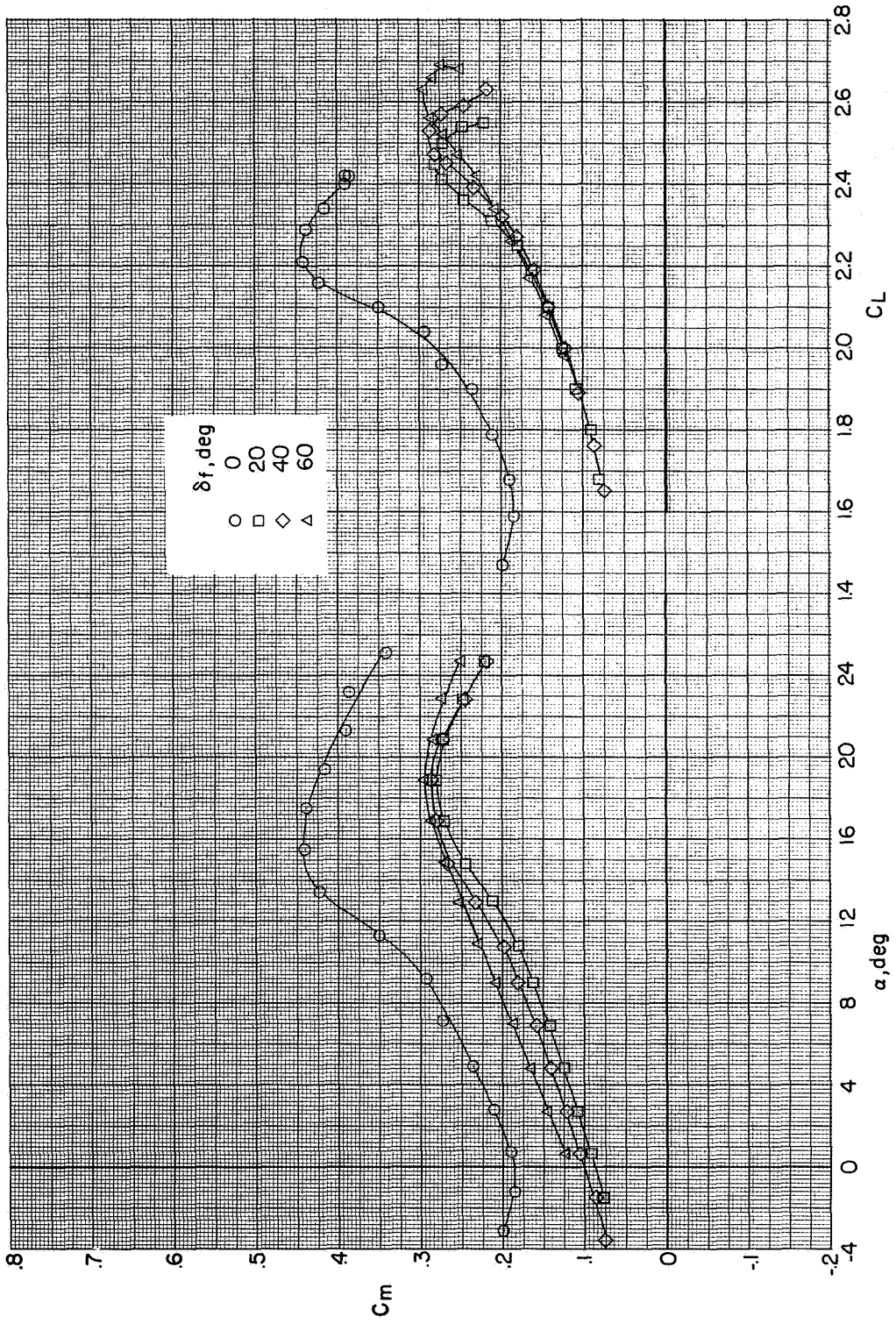

(c) Concluded.

Figure 12.- Continued.

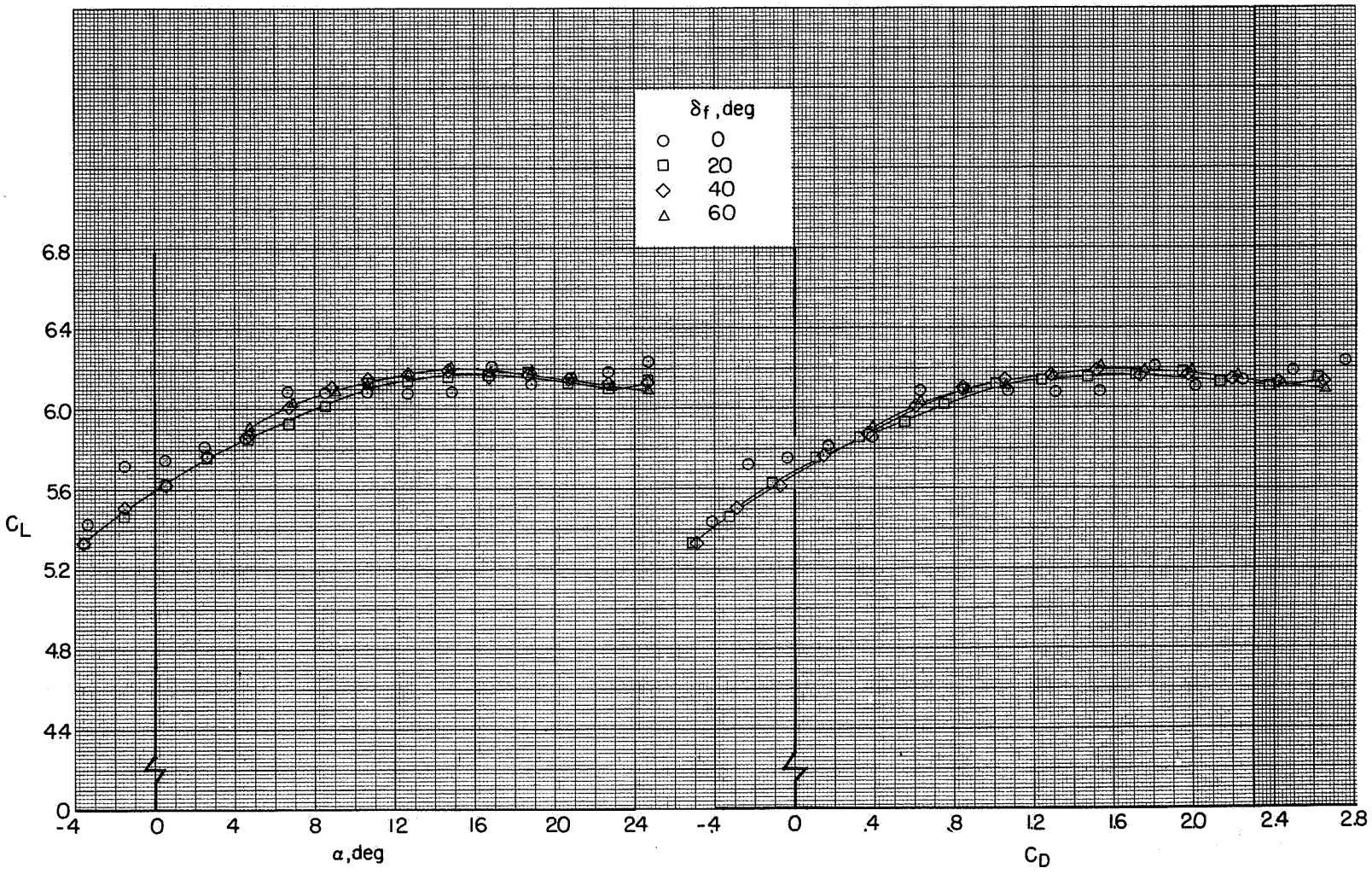

(d) $C_T = 6.0$.

Figure 12.- Continued.

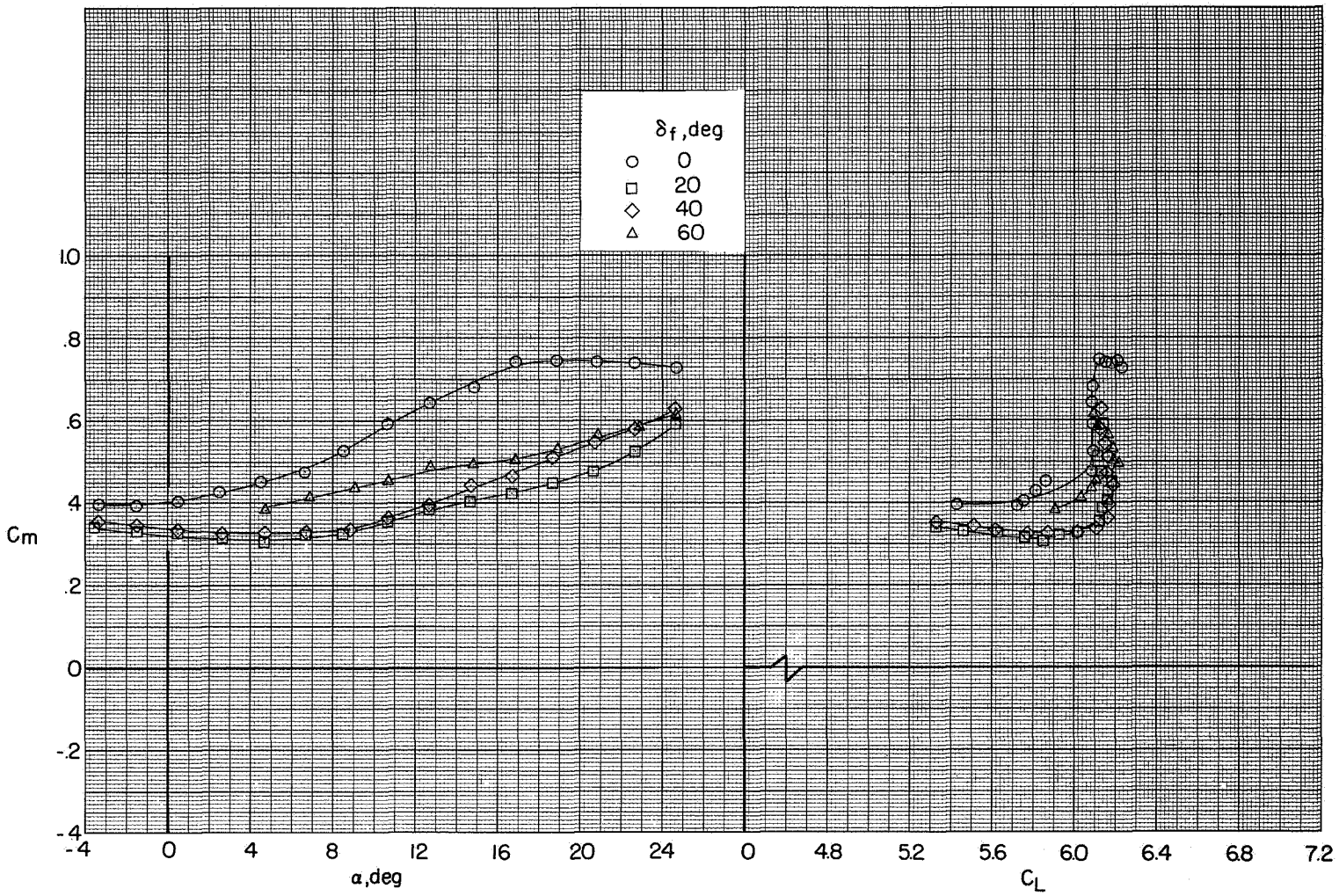

(d) Concluded.

Figure 12.- Concluded.

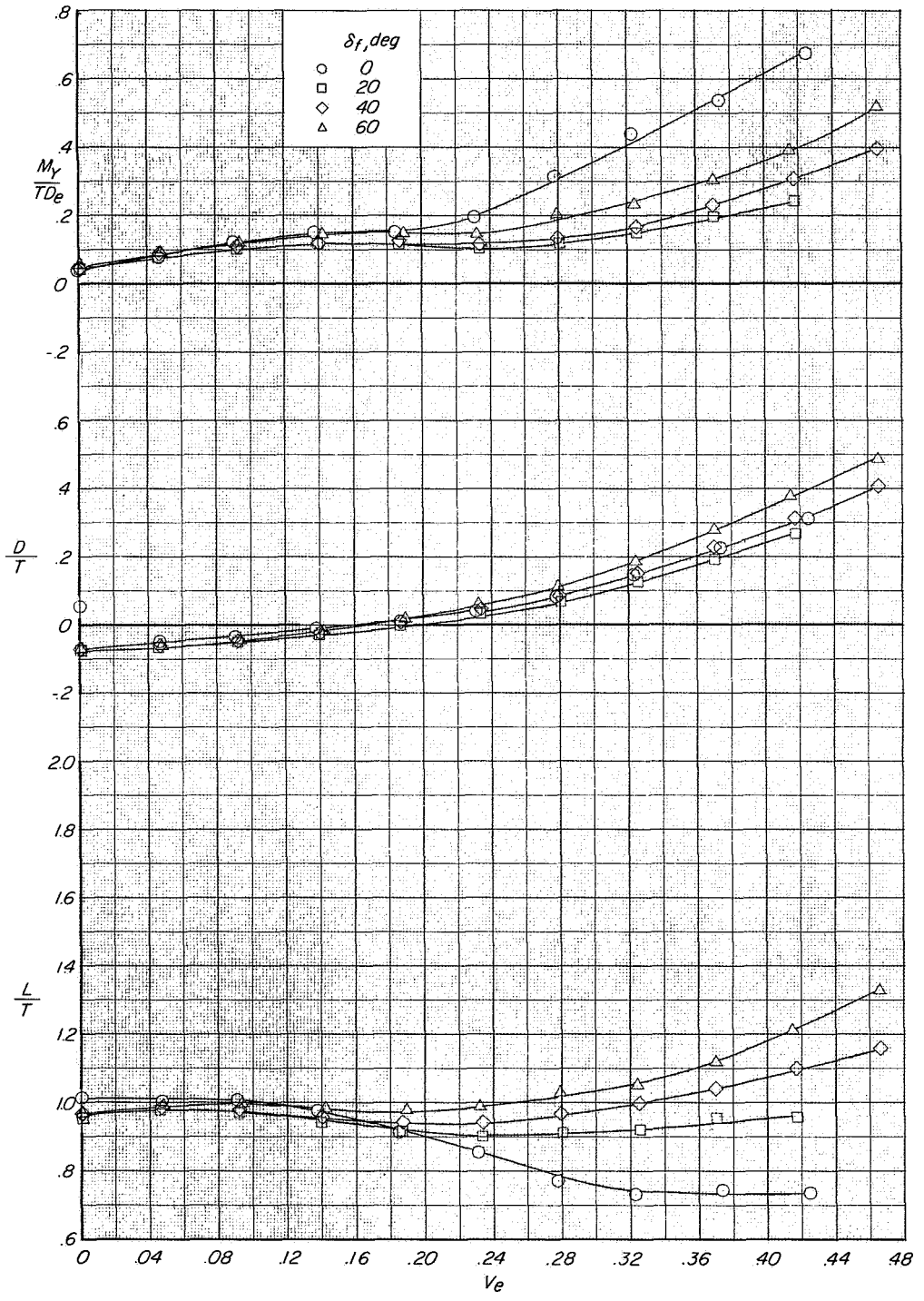

(a) Measured characteristics at $\alpha = 0^{\circ}$.

Figure 13.- Variation of longitudinal characteristics and interference increments with effective-velocity ratio showing effect of flap deflection. $\delta_n = 85^{\circ}$; $i_t = 0^{\circ}$.

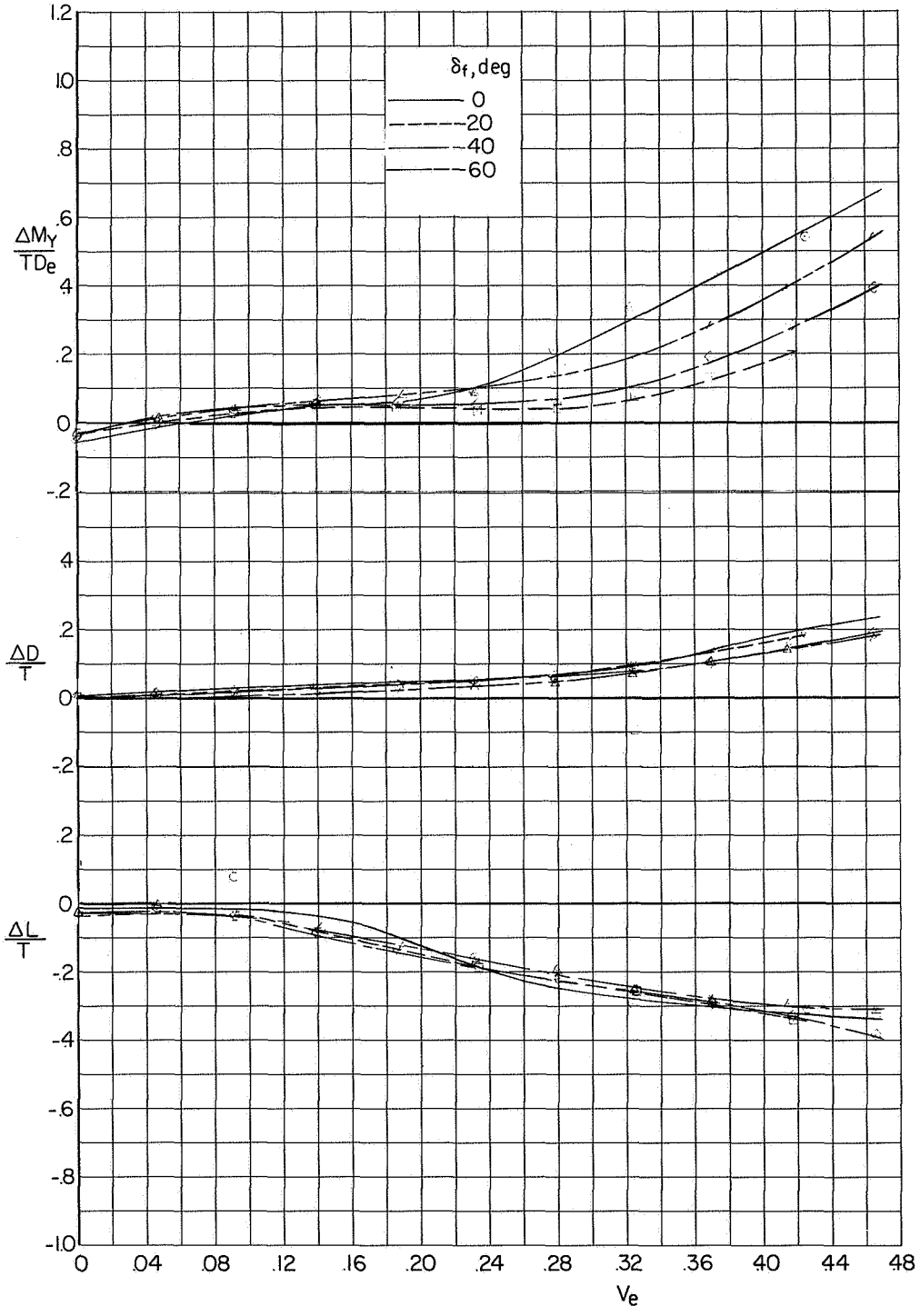

(b) Interference increments at $\alpha = 0^o$.

Figure 13.- Continued.

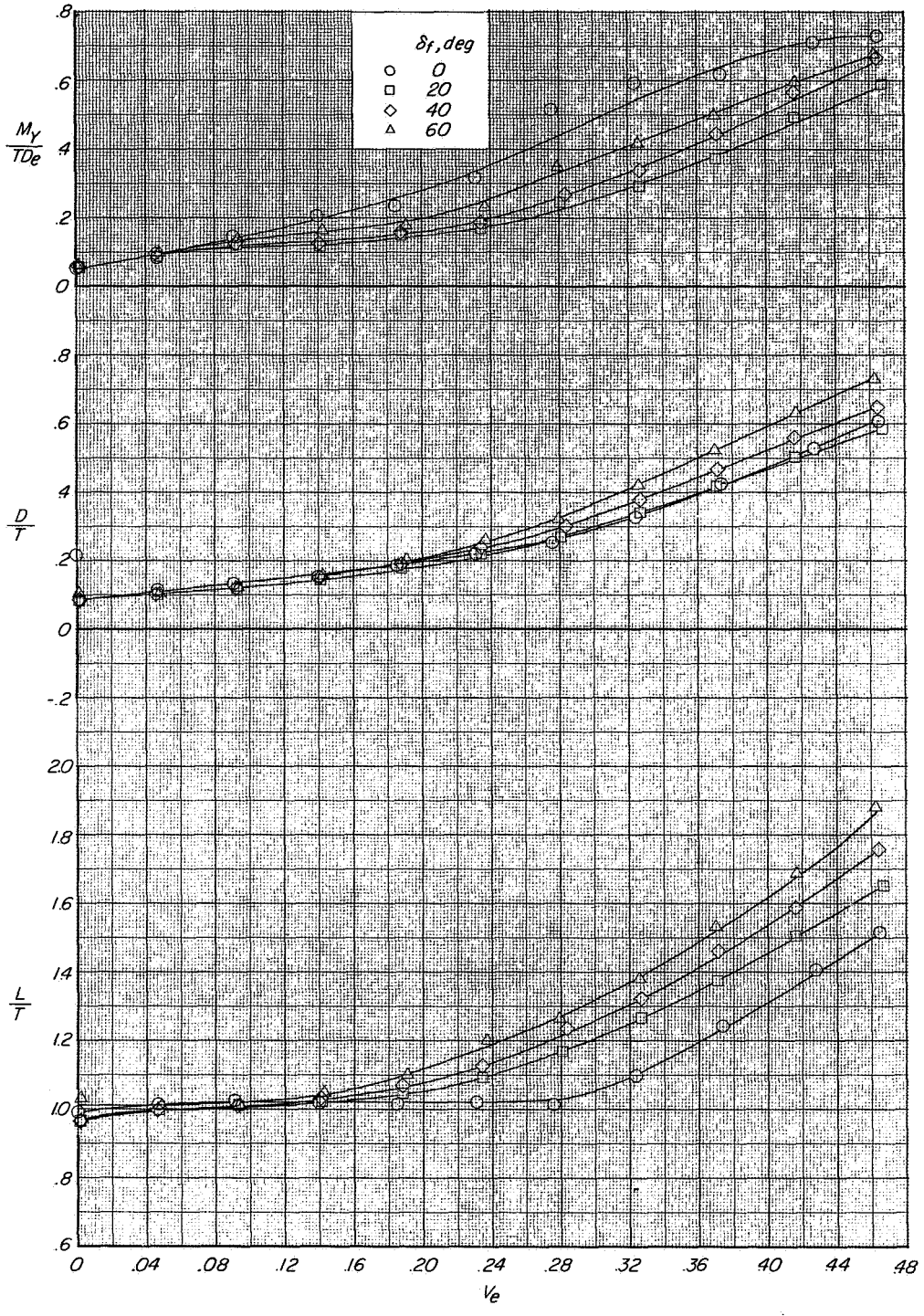

(c) Measured characteristics at $\alpha = 9^{o}$.

Figure 13.- Continued.

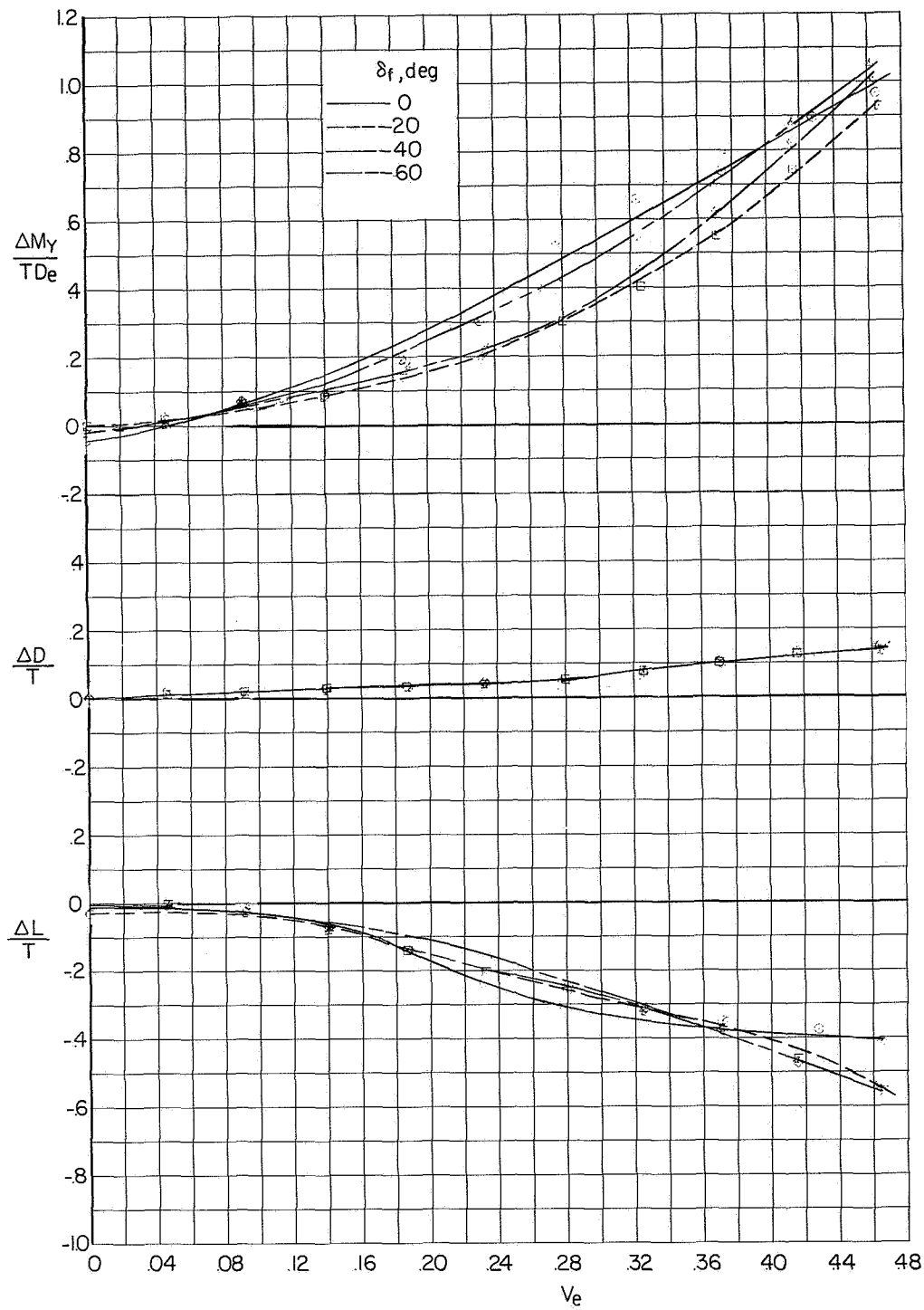

(d) Interference increments at $\alpha = 9^o$.

Figure 13.- Concluded.

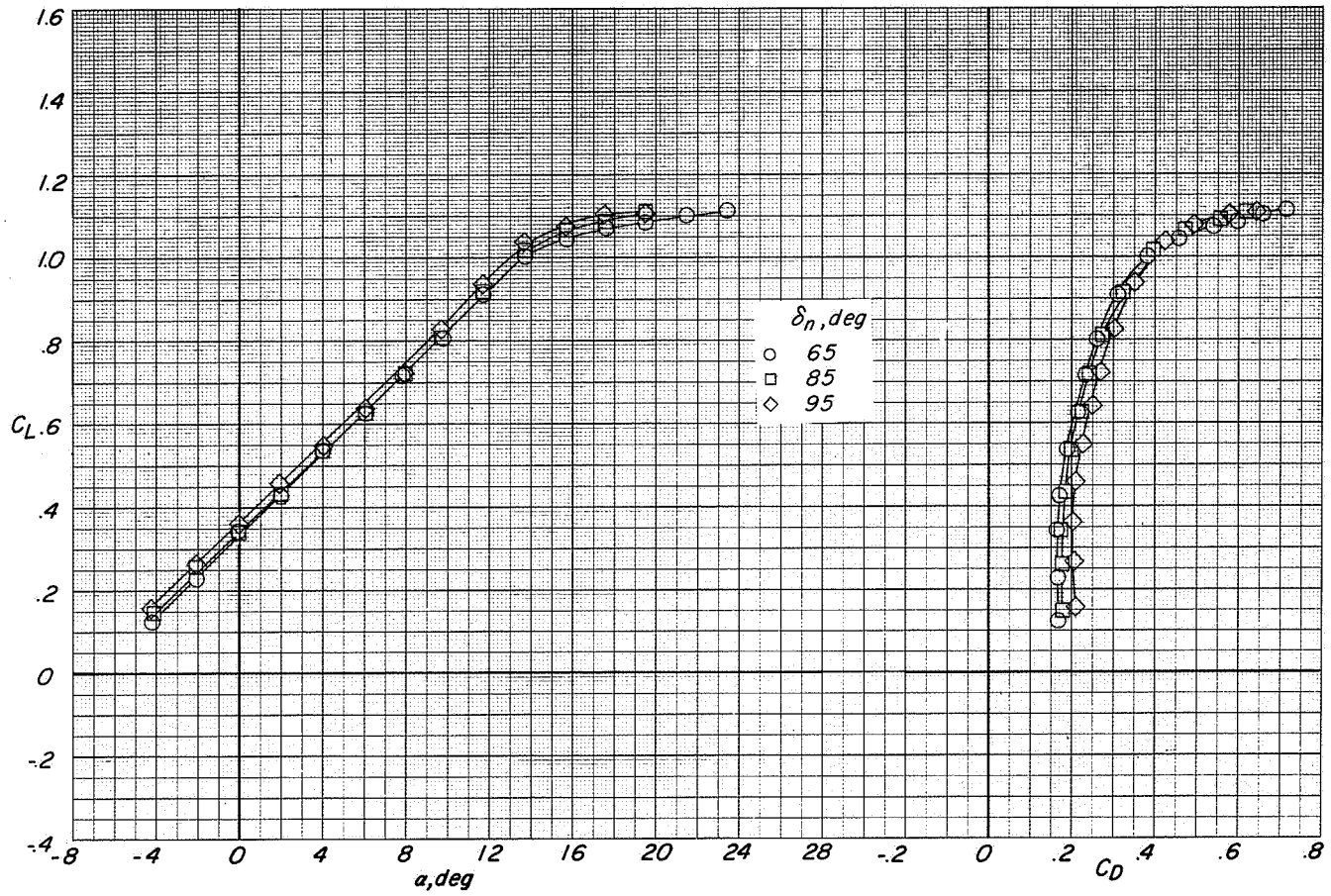

(a) $C_T = 0$.

Figure 14.- Longitudinal aerodynamic characteristics showing effects of nozzle deflection. $\delta_f = 60^o$; $i_t = 0^o$.

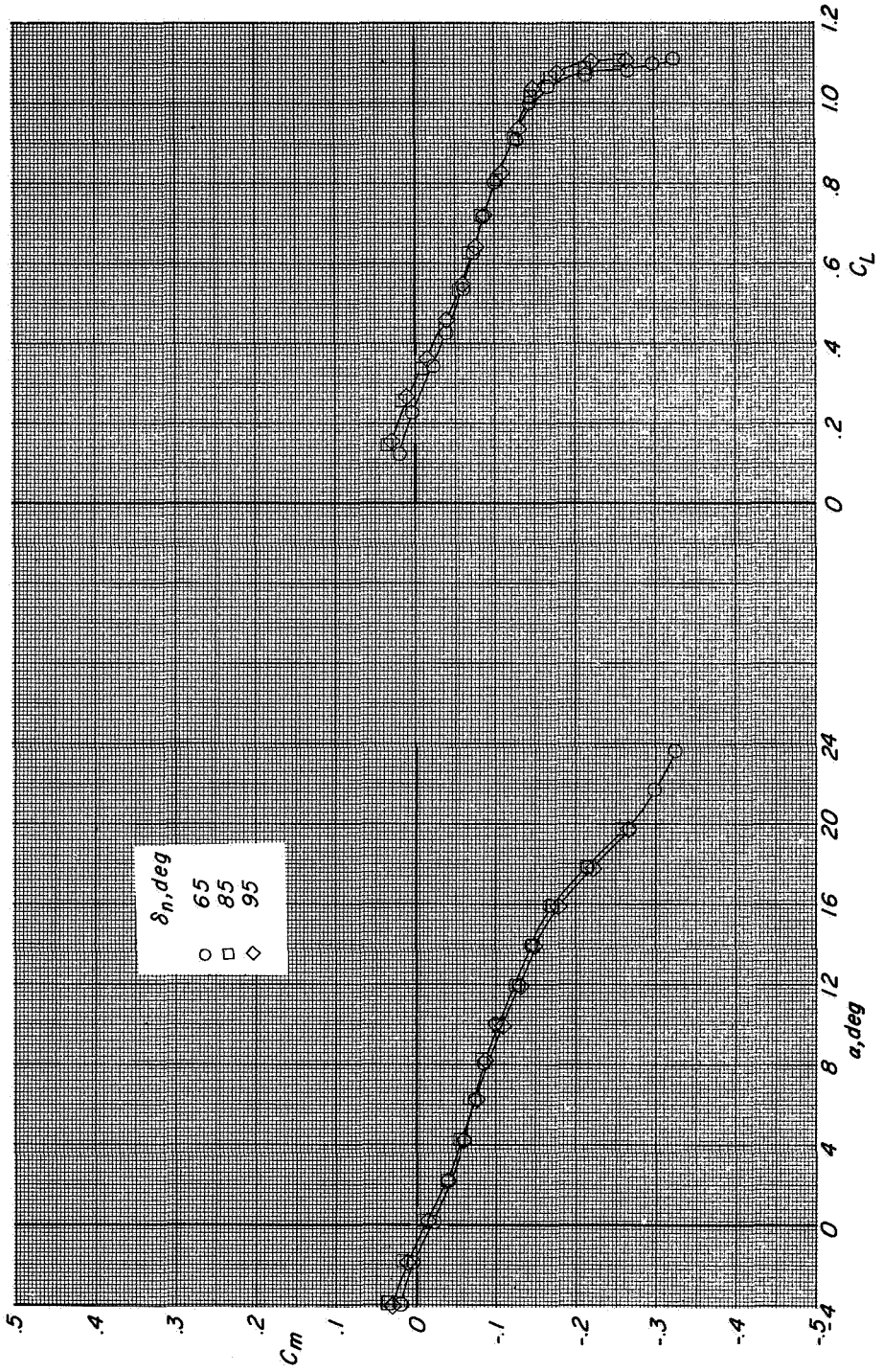

(a) Concluded.

Figure 14.- Continued.

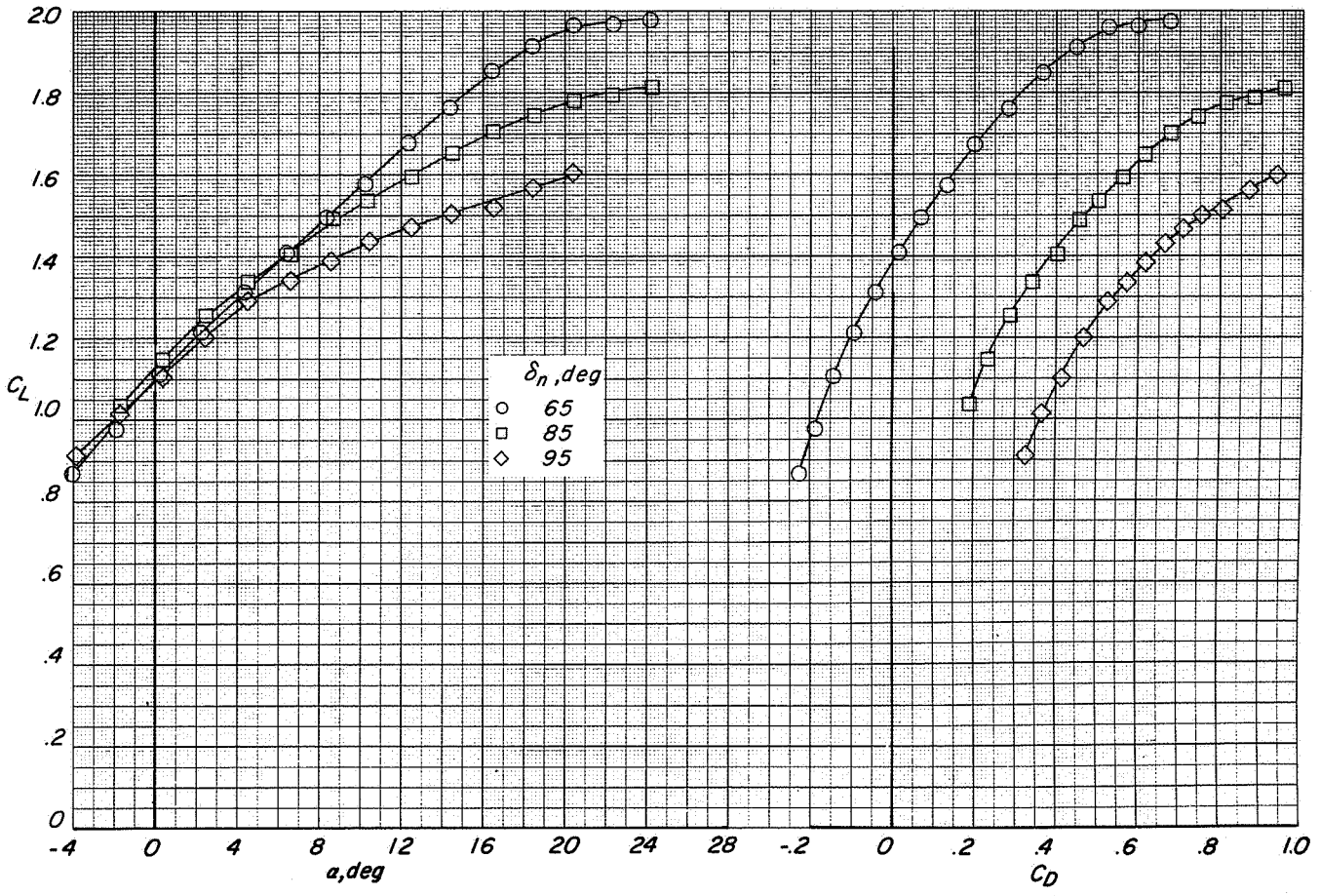

(b) $C_T = 1.1$.

Figure 14.- Continued.

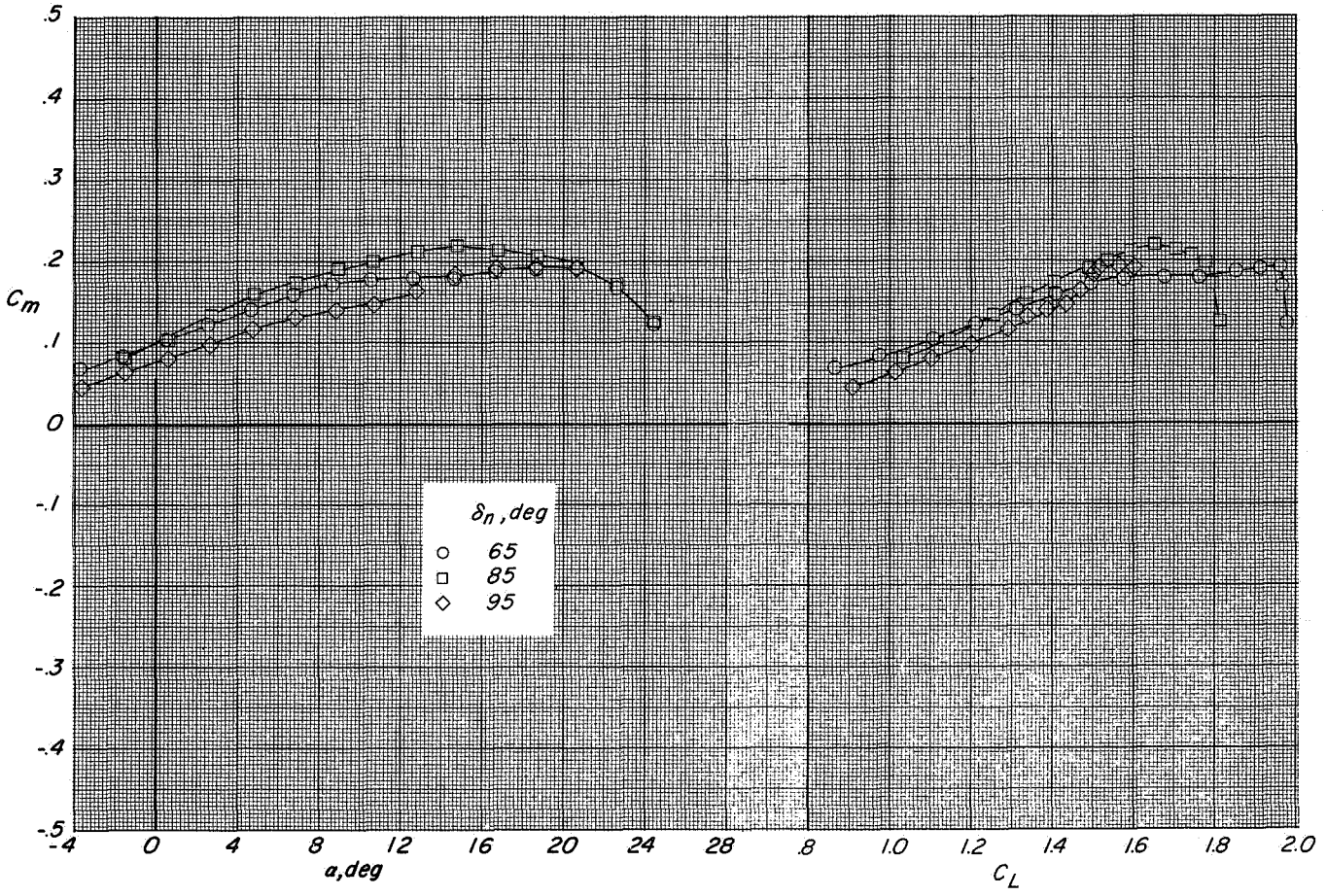

(b) Concluded.

Figure 14.- Continued.

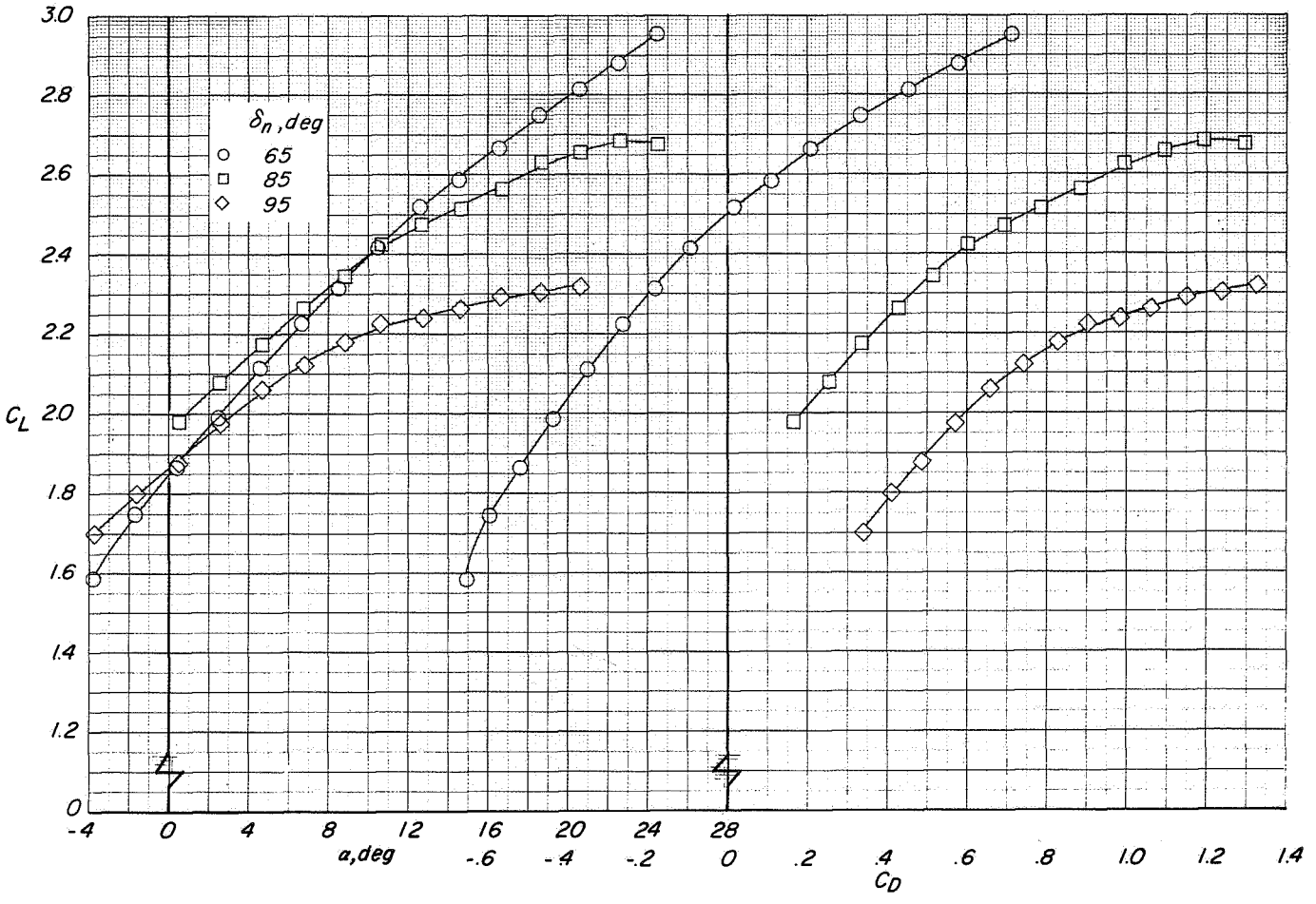

(c) $C_T = 2.0$.

Figure 14.- Continued.

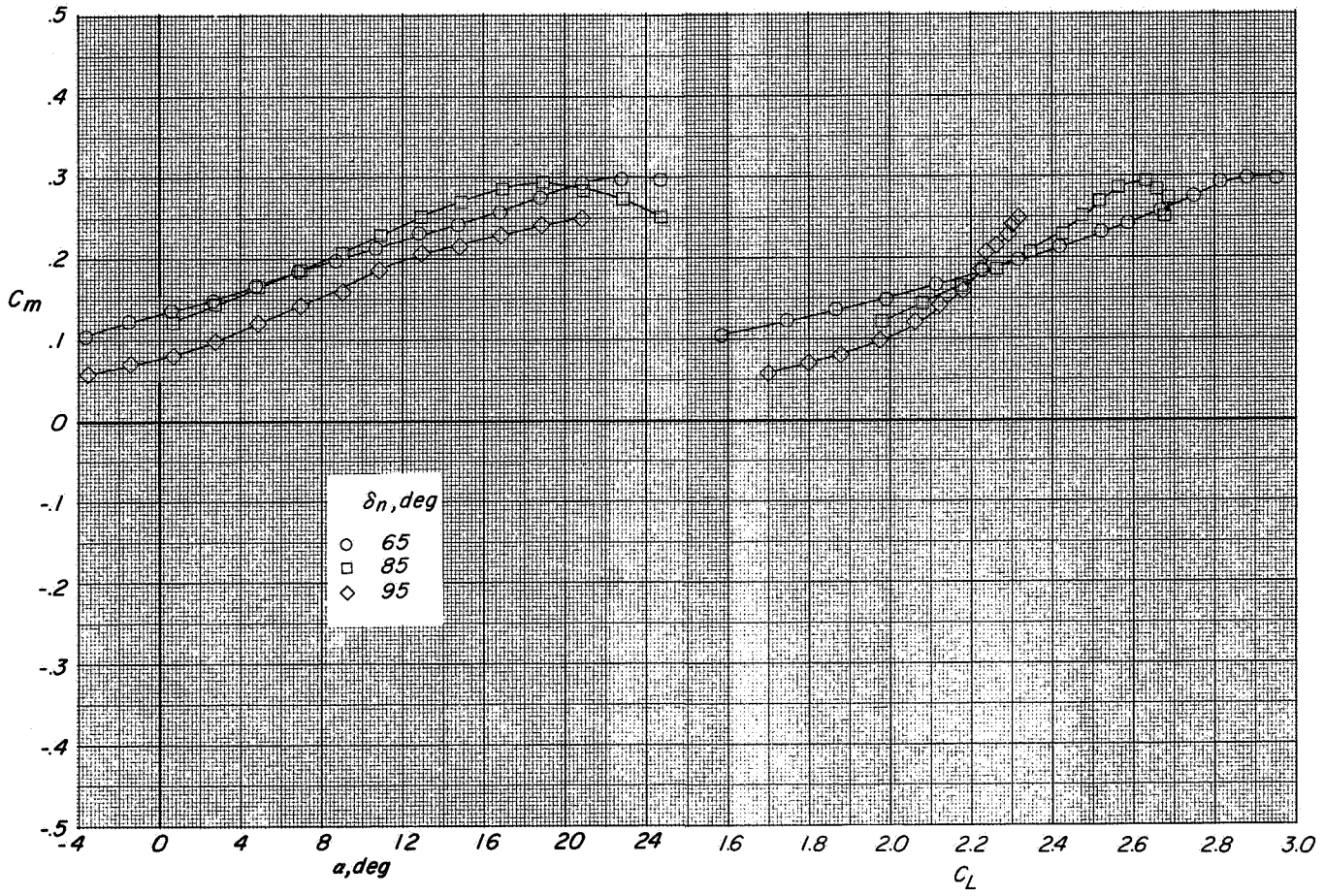

(c) Concluded.

Figure 14.- Continued.

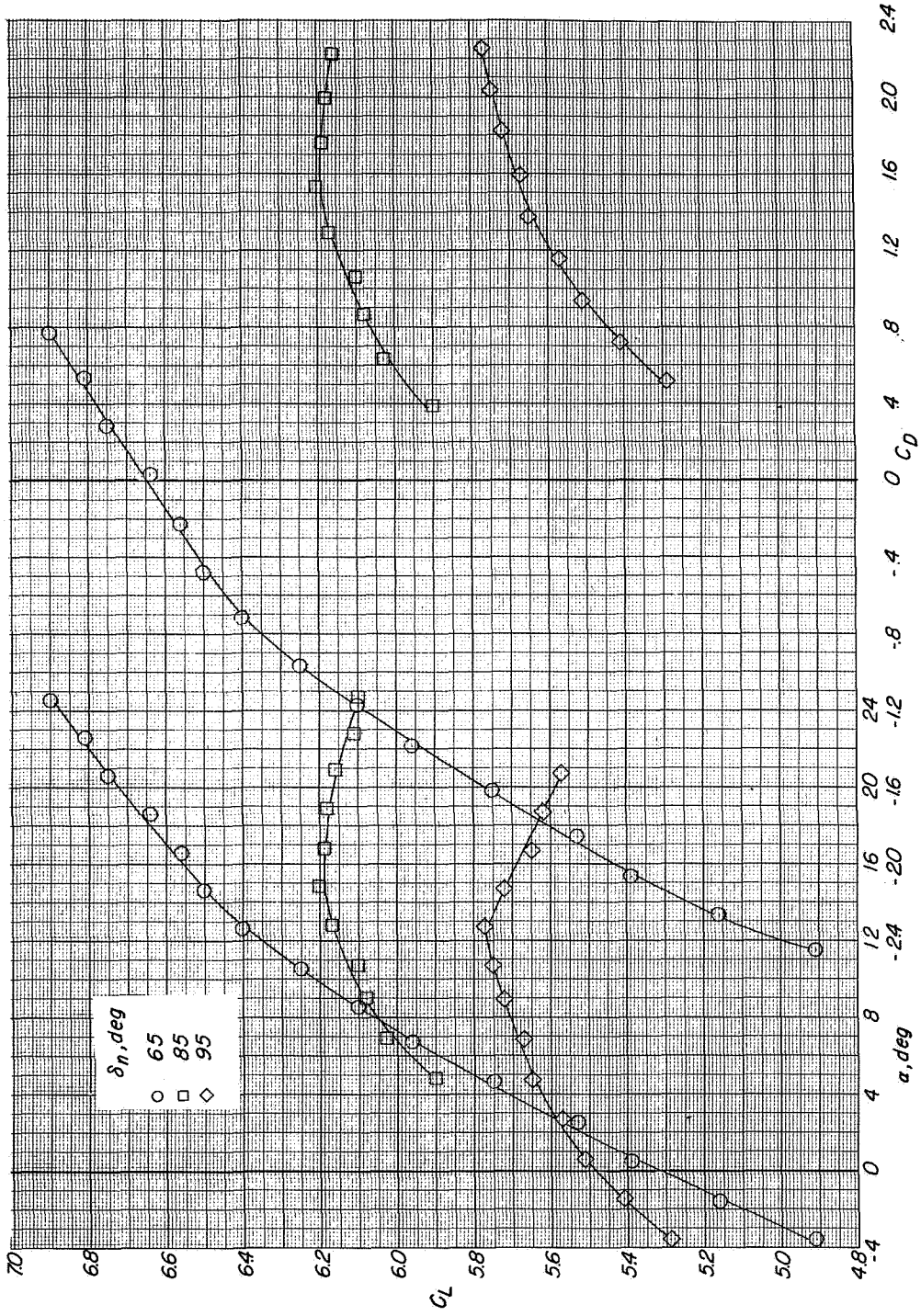

(d) $C_T = 6.0$.

Figure 14.- Continued.

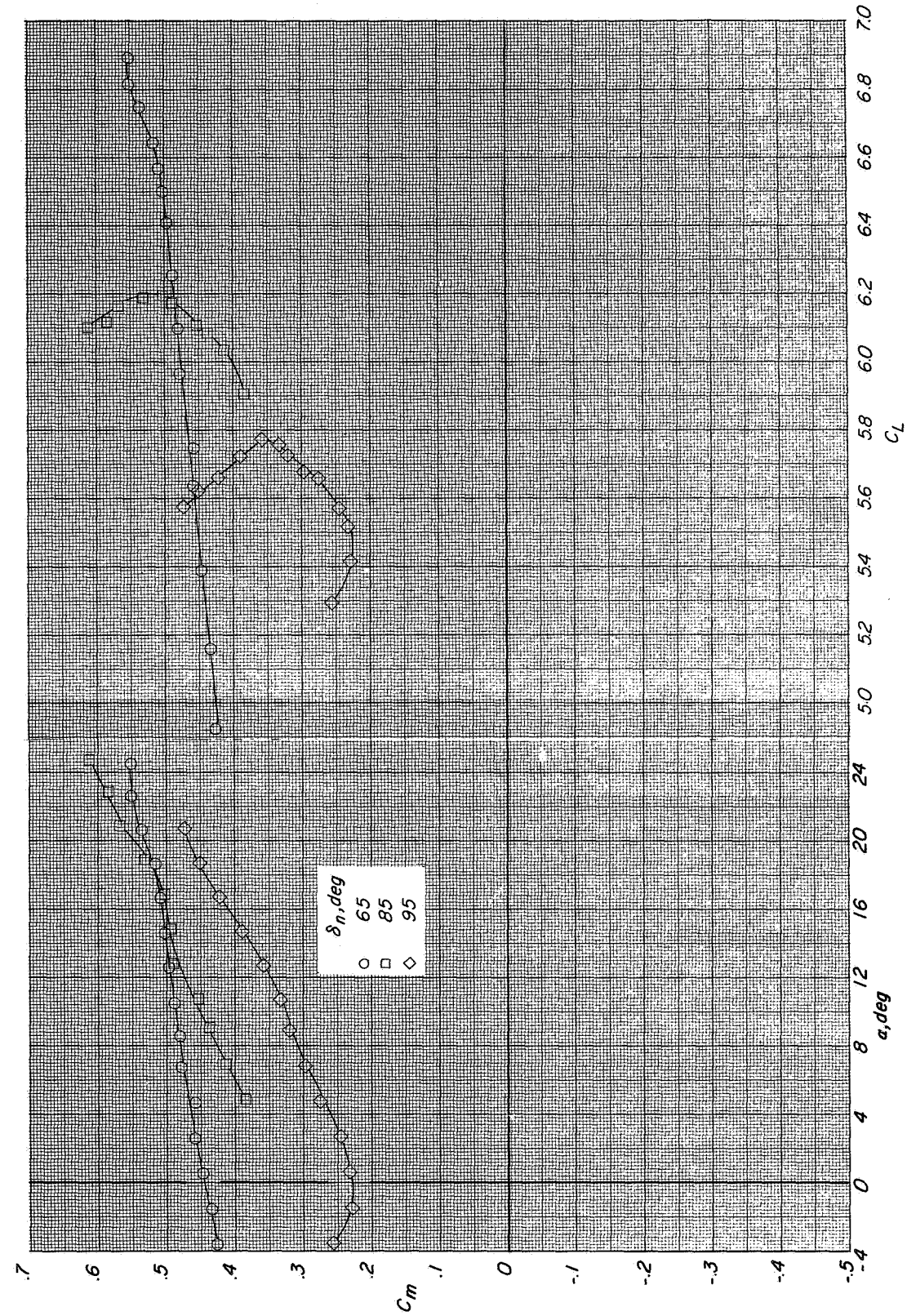

(d) Concluded.

Figure 14.- Concluded.

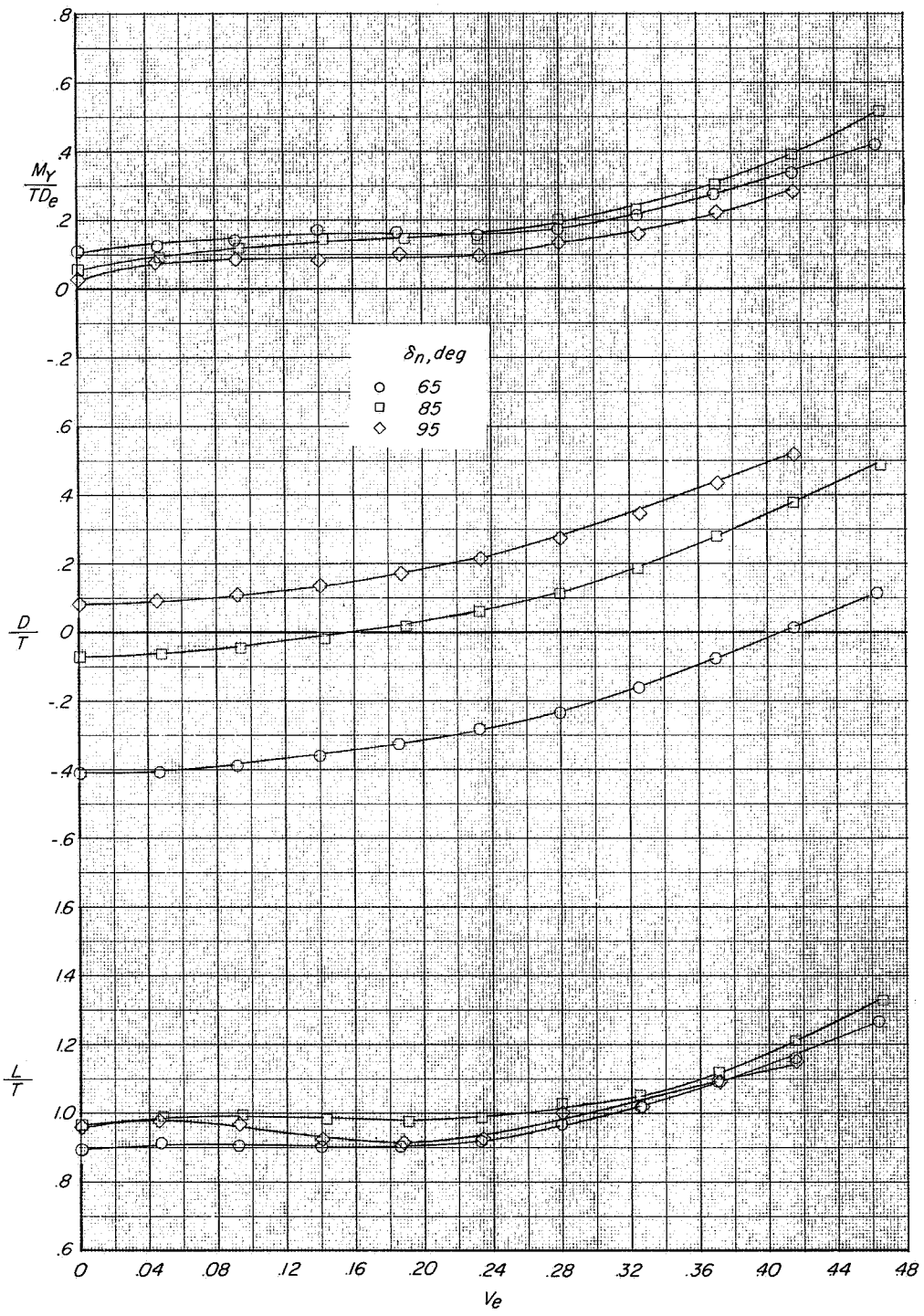

(a) Measured characteristics at $\alpha = 0^{o}$.

Figure 15.- Variation of longitudinal characteristics and interference increments with effective-velocity ratio showing effect of nozzle deflection. $\delta_f = 60^{o}$; $i_t = 0^{o}$.

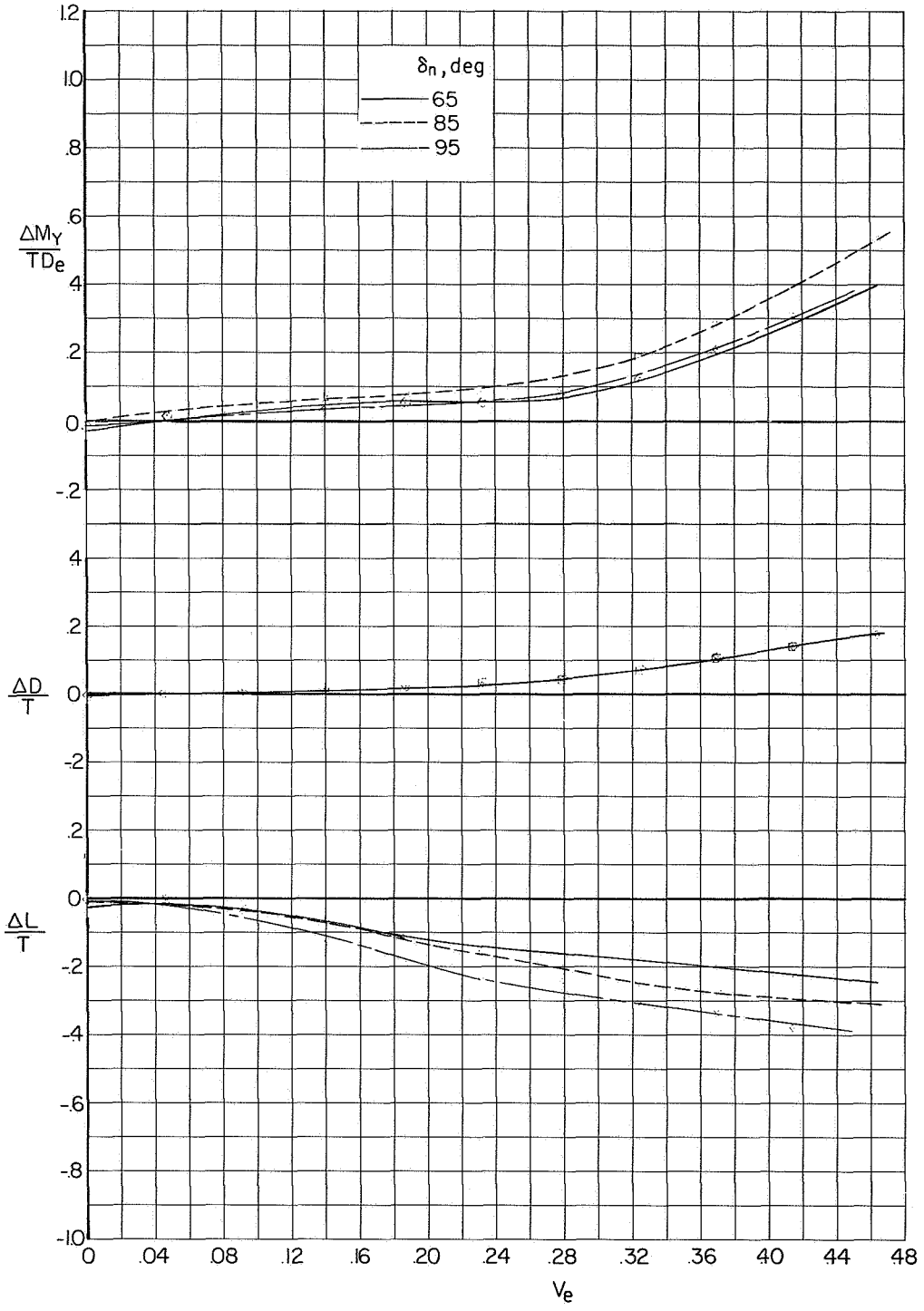

(b) Interference increments at $\alpha = 0^{o}$.

Figure 15.- Continued.

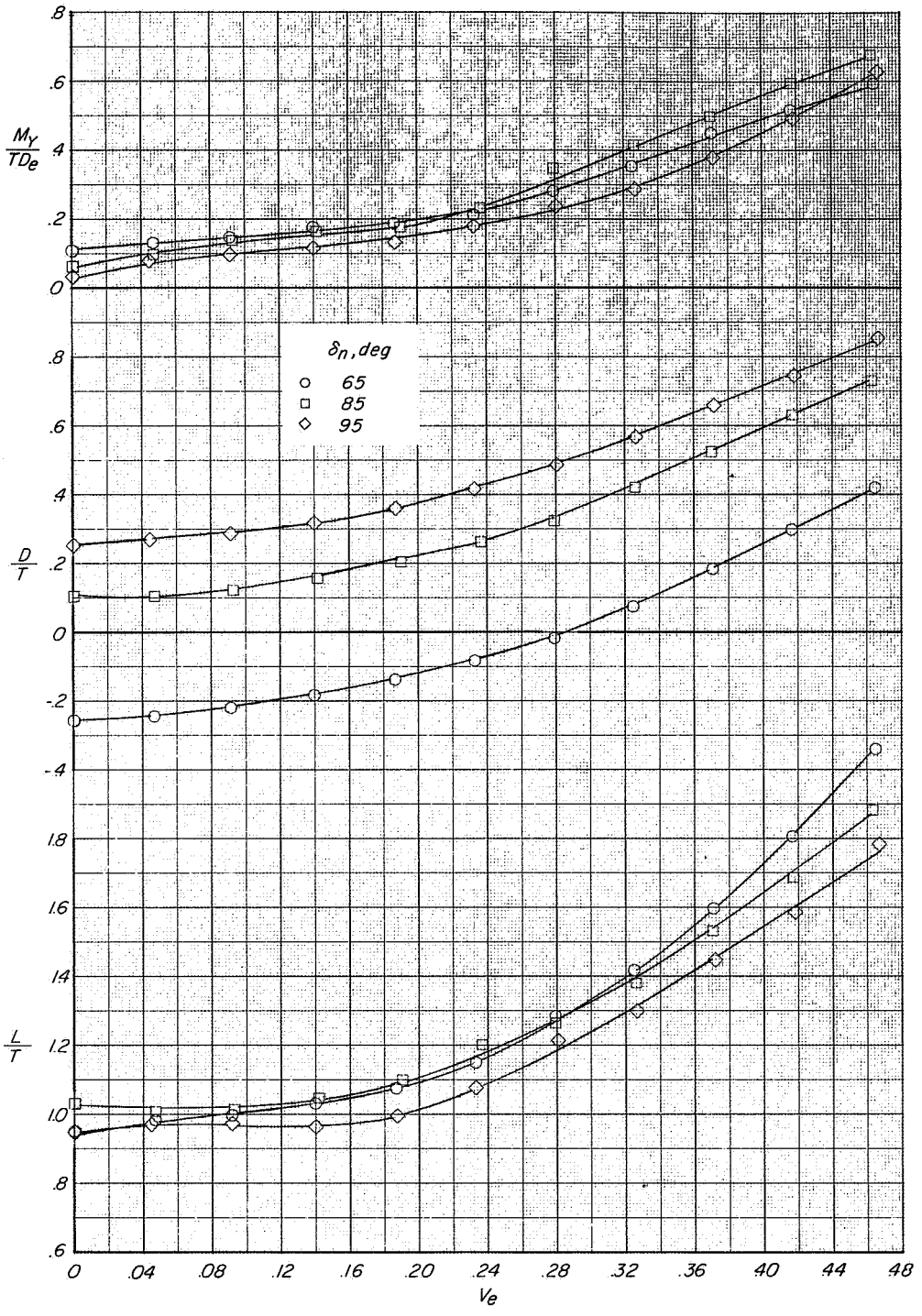

(c) Measured characteristics at $\alpha = 9^{o}$.

Figure 15.- Continued.

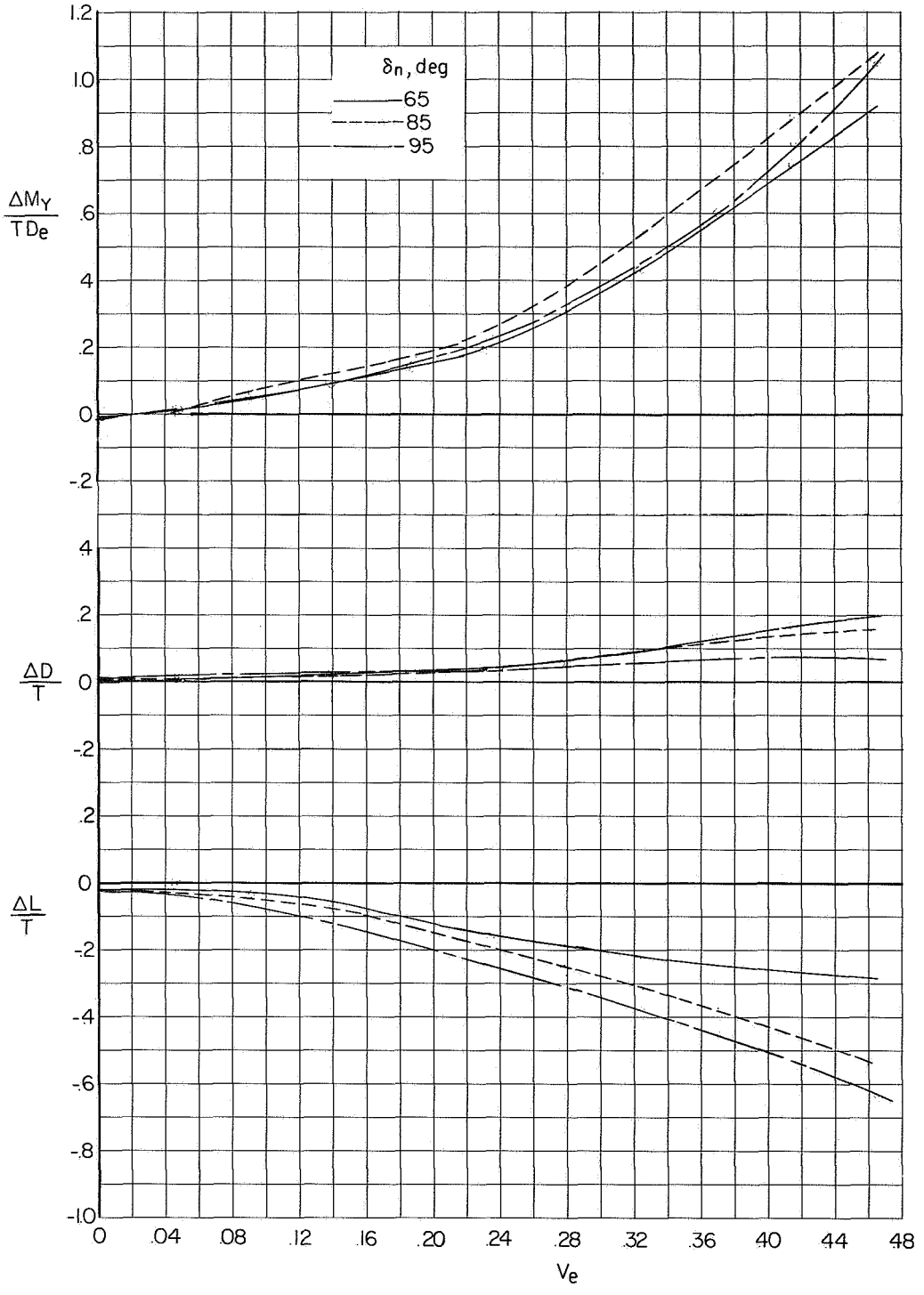

(d) Interference increments at $\alpha = 9^{o}$.

Figure 15.- Concluded.

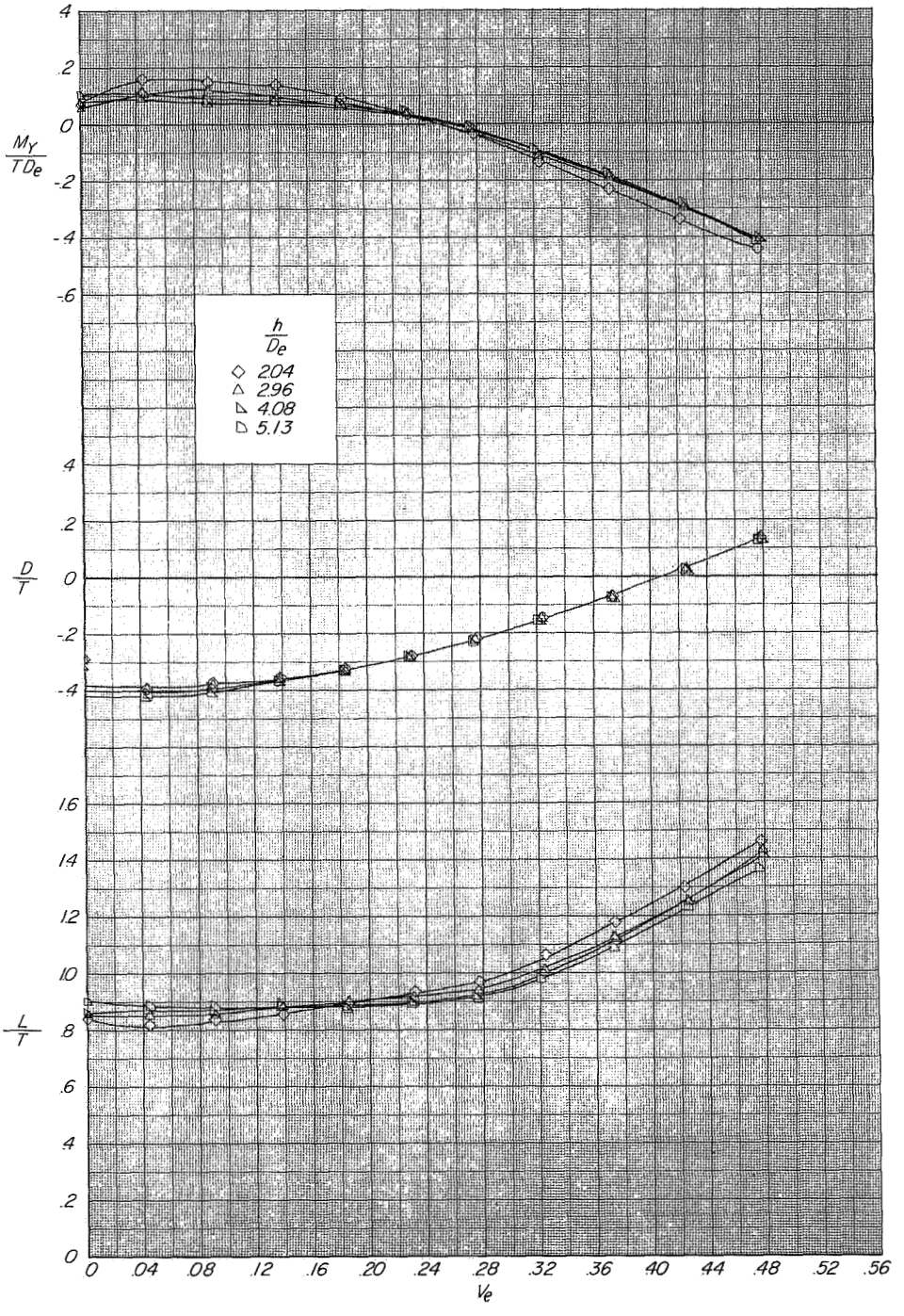

(a) Measured characteristics at $\alpha = 0^{o}$.

Figure 16.- Variation of longitudinal characteristics and interference increments with effective-velocity ratio showing effect of height above moving ground plane. $\delta_n = 65^{o}$; $\delta_f = 60^{o}$; horizontal tail off.

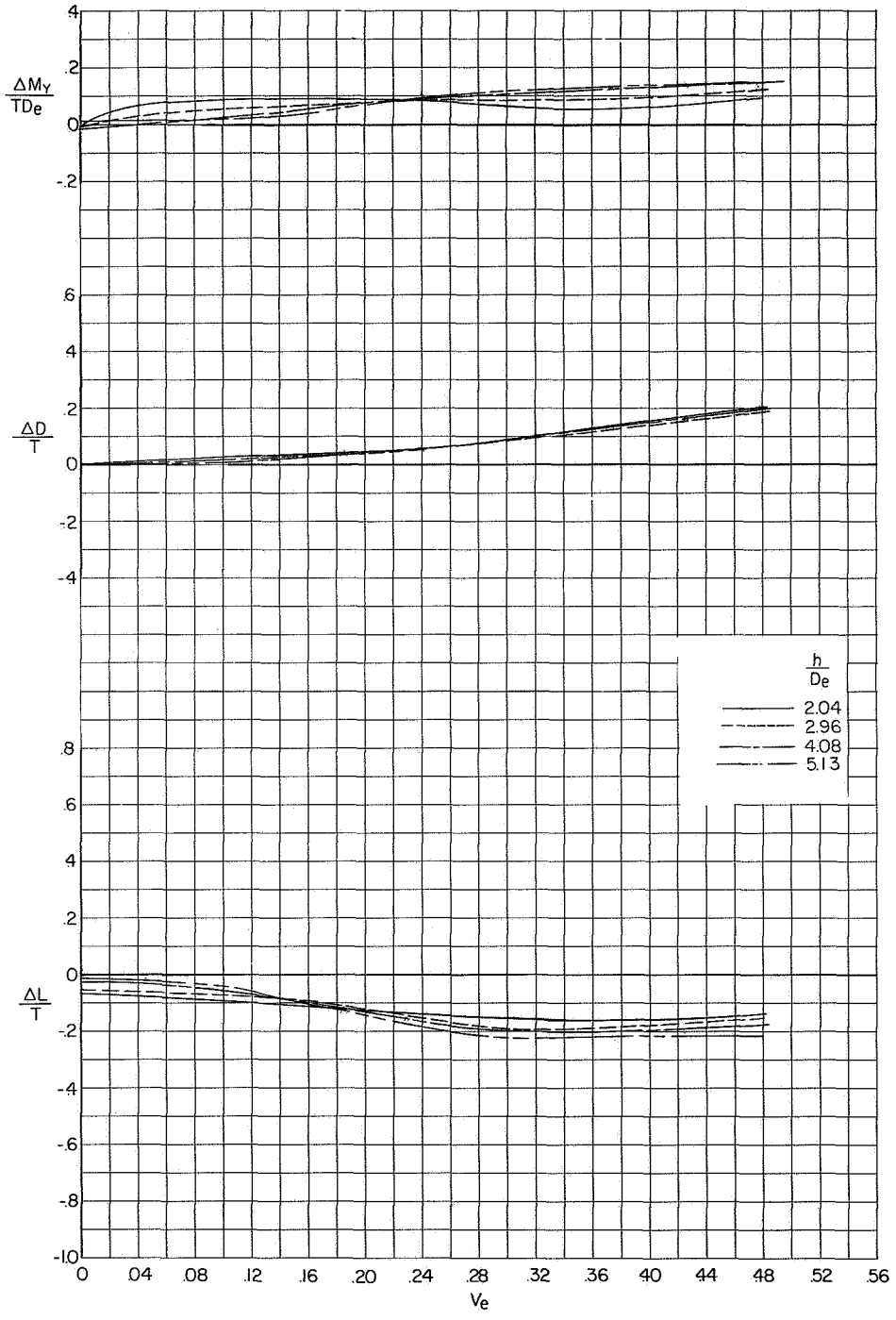

(b) Interference increments at $\alpha = 0^{o}$.

Figure 16.- Continued.

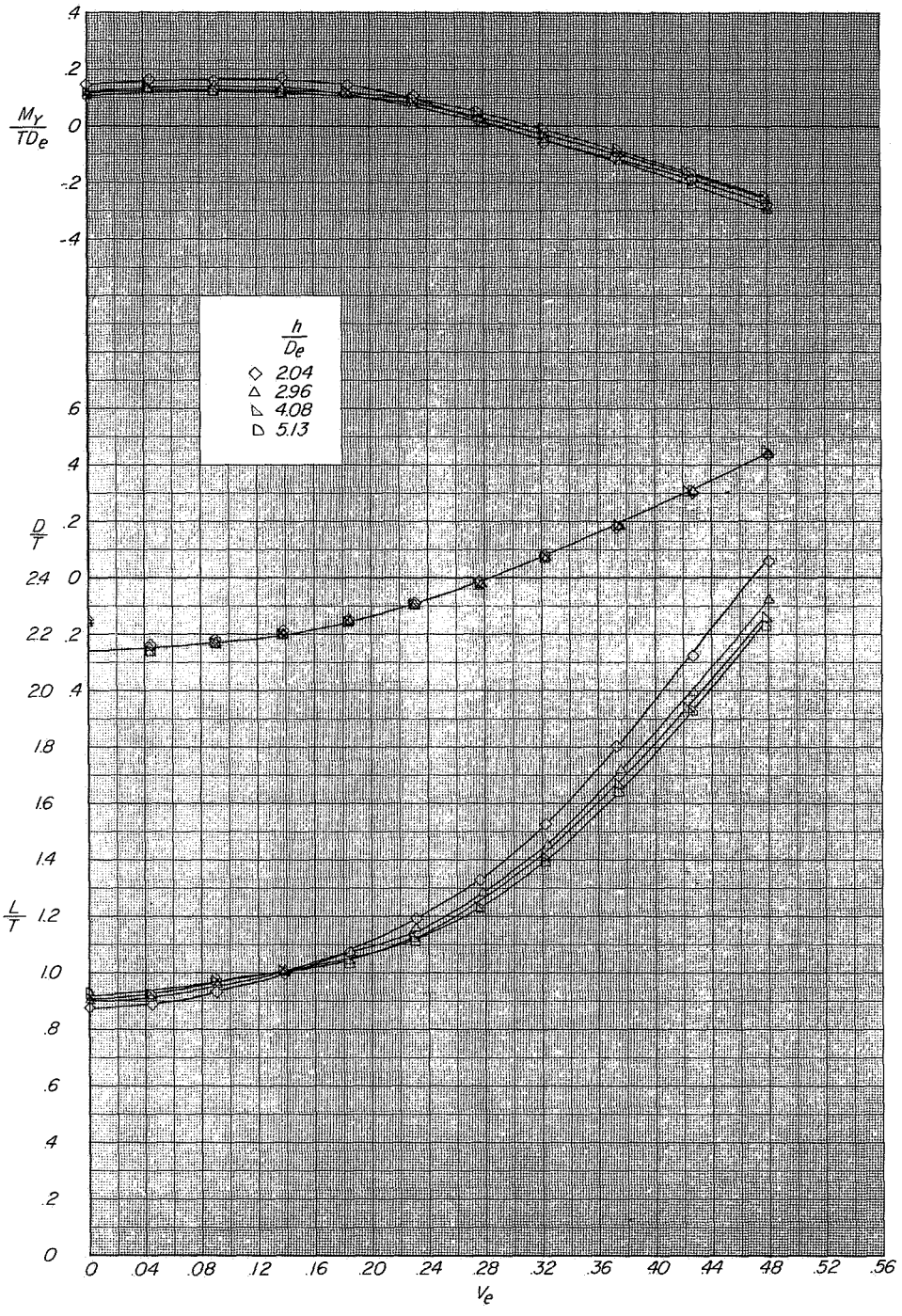

(c) Measured characteristics at $\alpha = 9^{o}$.

Figure 16.- Continued.

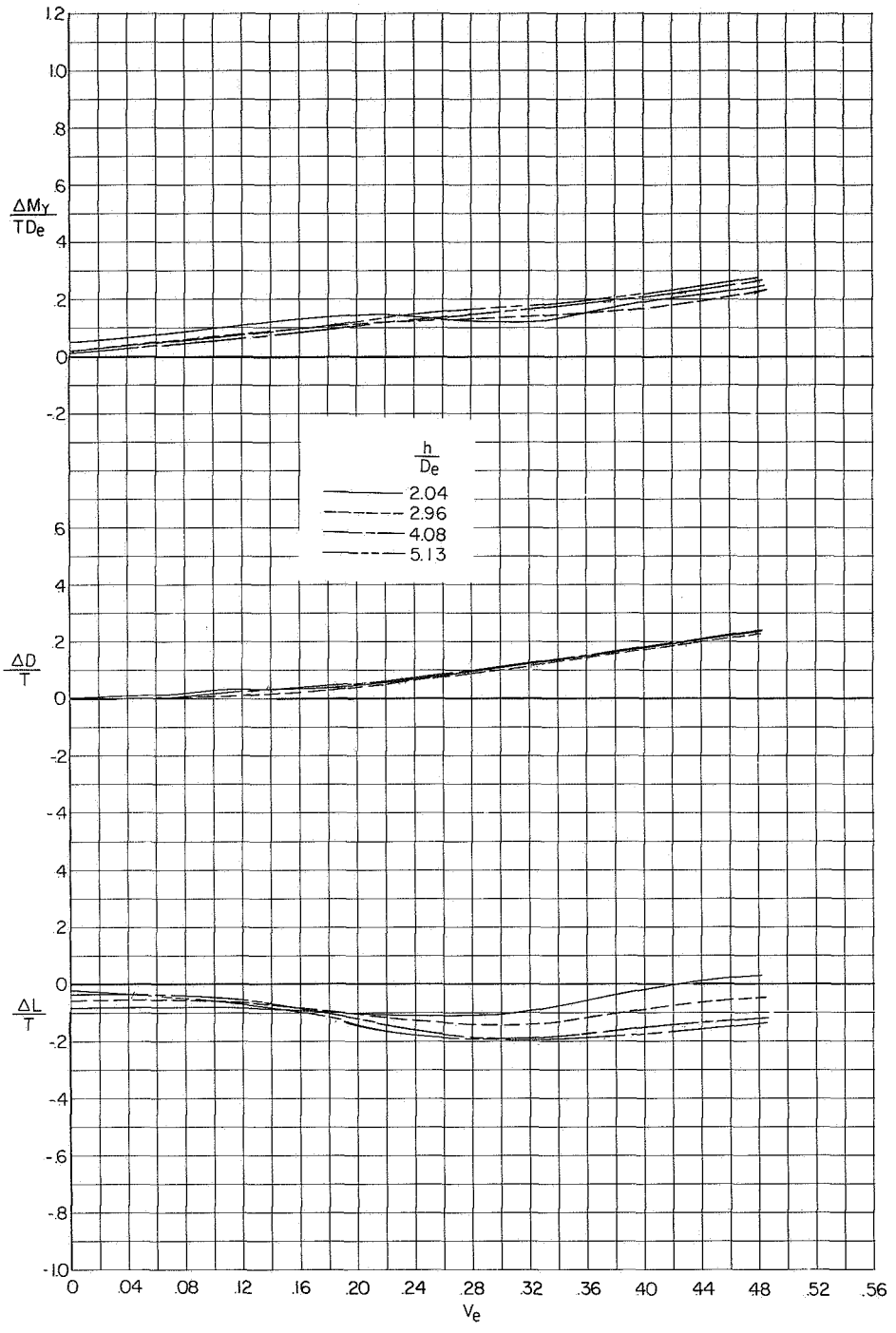

(d) Interference increments at $\alpha = 9^{o}$.

Figure 16.- Concluded.

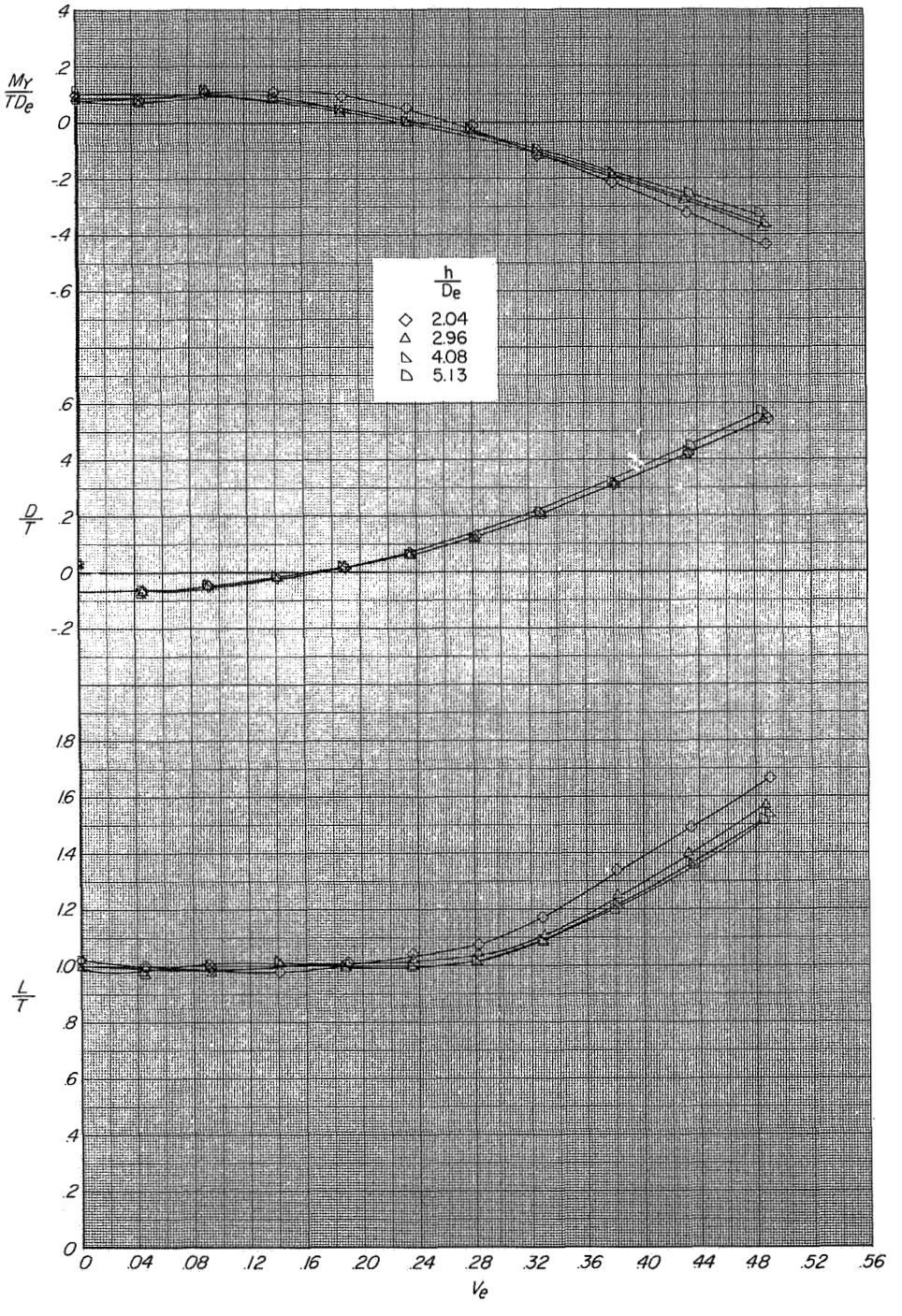

(a) Measured characteristics at $\alpha = 0^{o}$.

Figure 17.- Variation of longitudinal characteristics and interference increments with effective-velocity ratio showing effects of height above moving ground plane. $\delta_n = 85^{o}$; $\delta_f = 60^{o}$; horizontal tail off.

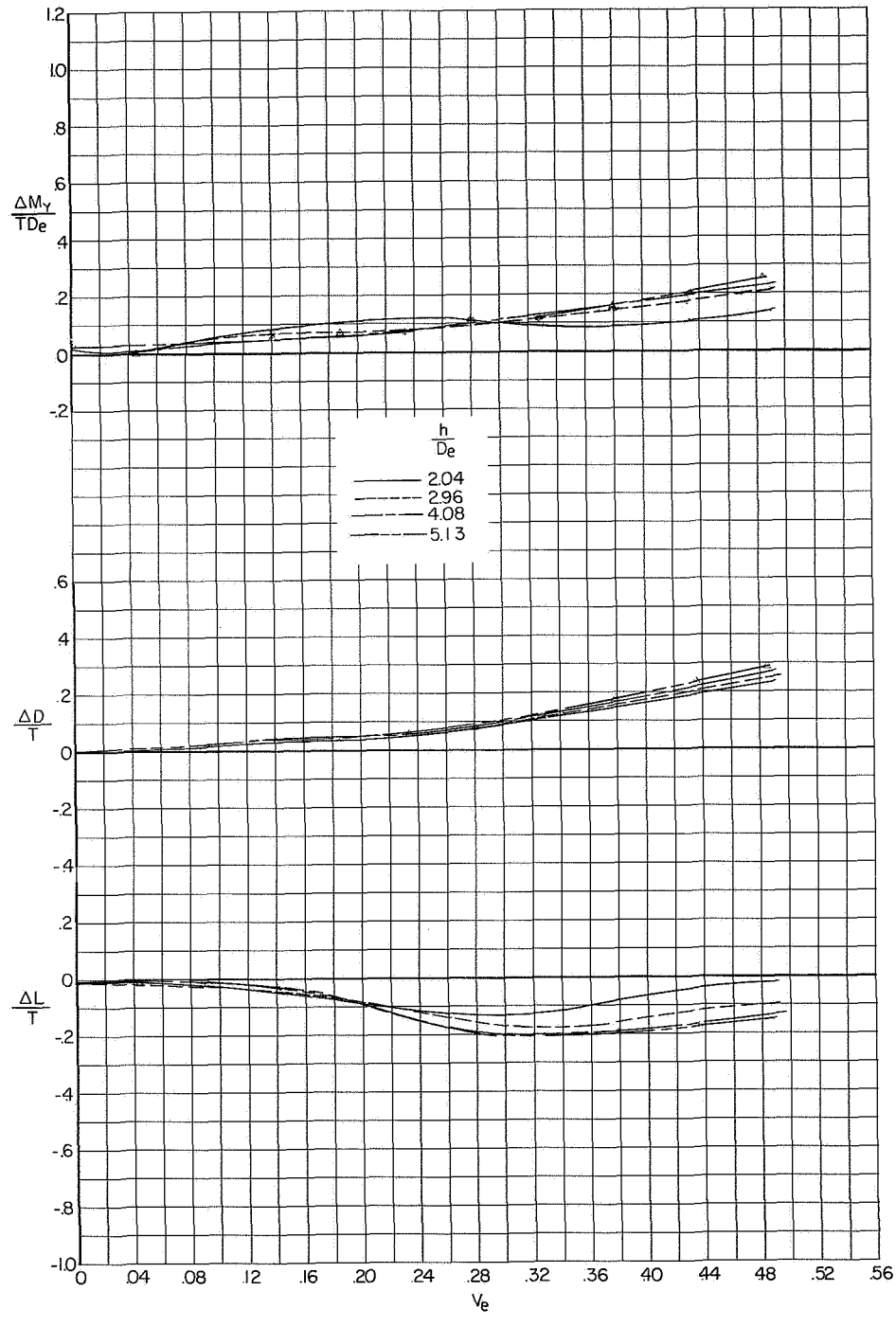

(b) Interference increments at $\alpha = 0^{o}$.

Figure 17.- Continued.

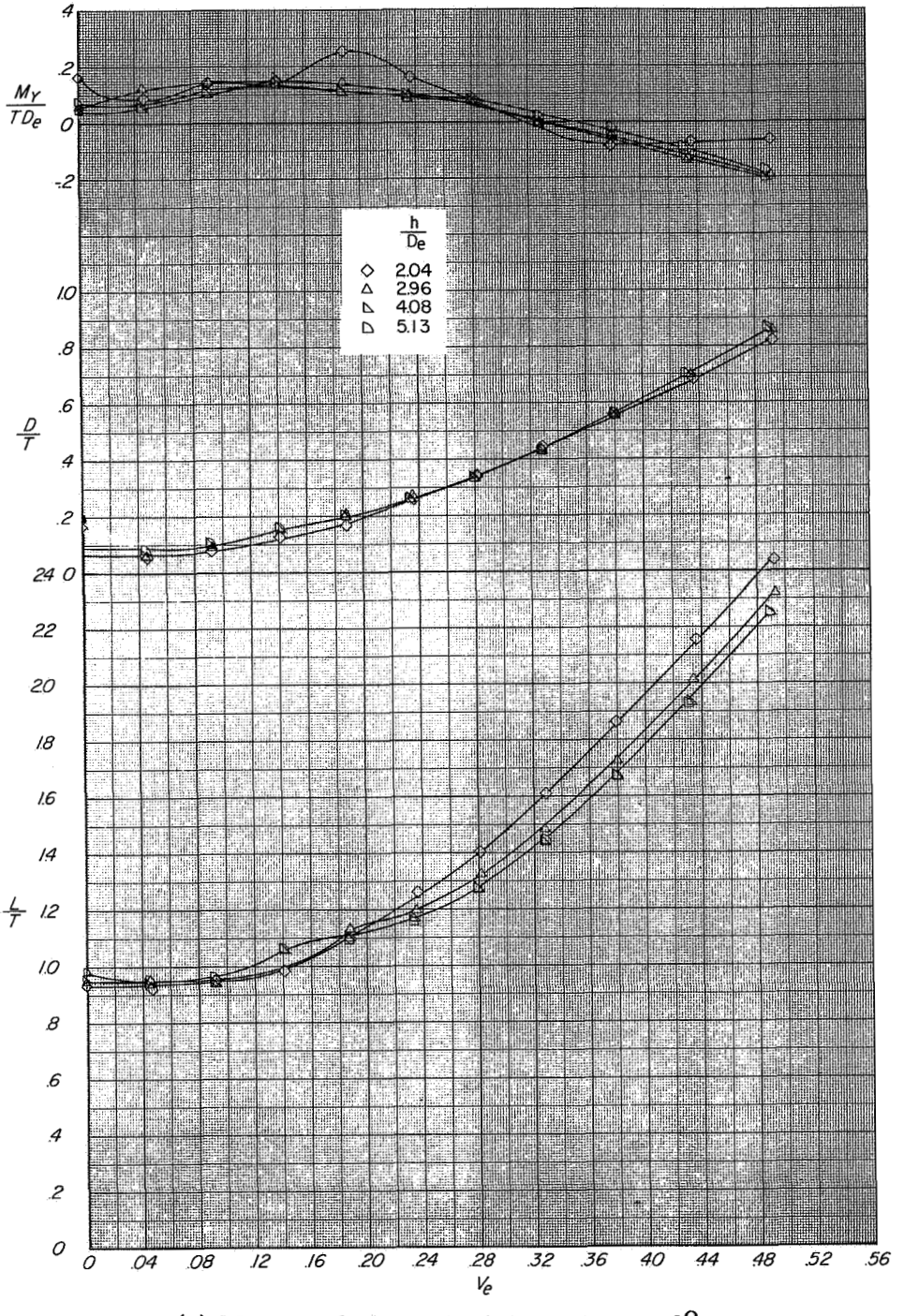

(c) Measured characteristics at $\alpha = 9^{O}$.

Figure 17.- Continued.

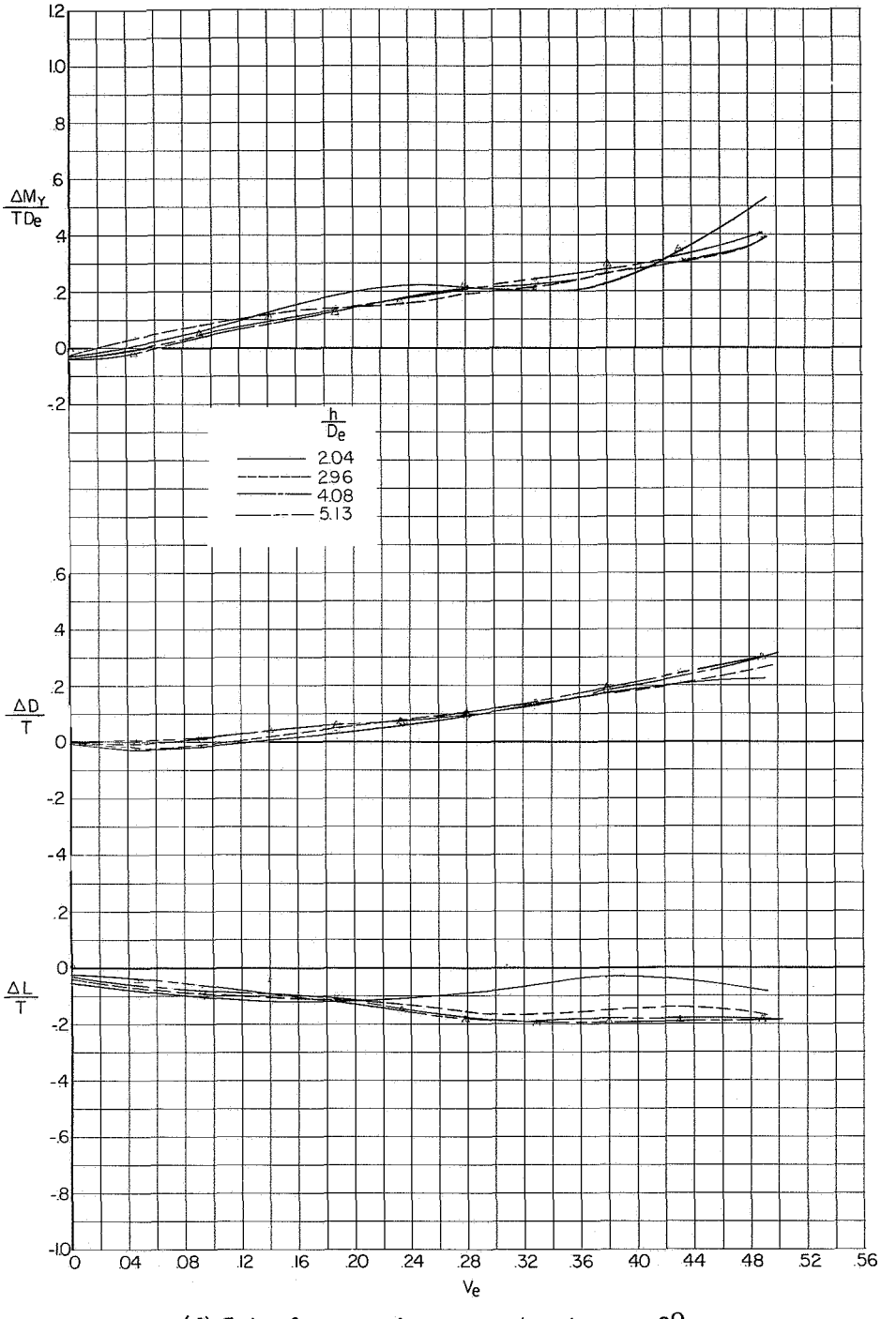

(d) Interference increments at $\alpha = 9^{o}$.

Figure 17.- Concluded.

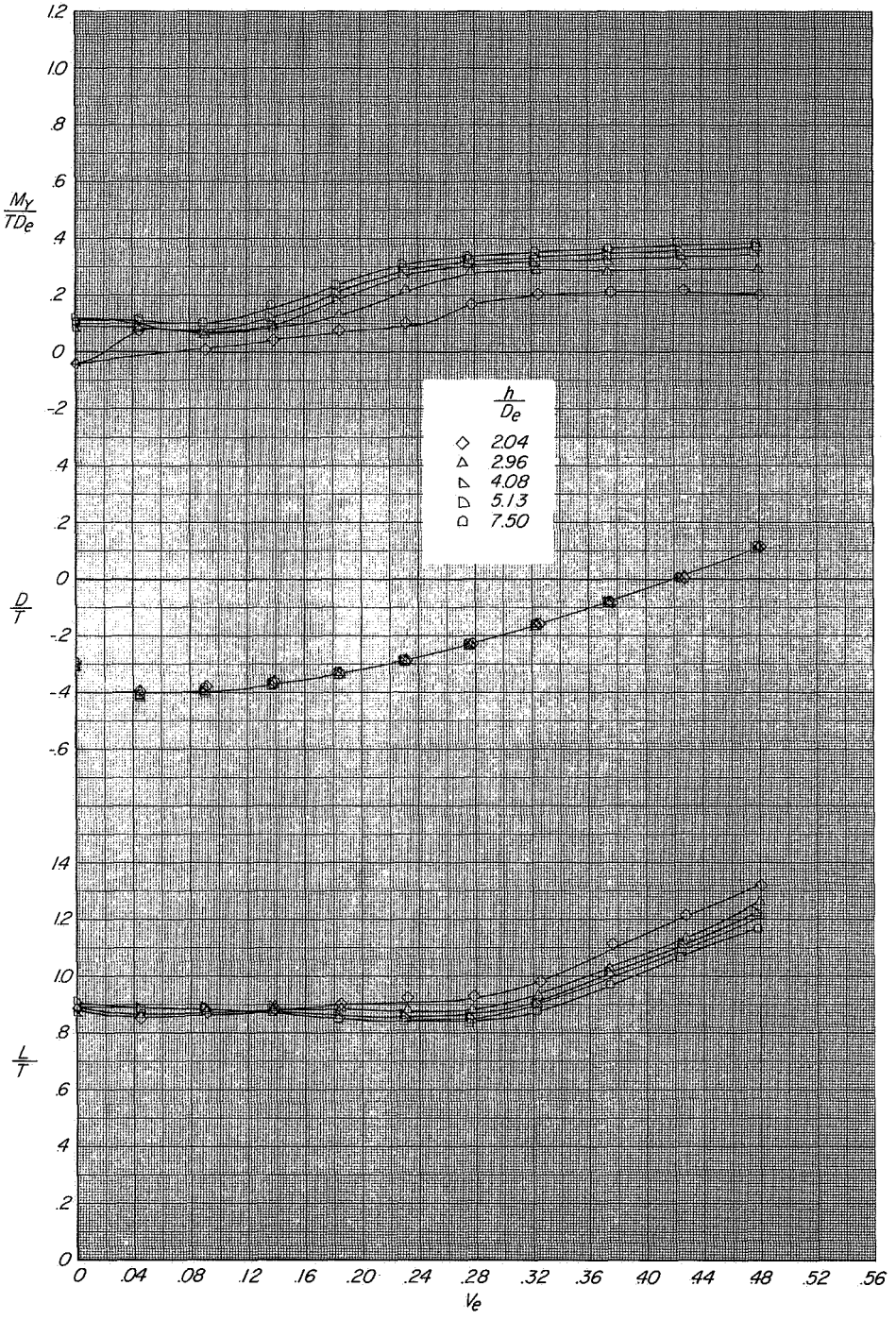

(a) Measured characteristics at $\alpha = 0^{o}$.

Figure 18.- Variation of longitudinal characteristics and interference increments with effective-velocity ratio showing effect of height above moving ground plane. $\delta_n = 65^{o}$; $\delta_f = 60^{o}$; $i_t = 0^{o}$.

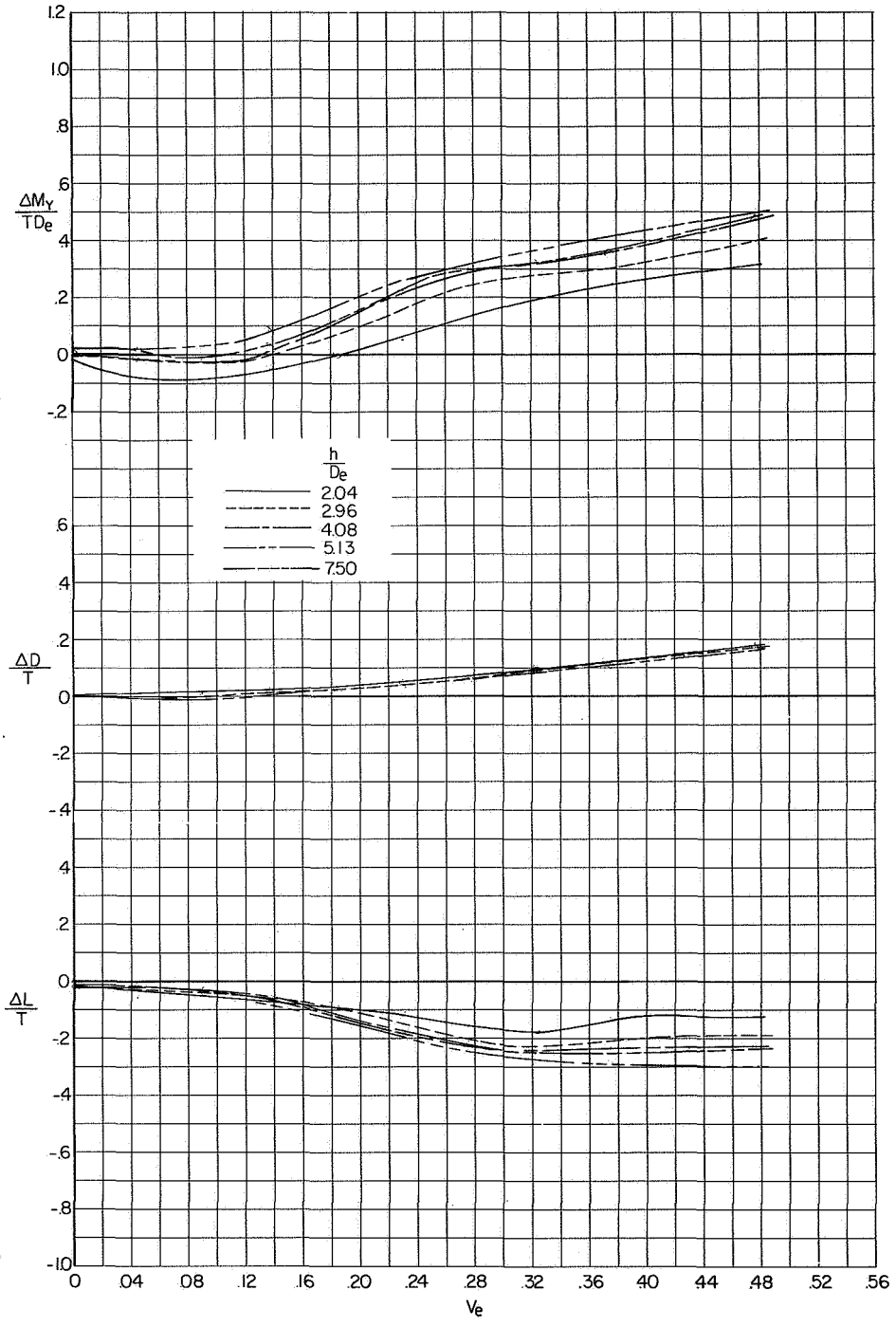

(b) Interference increments at $\alpha = 0^{o}$.

Figure 18.- Continued.

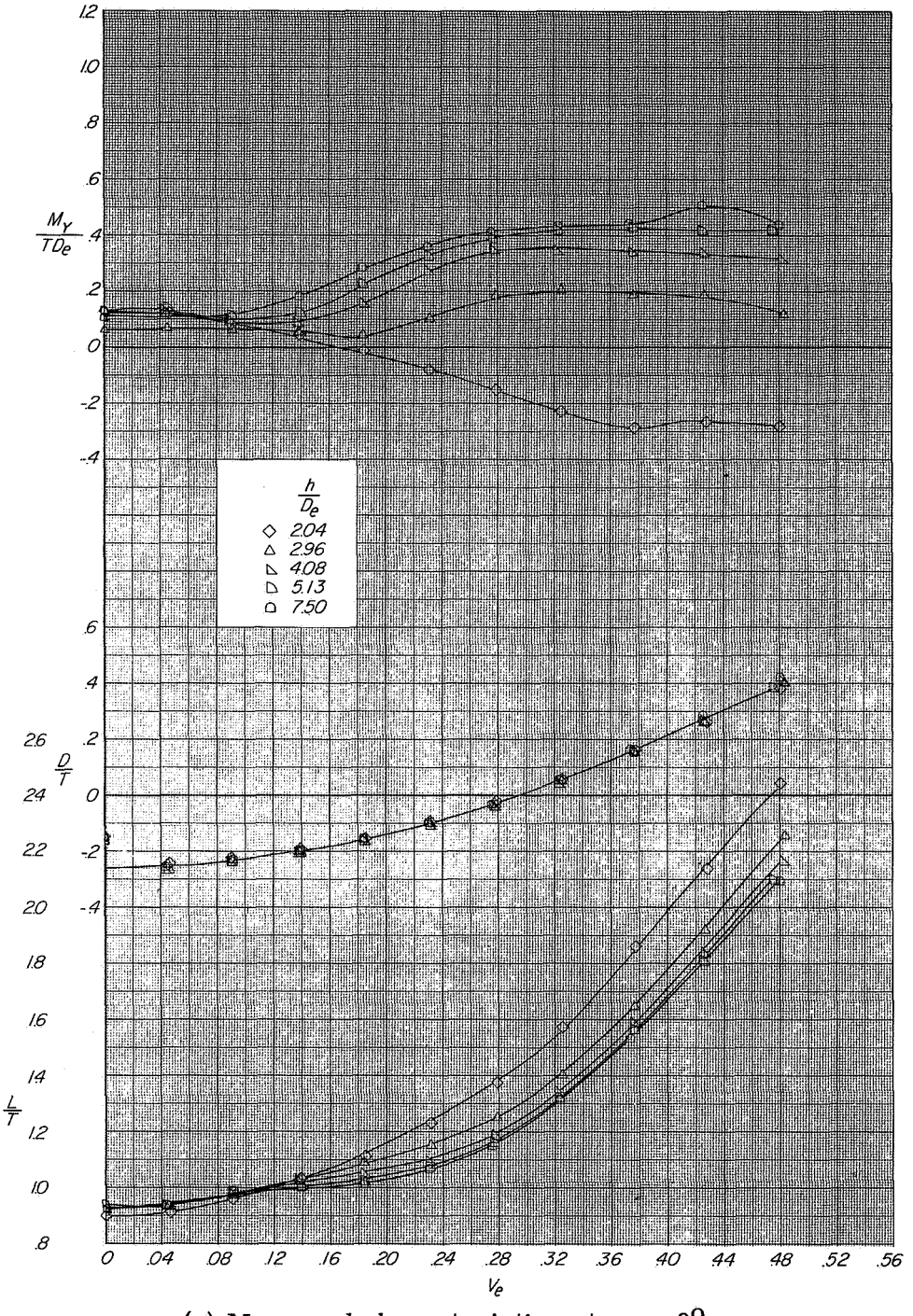

(c) Measured characteristics at $\alpha = 9^{o}$.

Figure 18.- Continued.

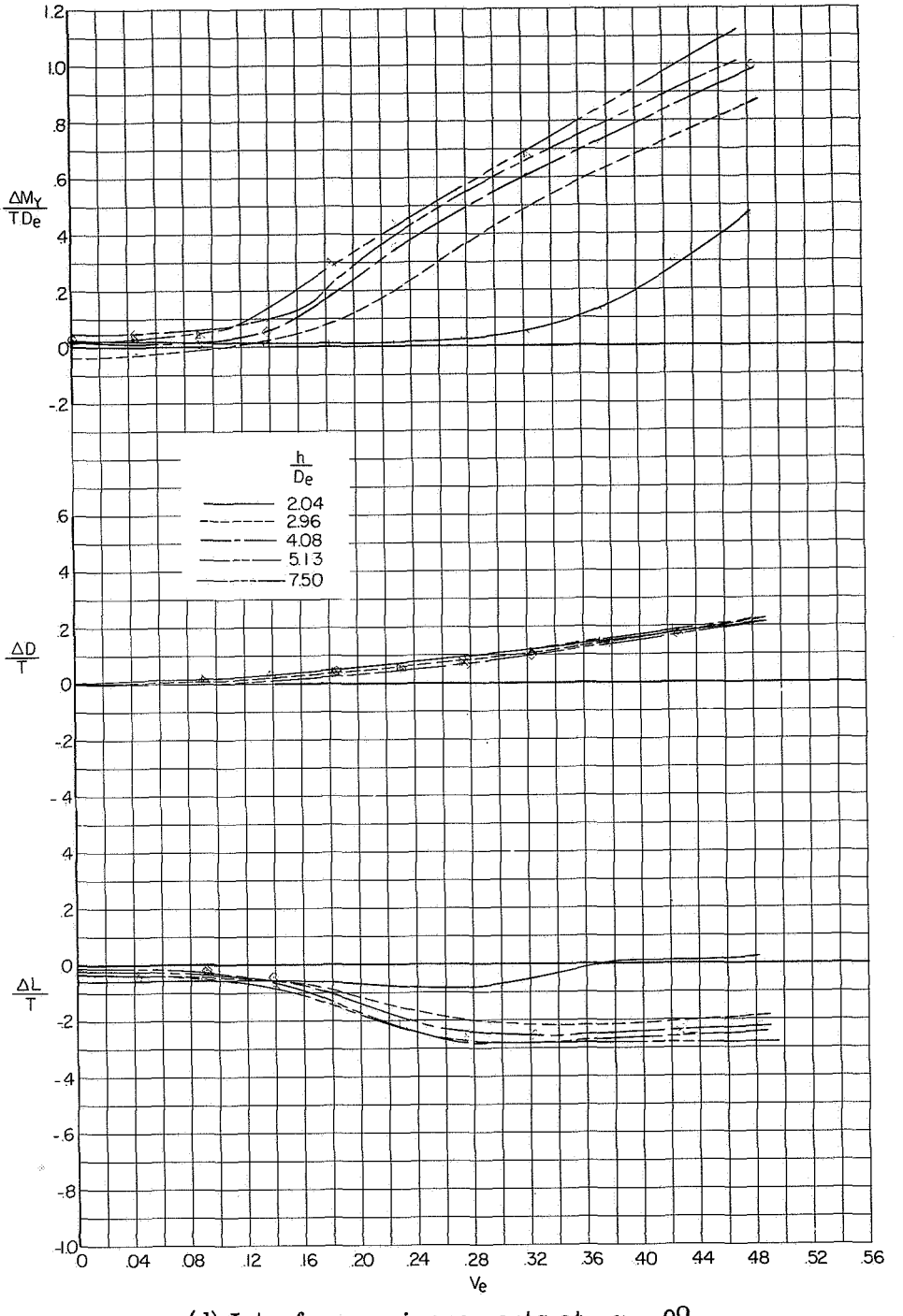

(d) Interference increments at $\alpha = 9^{o}$.

Figure 18.- Concluded.

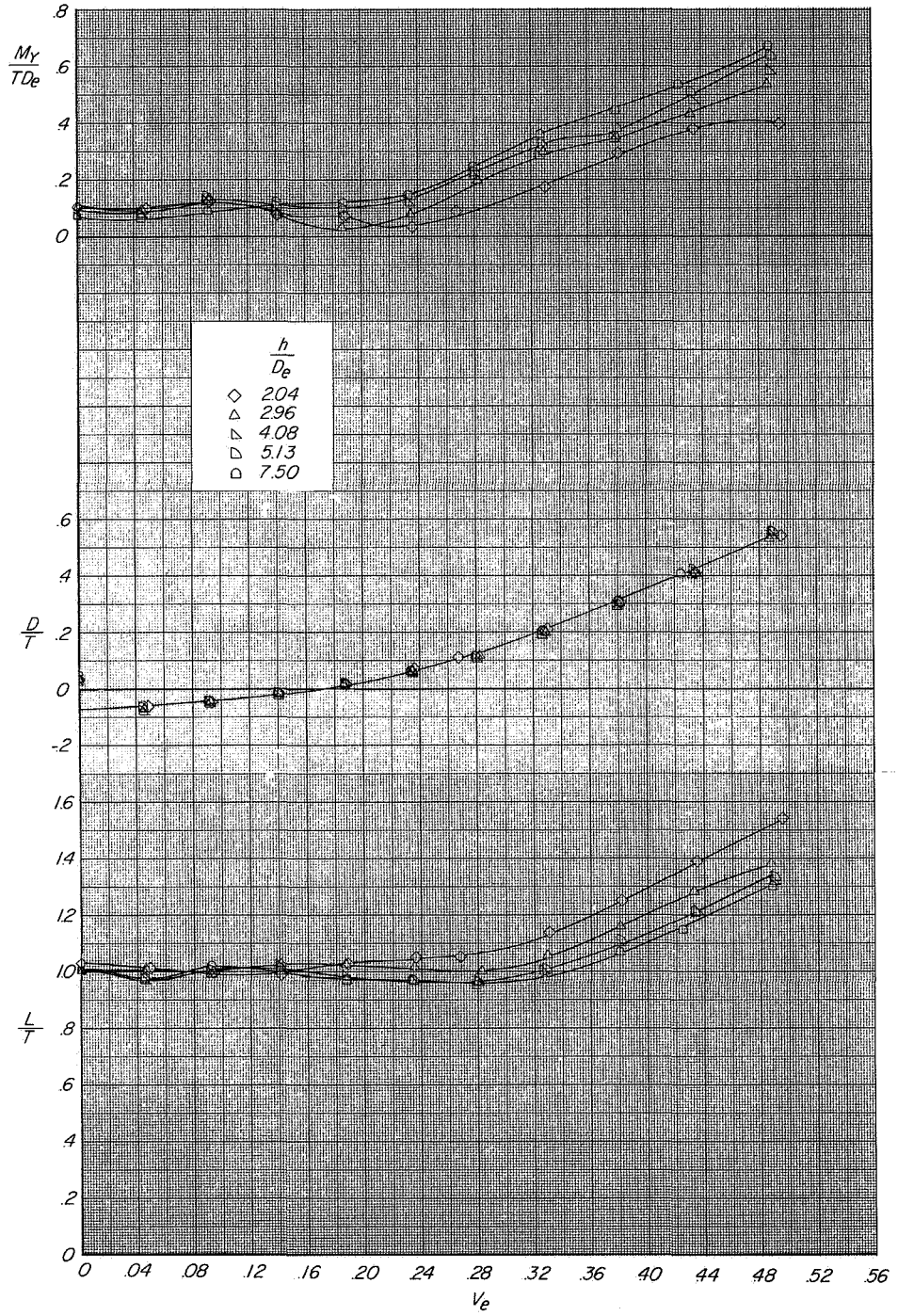

(a) Measured characteristics at $\alpha = 0^{o}$.

Figure 19.- Variation of longitudinal characteristics and interference increments with effective-velocity ratio showing effect of height above moving ground plane. $\delta_n = 85^{o}$; $\delta_f = 60^{o}$; $i_t = 0^{o}$.

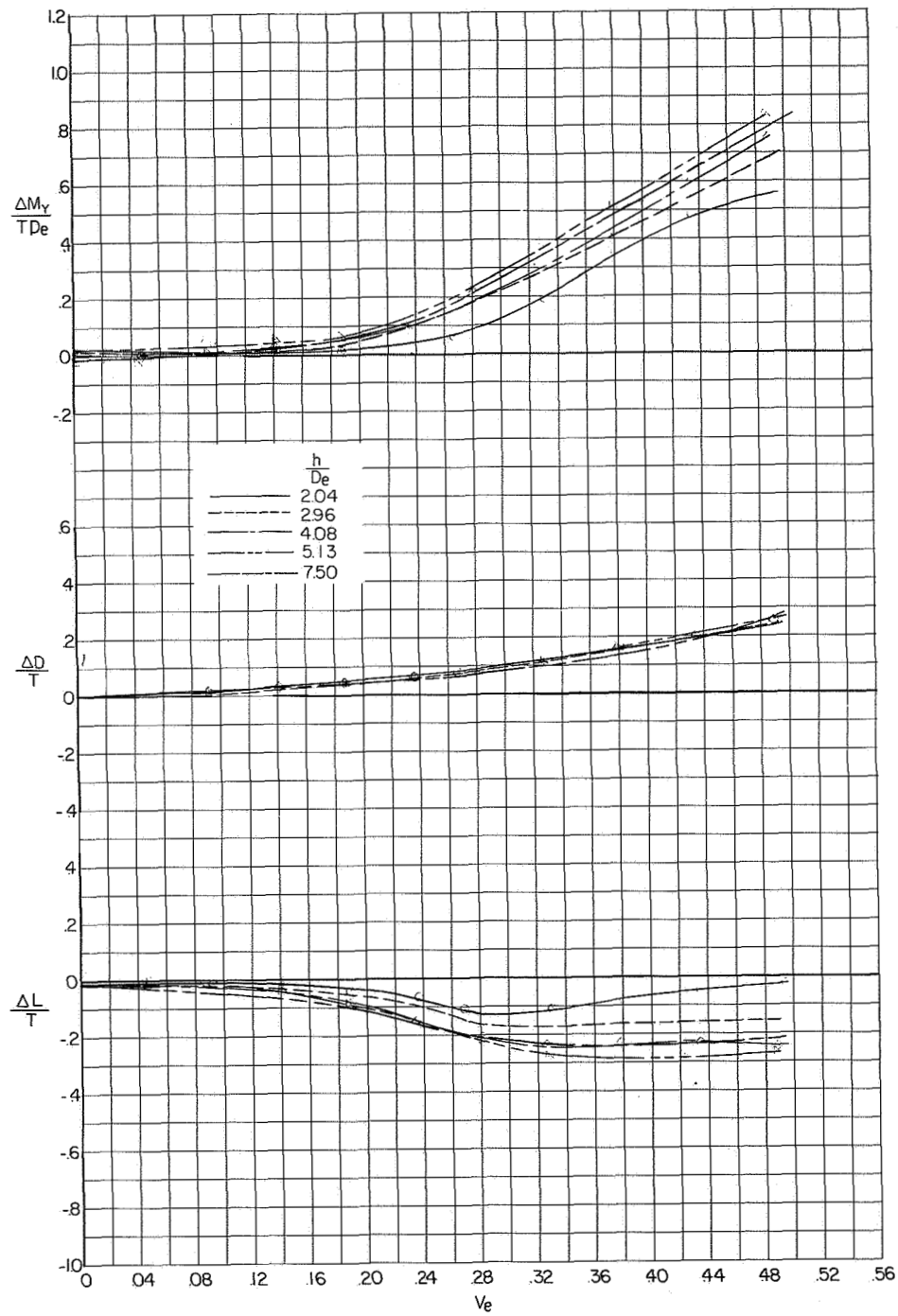

(b) Interference increments at $\alpha = 0^{o}$.

Figure 19.- Continued.

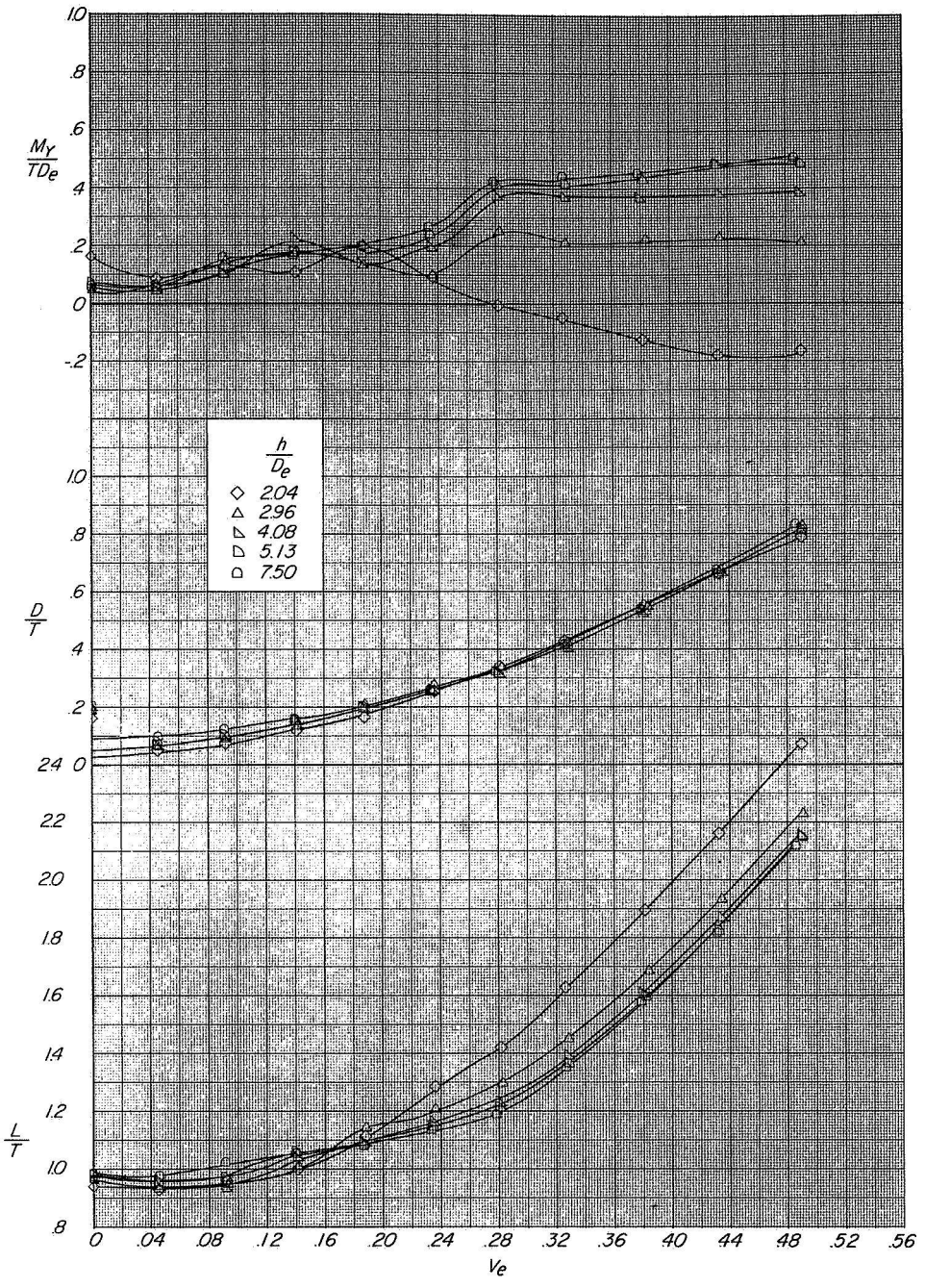

(c) Measured characteristics at $\alpha = 9^{o}$.

Figure 19.- Continued.

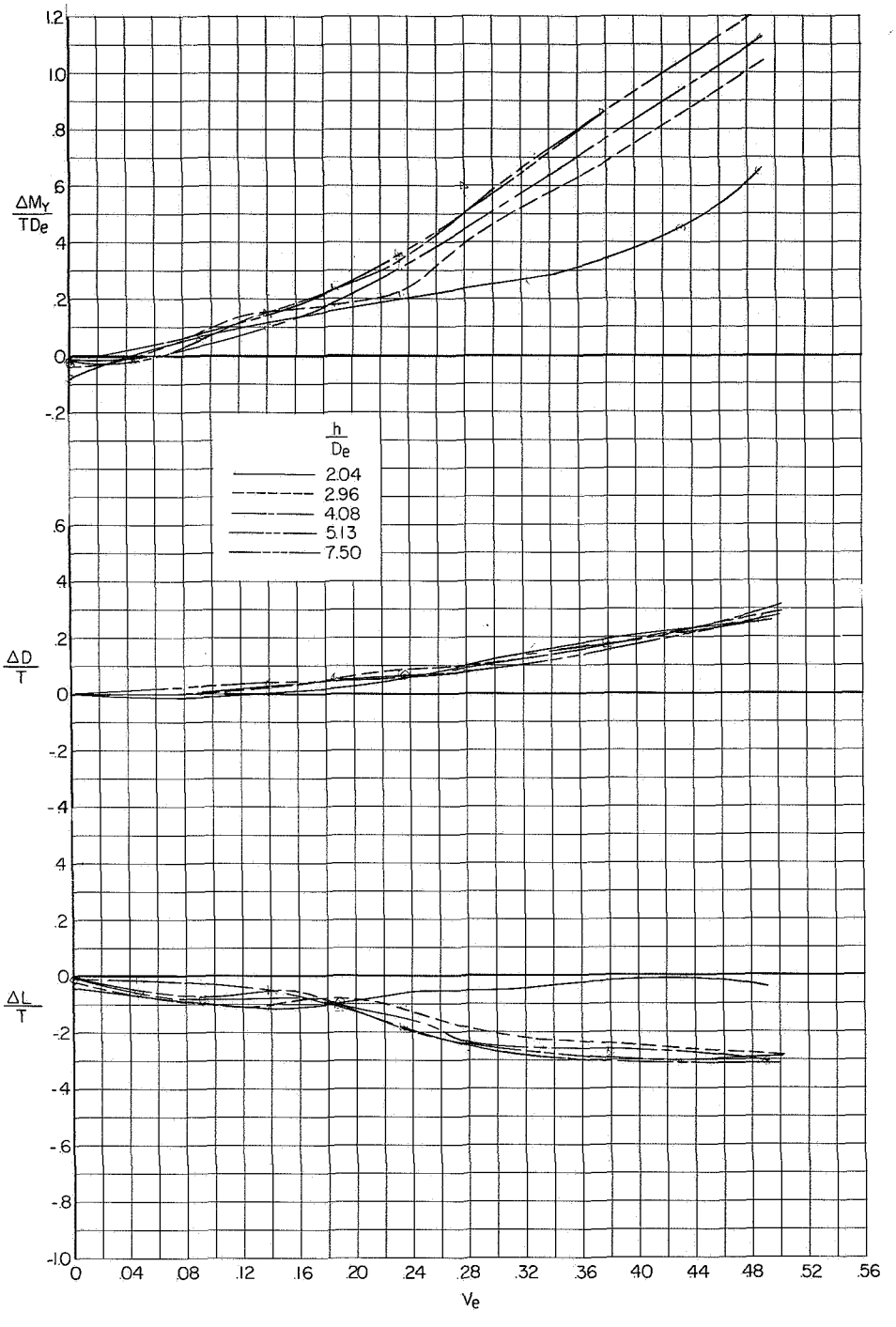

(d) Interference increments at $\alpha = 9^{o}$.

Figure 19.- Concluded.

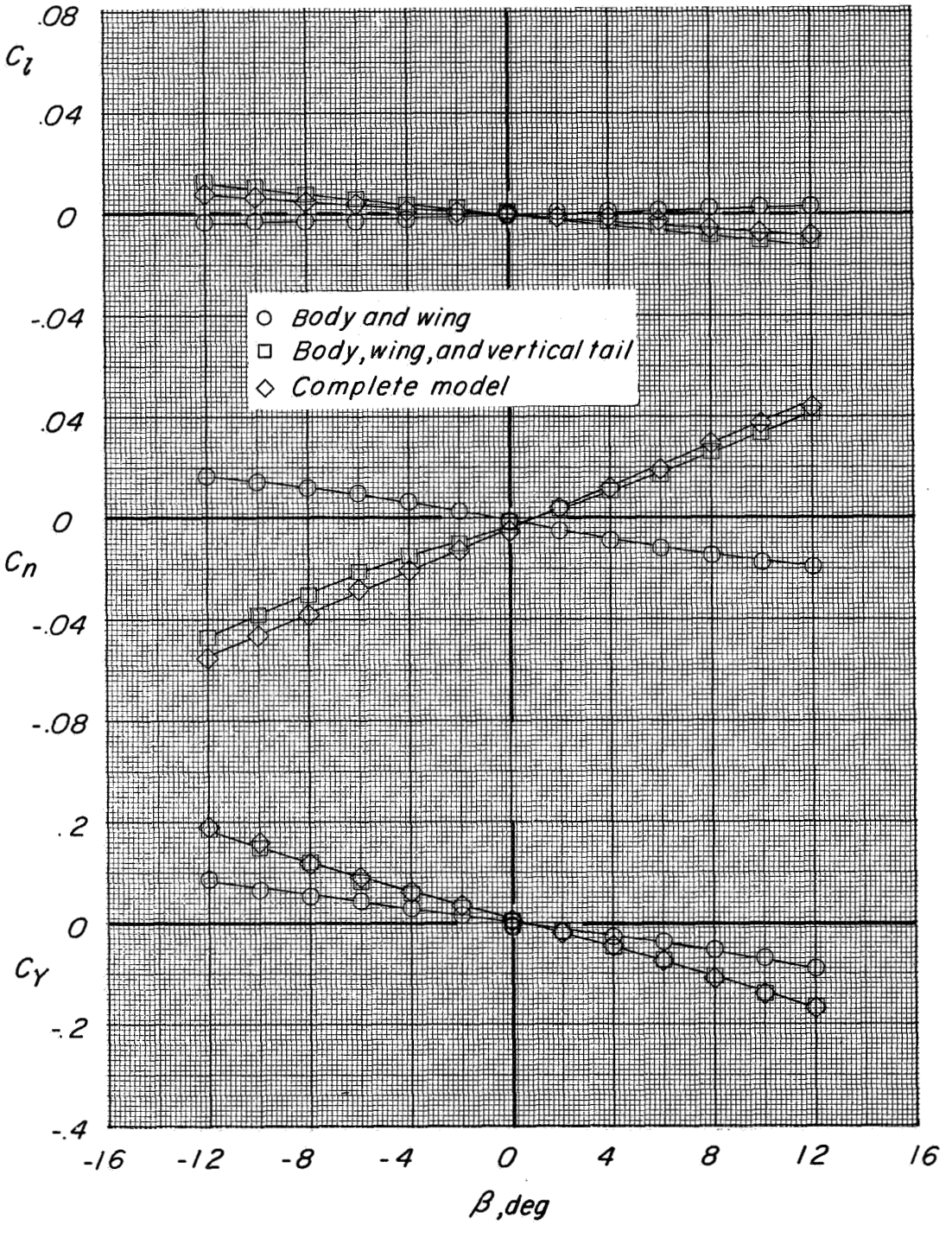

(a) $C_T = 0$.

Figure 20.- Characteristics of model in sideslip showing contributions of major components. Cruise configuration. $\delta_f = 0^o$; $\delta_n = 0^o$; landing gear up.

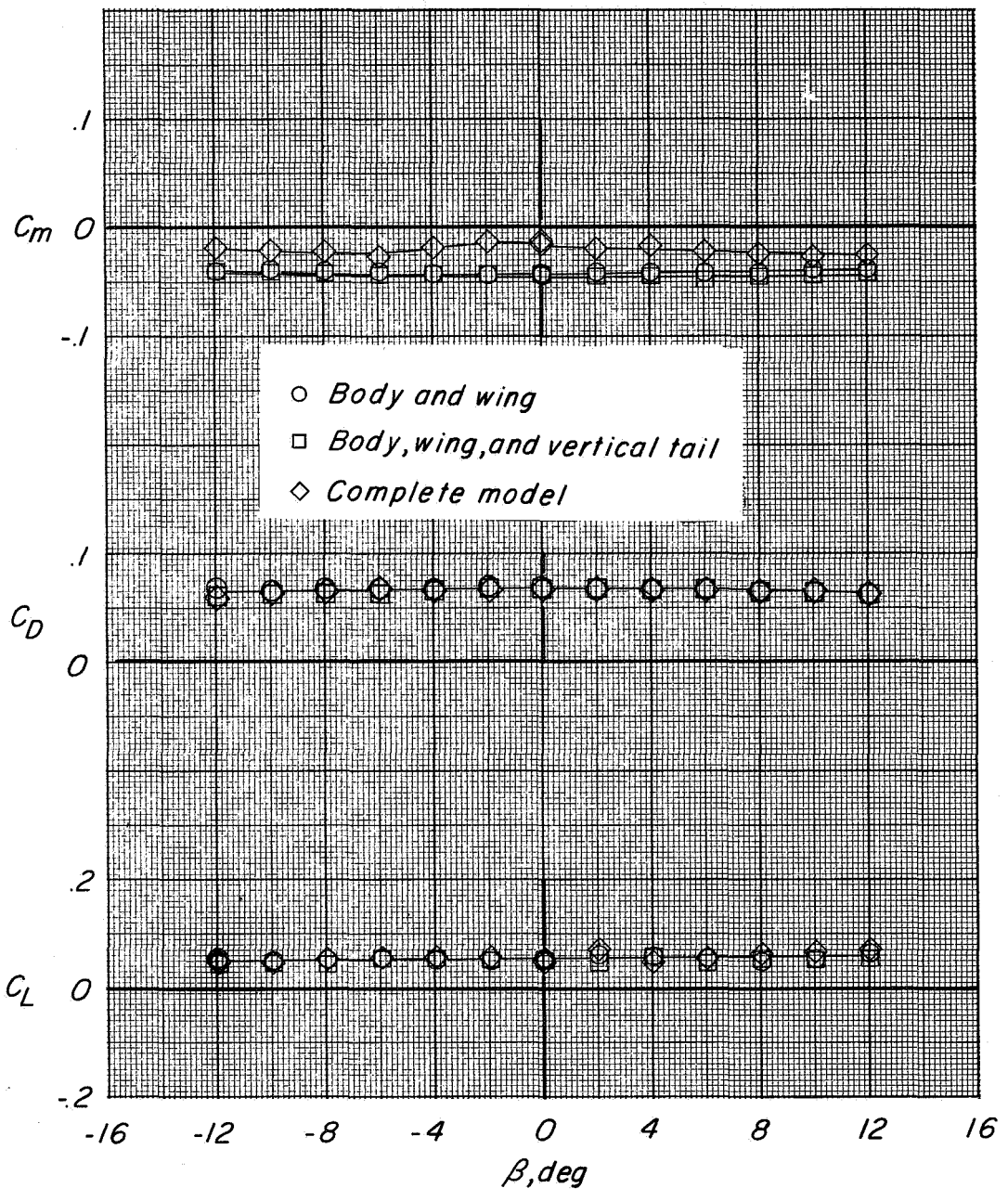

(a) Concluded.

Figure 20.- Continued.

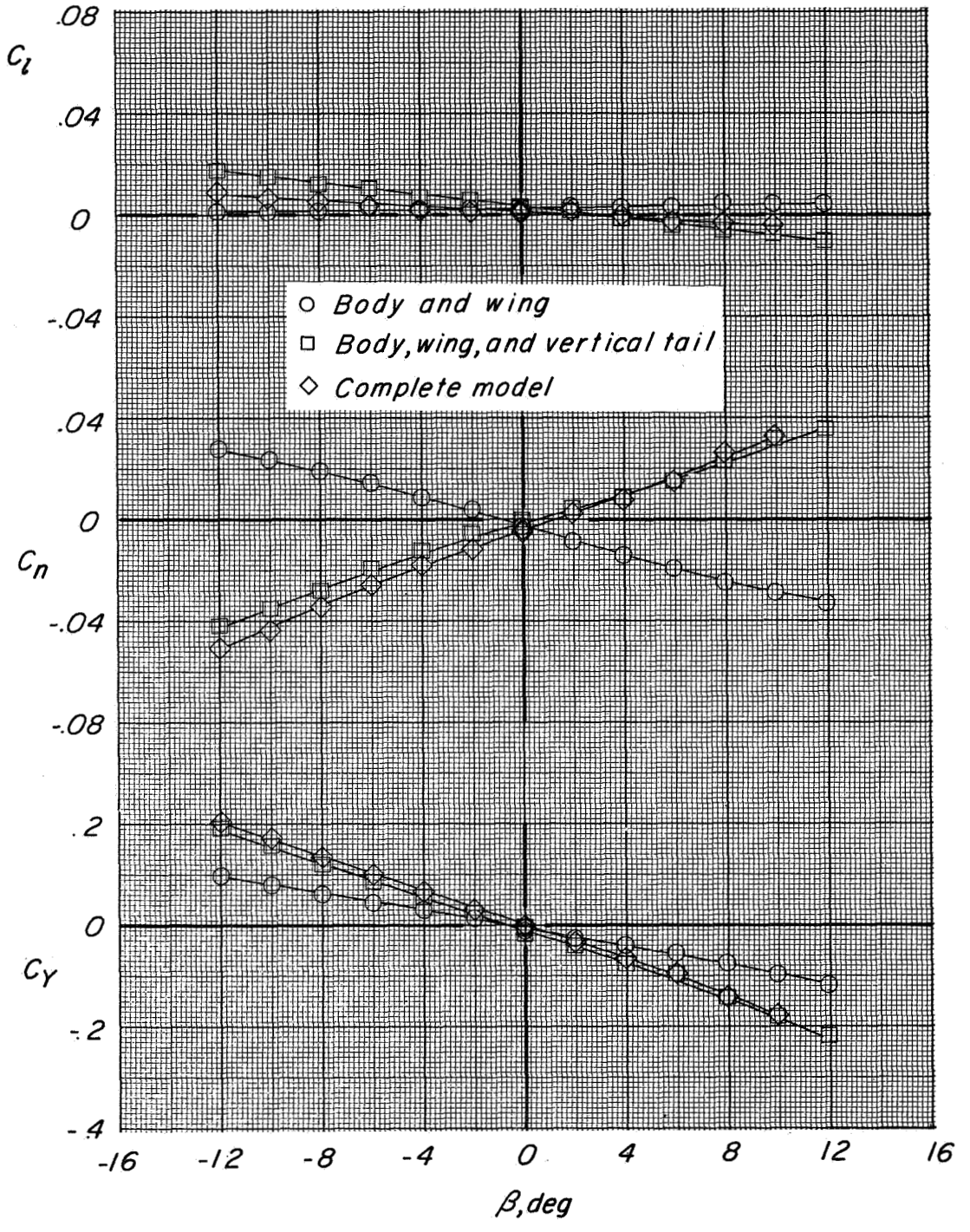

(b) $C_T = 0.6$.

Figure 20.- Continued.

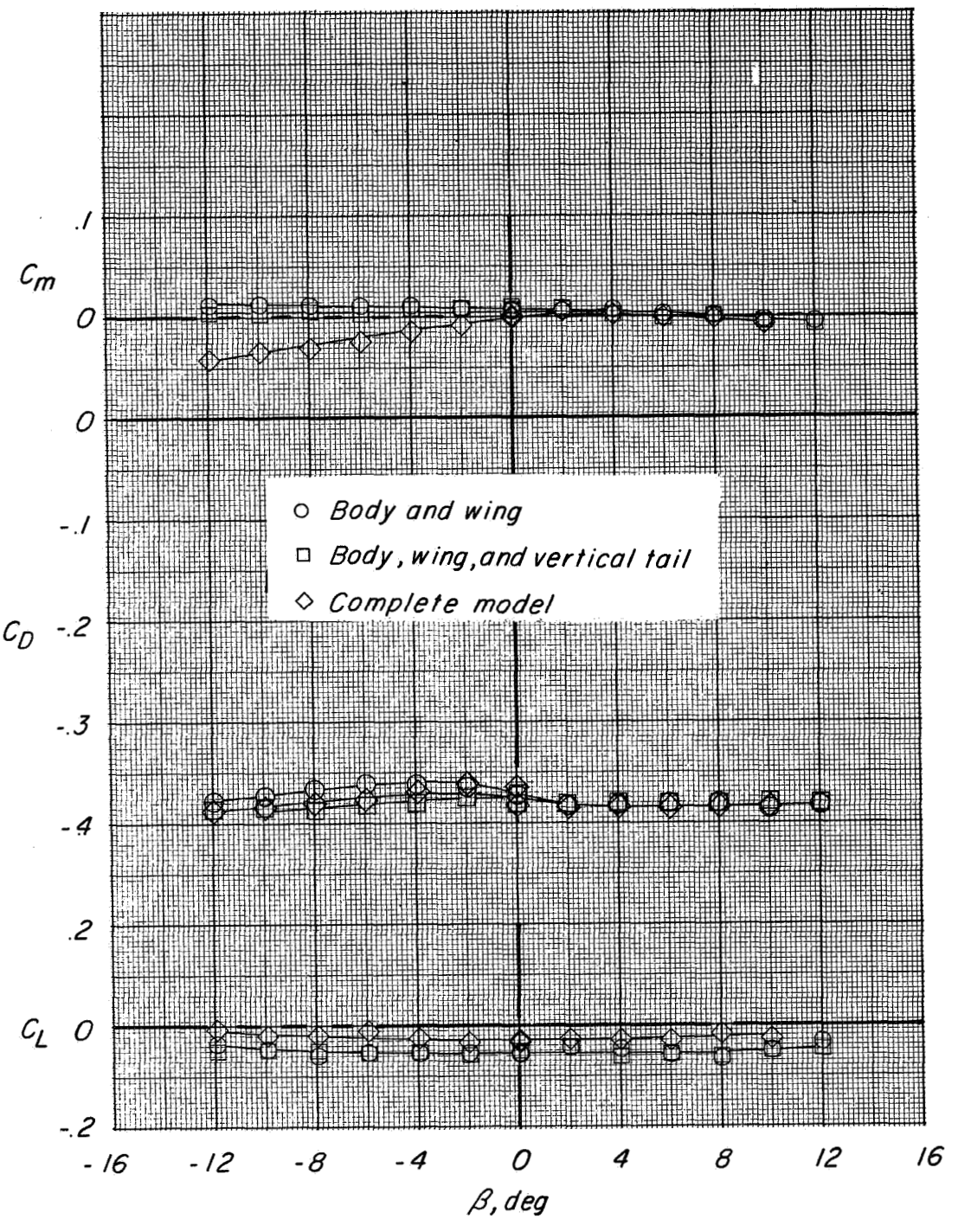

(b) Concluded.

Figure 20.- Continued.

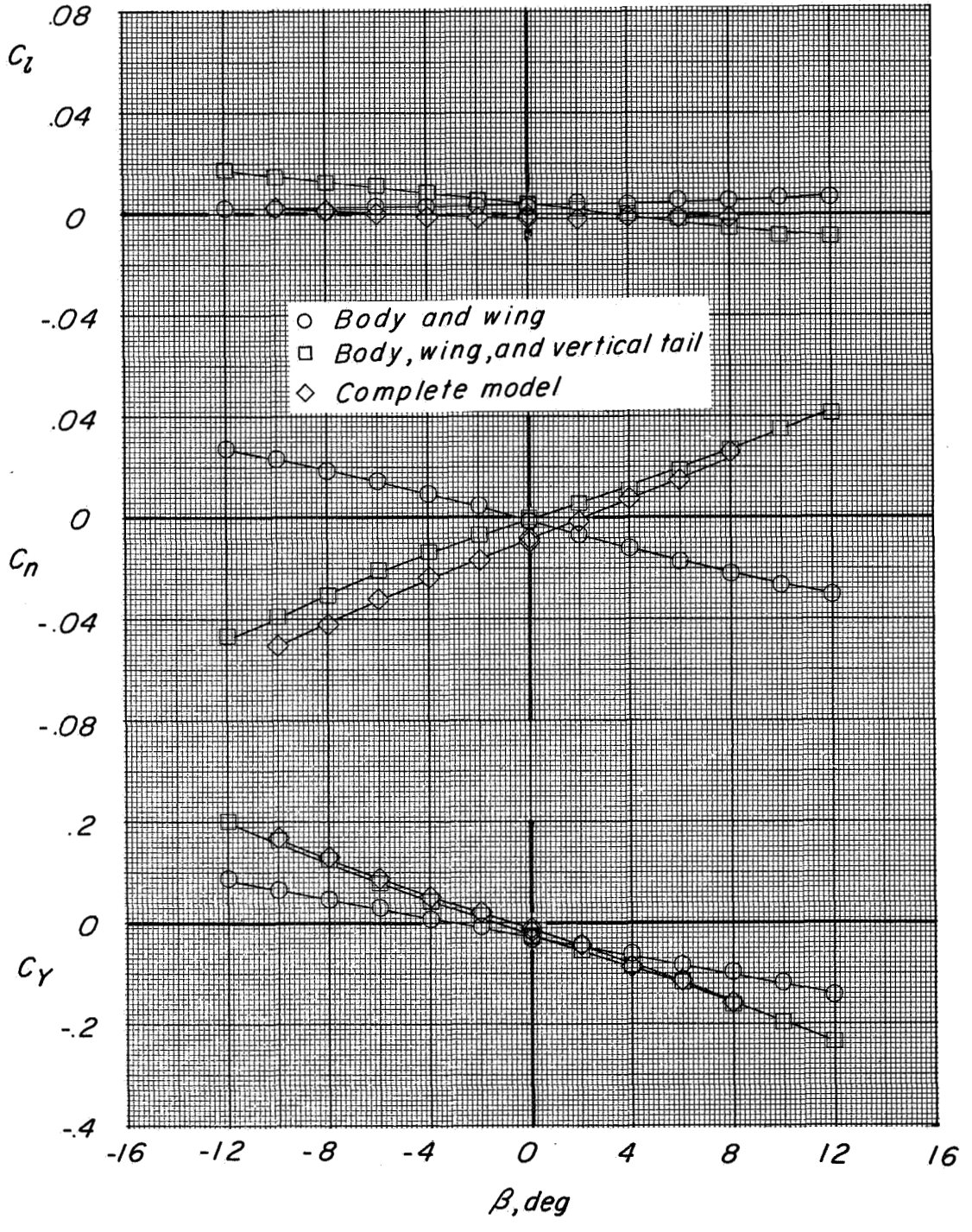

(c) $C_T = 1.1$.

Figure 20.- Continued.

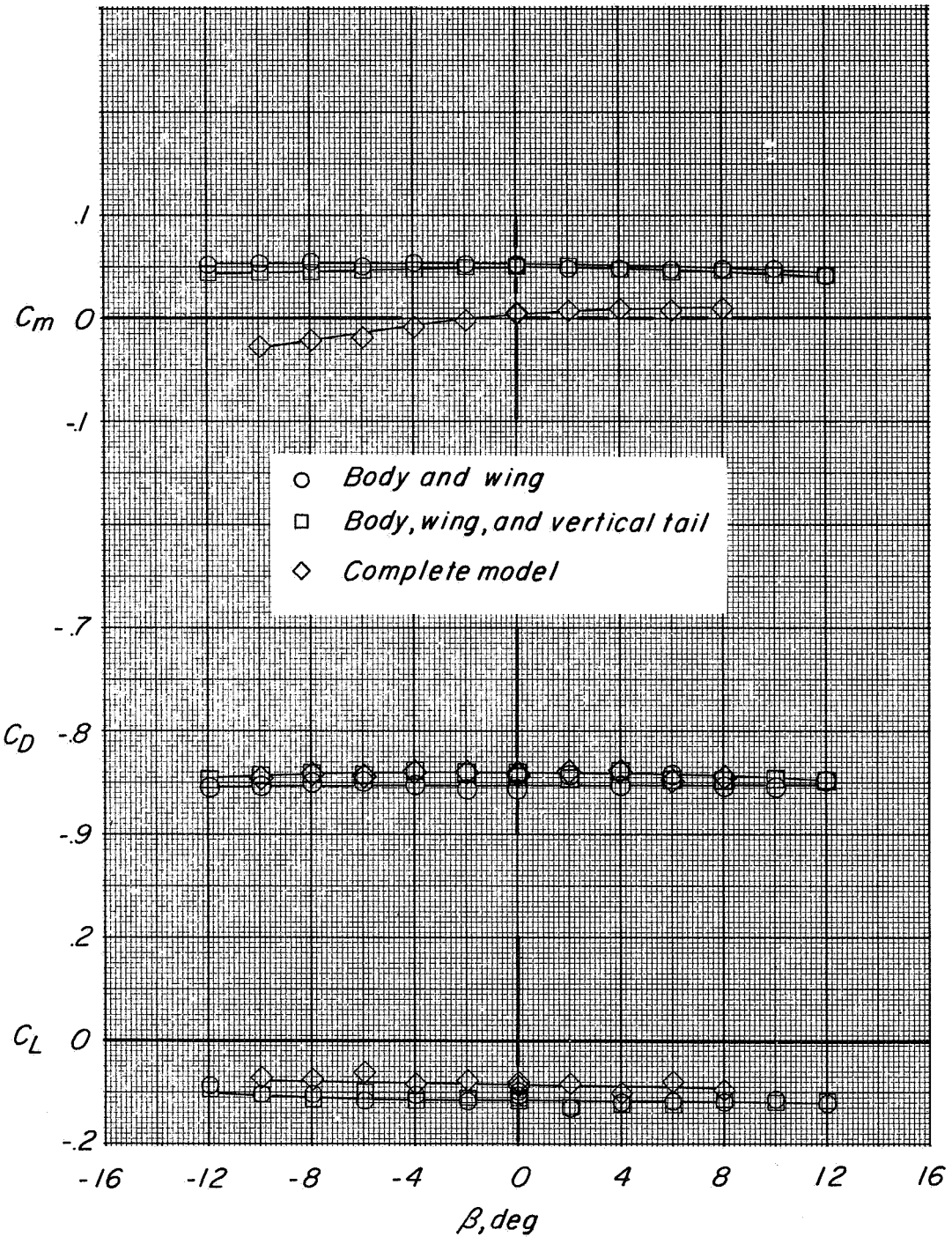

(c) Concluded.

Figure 20.- Concluded.

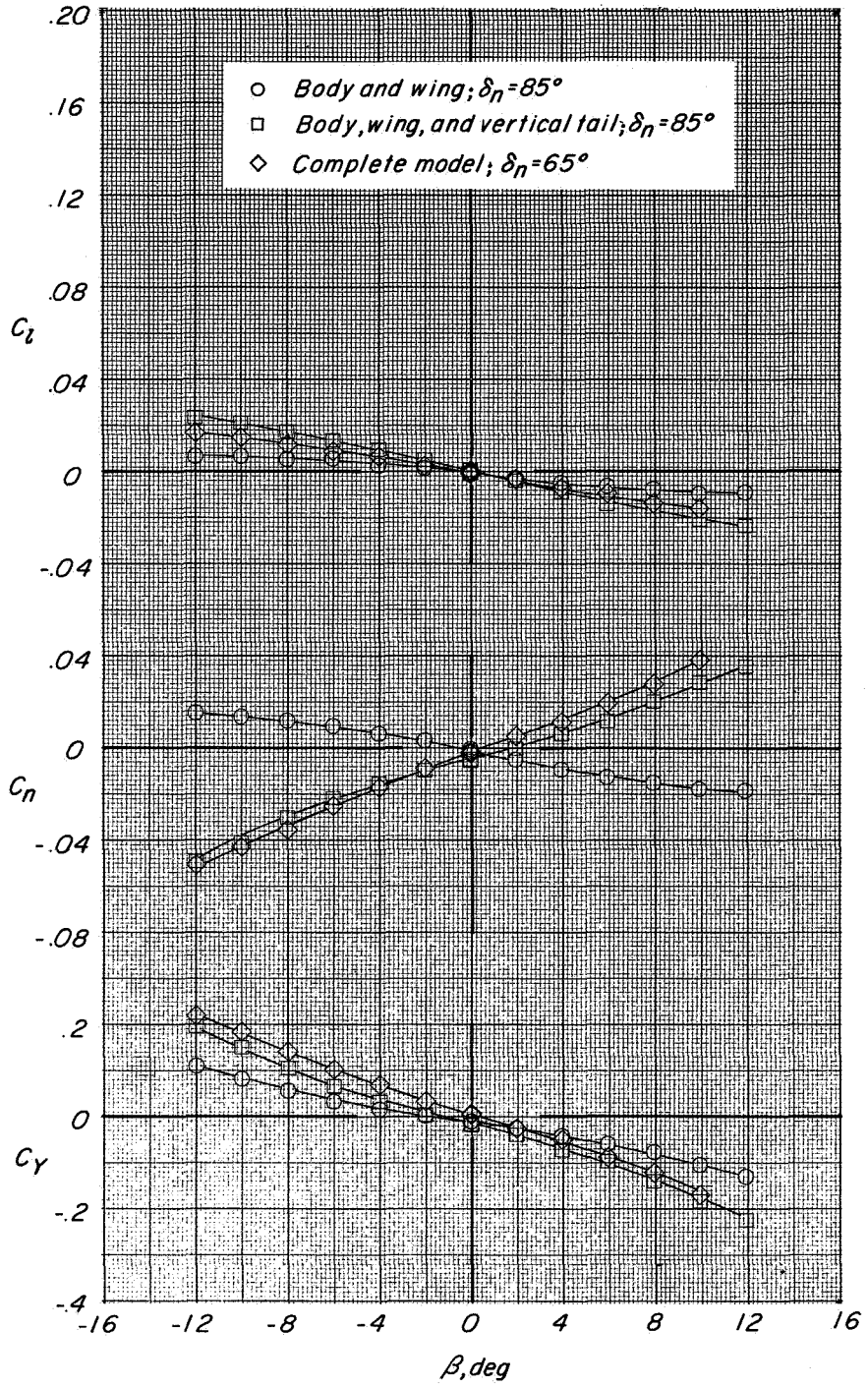

(a) $C_T = 0$.

Figure 21.- Characteristics of model in sideslip showing contributions of major components. $\delta_f = 60^o$; $\alpha = 0^o$.

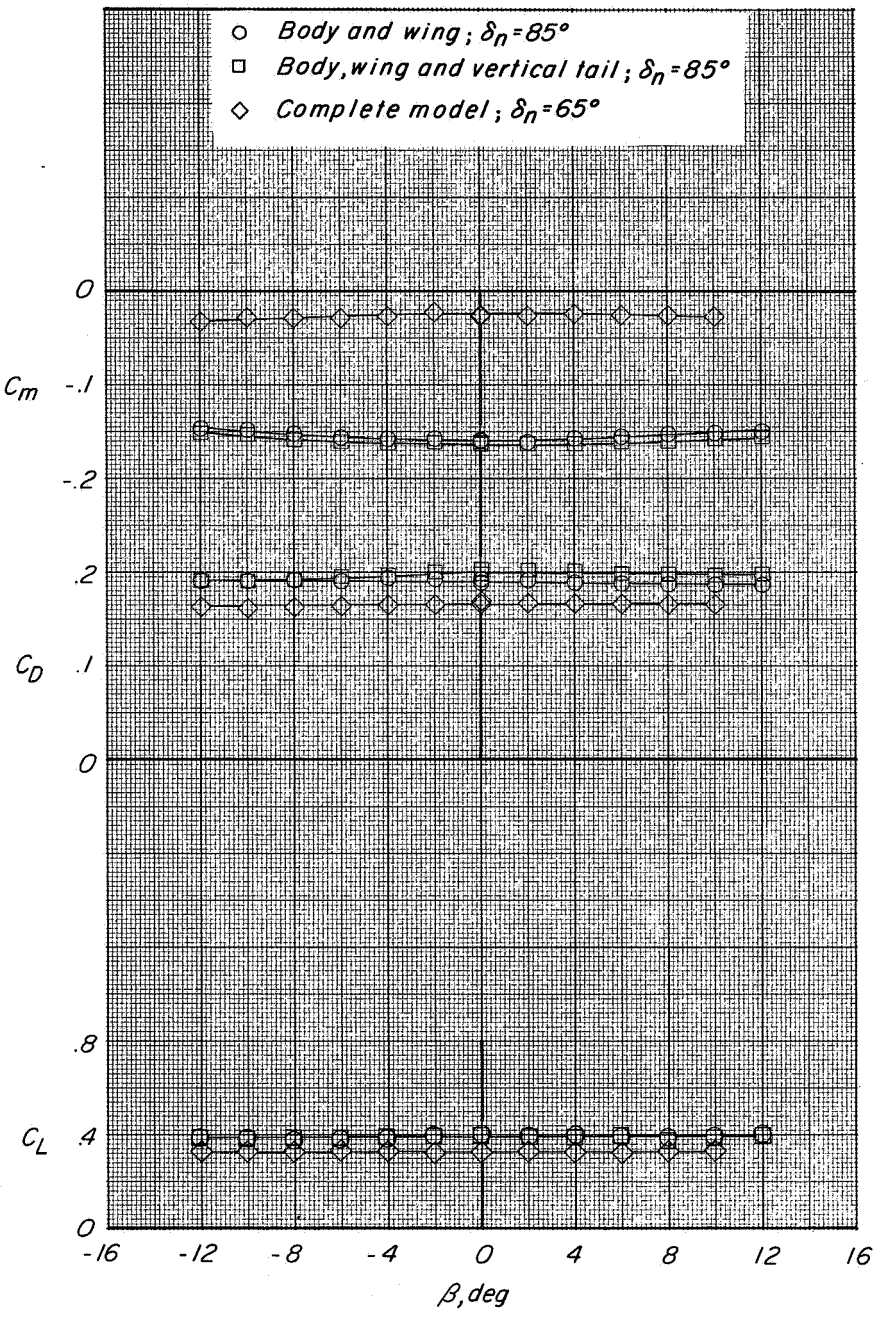

(a) Concluded.

Figure 21.- Continued.

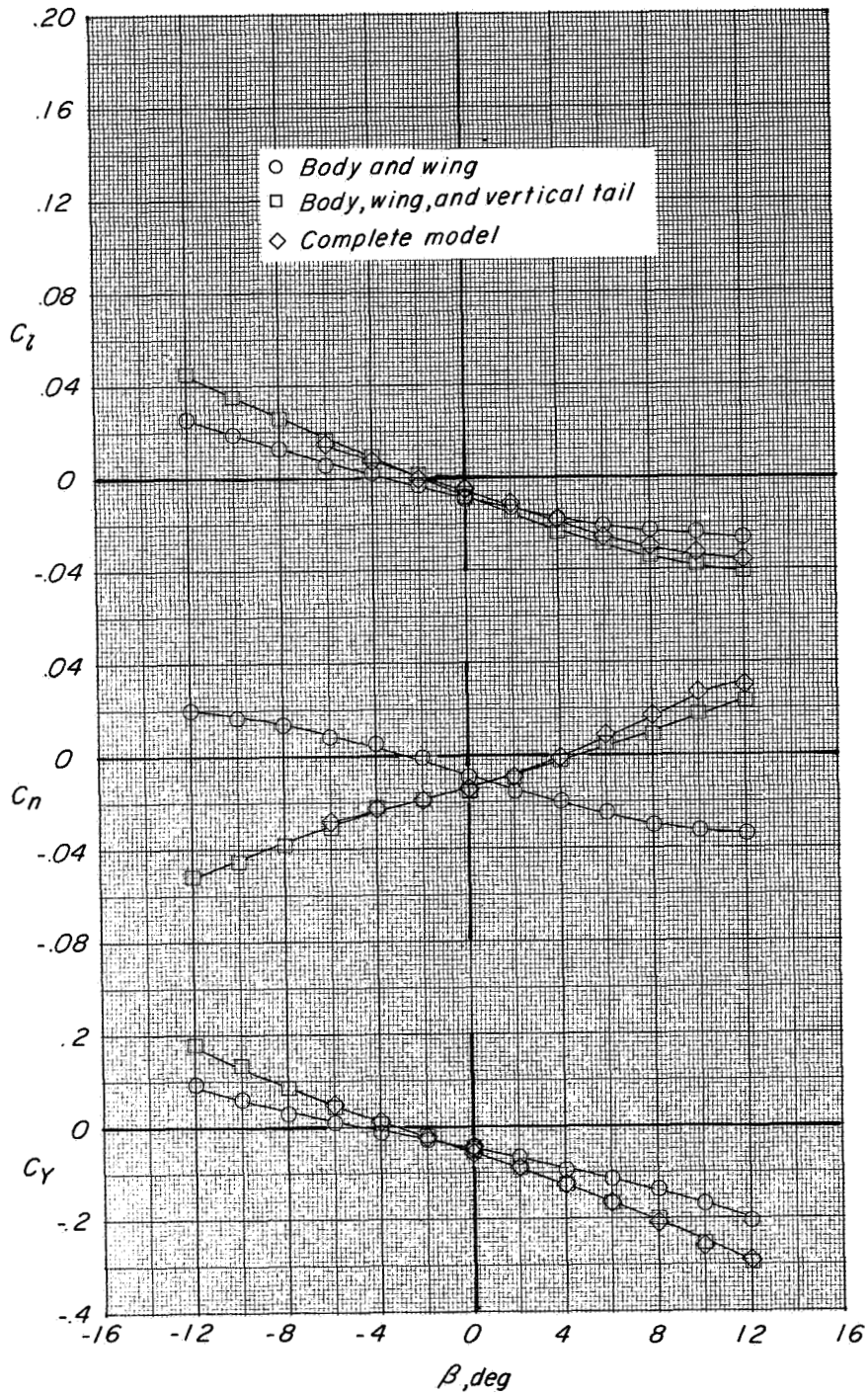

(b) $C_T = 1.1$; $\delta_n = 85^o$.

Figure 21.- Continued.

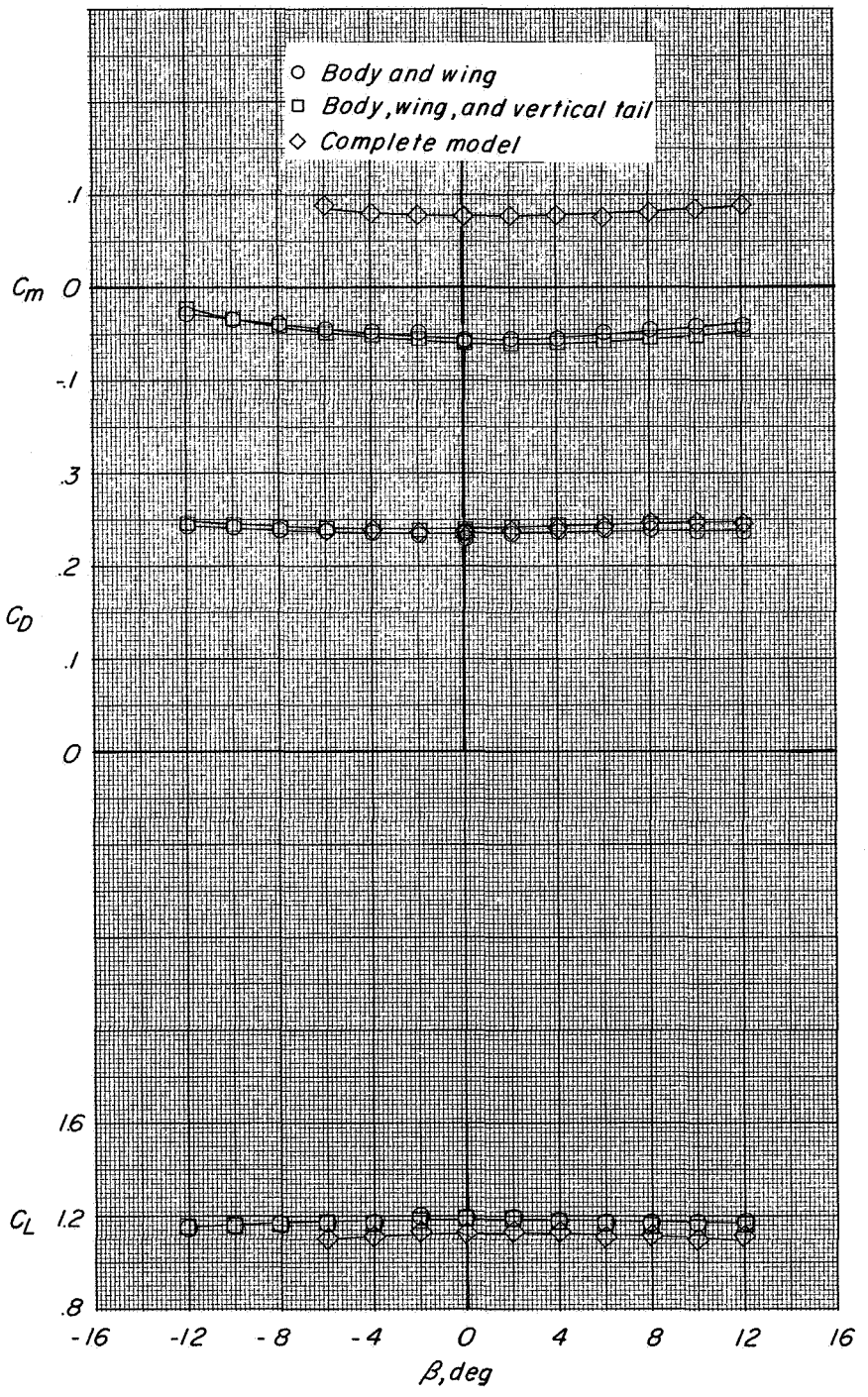

(b) Concluded.

Figure 21.- Continued.

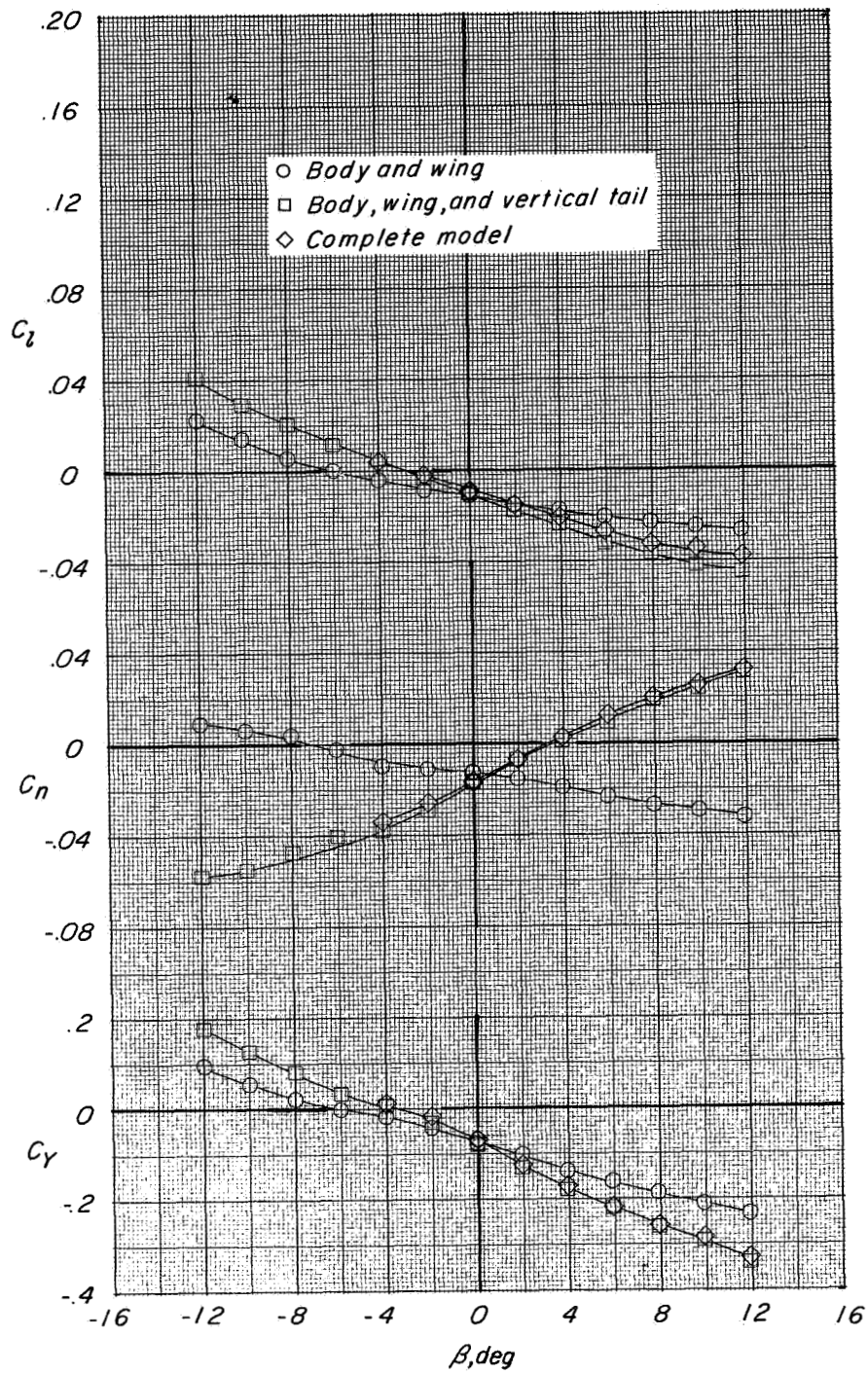

(c) $C_T = 2.1$; $\delta_n = 85^o$.

Figure 21.- Continued.

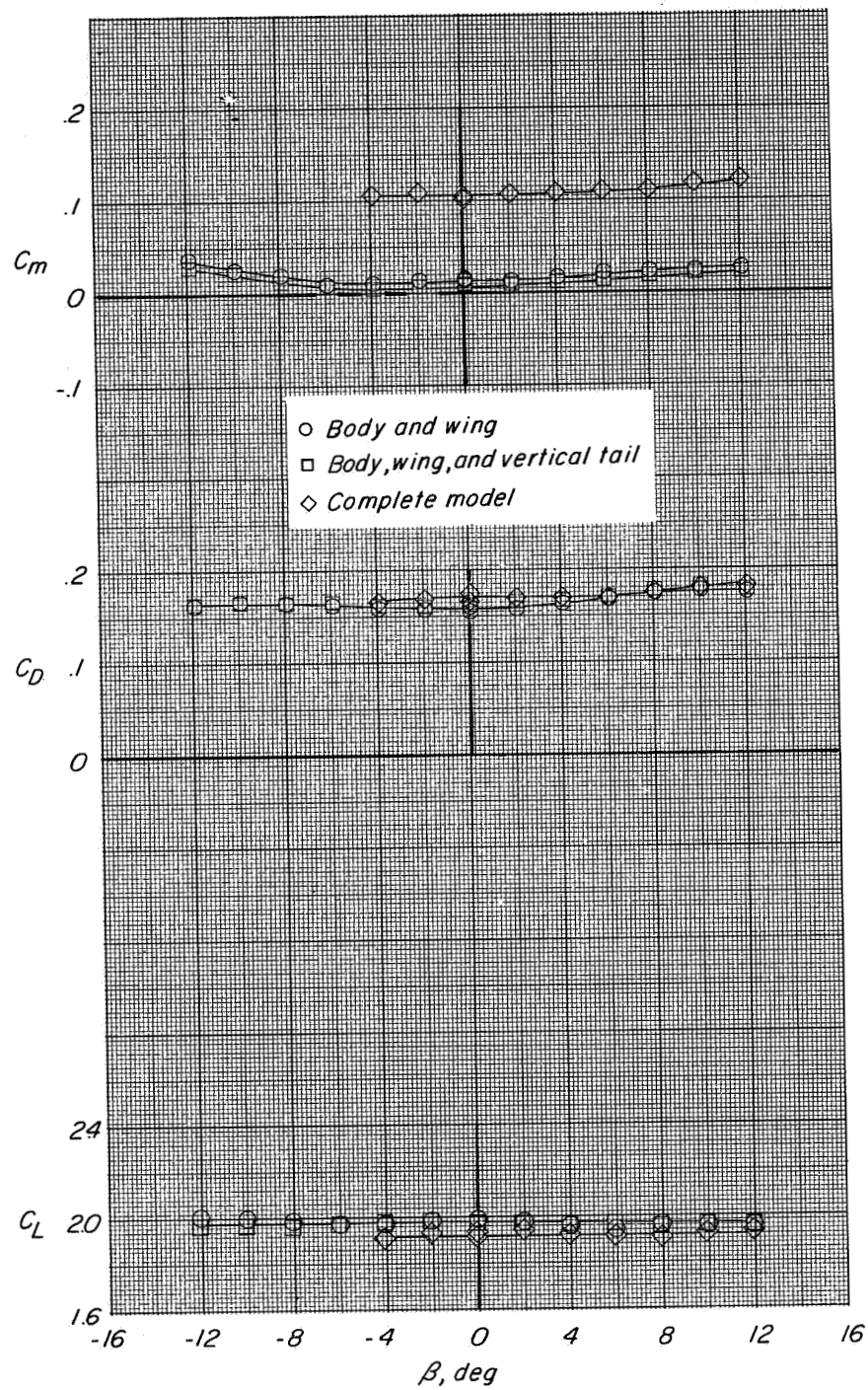

(c) Concluded.

Figure 21.- Continued.

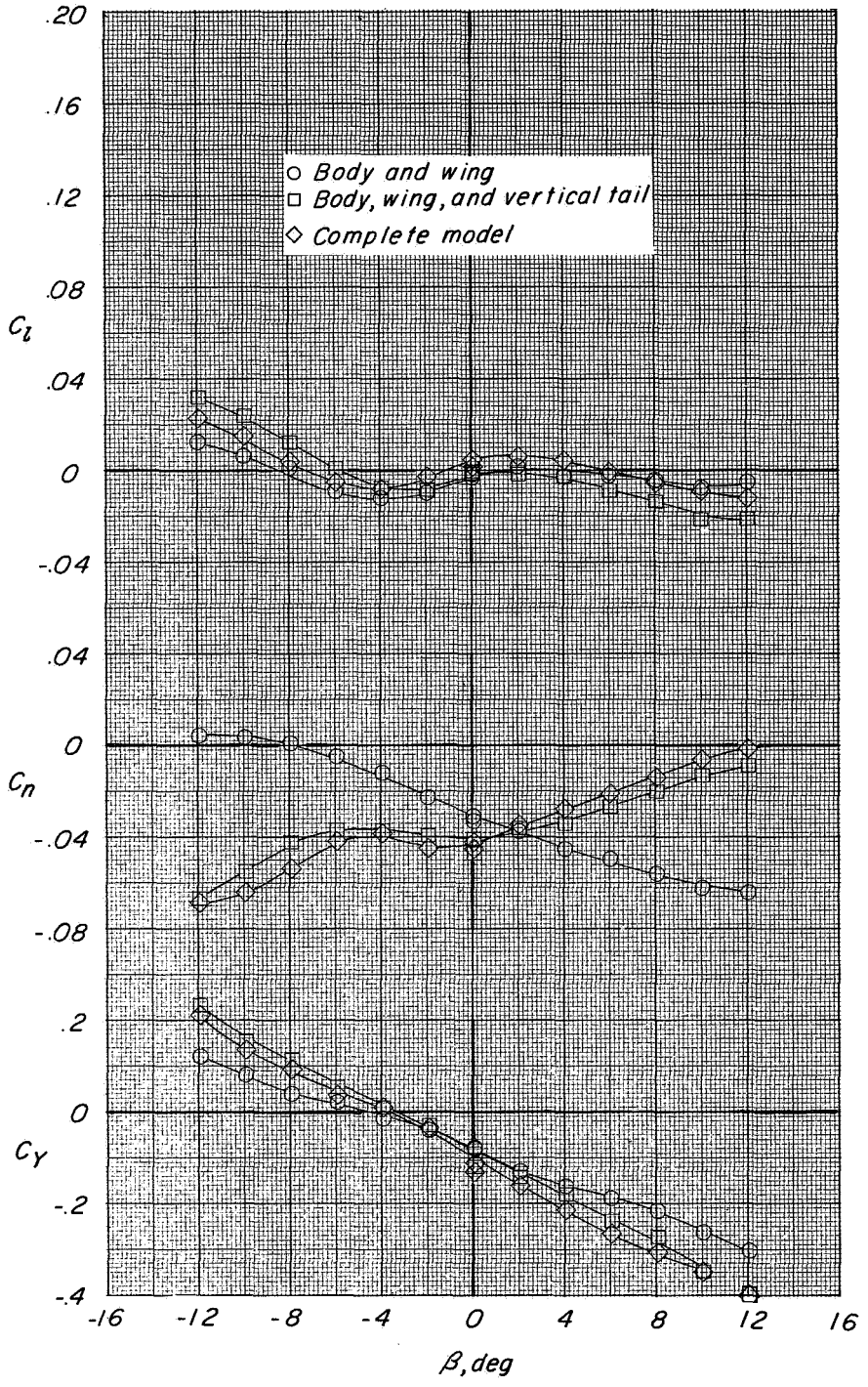

(d) $C_T = 6.1$; $\delta_n = 85^o$.

Figure 21.- Continued.

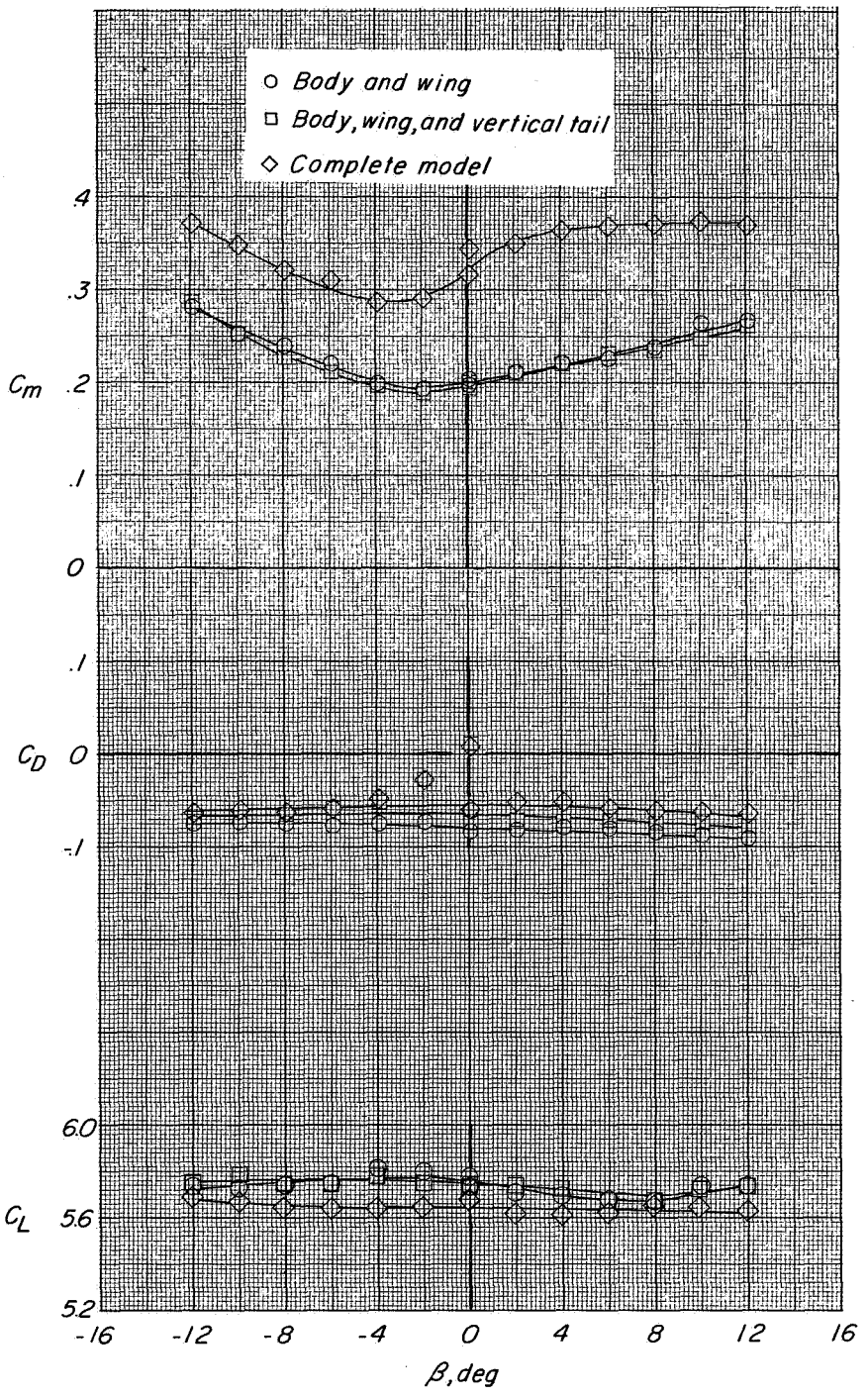

(d) Concluded.

Figure 21.- Concluded.

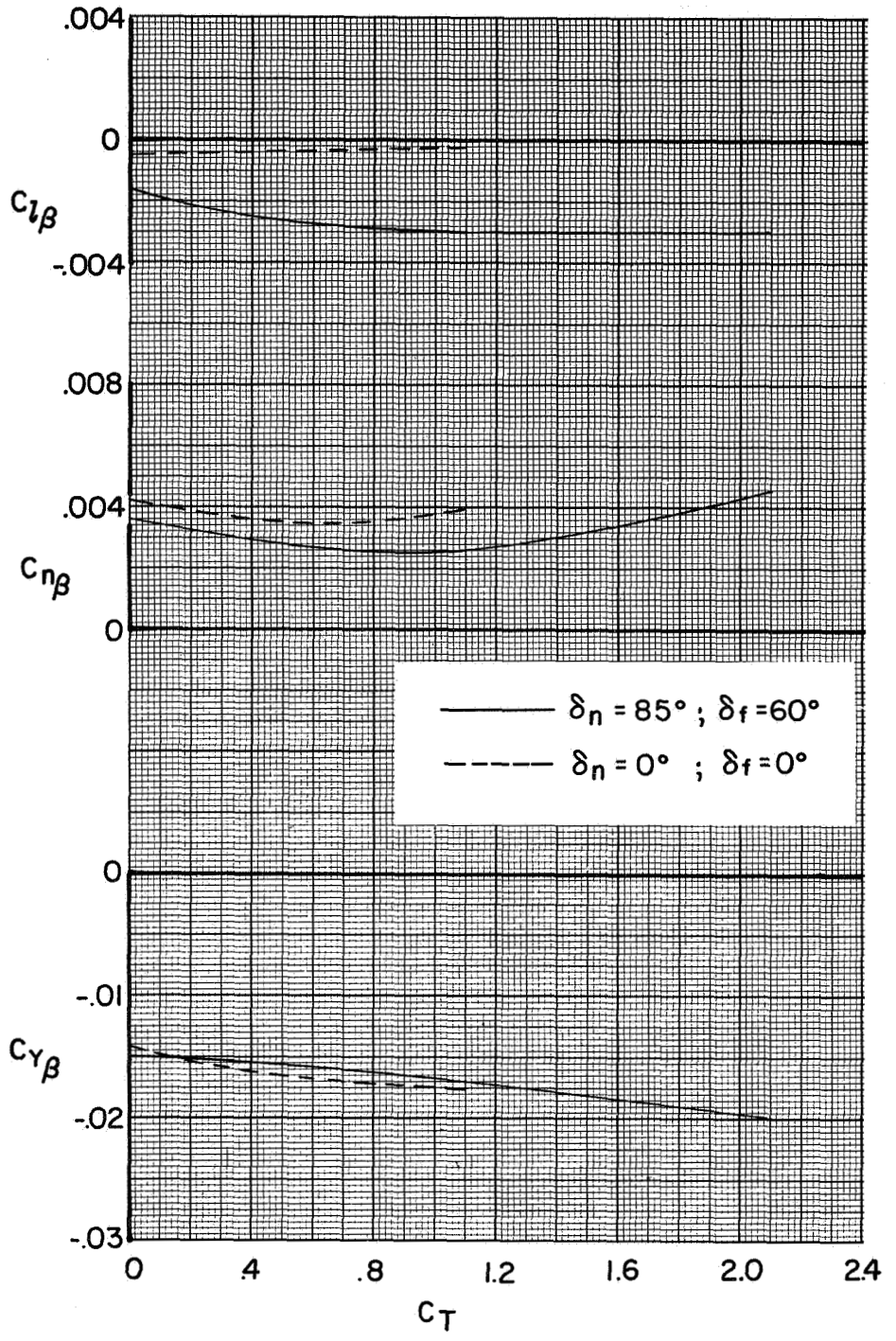

Figure 22.- Variation of lateral-stability parameters with thrust coefficient. $\alpha = 0^o$.

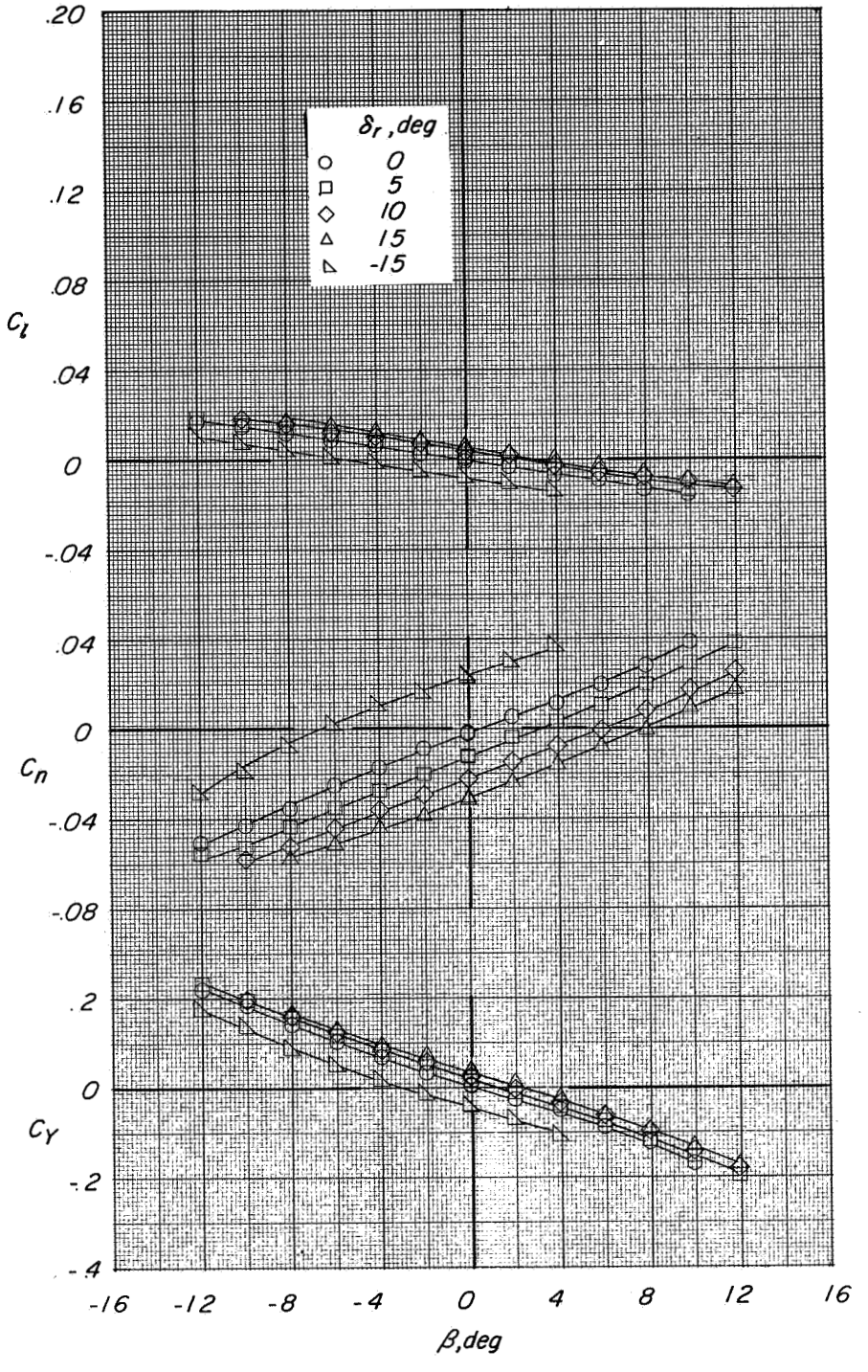

(a) $C_T = 0$.

Figure 23.- Variation of lateral-directional characteristics with sideslip angle showing effects of rudder deflection. $\delta_n = 85^o$; $\delta_f = 60^o$; $i_t = 0^o$; $\alpha = 0^o$.

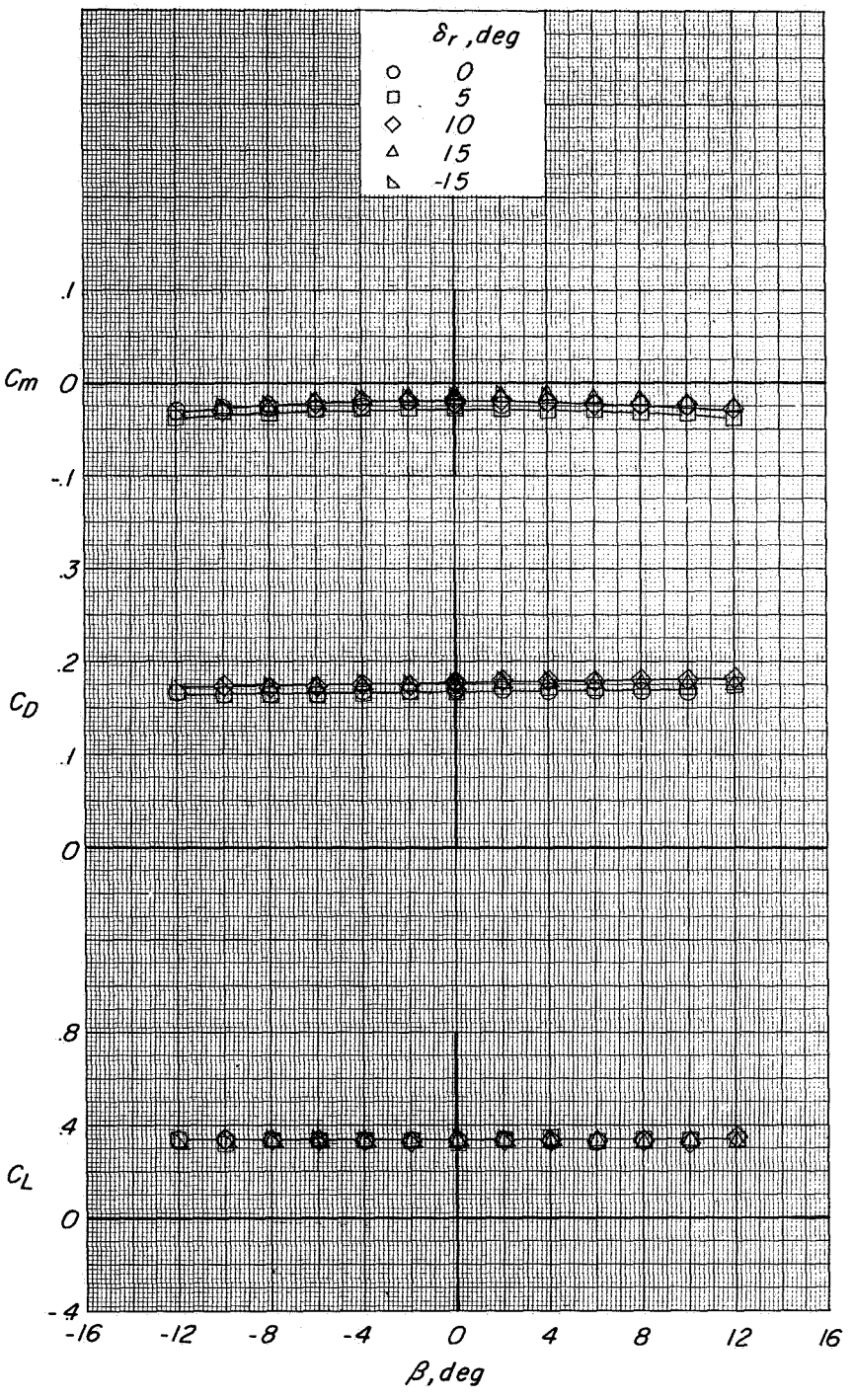

(a) Concluded.

Figure 23.- Continued.

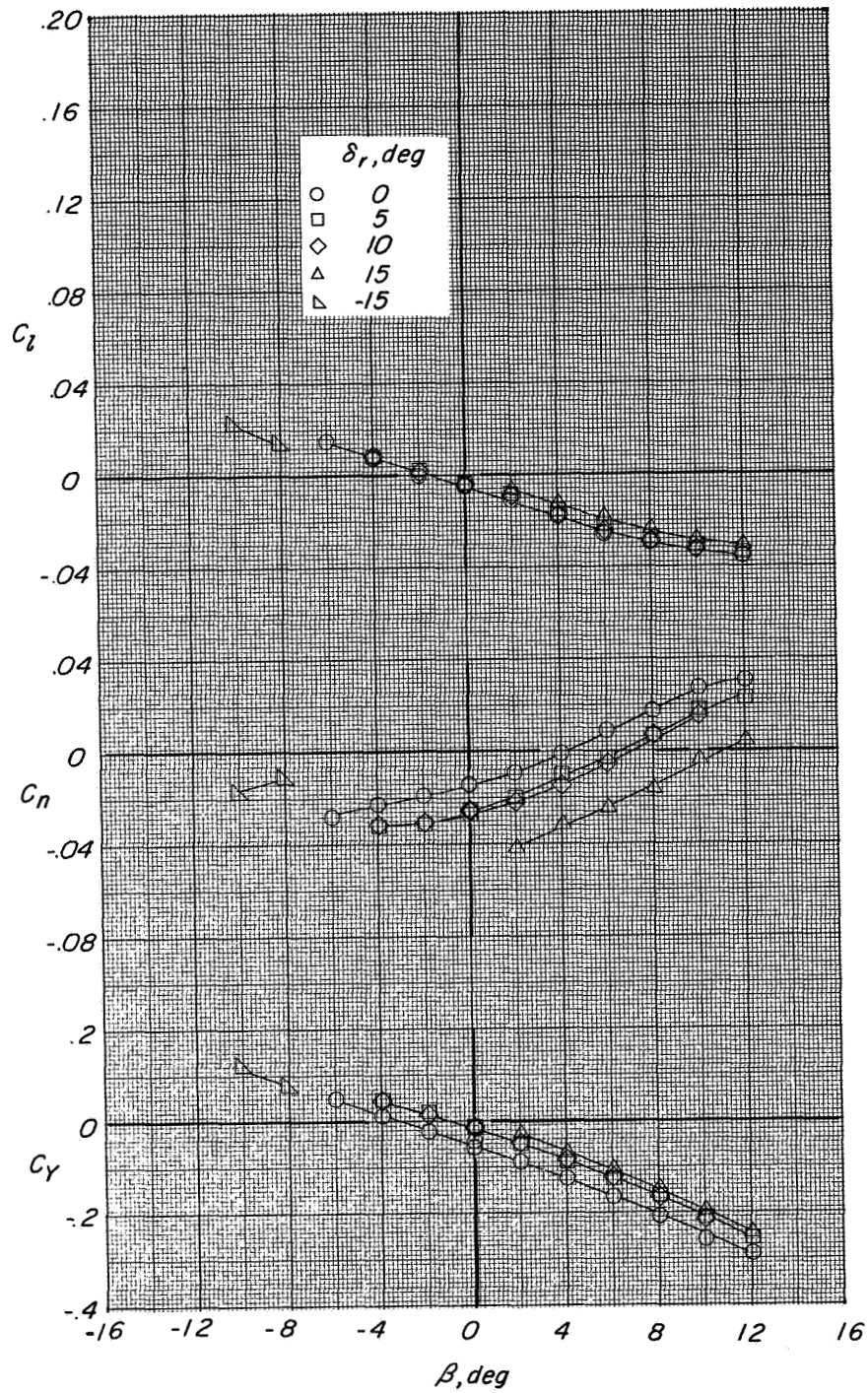

(b) $C_T = 1.1$.

Figure 23.- Continued.

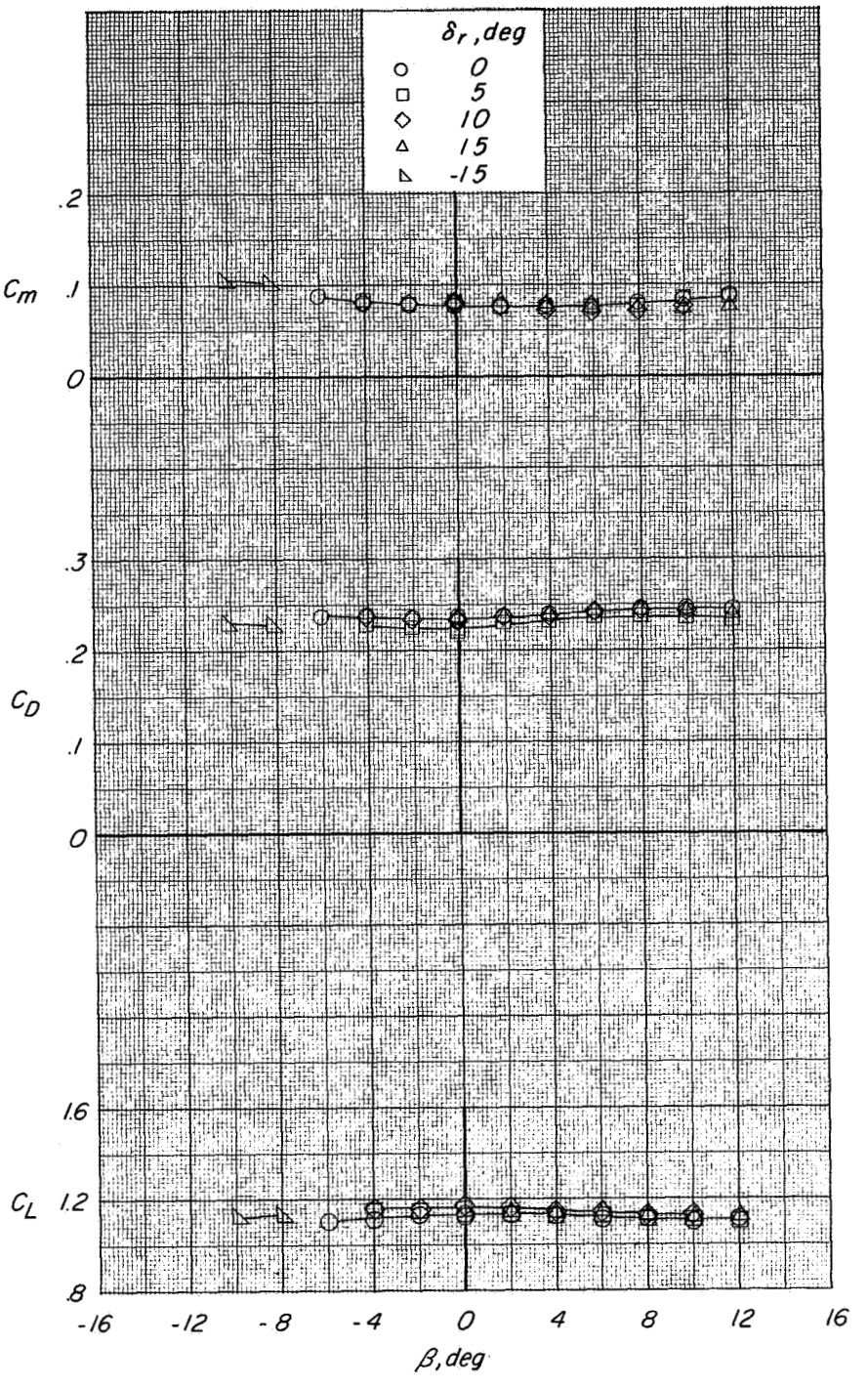

(b) Concluded.

Figure 23.- Continued.

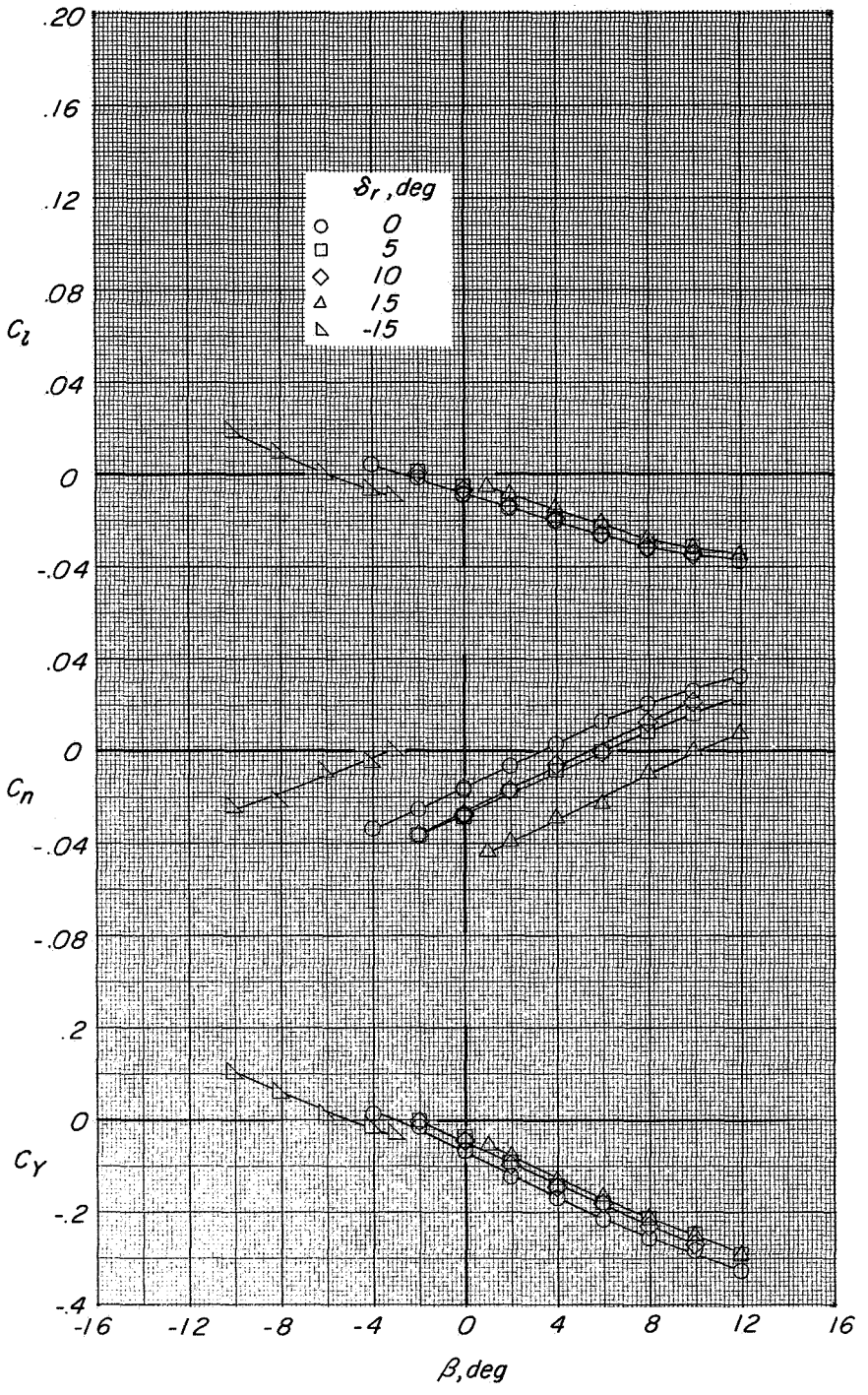

(c) $C_T = 2.1$.

Figure 23.- Continued.

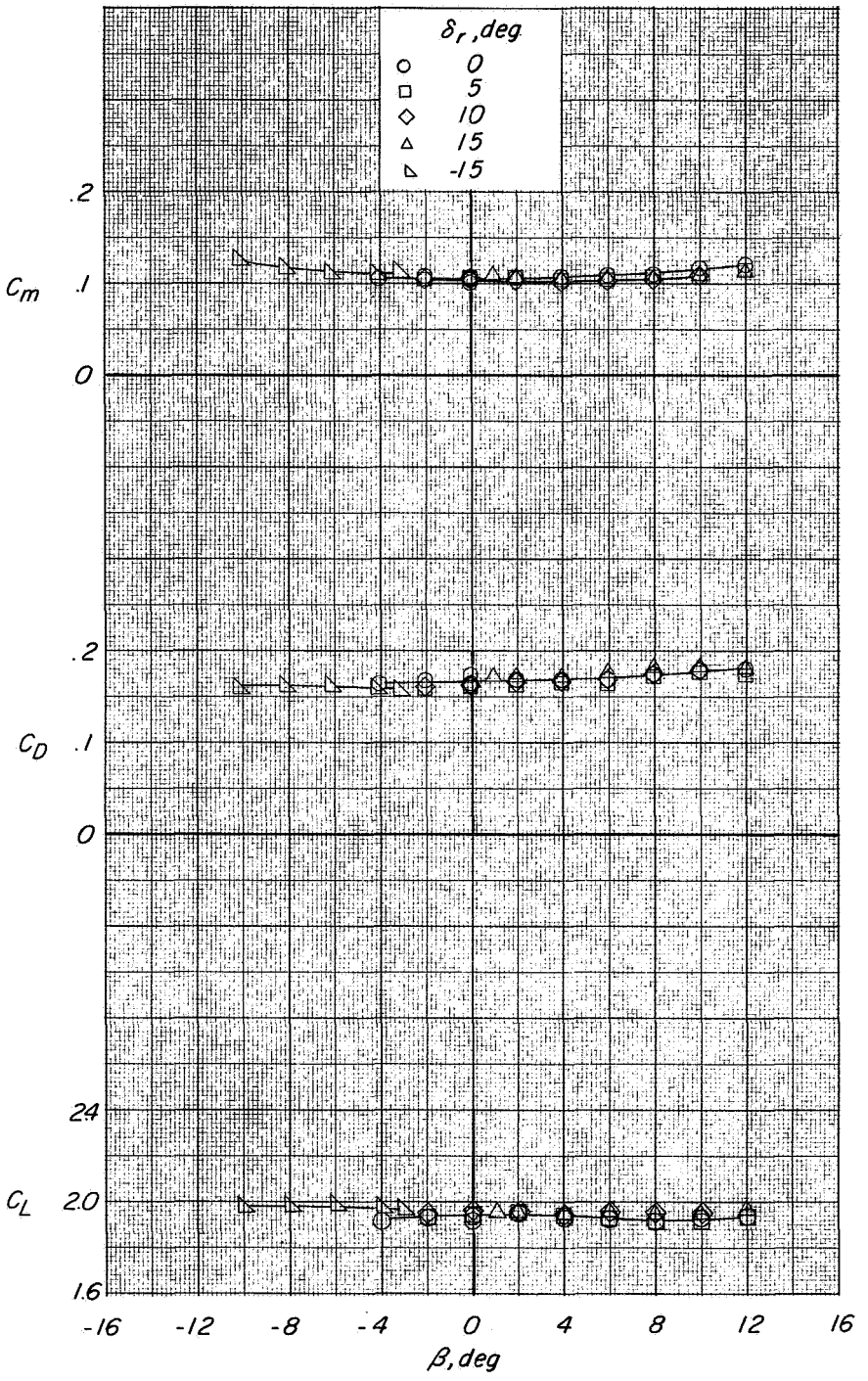

(c) Concluded.

Figure 23.- Continued.

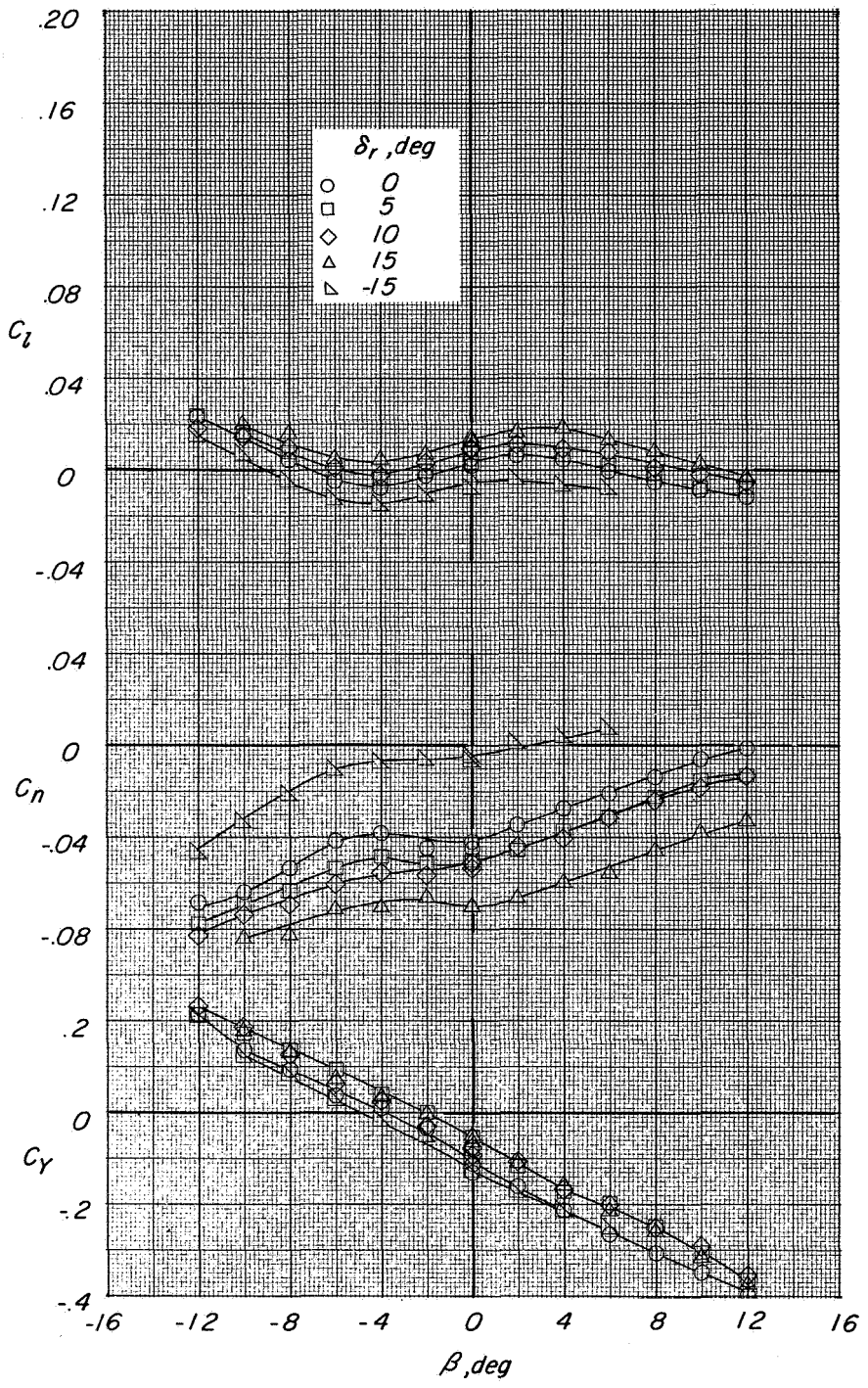

(d) $C_T = 6.1$.

Figure 23.- Continued.

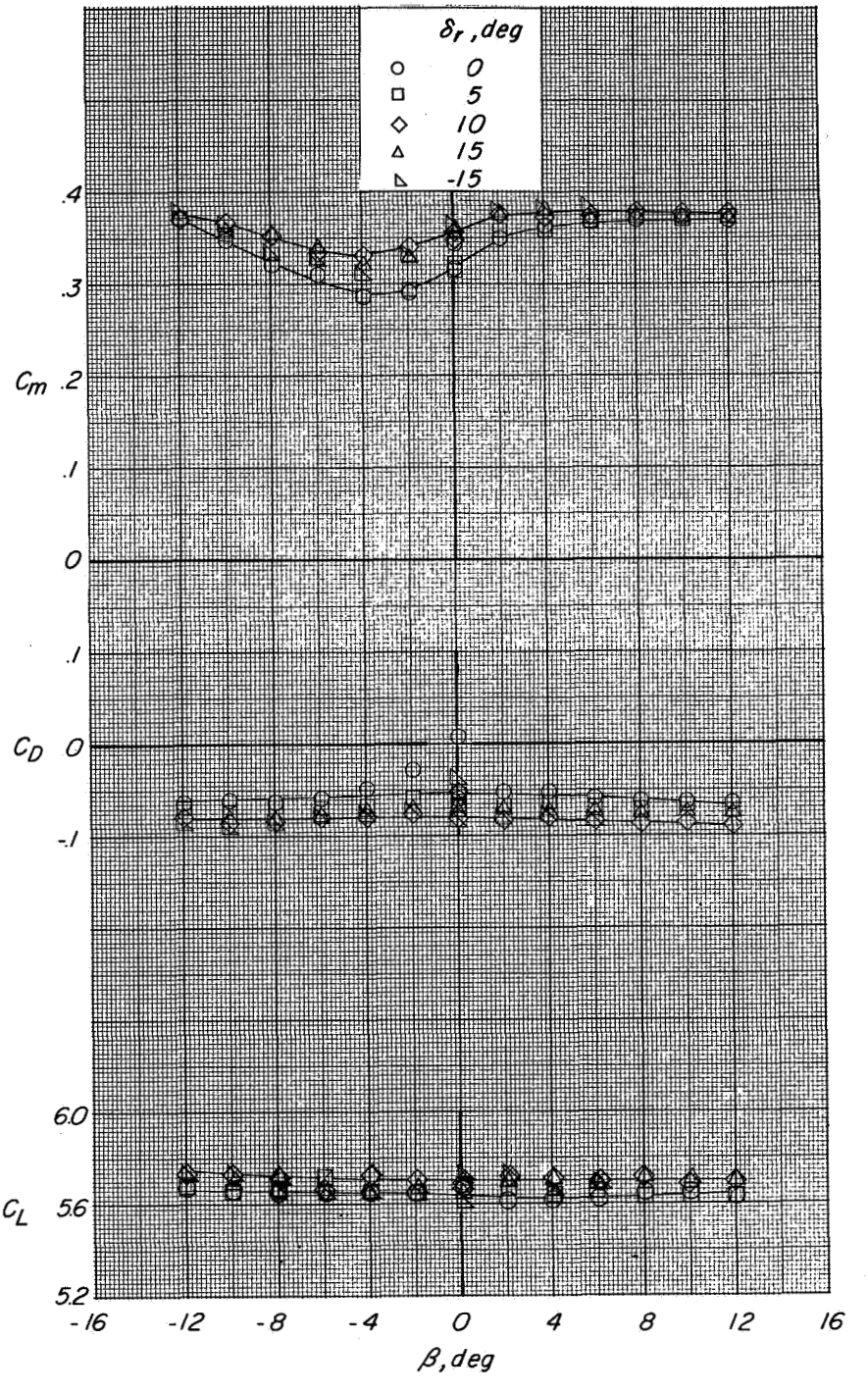

(d) Concluded.

Figure 23.- Concluded.

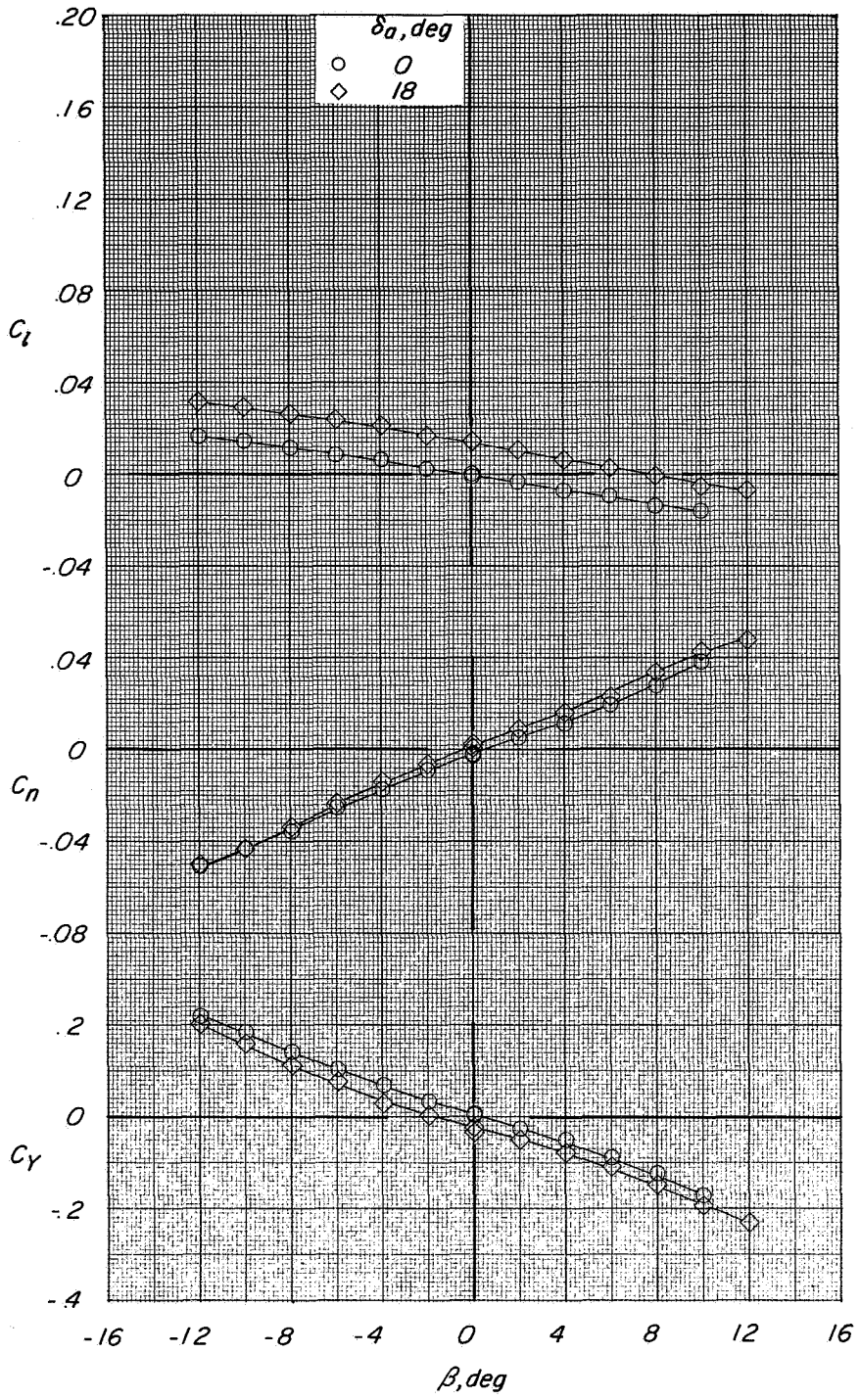

(a) $C_T = 0$.

Figure 24.- Variation of lateral-directional characteristics with sideslip angle showing effect of aileron deflection. $\delta_n = 85^o$; $\delta_f = 60^o$; $i_t = 0^o$; $\alpha = 0^o$.

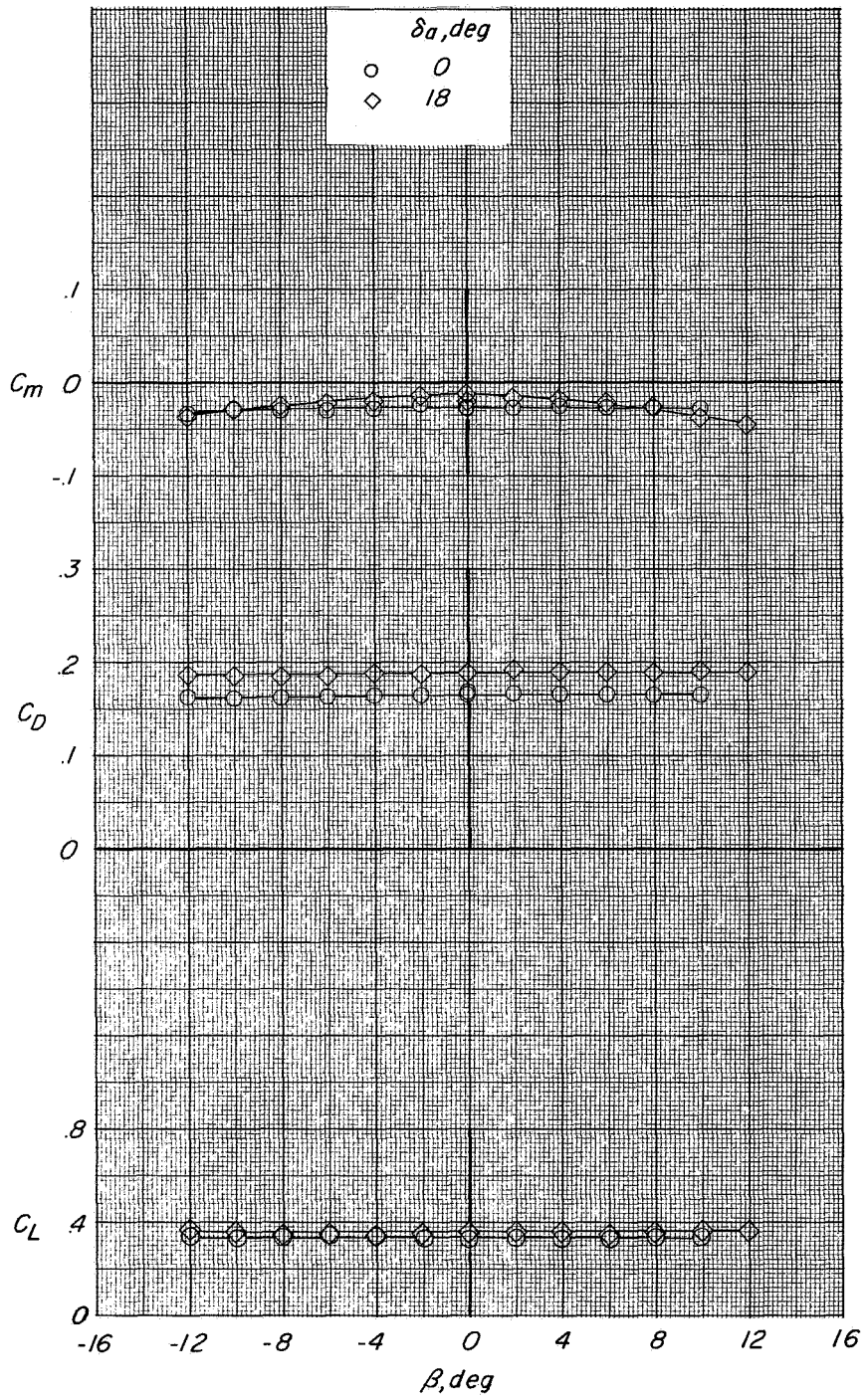

(a) Concluded.

Figure 24.- Continued.

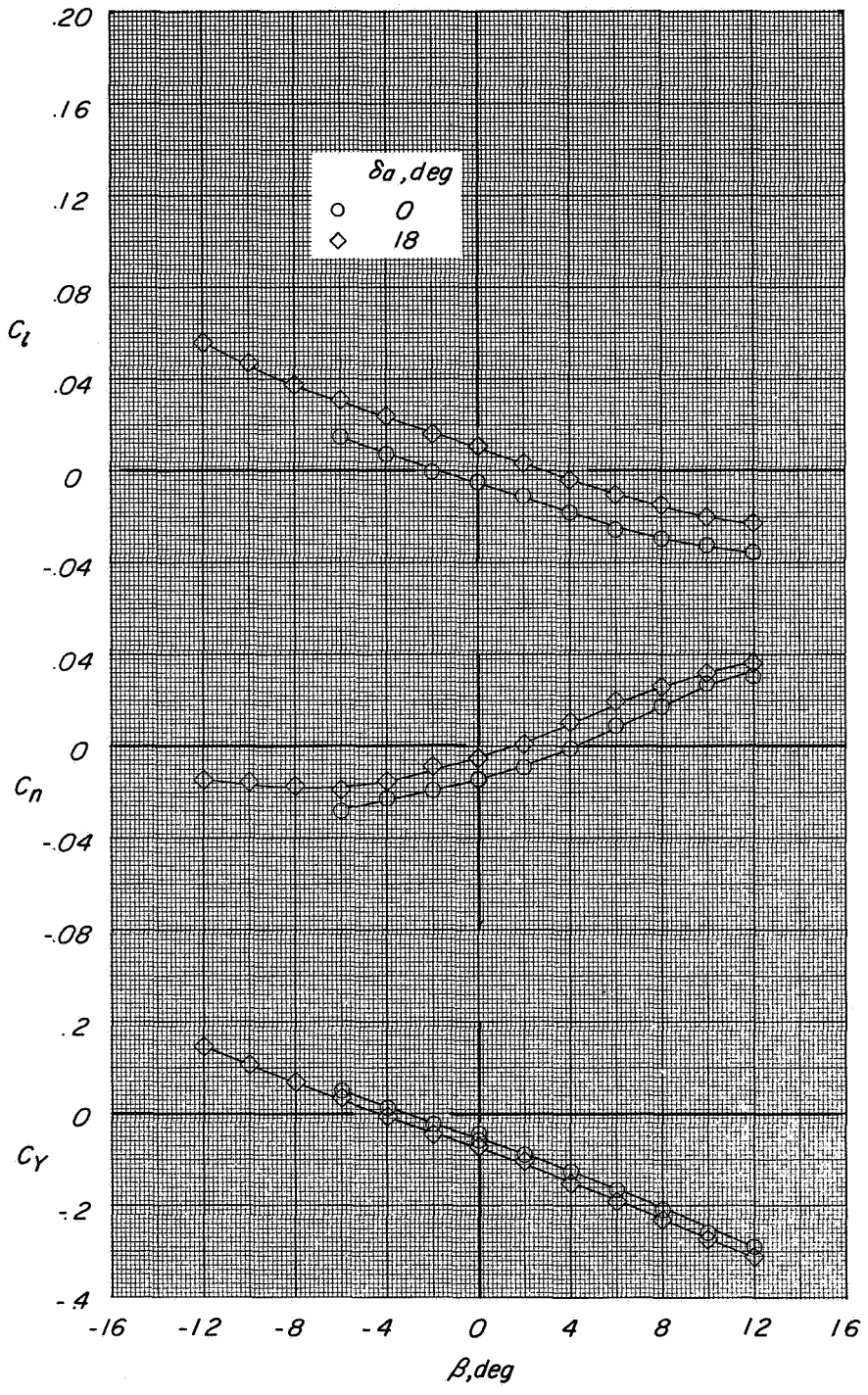

(b) $C_T = 1.1$.

Figure 24.- Continued.

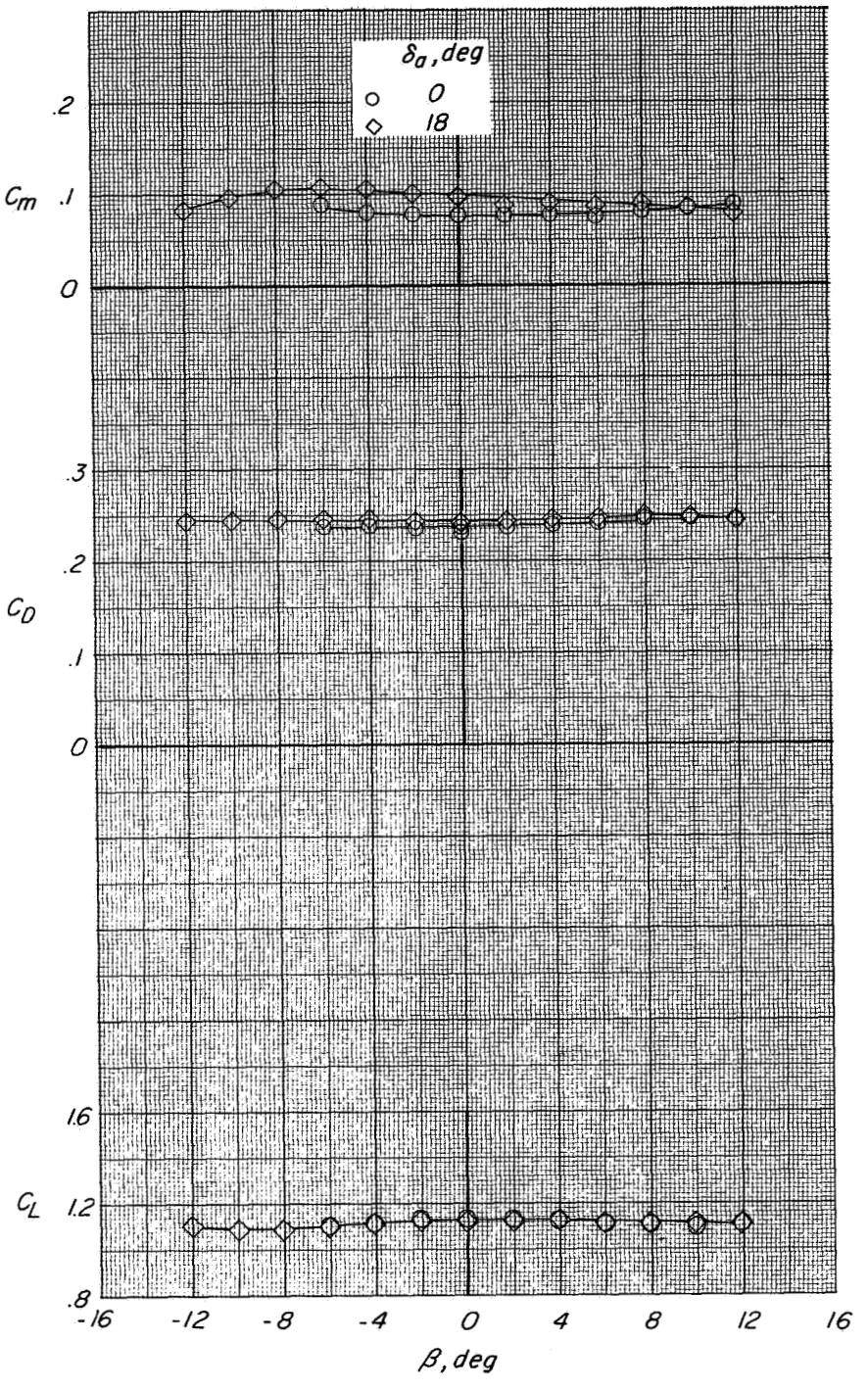

(b) Concluded.

Figure 24.- Continued.

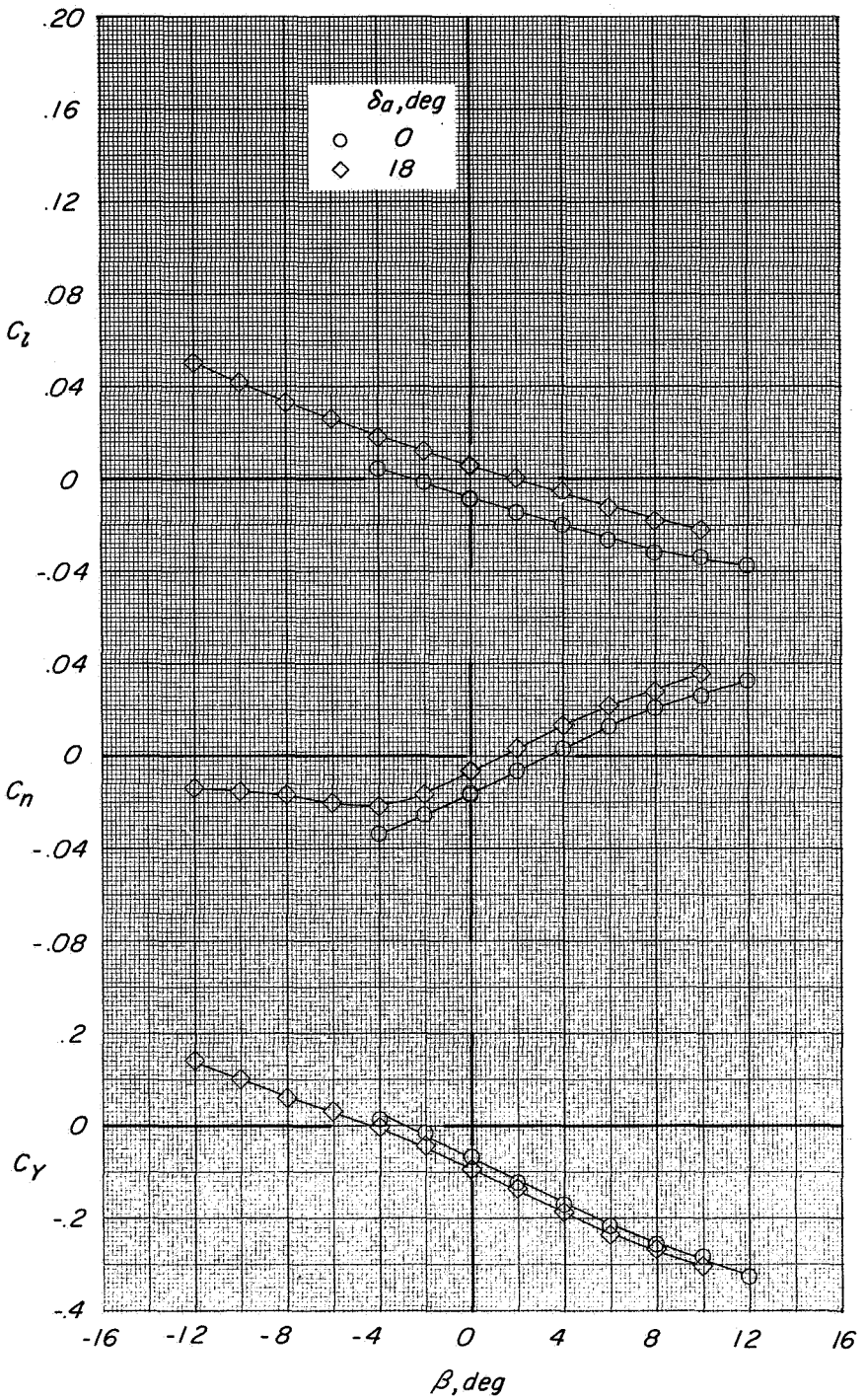

(c) $C_T = 2.1$.

Figure 24.- Continued.

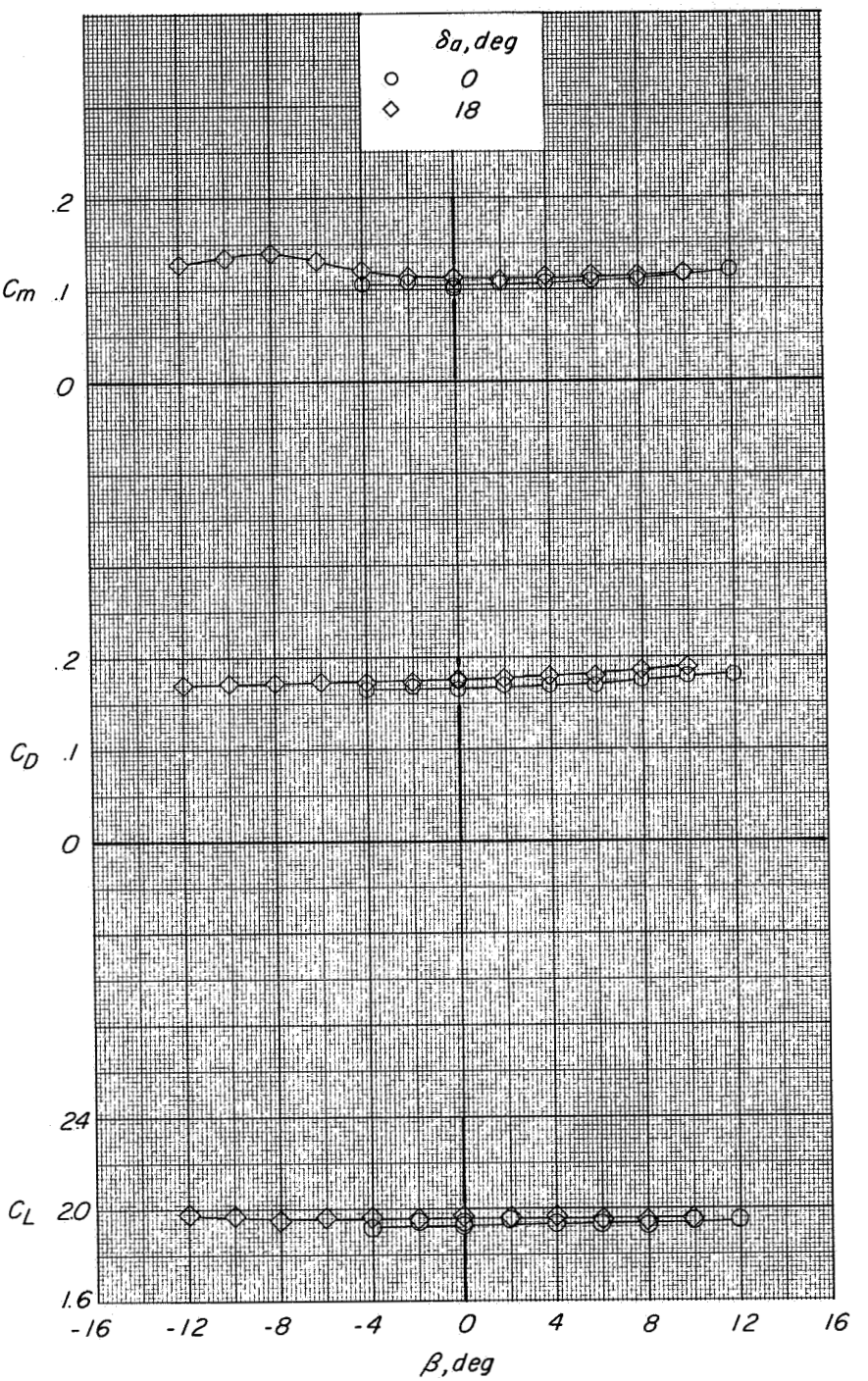

(c) Concluded.

Figure 24.- Continued.

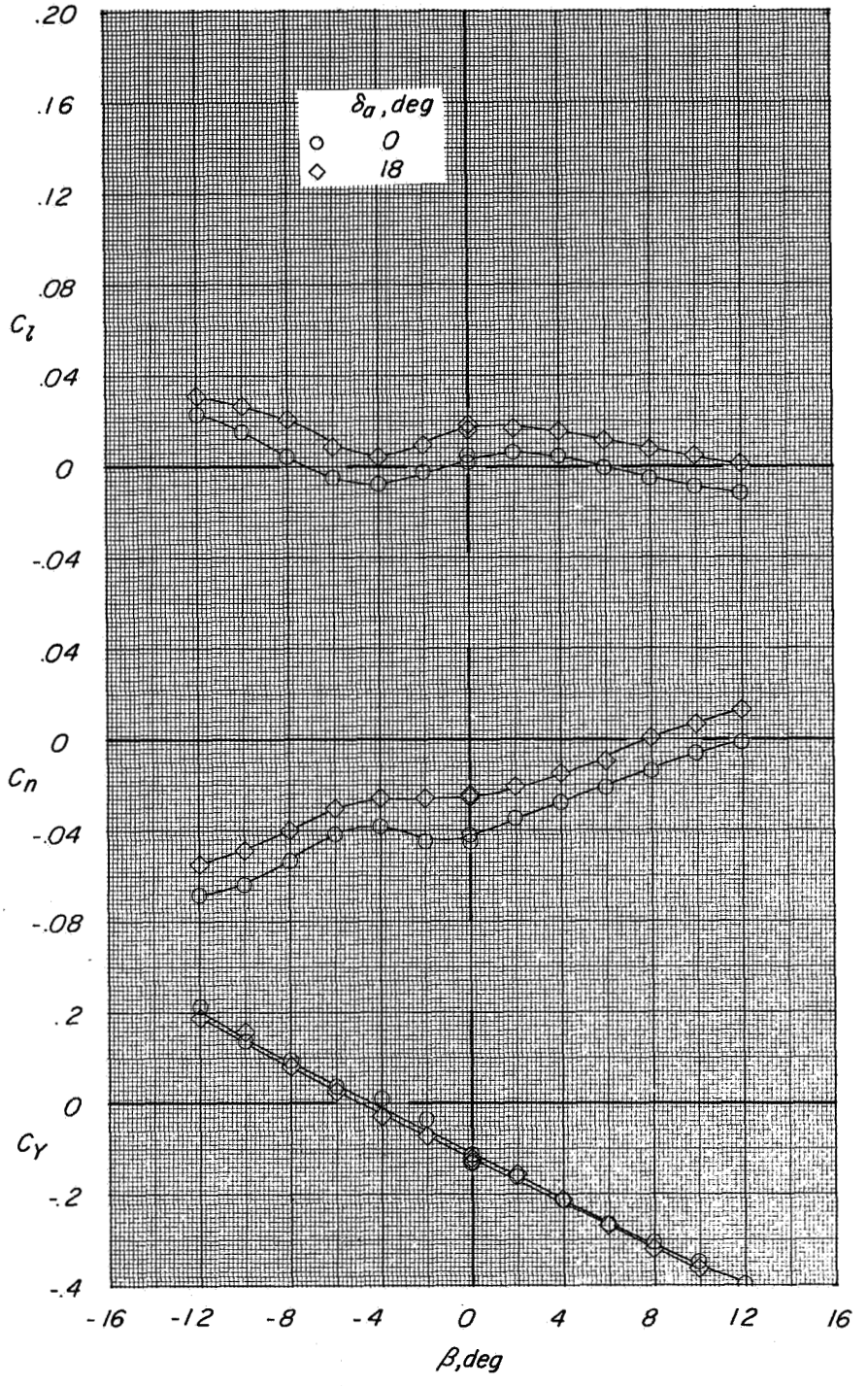

(d) $C_T = 6.1$.

Figure 24.- Continued.

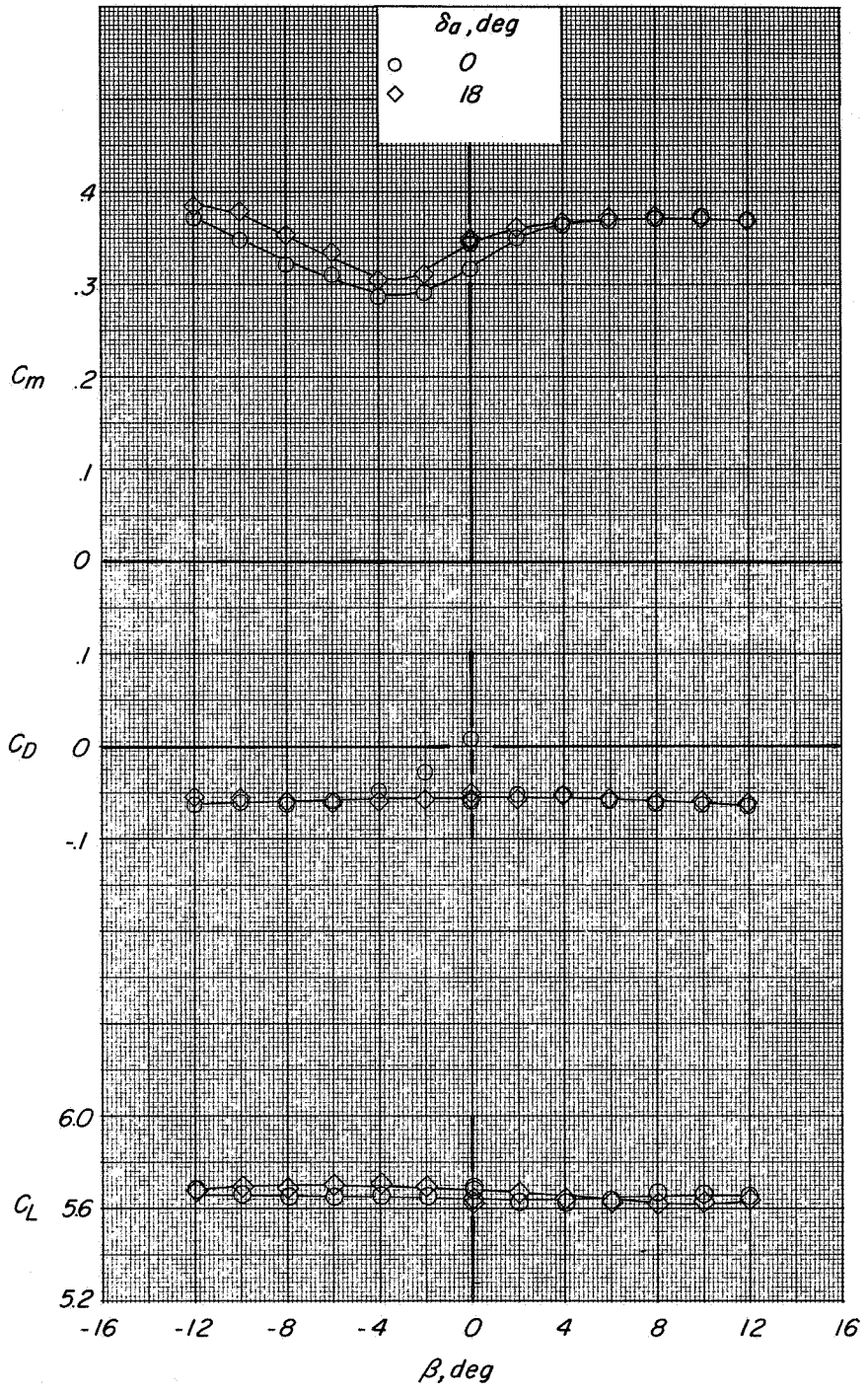

(d) Concluded.

Figure 24.- Concluded.

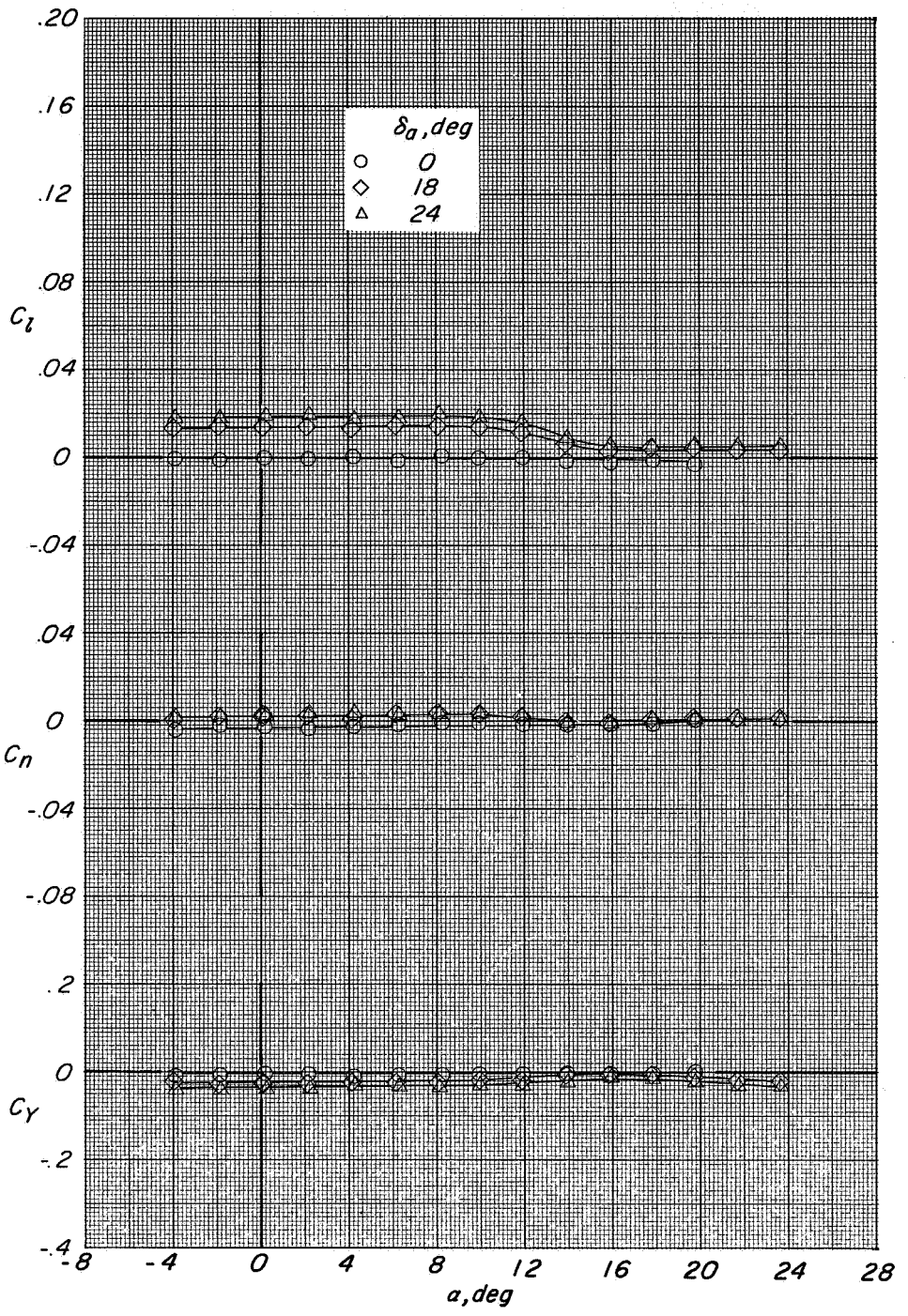

(a) $C_T = 0$.

Figure 25.- Variation of lateral-directional characteristics with angle of attack showing effect of aileron deflection. $\delta_n = 85^o$; $\delta_f = 60^o$; $i_t = 0^o$; $\beta = 0^o$.

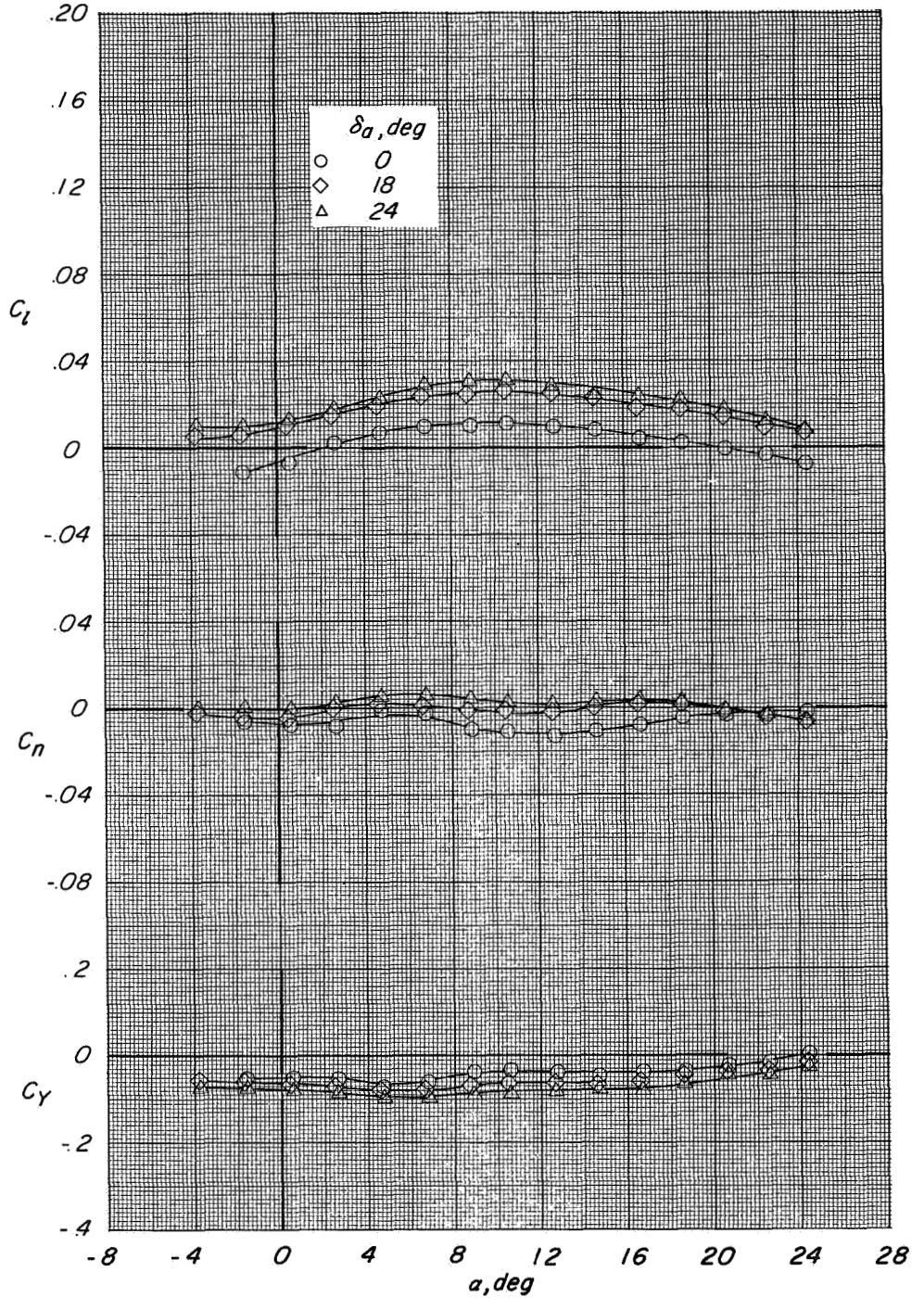

(b) $C_T = 1.1$.

Figure 25.- Continued.

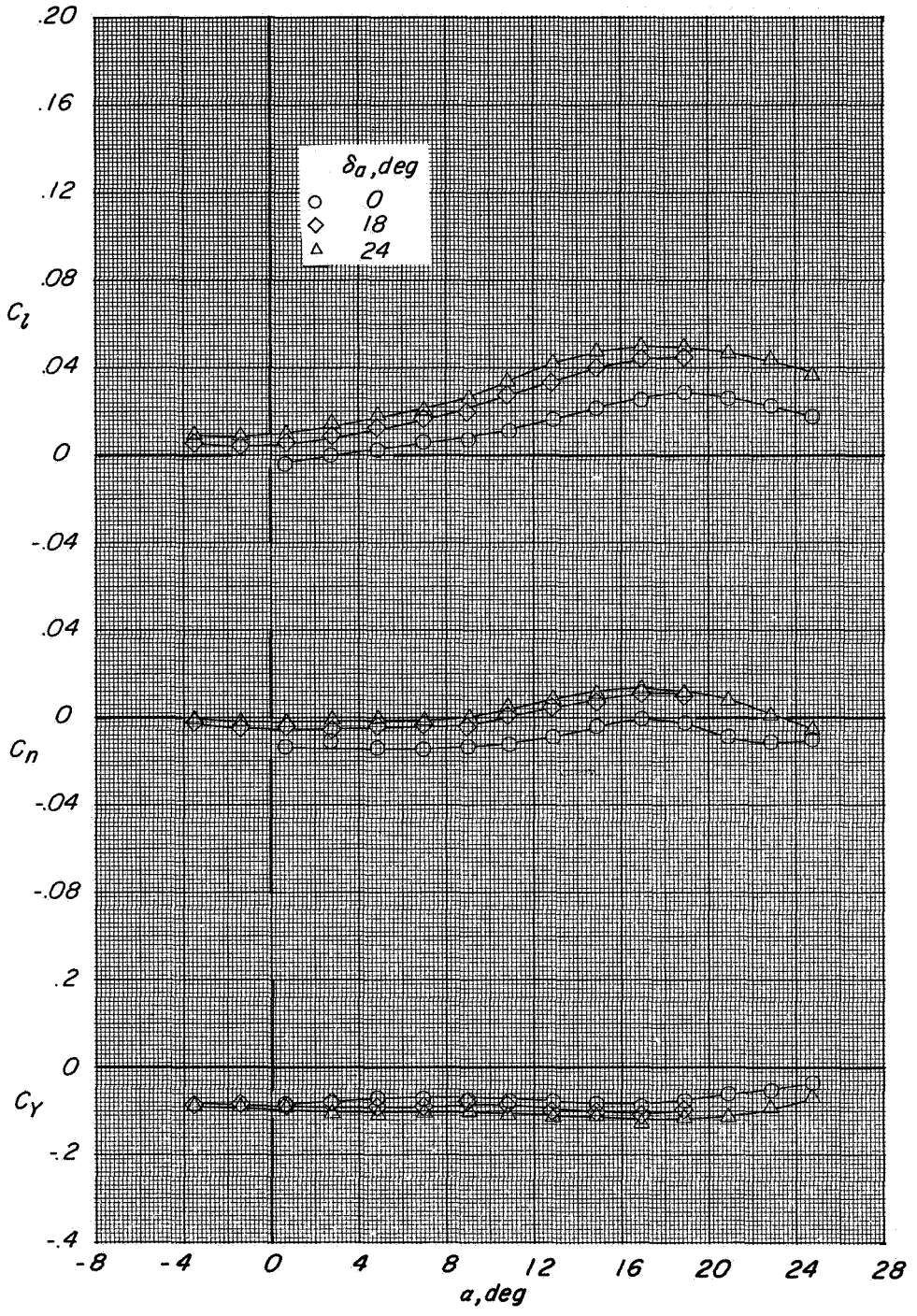

(c) $C_T = 2.1$.

Figure 25.- Continued.

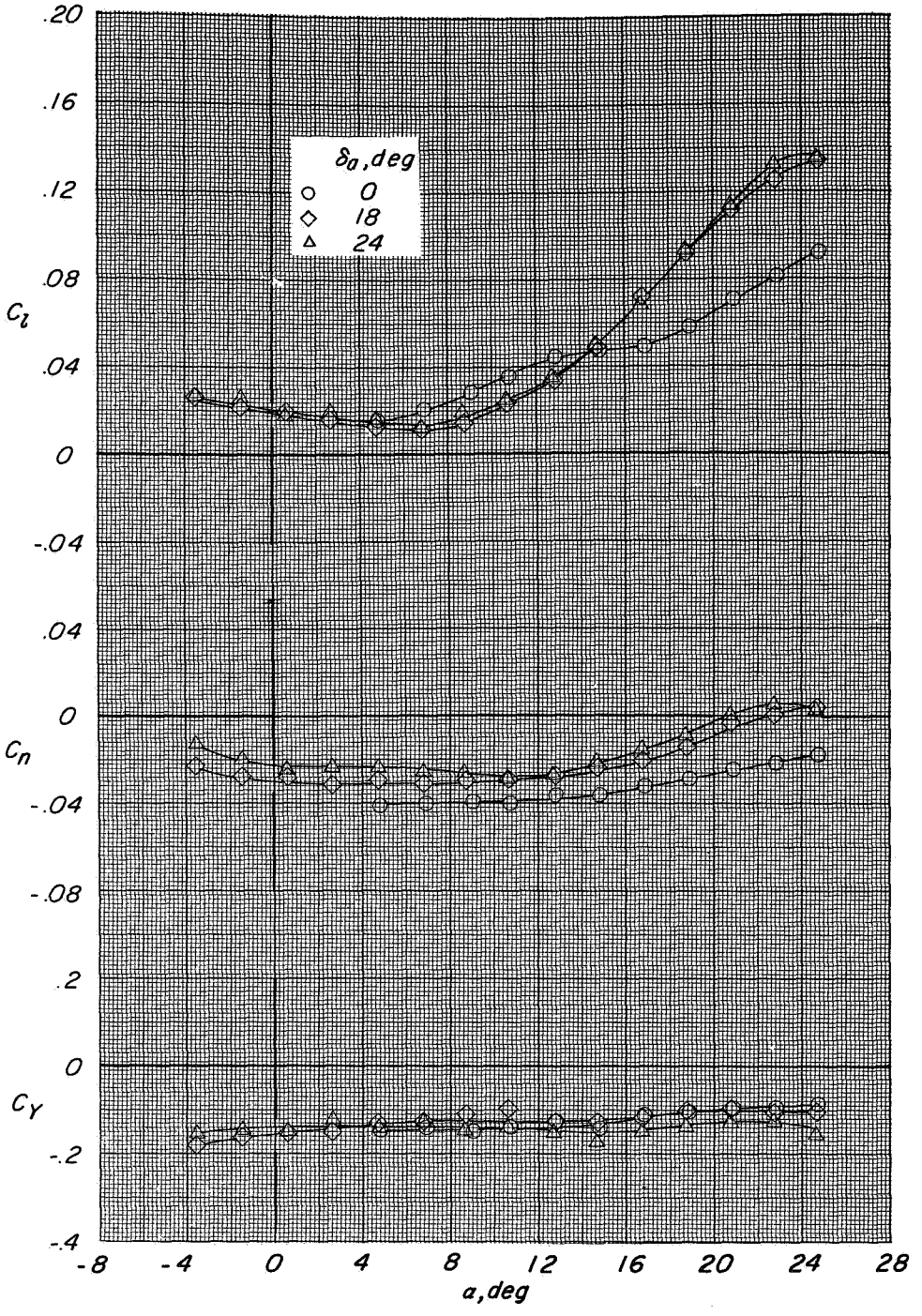

(d) $C_T = 6.1$.

Figure 25.- Concluded.

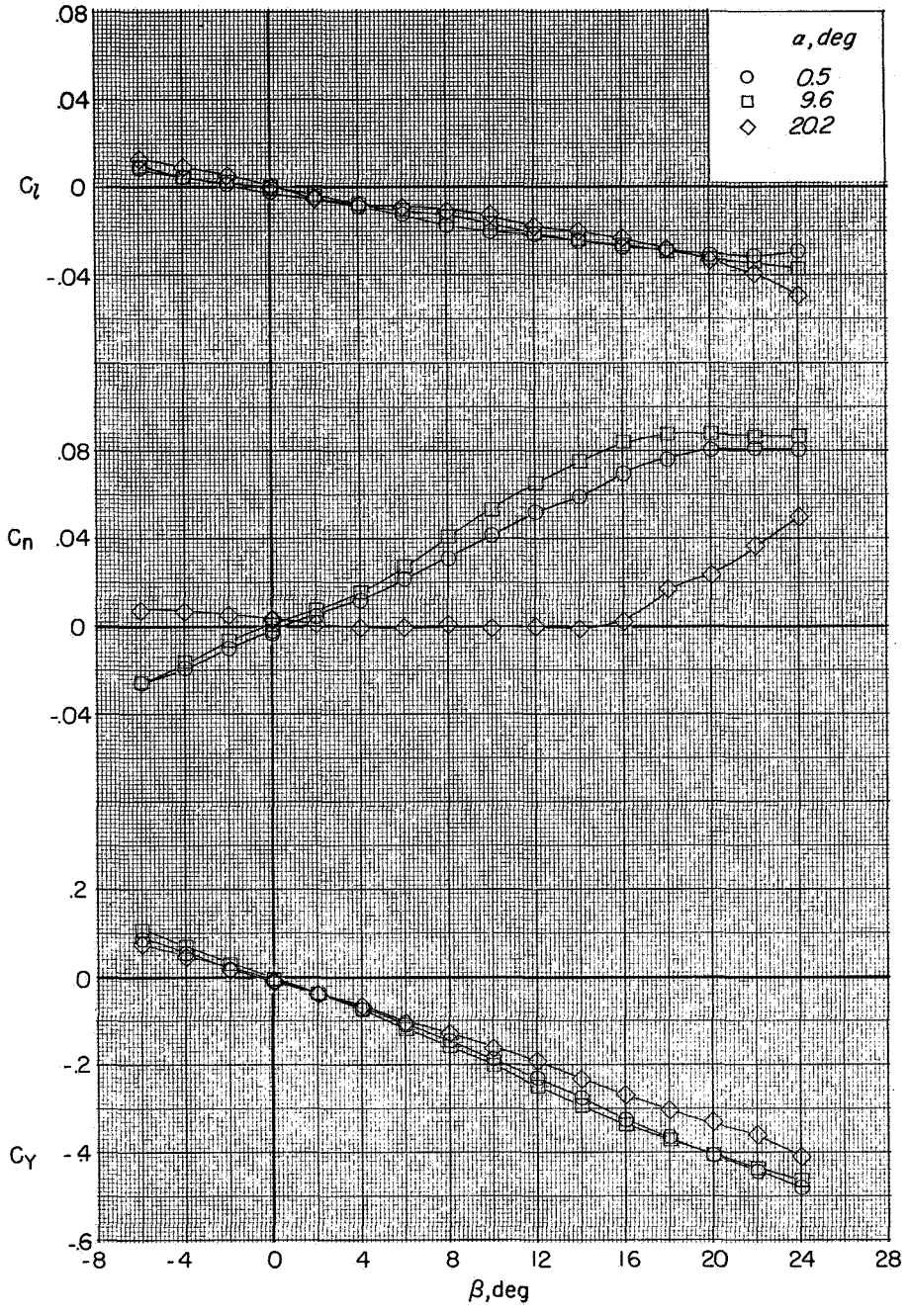

(a) $C_T = 0$.

Figure 26.- Variation of lateral-directional characteristics with sideslip angle showing effect of angle of attack. $\delta_n = 85^o$; $\delta_f = 60^o$; $i_t = 0^o$.

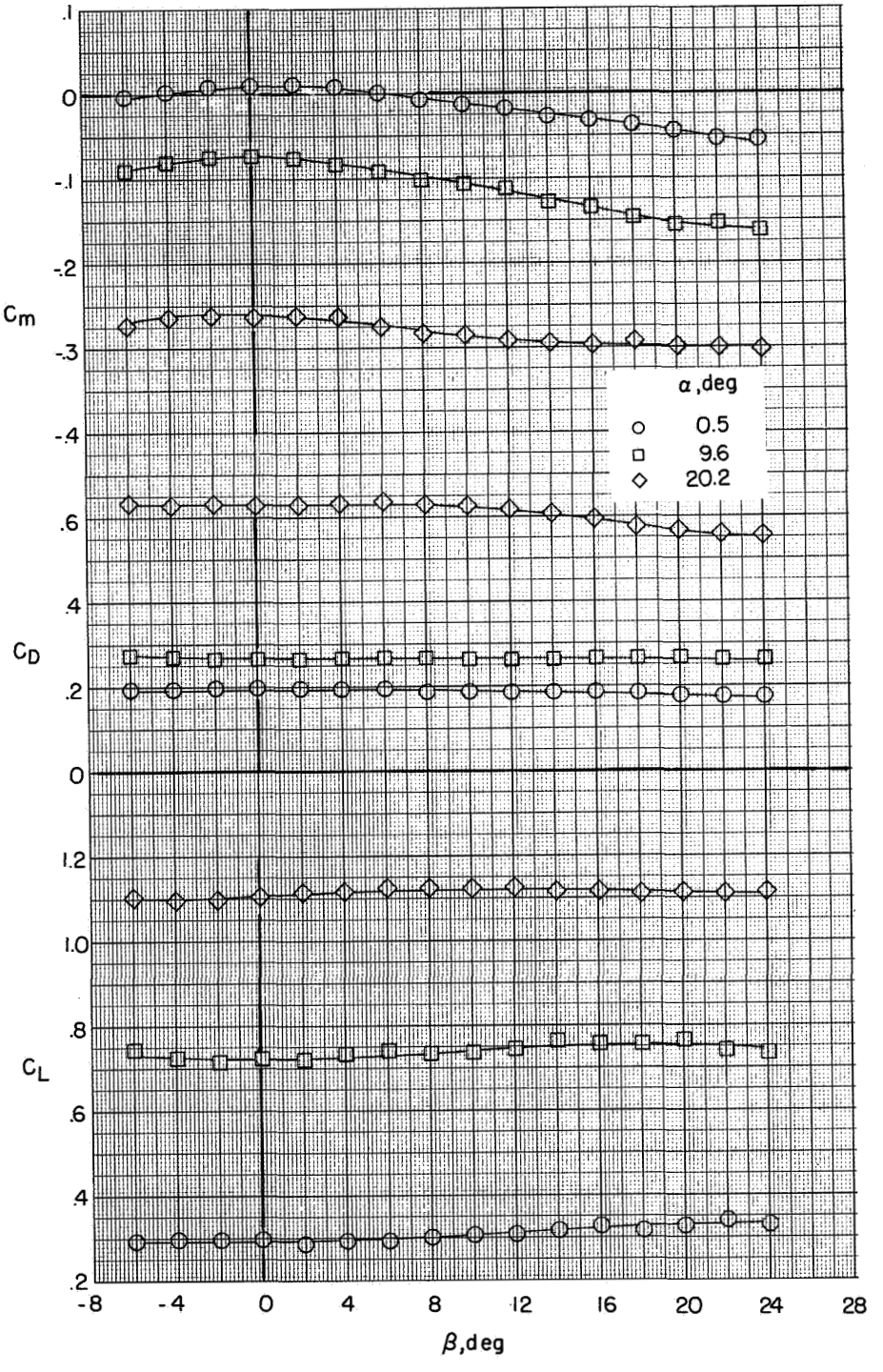

(a) Concluded.

Figure 26.- Continued.

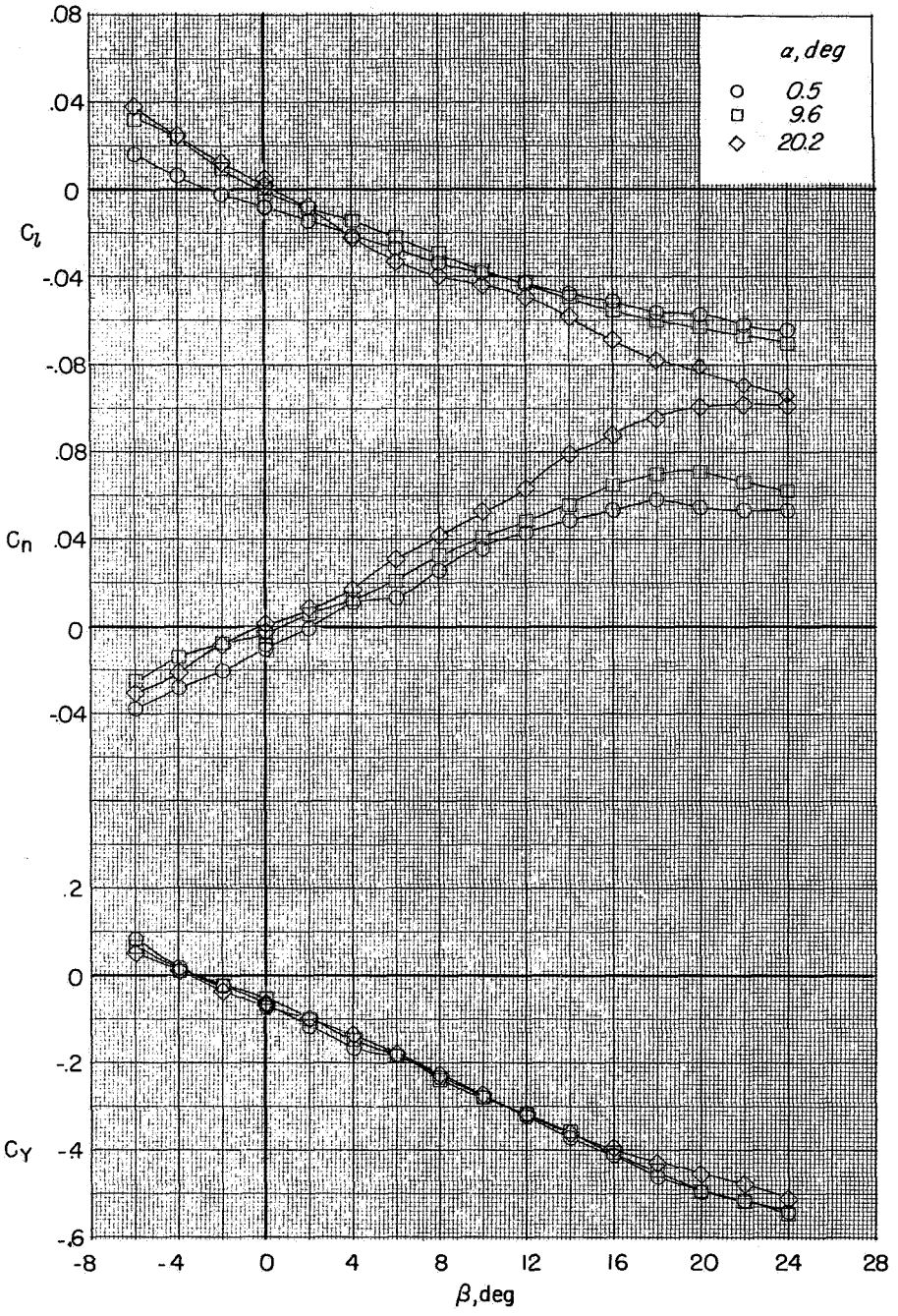

(b) $C_T = 1.1$.

Figure 26.- Continued.

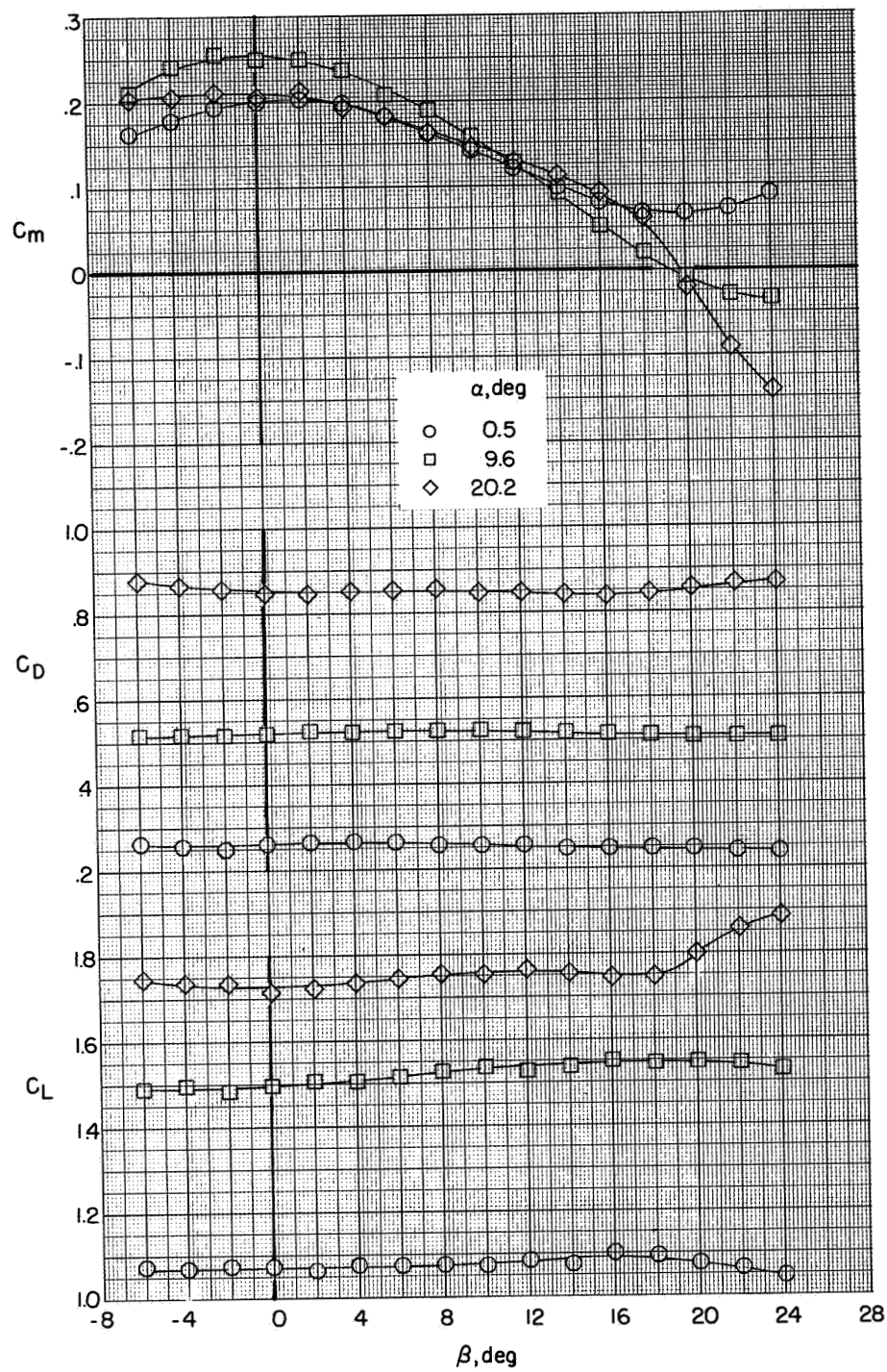

(b) Concluded.

Figure 26.- Continued.

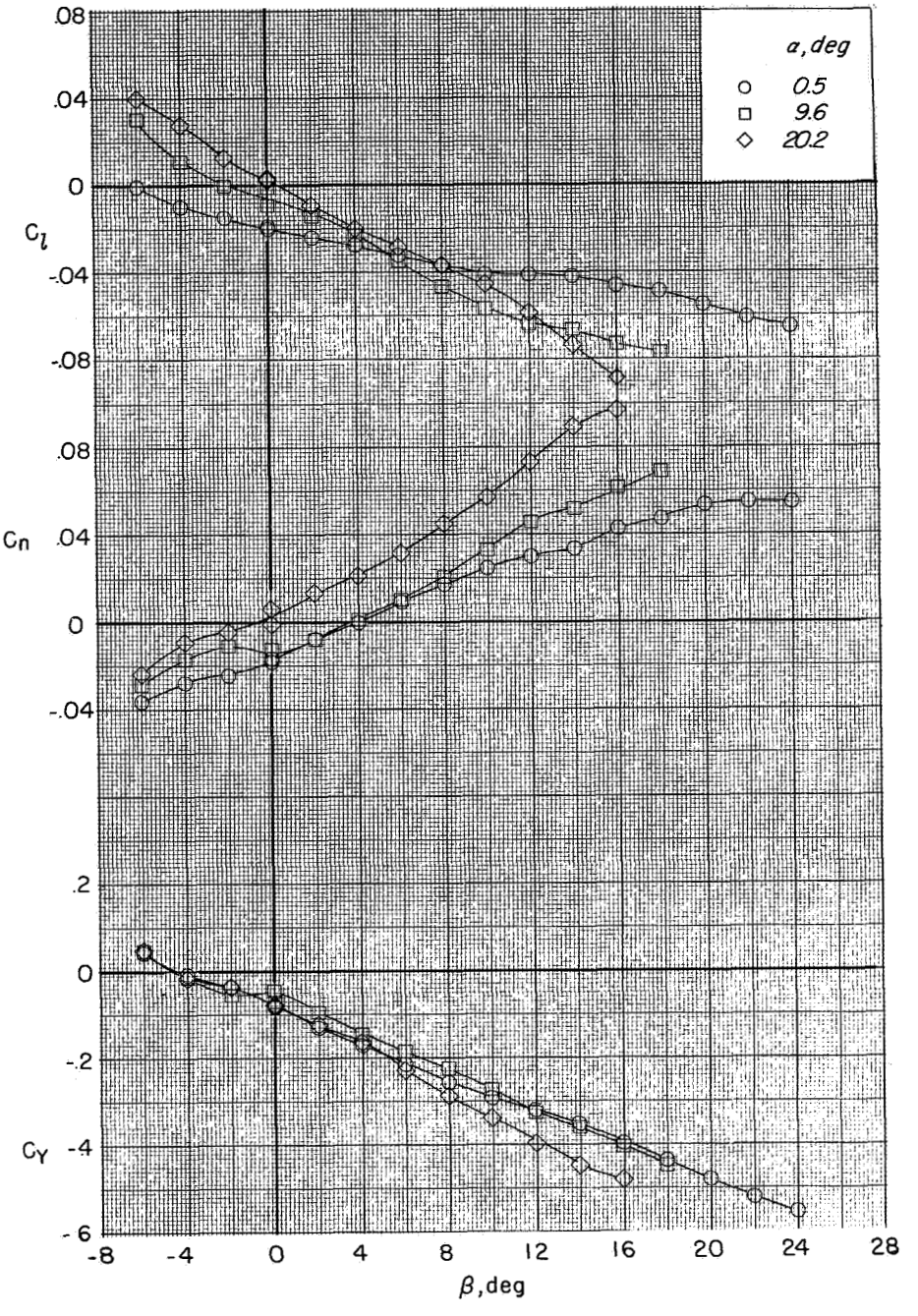

(c) $C_T = 2.1$.

Figure 26.- Continued.

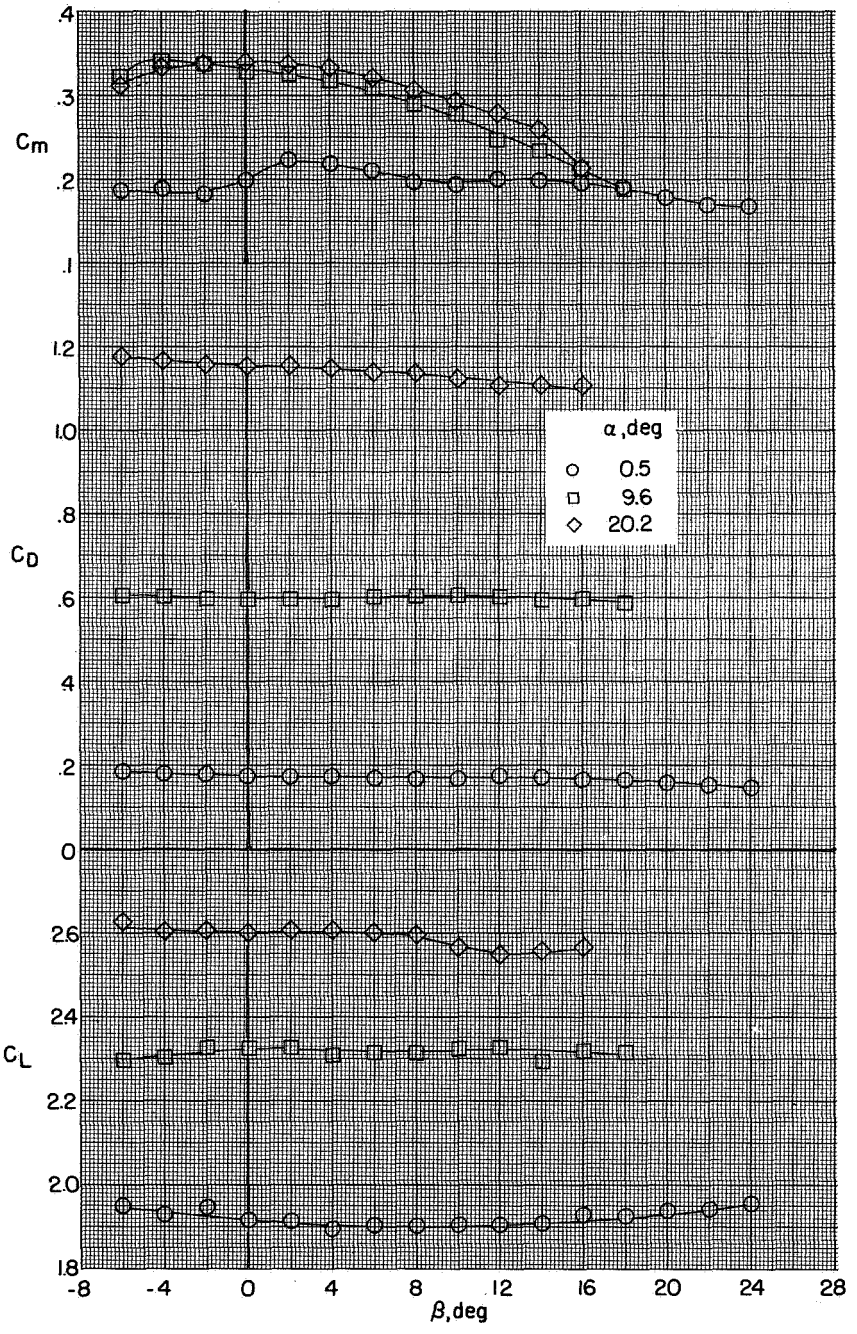

(c) Concluded.

Figure 26.- Continued.

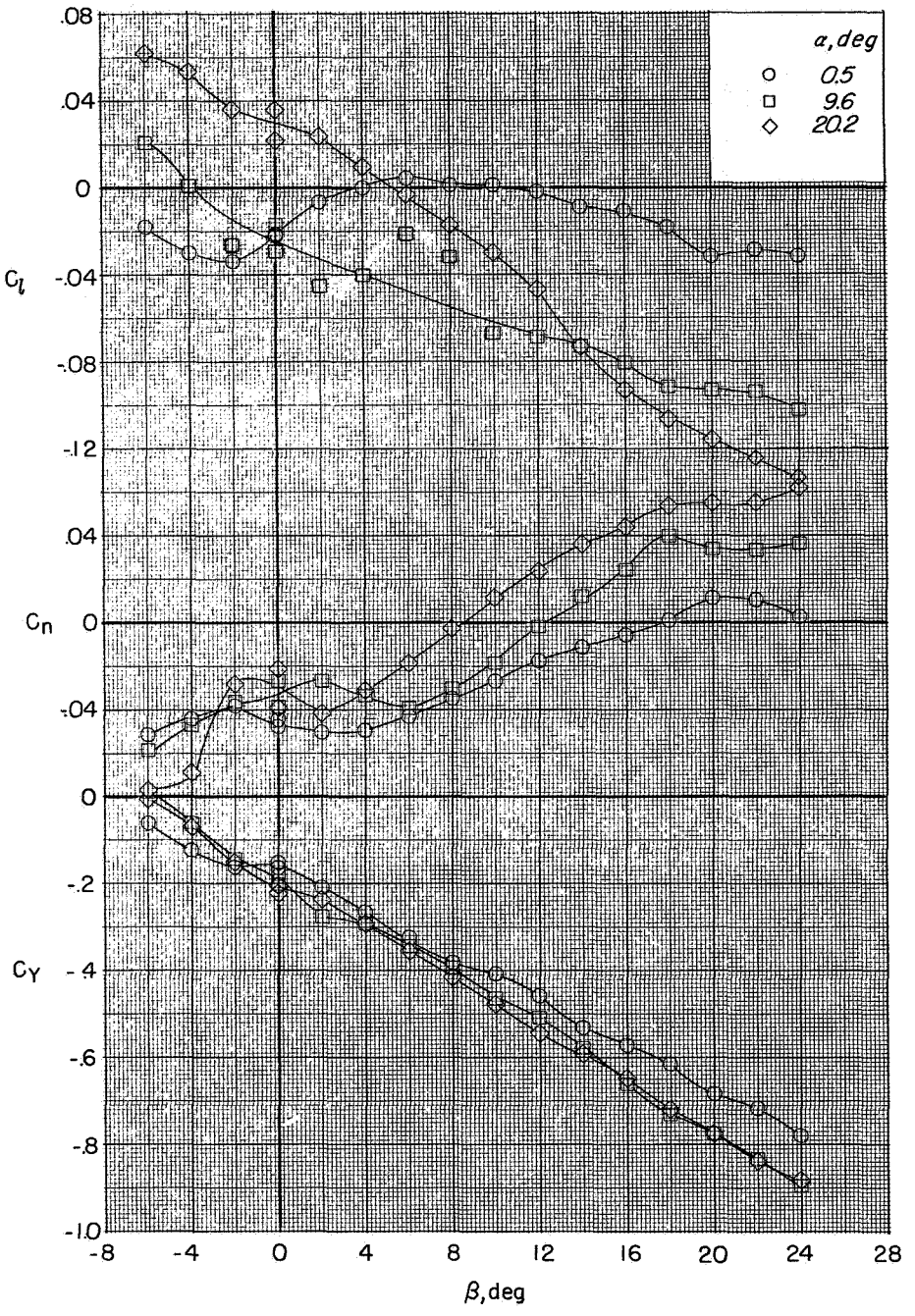

(d) $C_T = 6.1$.

Figure 26.- Continued.

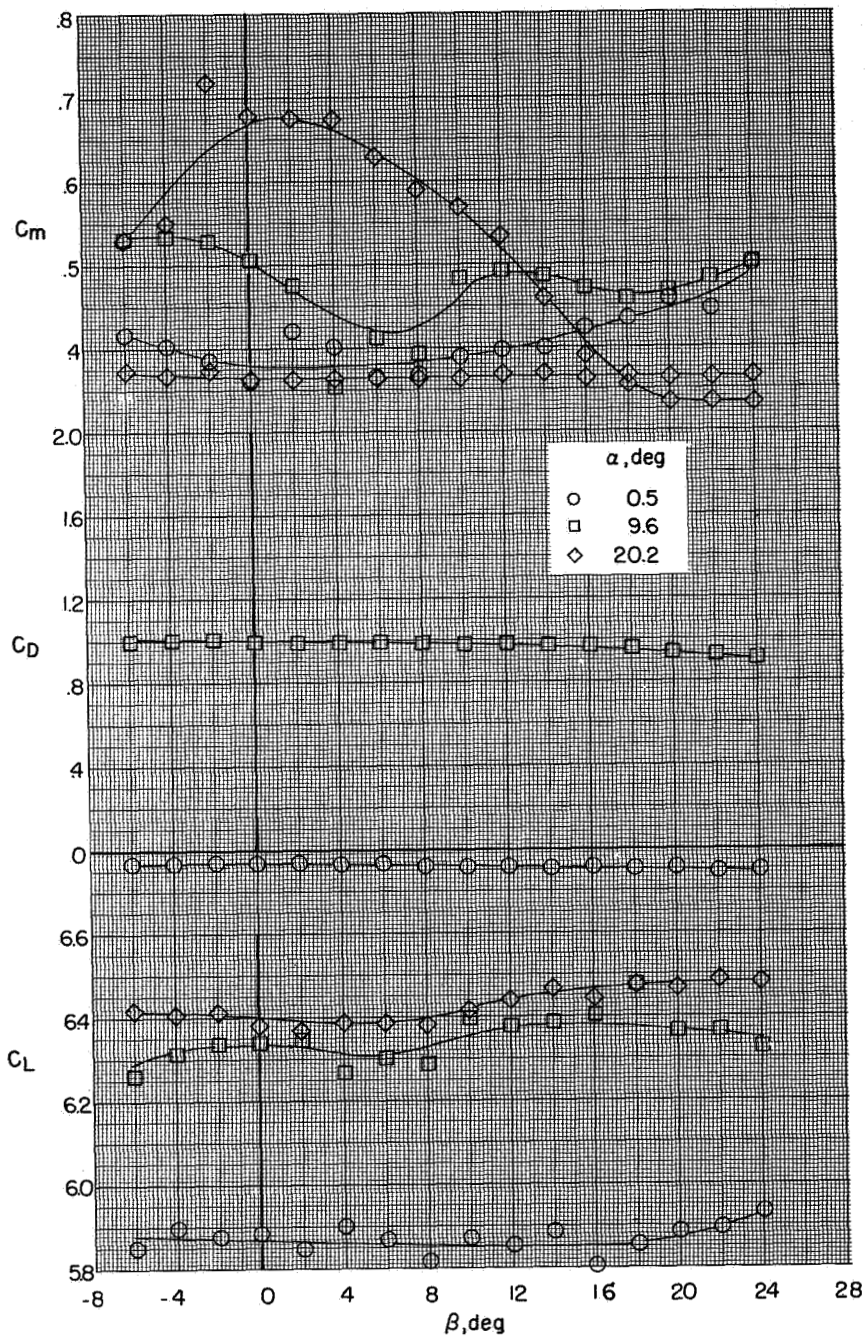

(d) Concluded.

Figure 26.- Concluded.

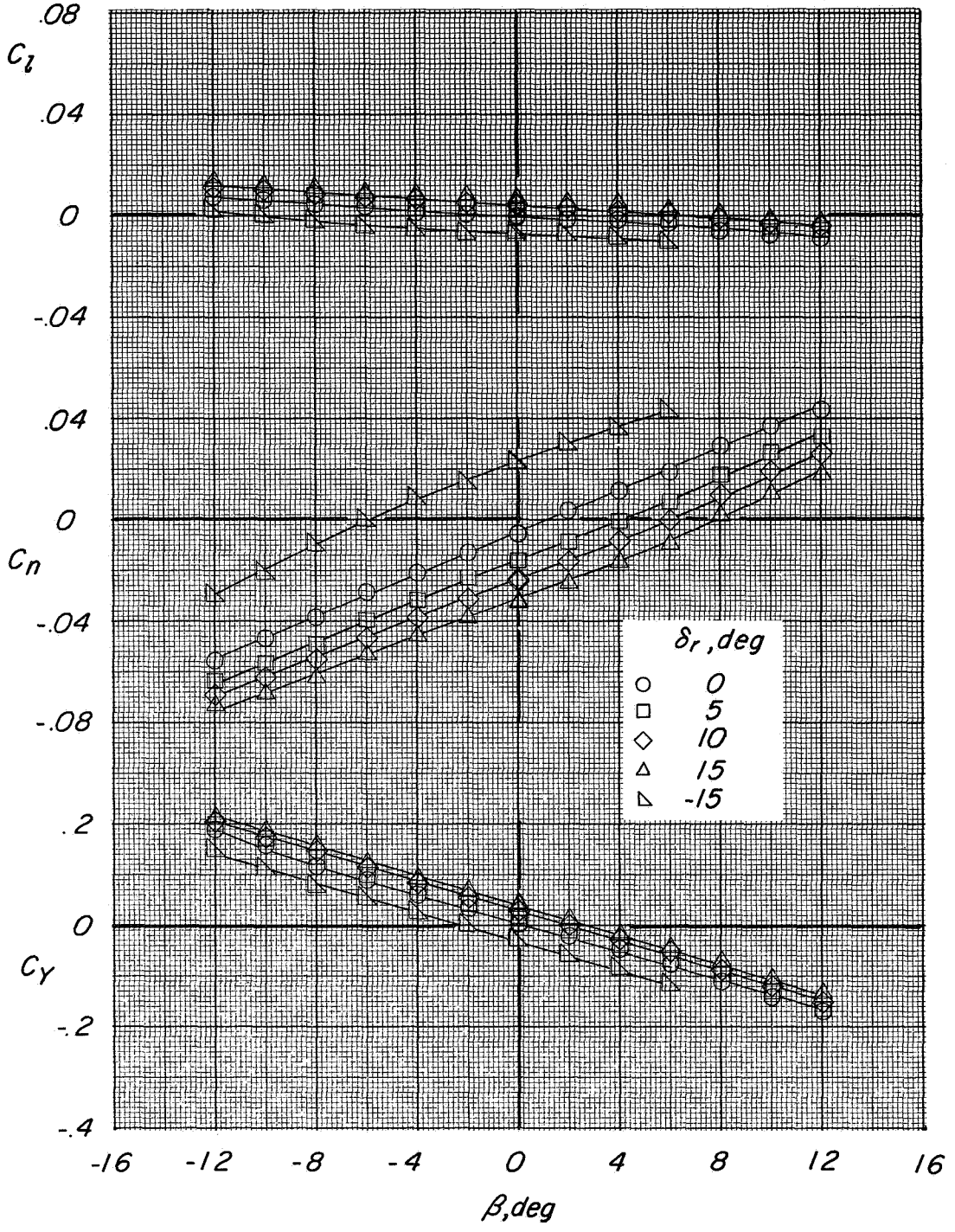

(a) $C_T = 0$.

Figure 27.- Variation of lateral-directional characteristics with sideslip angle showing rudder effectiveness in cruise. $\delta_f = 0^o$; $\delta_n = 0^o$; landing gear up; $\alpha = 0^o$.

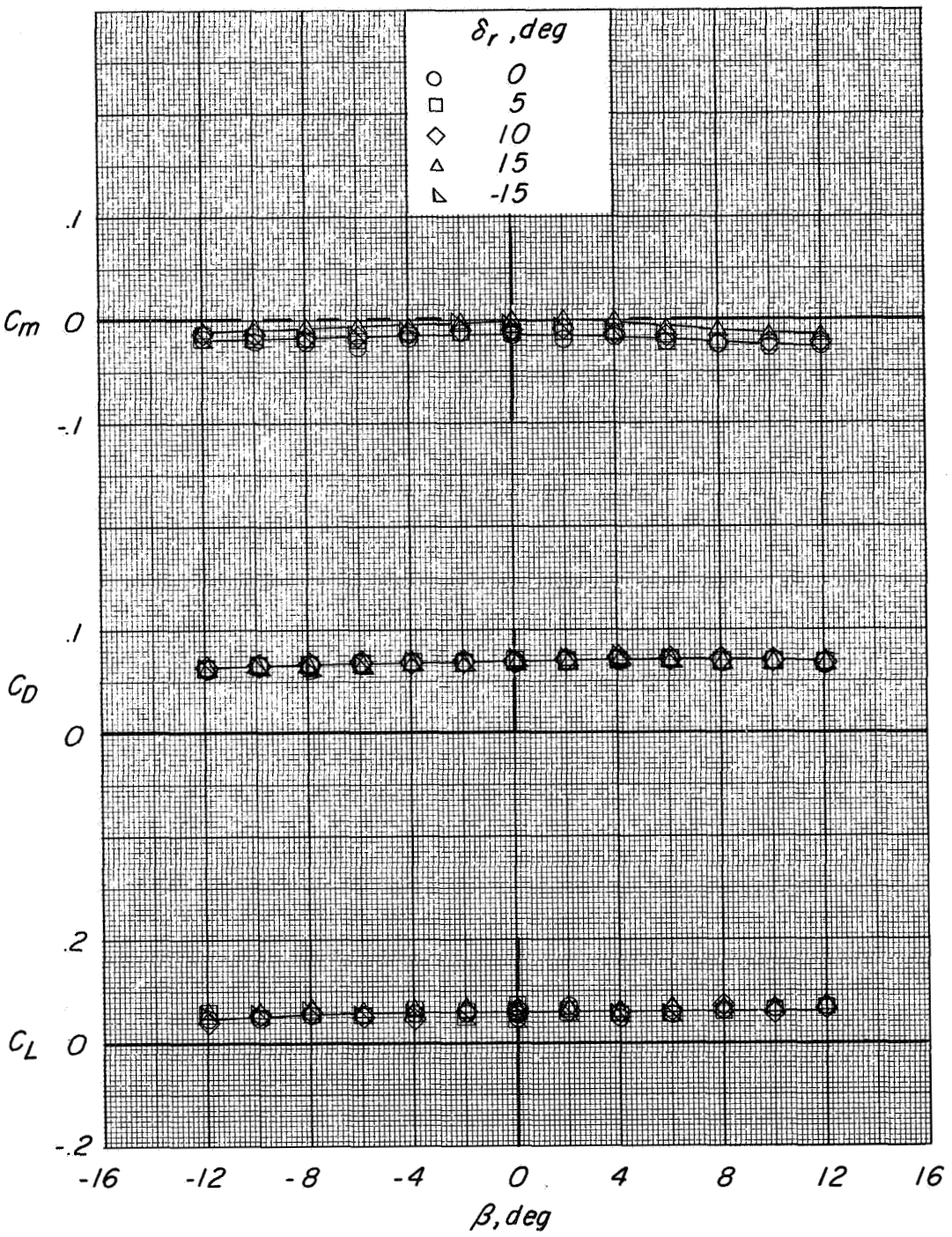

(a) Concluded.

Figure 27.- Continued.

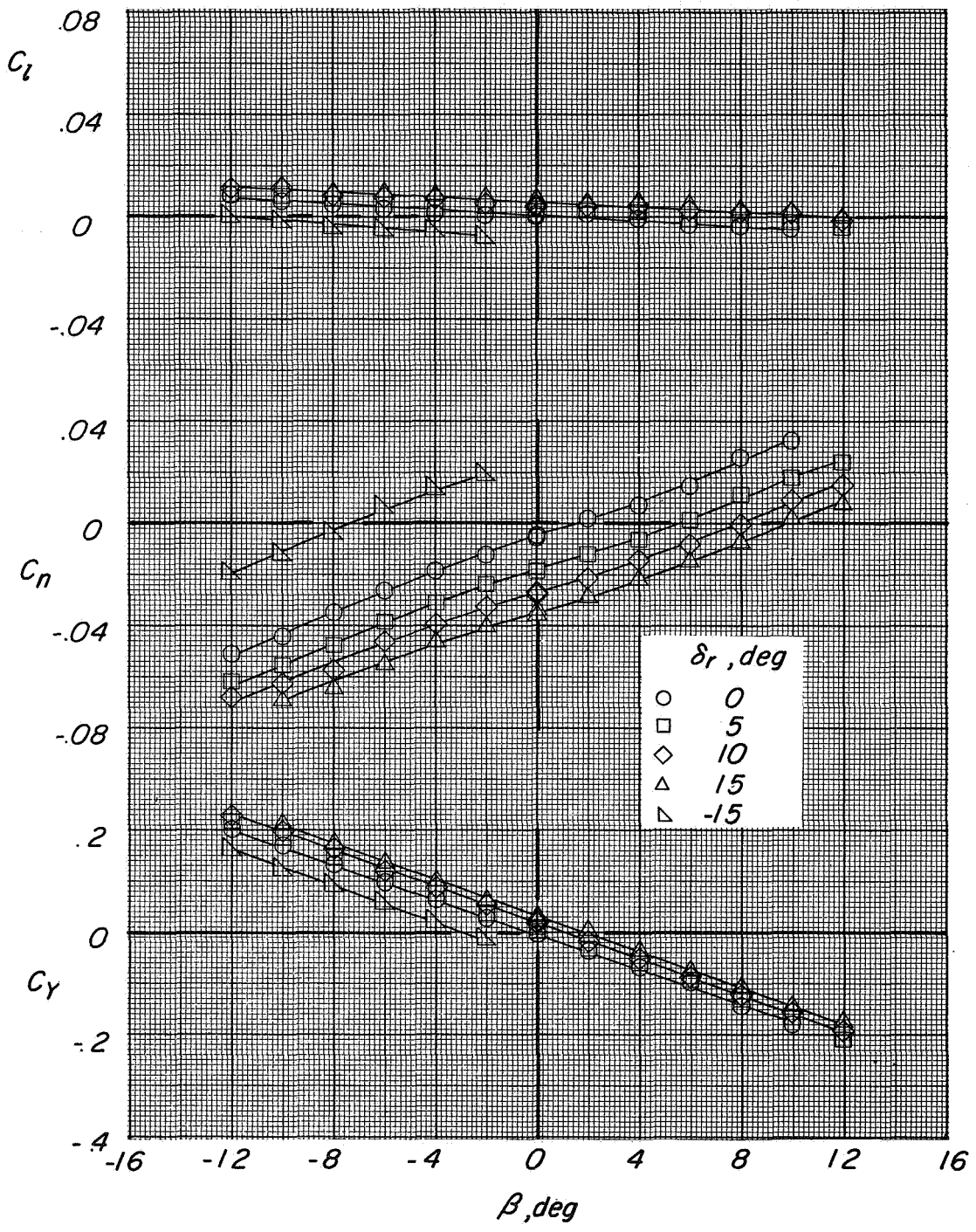

(b) $C_T = 0.6$.

Figure 27.- Continued.

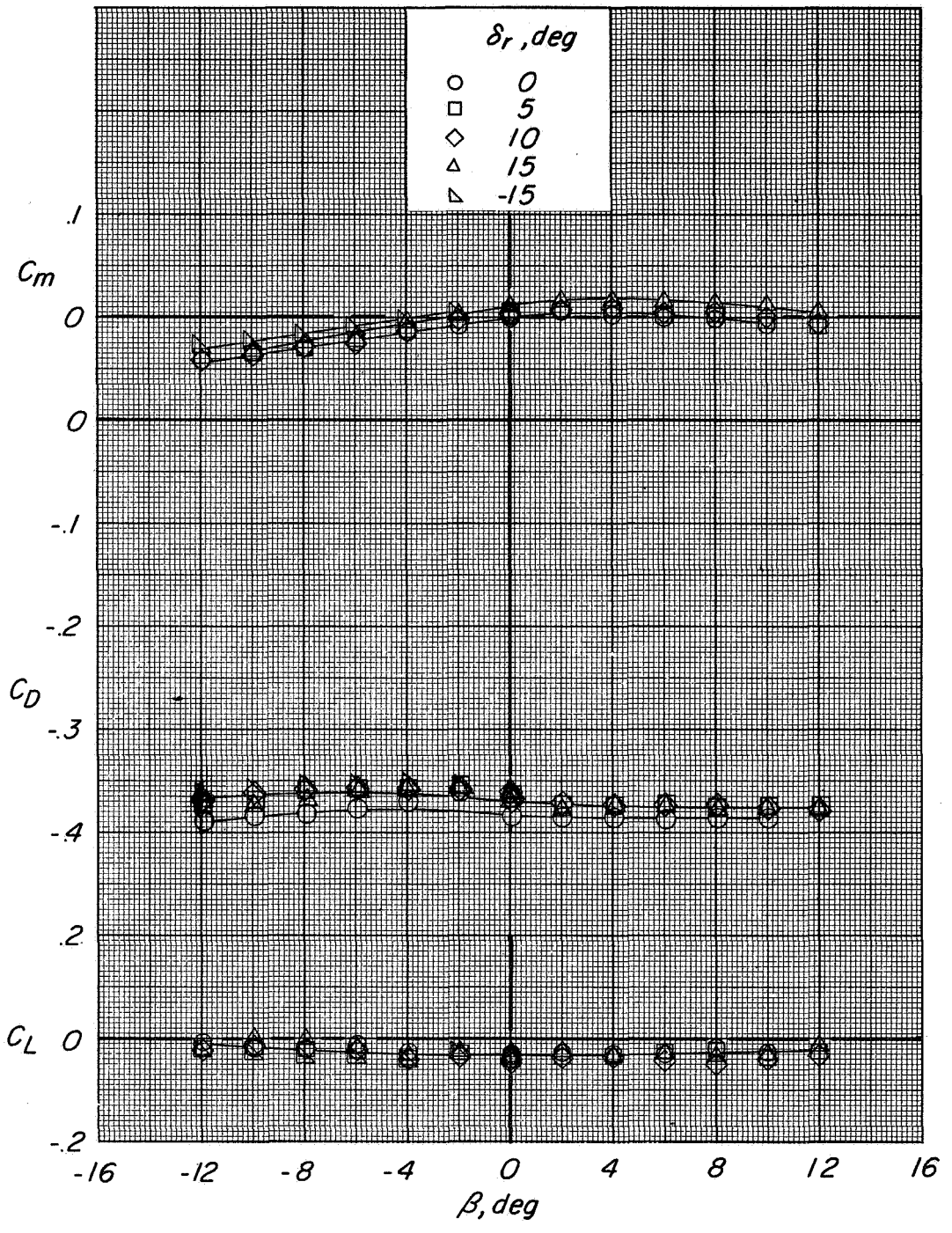

(b) Concluded.

Figure 27.- Continued.

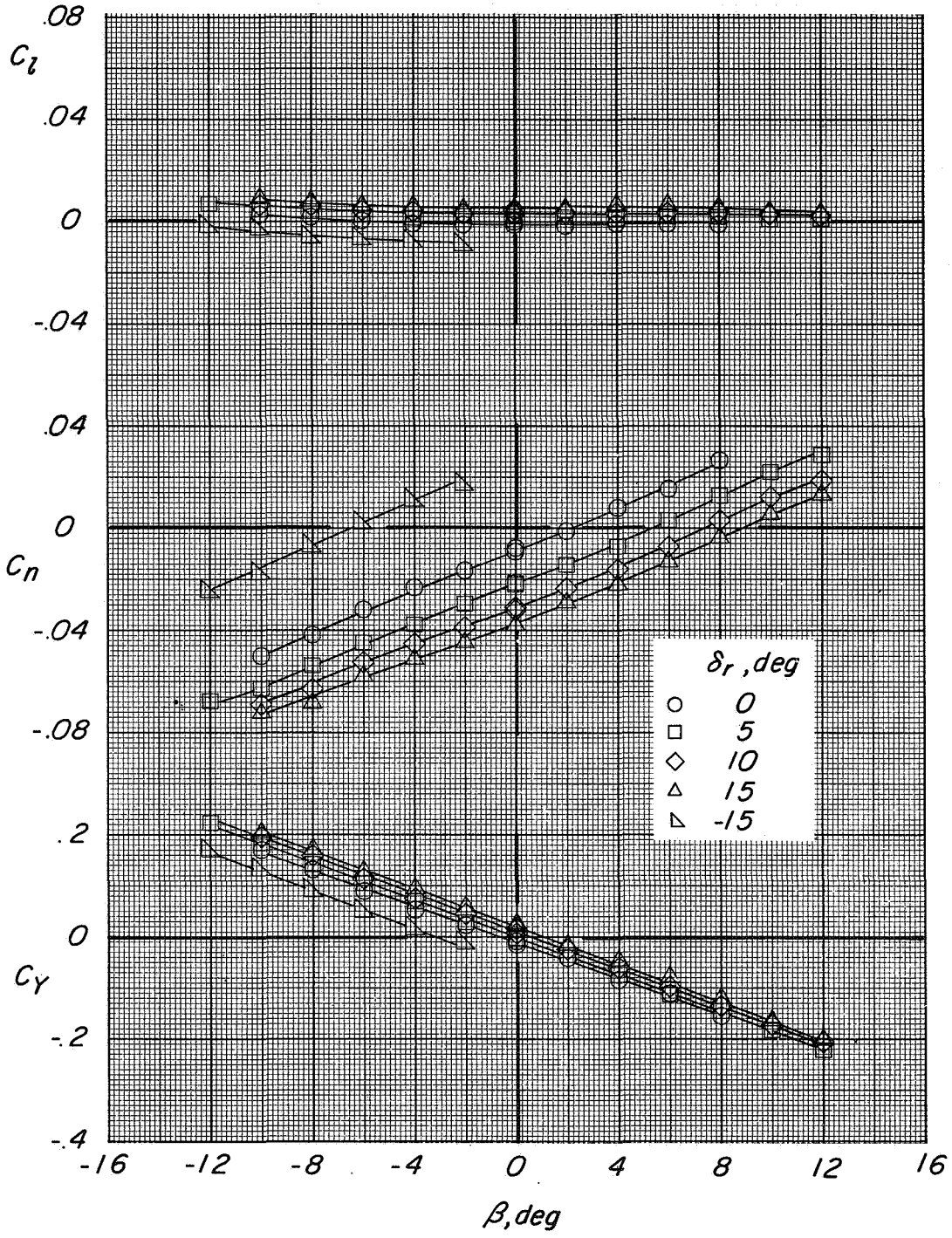

(c) $C_T = 1.1$.

Figure 27.- Continued.

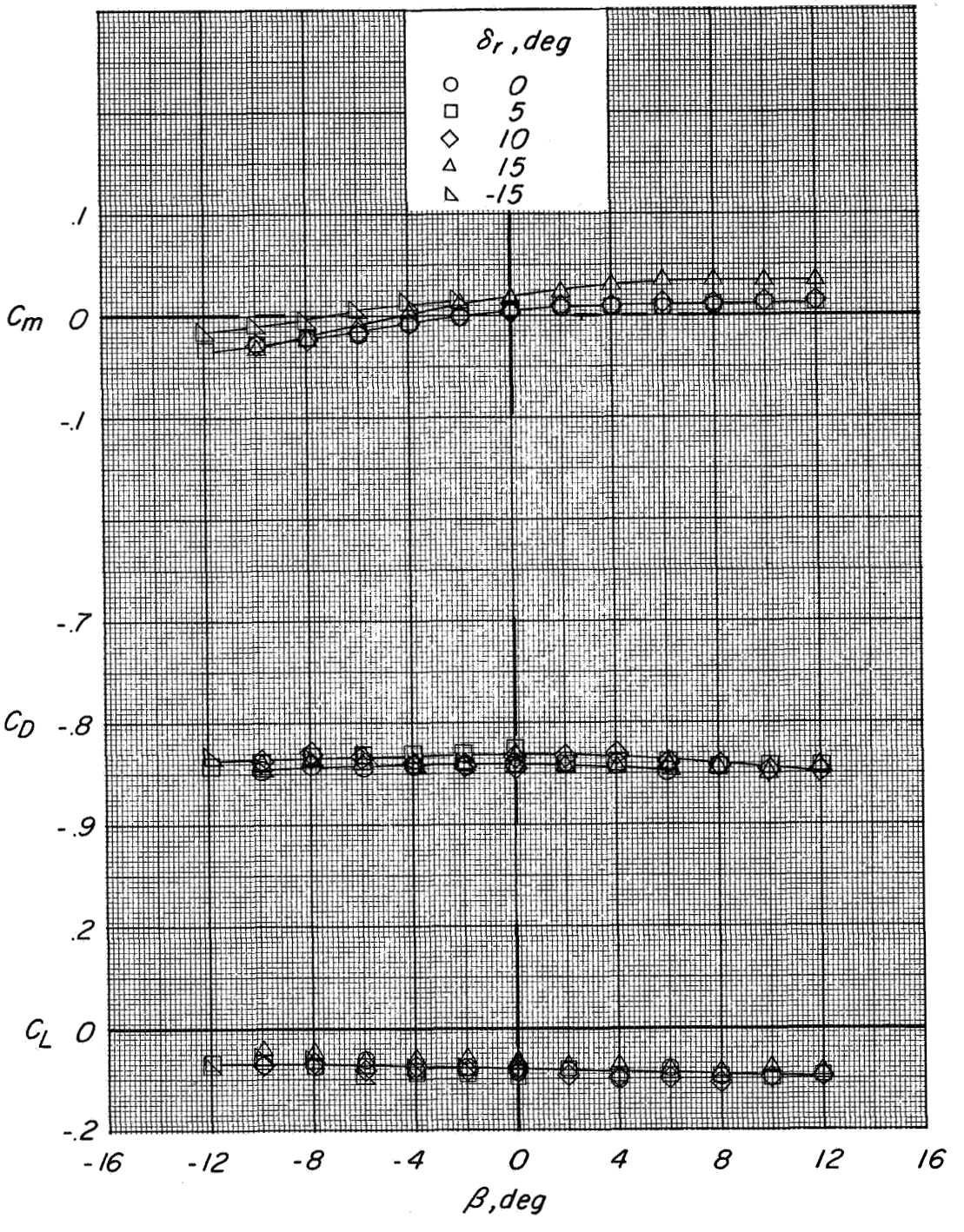

(c) Concluded.

Figure 27.- Concluded.

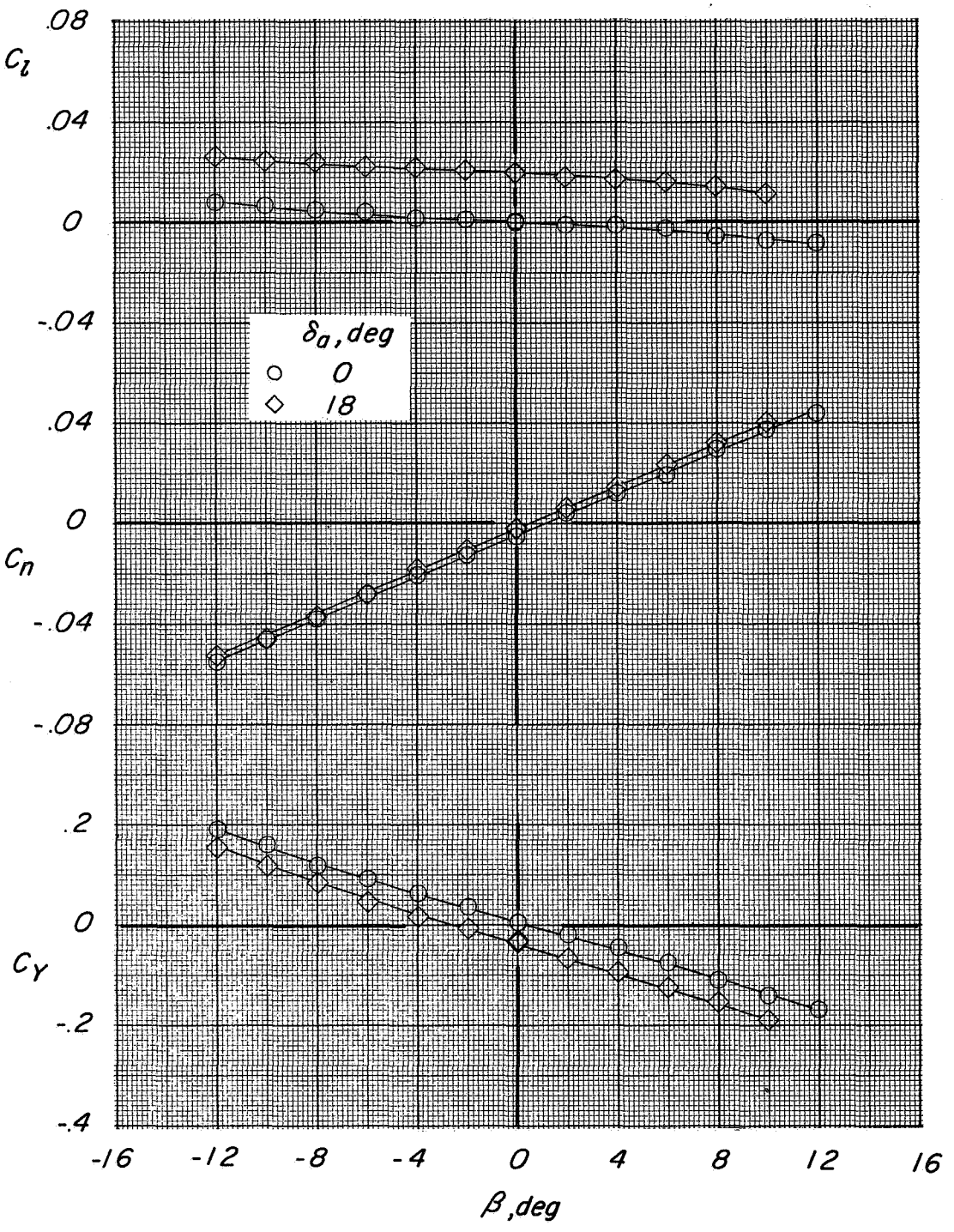

(a) $C_T = 0$.

Figure 28.- Variation of lateral-directional characteristics with sideslip angle showing effect of aileron deflection in cruise. $\delta_f = 0^o$; $\delta_n = 0^o$; landing gear up; $\alpha = 0^o$.

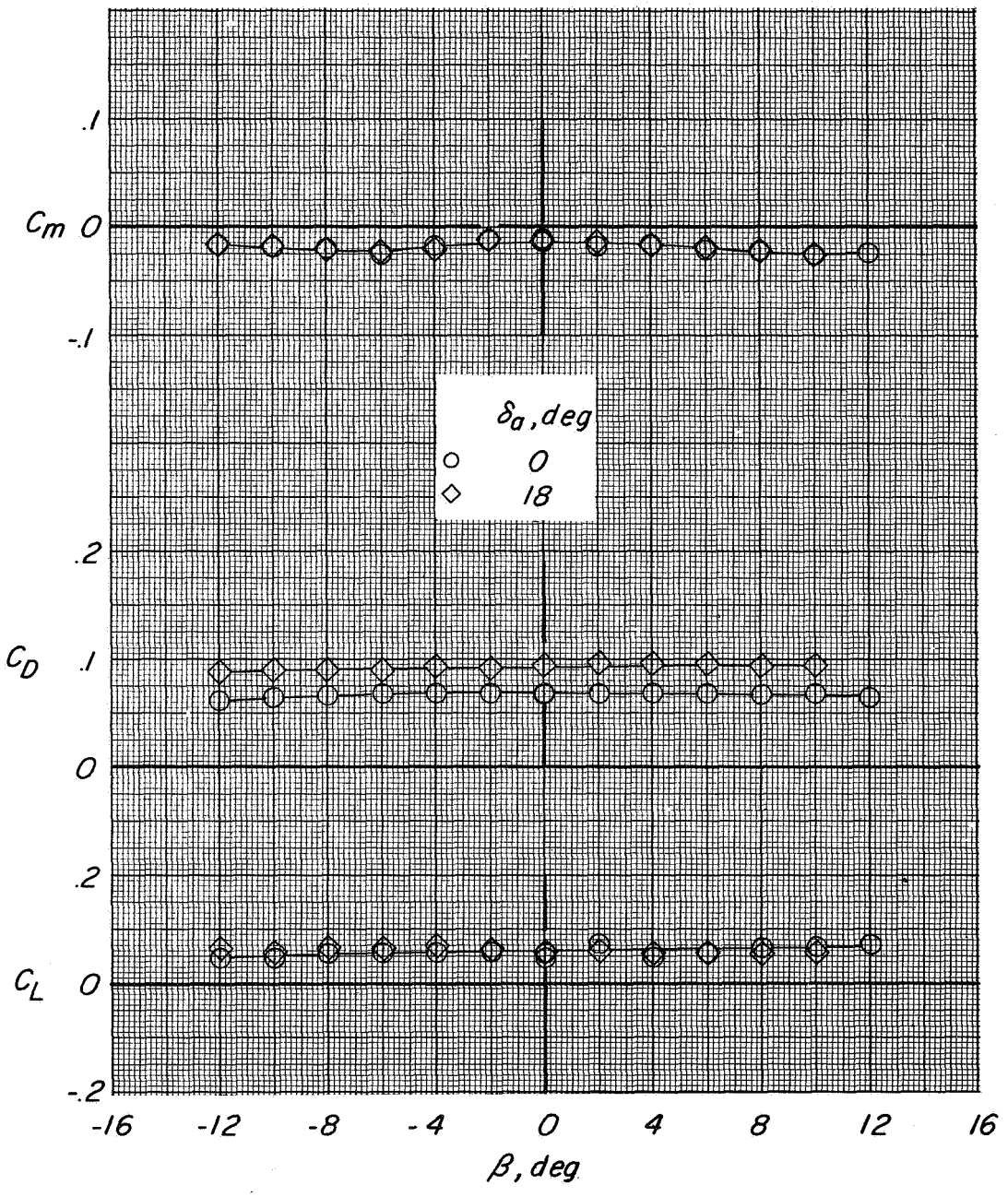

(a) Concluded.

Figure 28.- Continued.

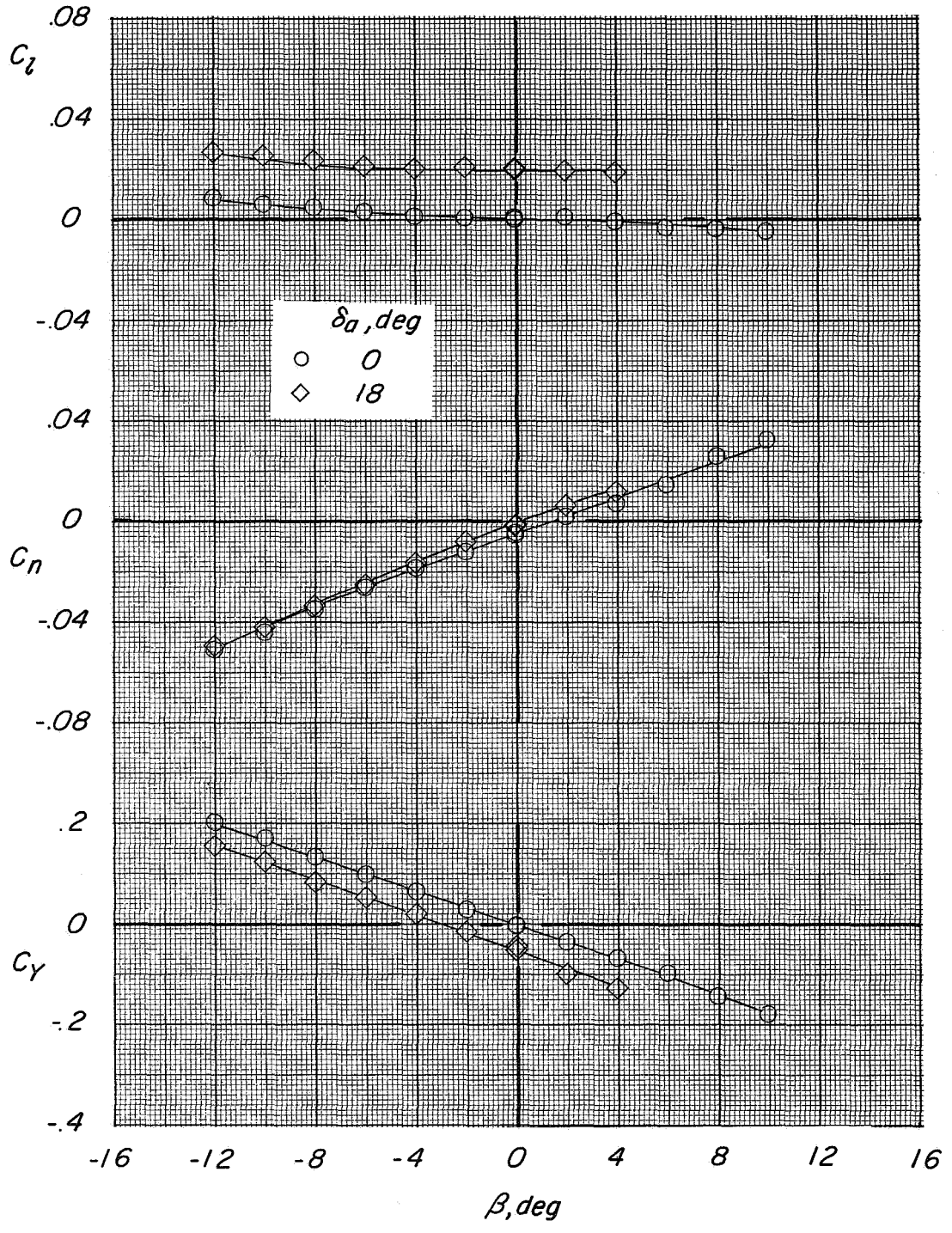

(b) $C_T = 0.6$.

Figure 28.- Continued.

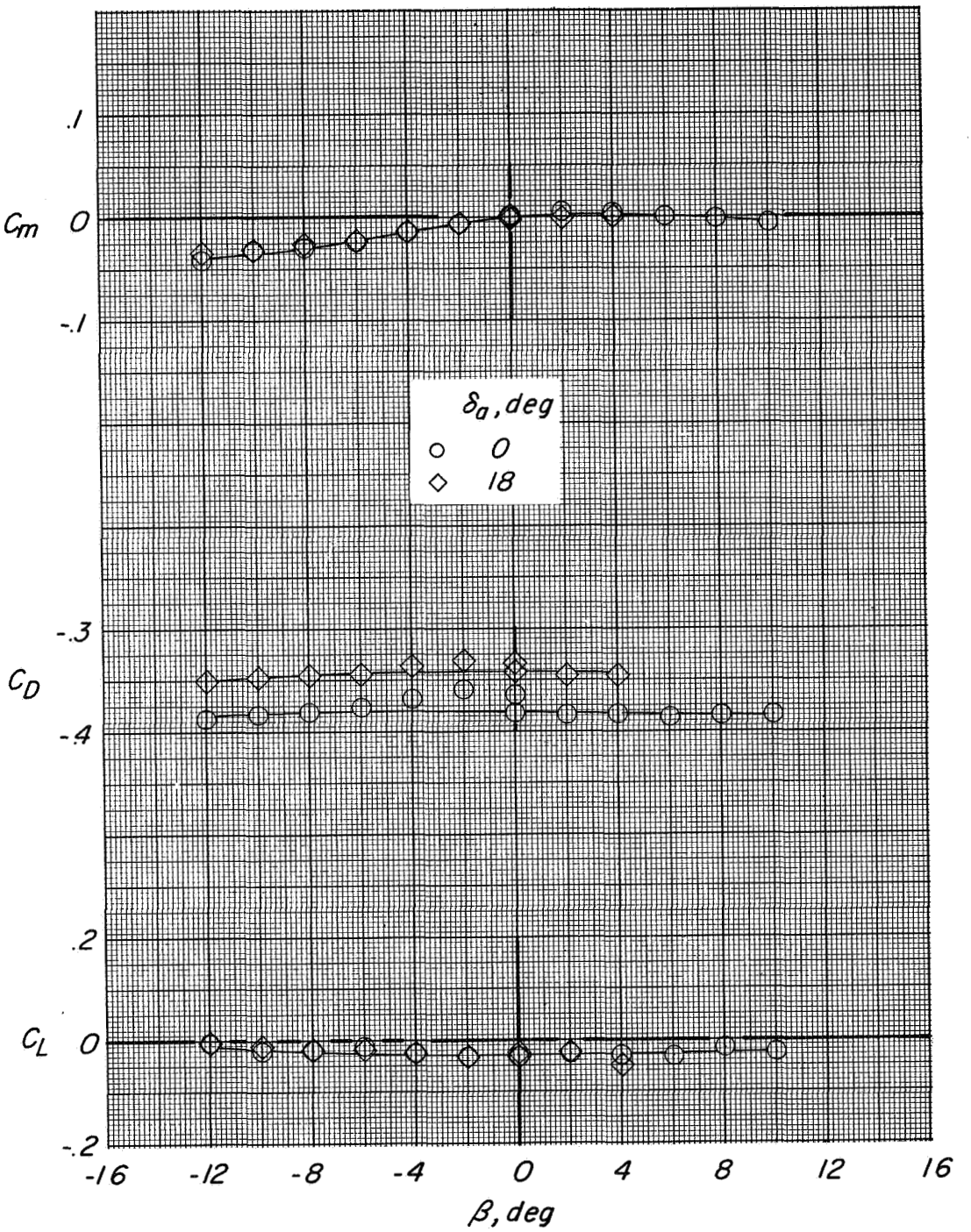

(b) Concluded.

Figure 28.- Continued.

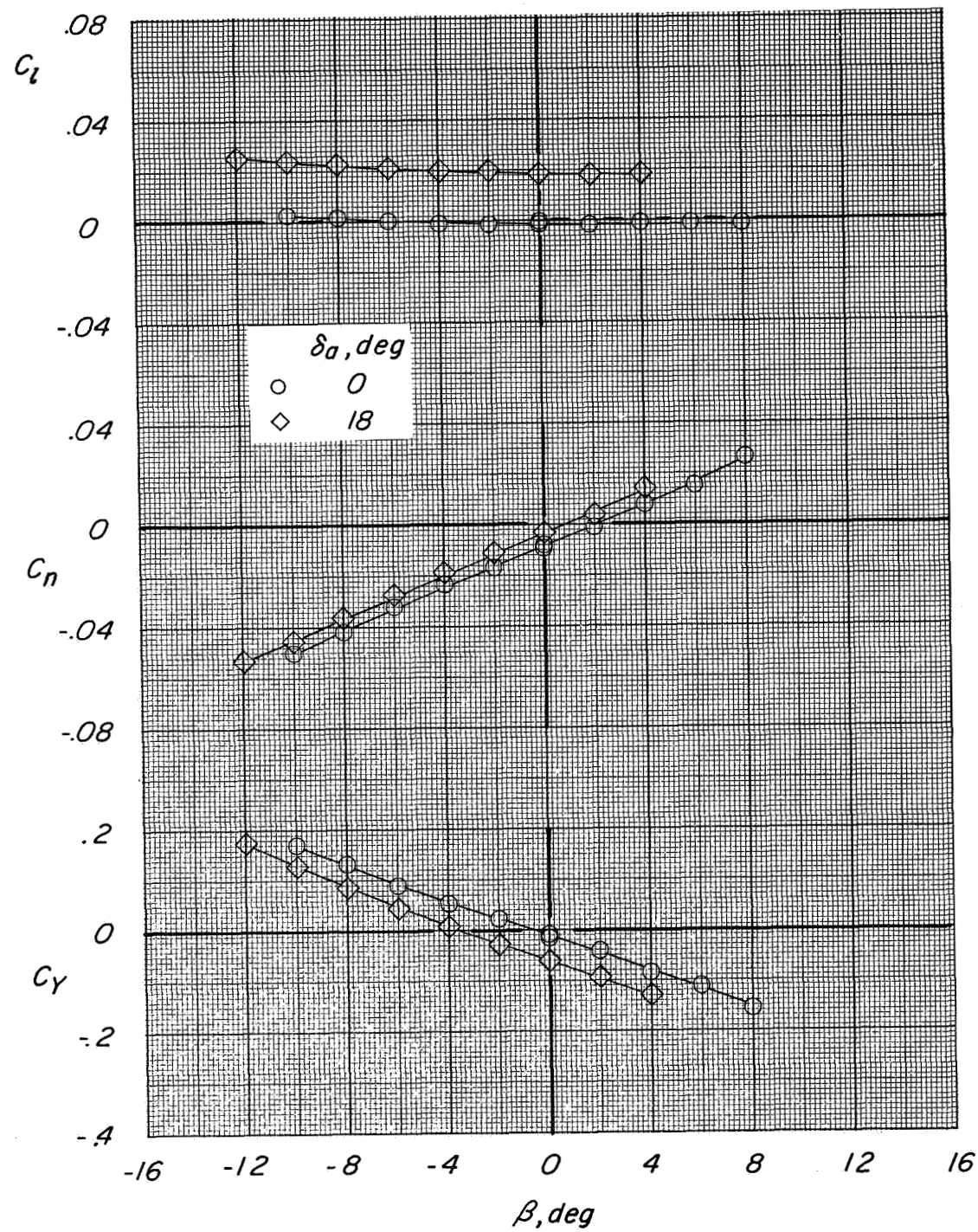

(c) $C_T = 1.1$.

Figure 28.- Continued.

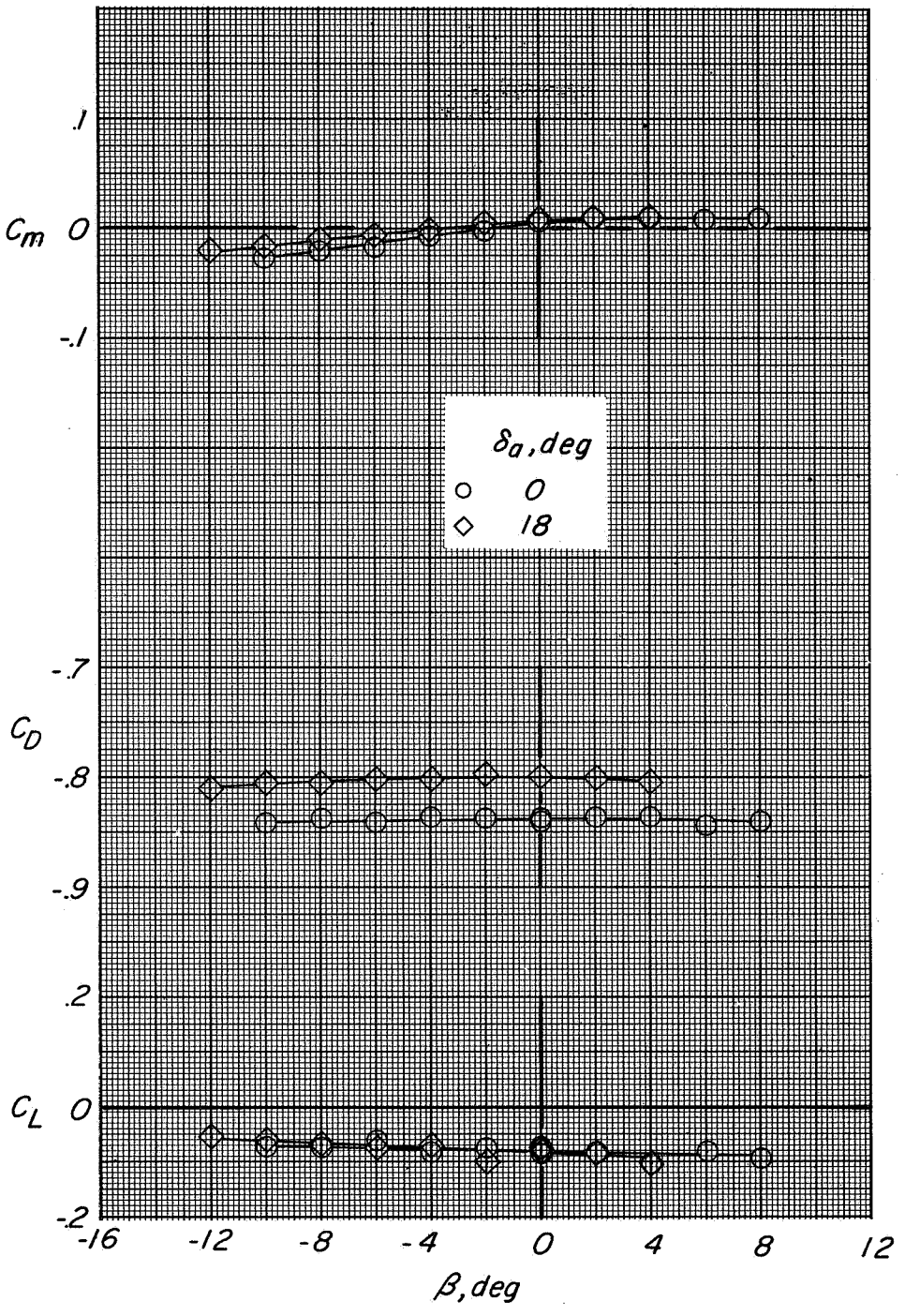

(c) Concluded.

Figure 28.- Concluded.

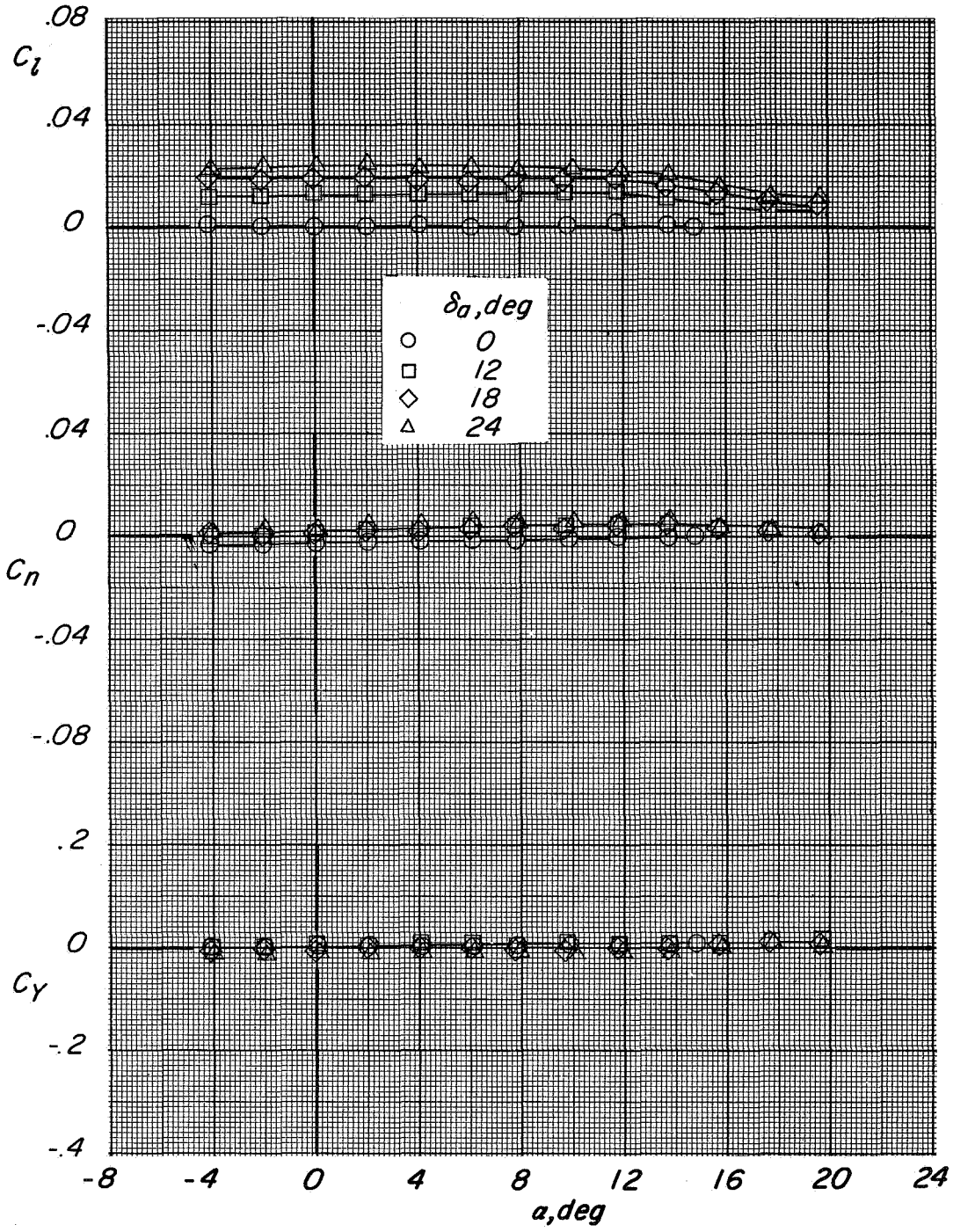

(a) $C_T = 0$.

Figure 29.- Variation of lateral-directional characteristics with angle of attack showing aileron effectiveness in cruise. $\delta_f = 0^o$; $\delta_n = 0^o$; landing gear up; $\beta = 0^o$.

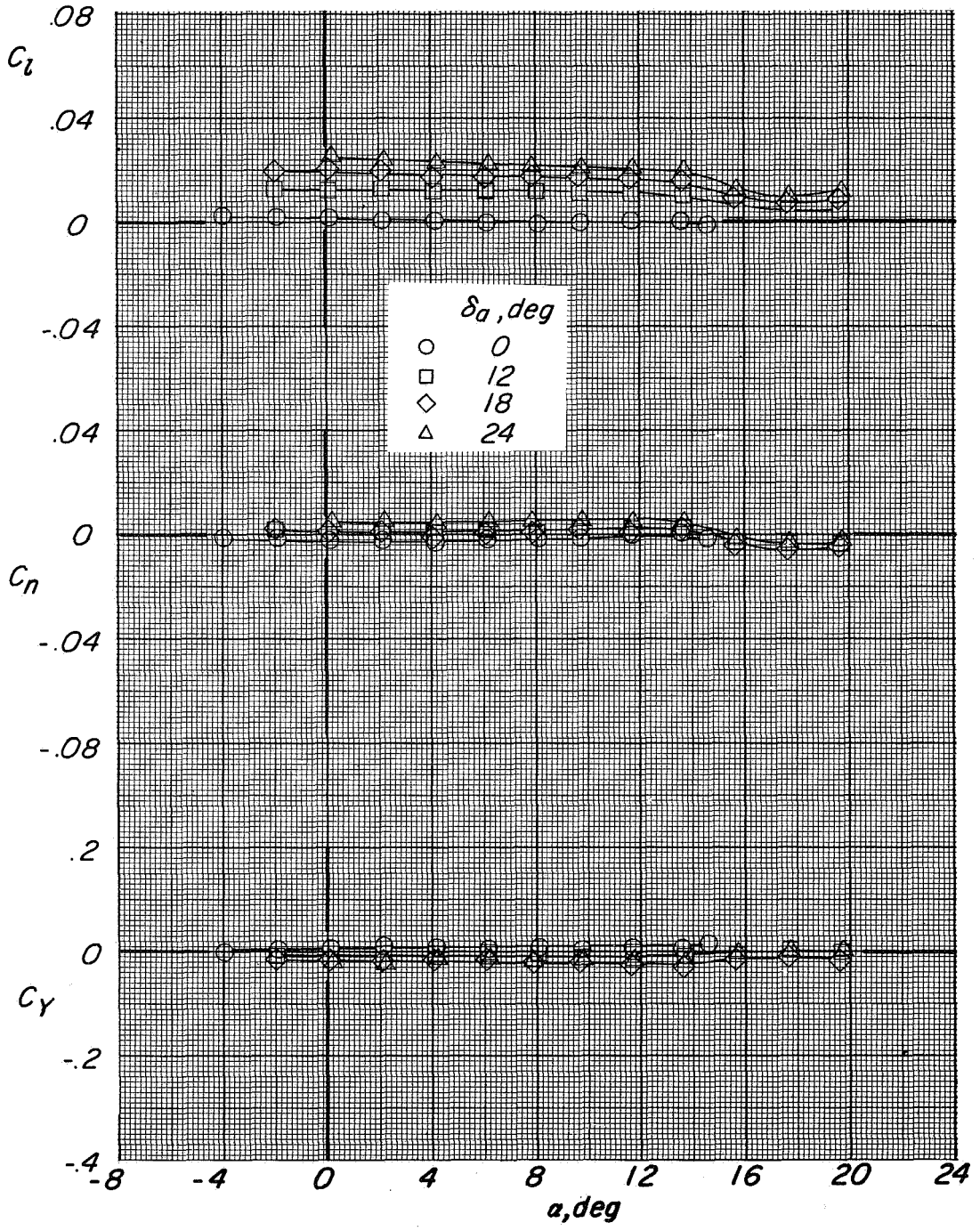

(b) $C_T = 0.6$.

Figure 29.- Continued.

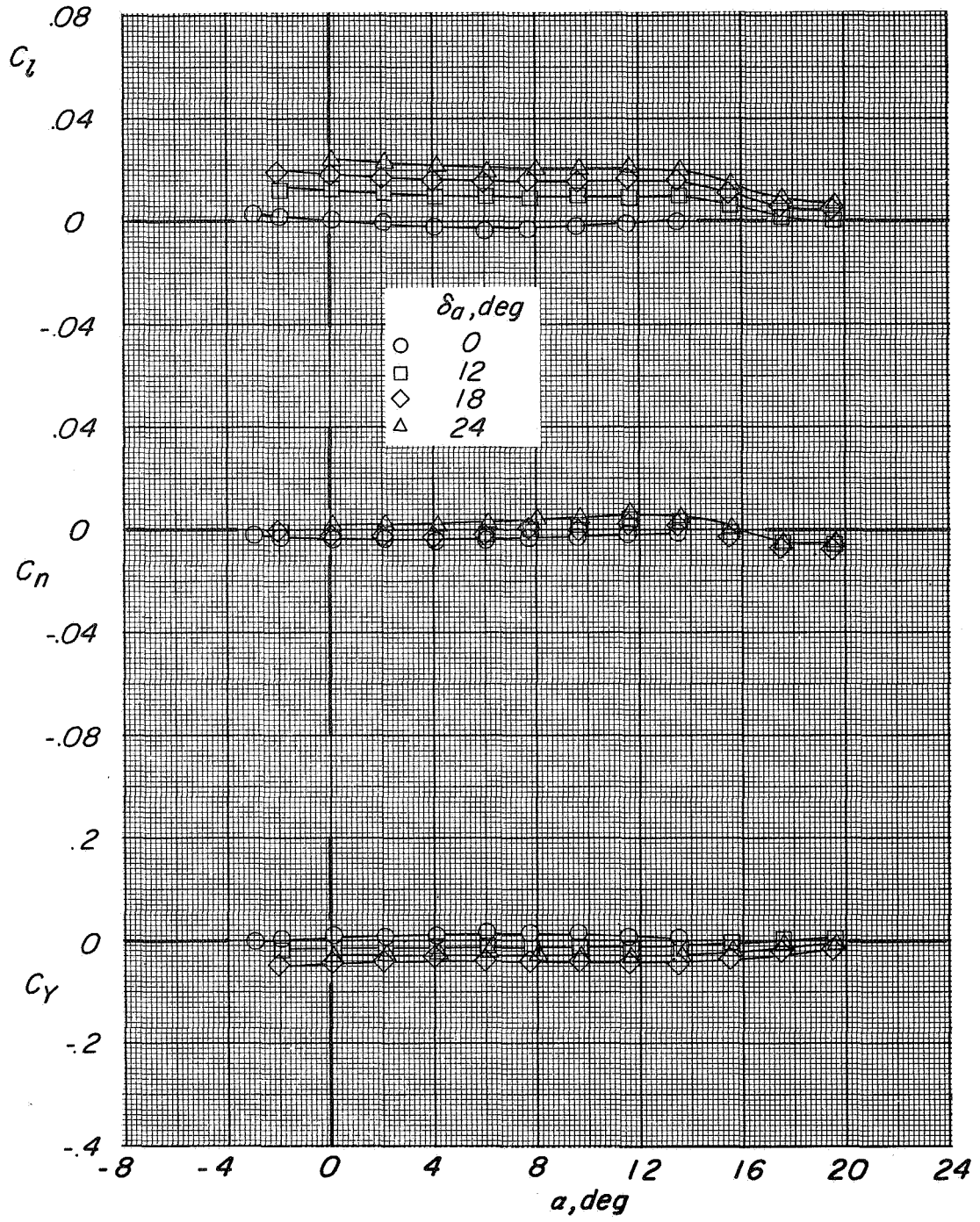

(c) $C_T = 1.1$.

Figure 29.- Concluded.

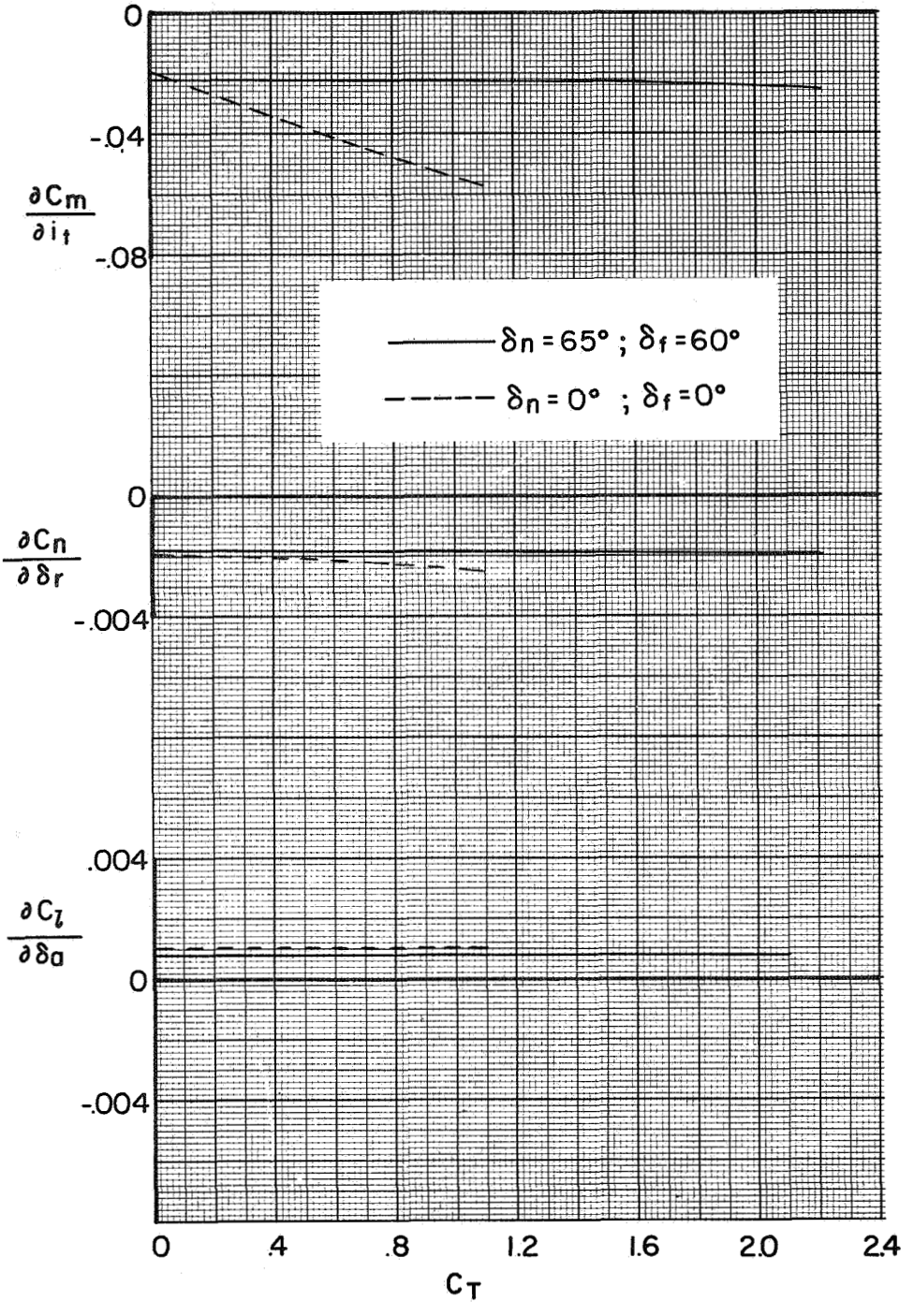

Figure 30.- Variation of control-surface effectiveness with thrust coefficient. $\alpha = 0^o$; $\beta = 0^o$.

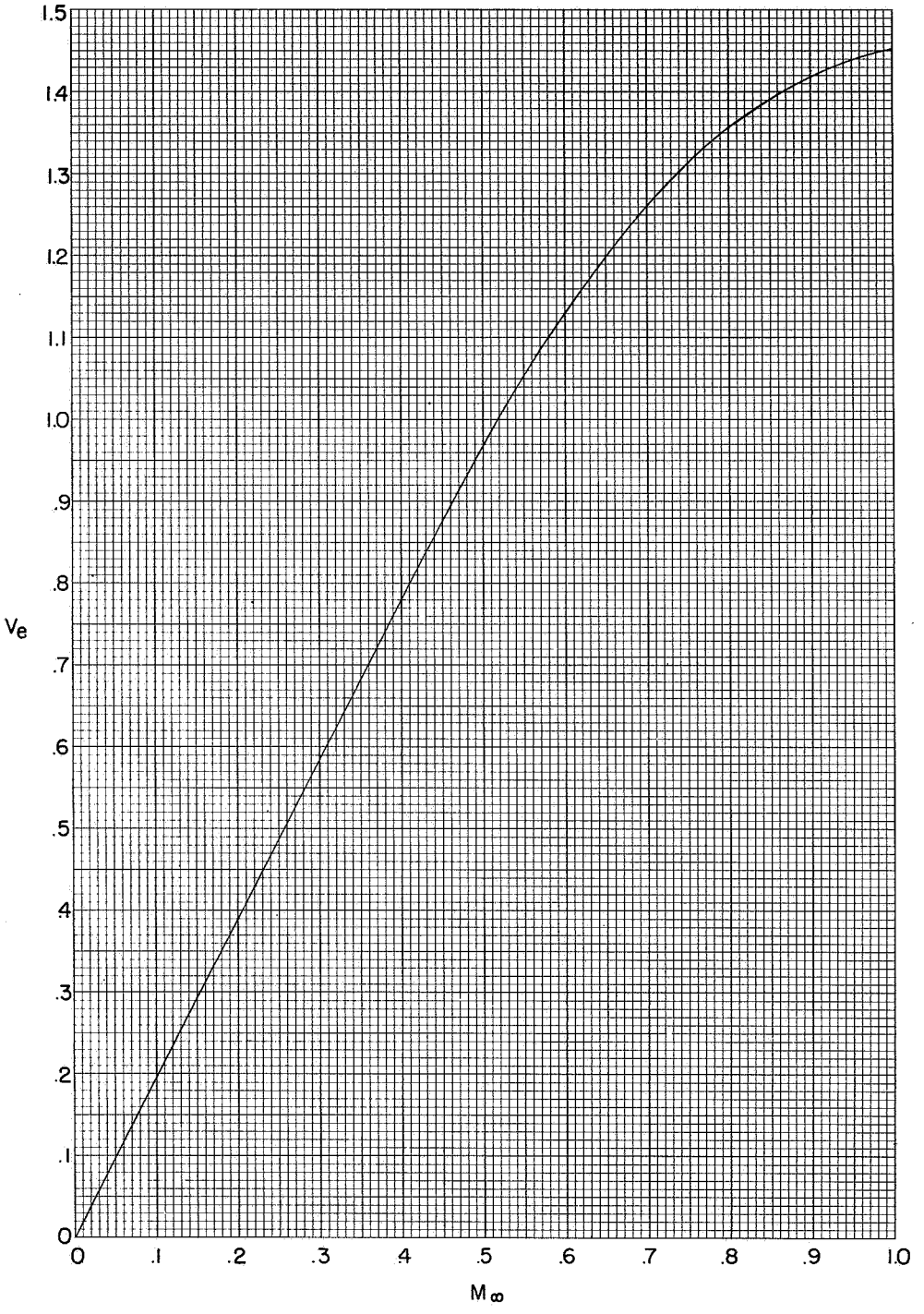

Figure 31.- Variation of effective-velocity ratio with Mach number at an altitude of 4572 meters (15 000 feet).

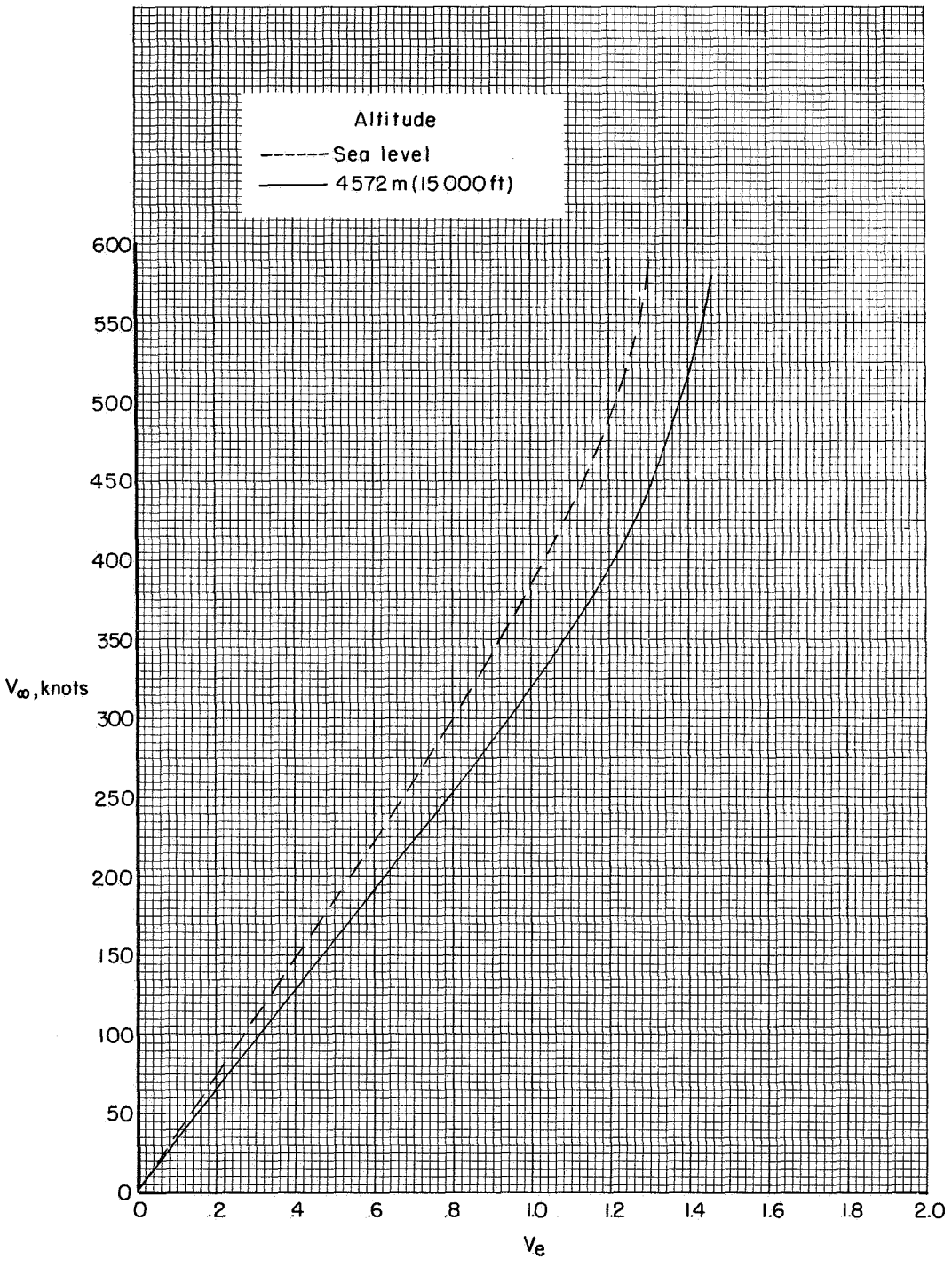

Figure 32.- Variation of free-stream velocity with effective-velocity ratio.

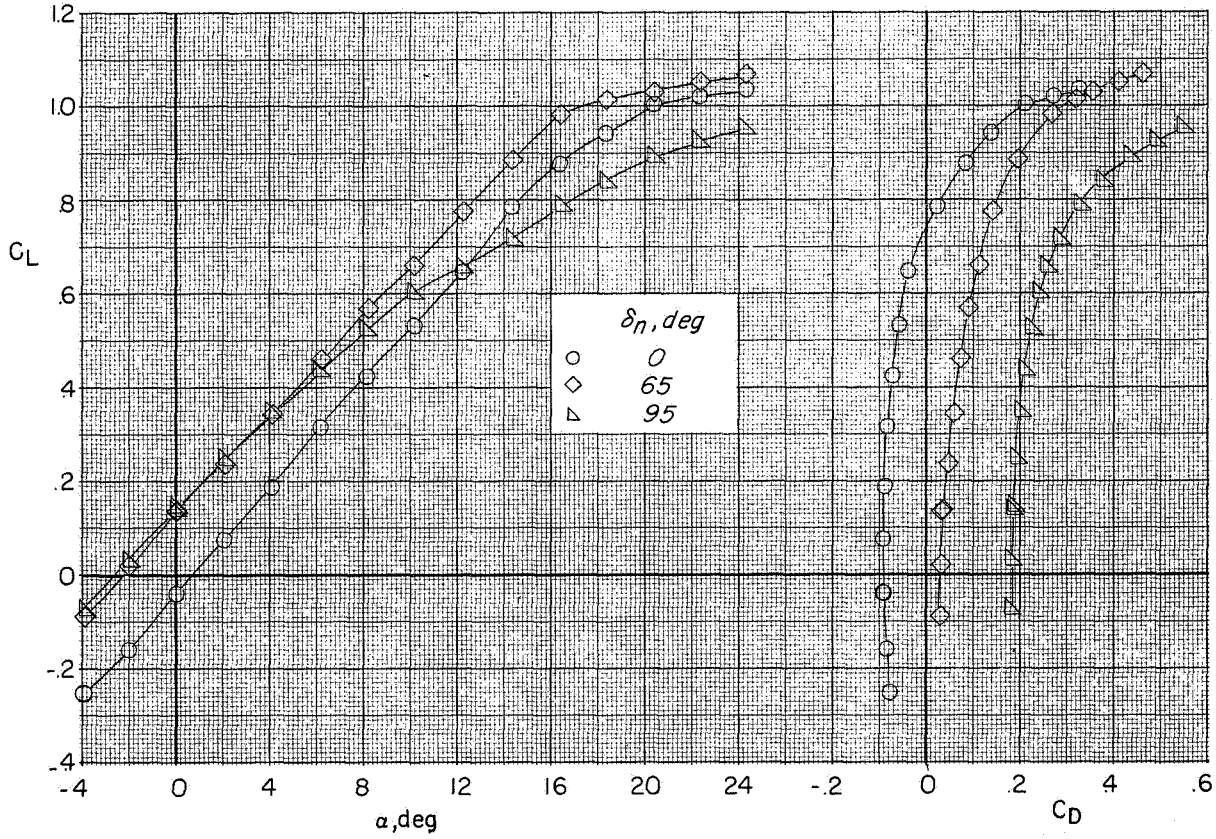

(a) Variations of C_L with α and C_D at $C_T = 0.2(V_e = 0.80)$.

Figure 33.- Longitudinal aerodynamic characteristics showing effect of nozzle deflection of cruise configuration. Landing gear up; $\delta_f = 0^o$; tail off.

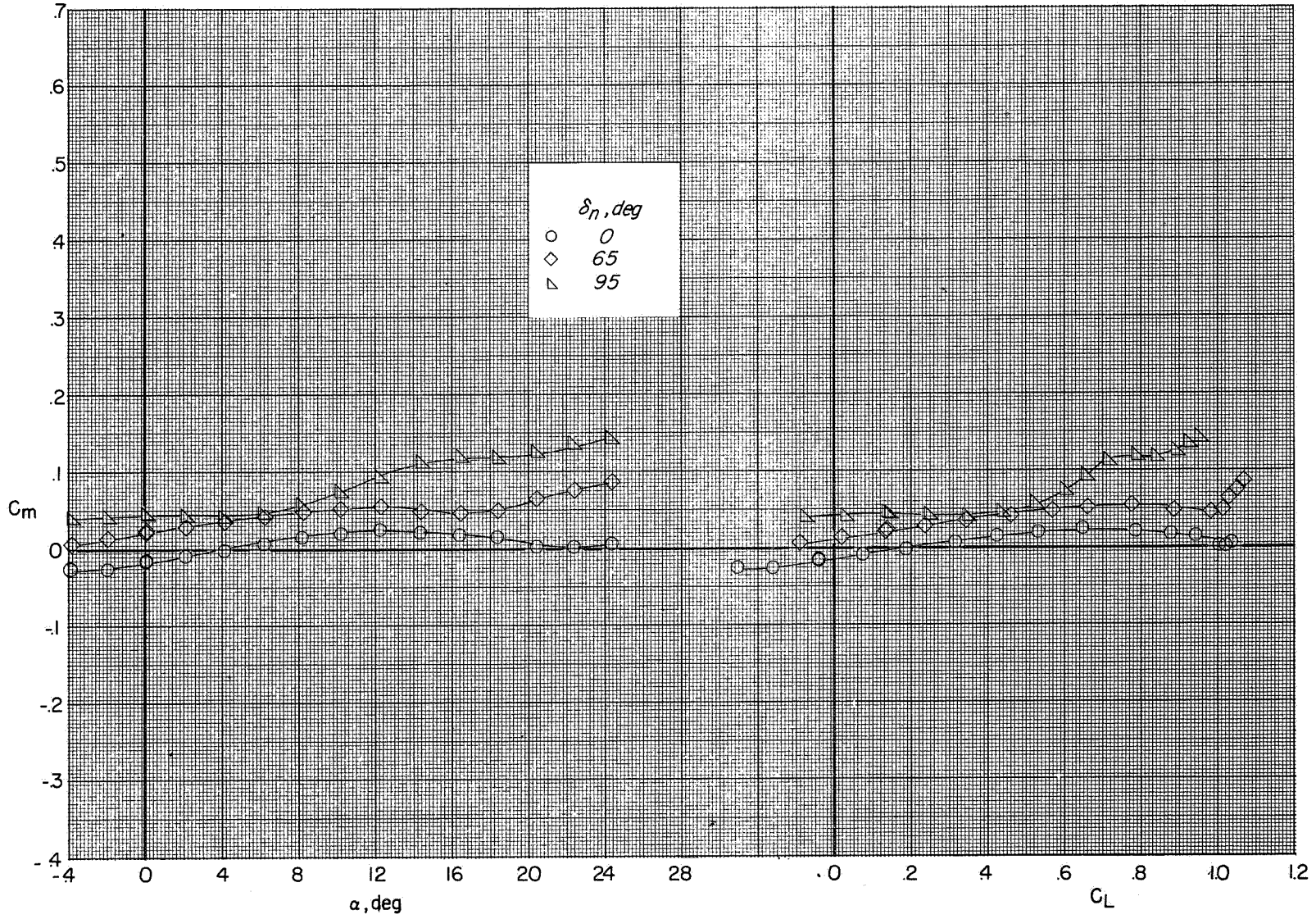

(b) Variations of C_m with α and C_L at $C_T = 0.2(V_e = 0.80)$.

Figure 33.- Concluded.

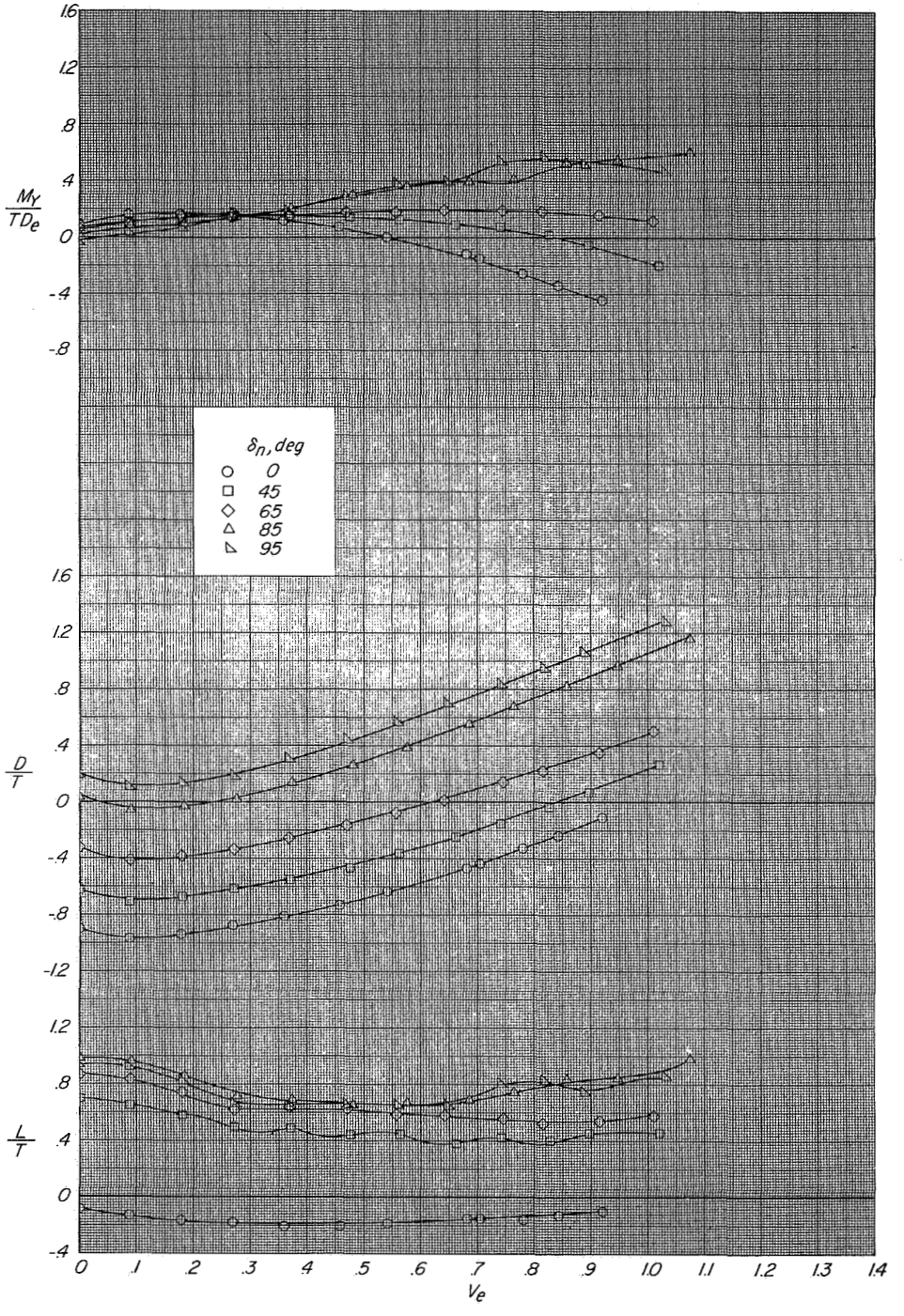

Figure 34.- Effect of effective-velocity ratio on longitudinal aerodynamic characteristics of cruise configuration. Landing gear up; $\delta_f = 0^o$; $\alpha = 0^o$; tail off.

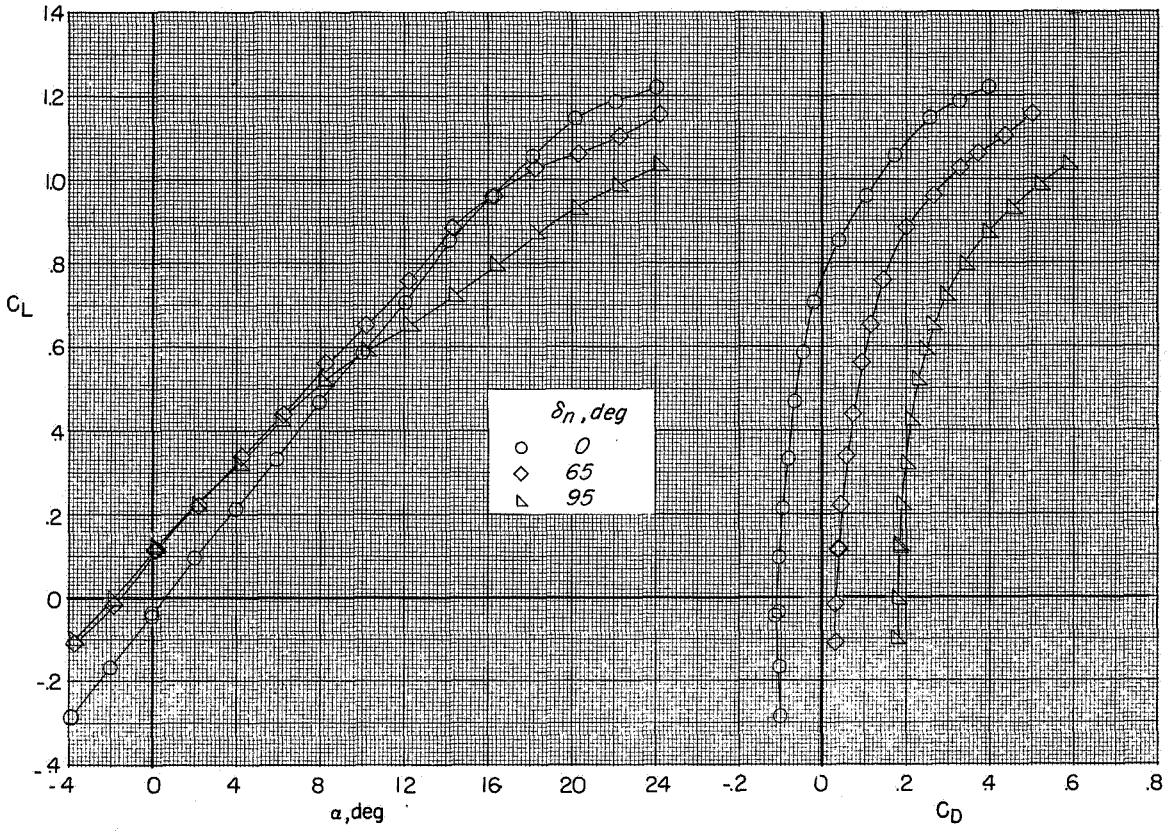

(a) $C_T = 0.2(V_e = 0.80)$.

Figure 35.- Longitudinal aerodynamic characteristics showing effect of nozzle deflection of cruise configuration. Landing gear up; $\delta_f = 0^o$; $i_t = 0^o$.

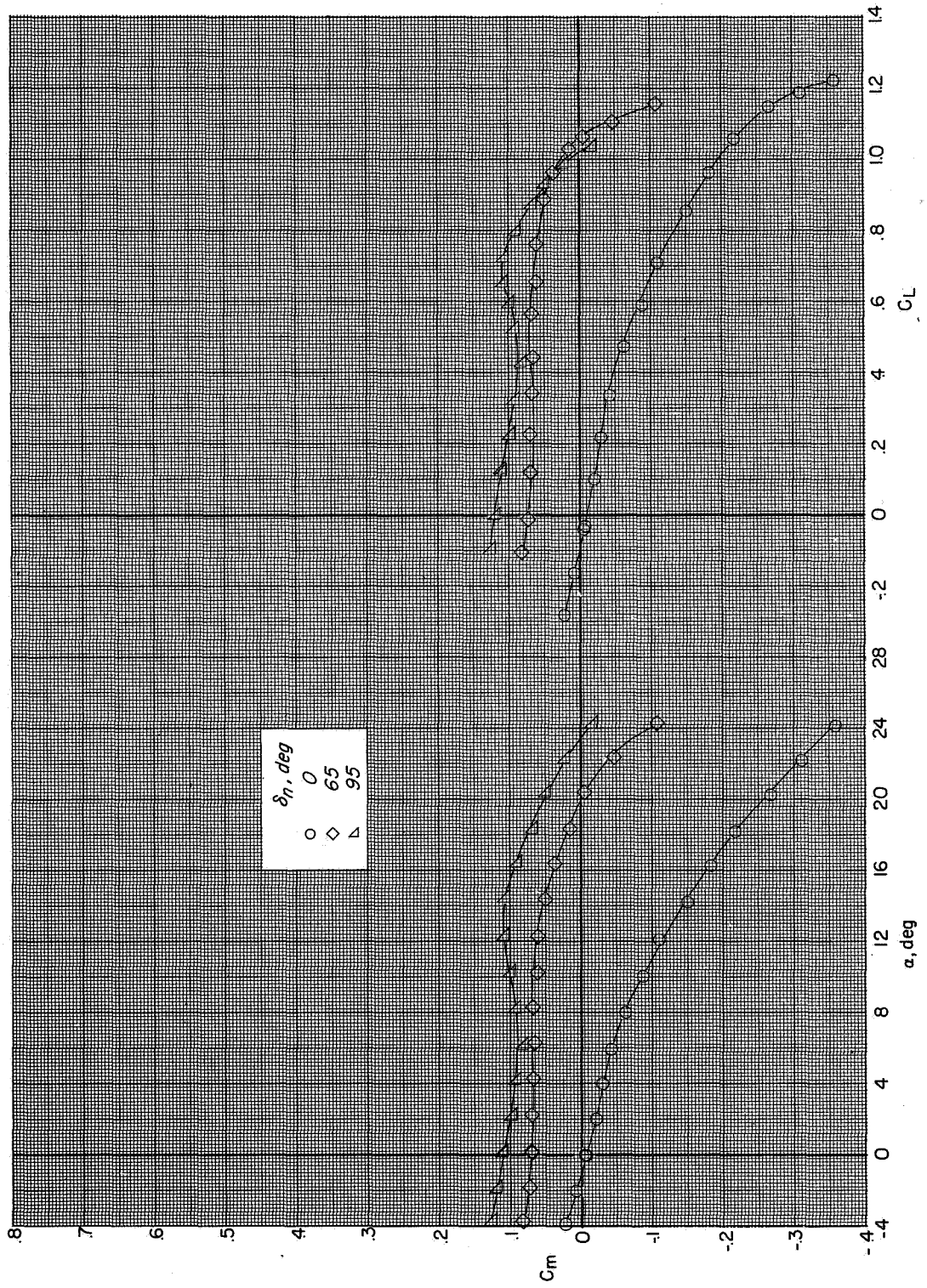

(a) Concluded.

Figure 35.- Concluded.

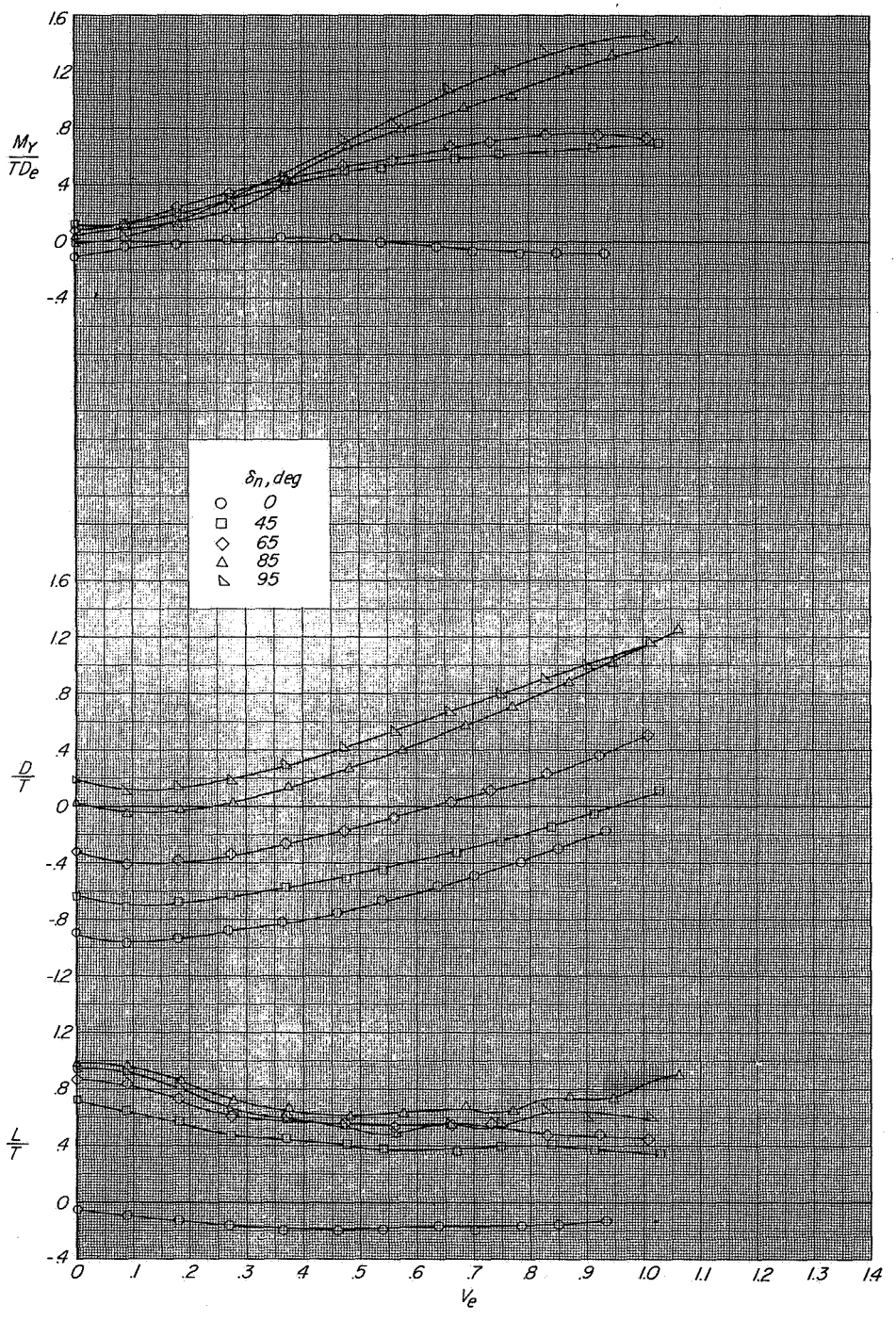

(a) $i_t = 0^o$.

Figure 36.- Effect of effective-velocity ratio on longitudinal aerodynamic characteristics of cruise configuration. Landing gear up; $\delta_f = 0^o$; $\alpha = 0^o$.

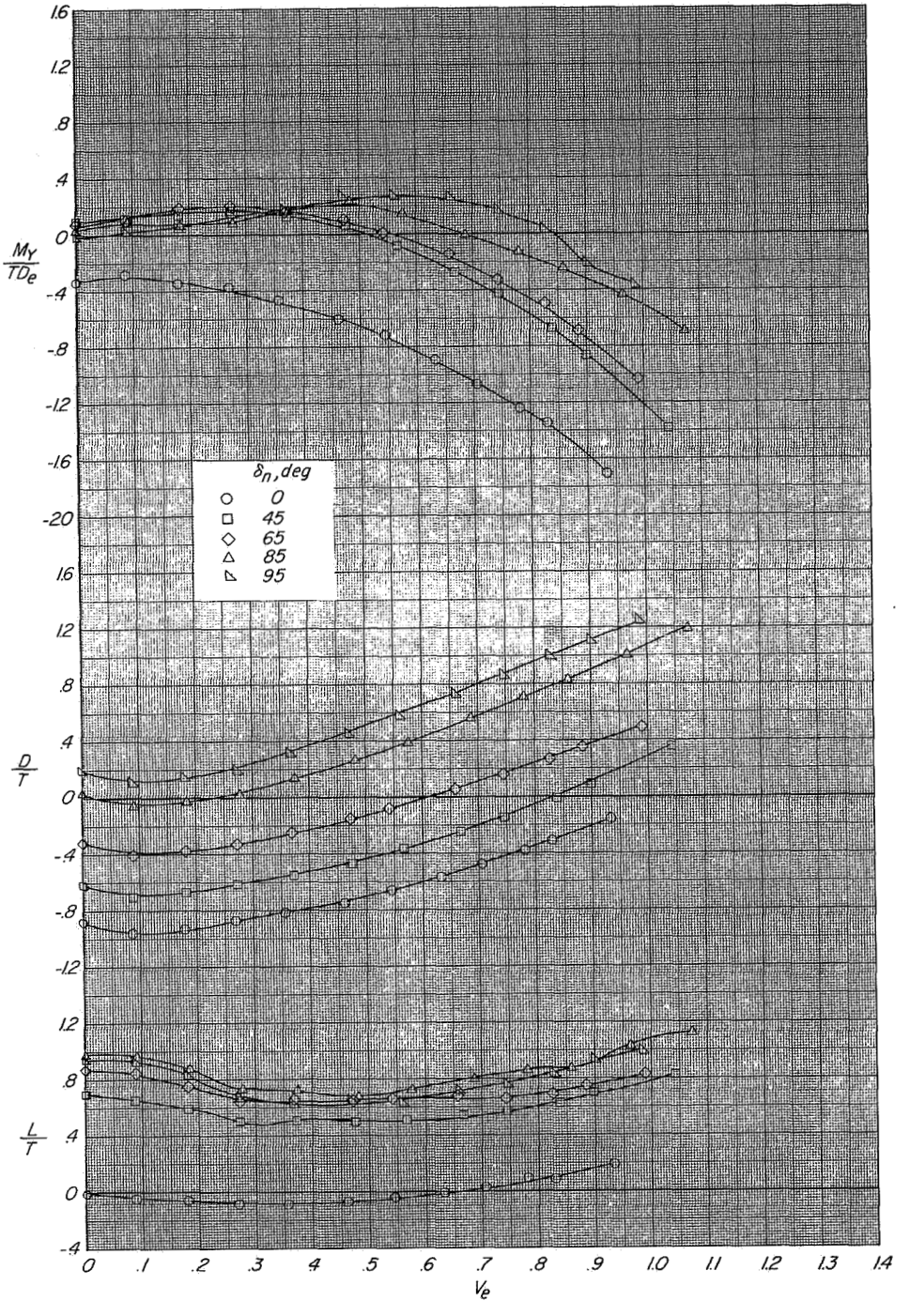

(b) $i_t = 4^o$.

Figure 36.- Concluded.

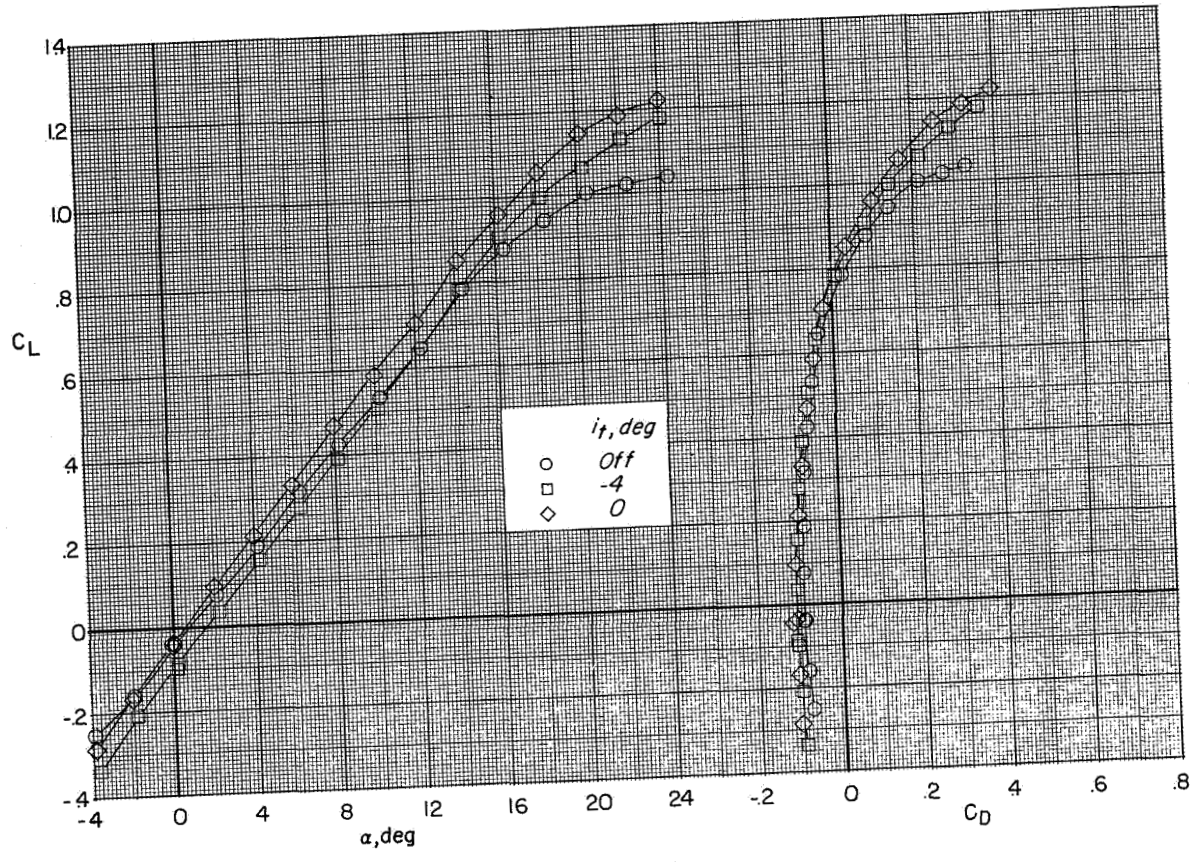

(a) $\delta_n = 0^o$.

Figure 37.- Longitudinal aerodynamic characteristics showing effect of horizontal-tail incidence of cruise configuration. Landing gear up; $\delta_f = 0^o$; $C_T = 0.2$.

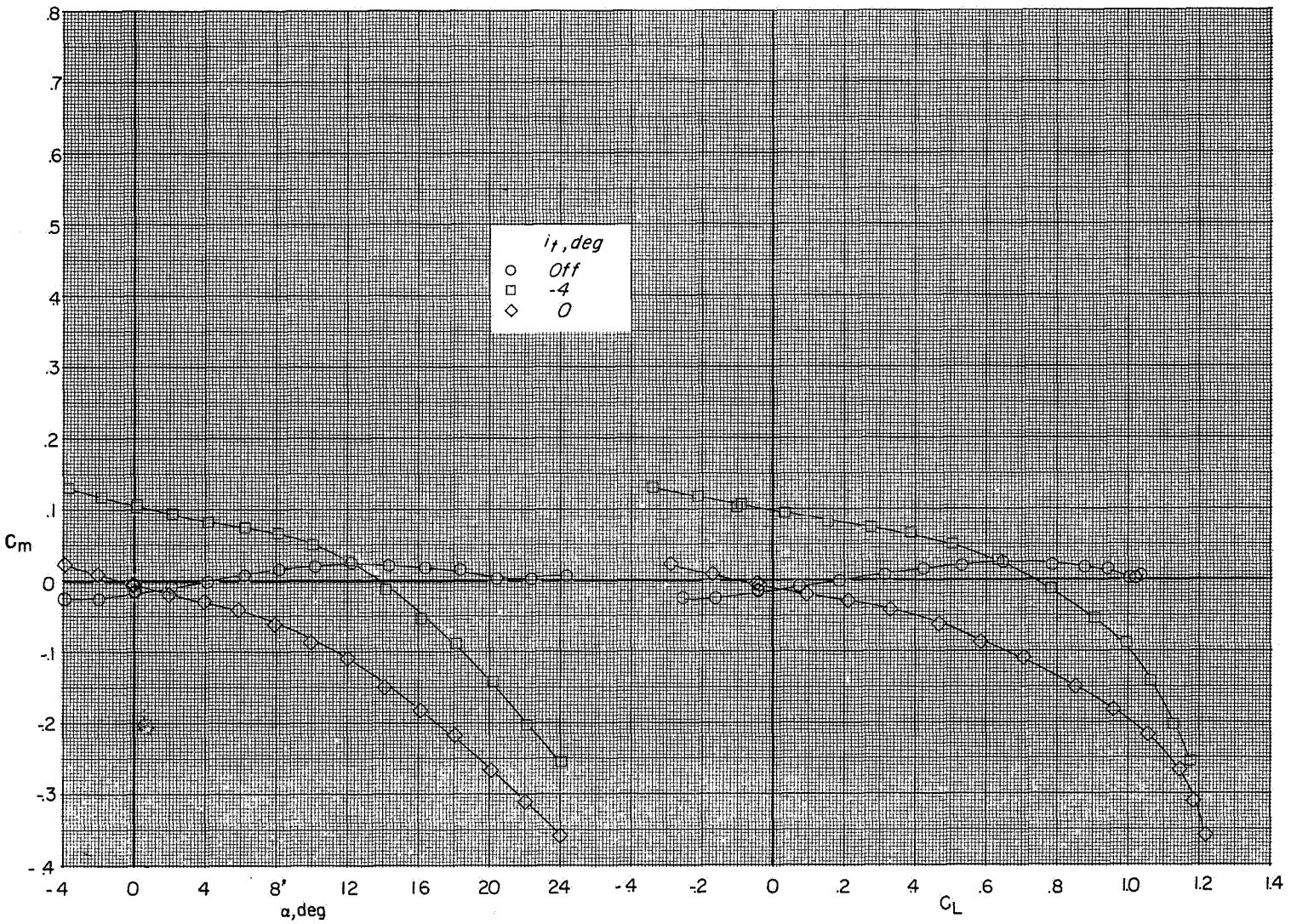

(a) Concluded.

Figure 37.- Continued.

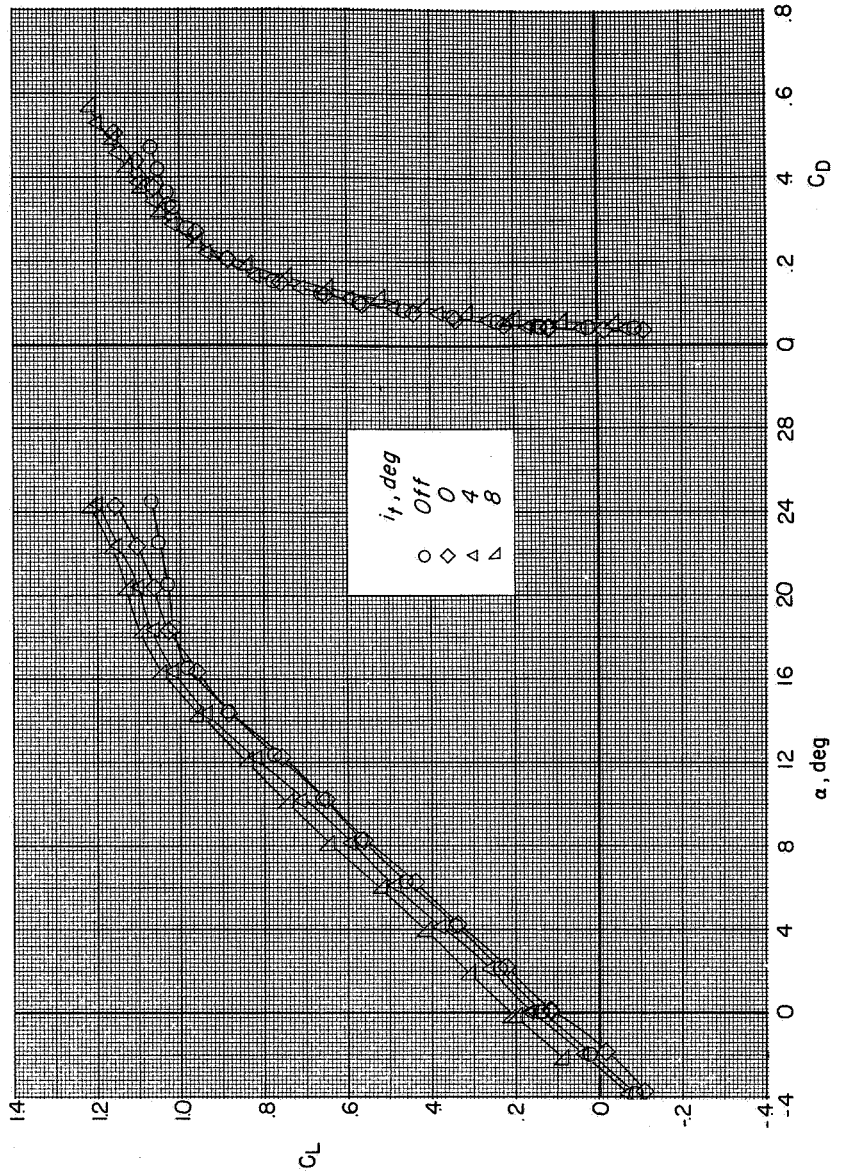

(b) $\delta_n = 65^o$.

Figure 37.- Continued.

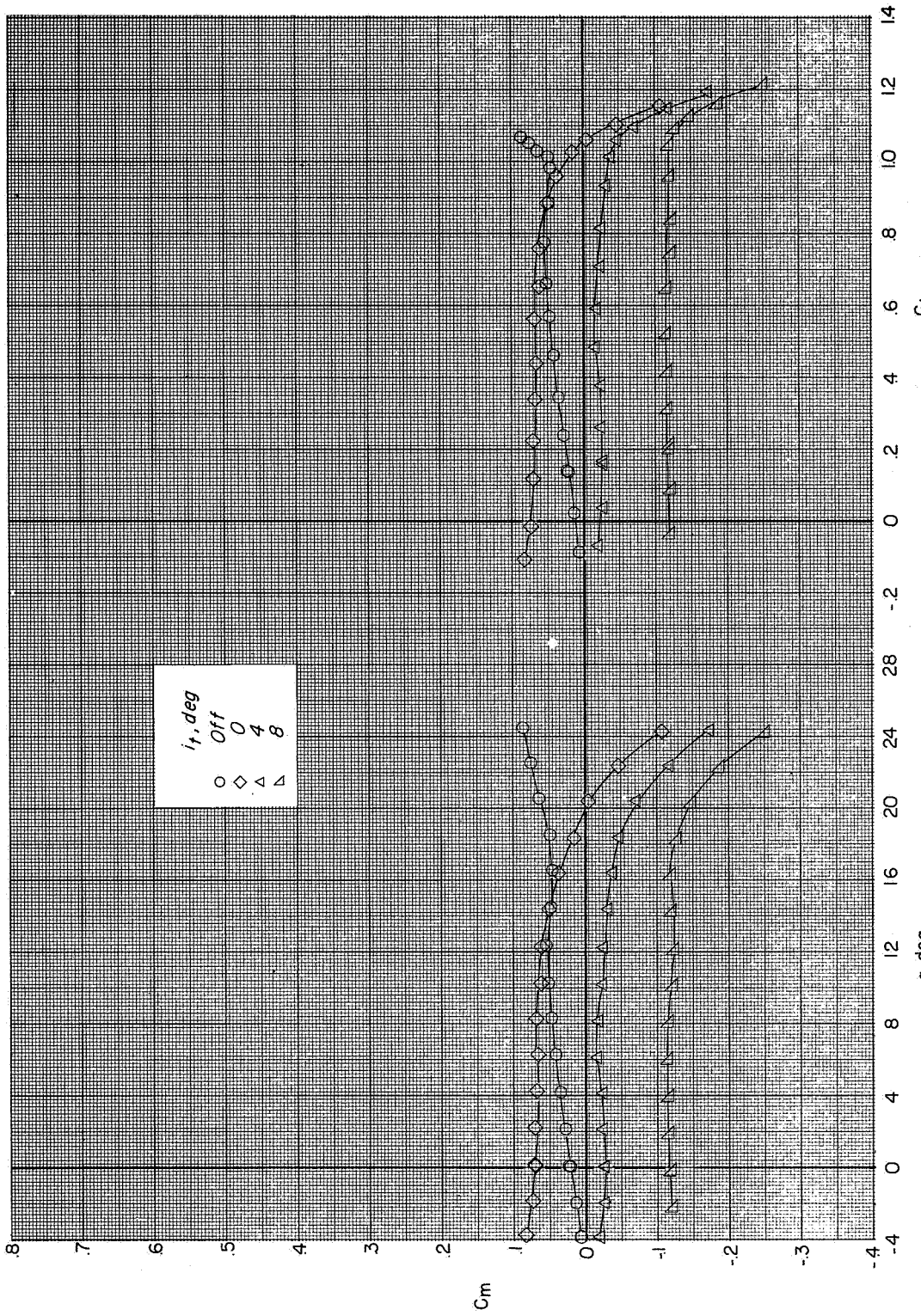

(b) Concluded.

Figure 37.- Continued.

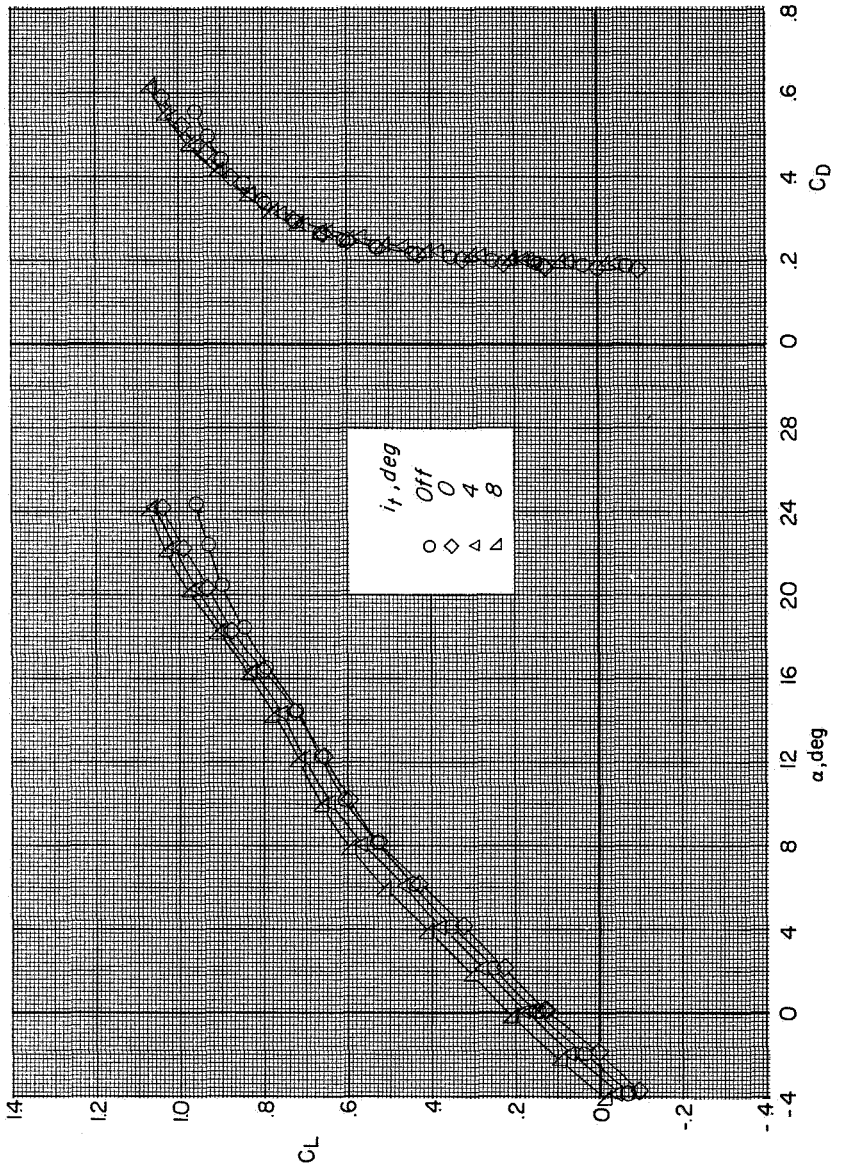

(c) $\delta_n = 95^o$.

Figure 37.- Continued.

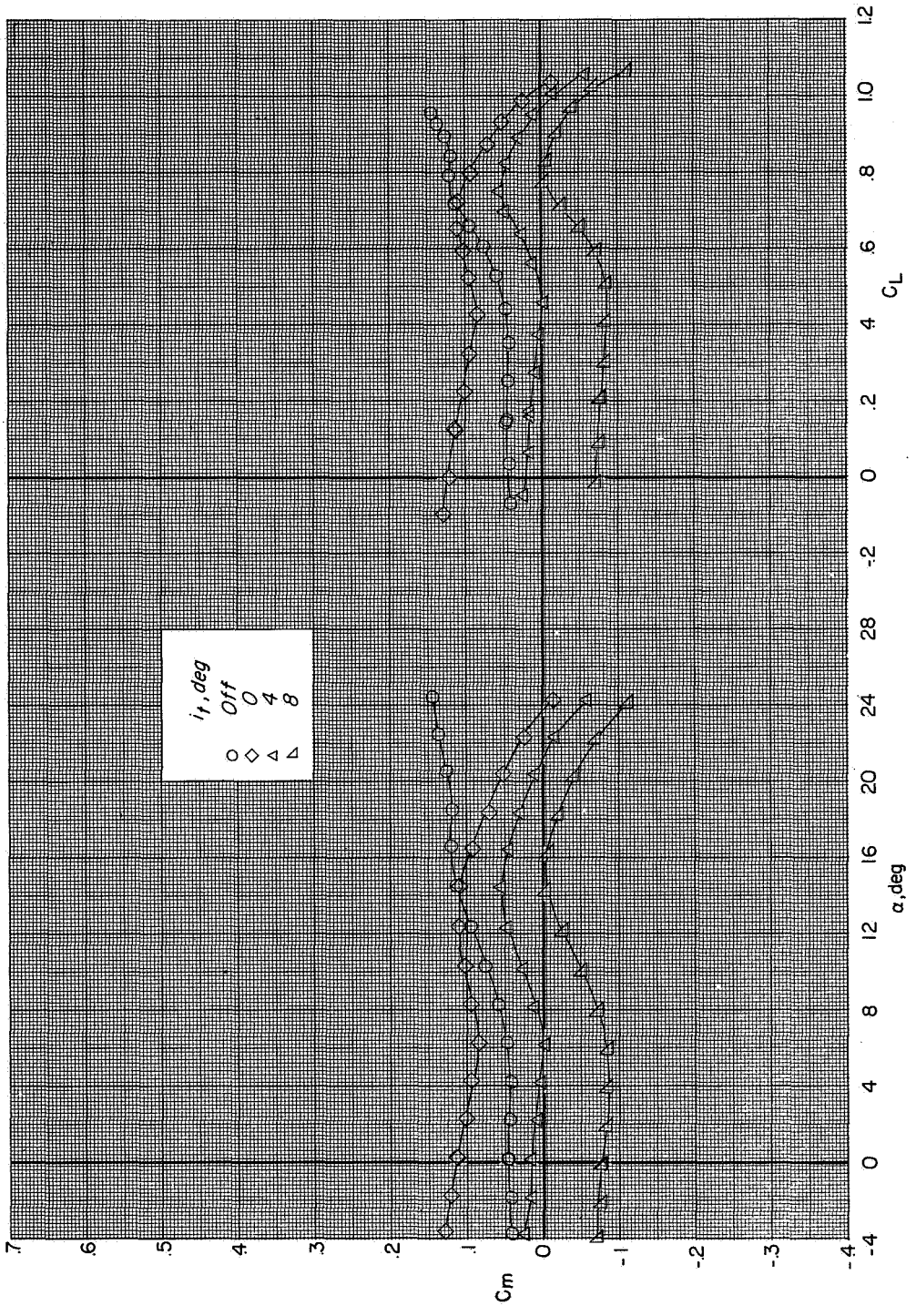

(c) Concluded.

Figure 37.- Concluded.

NASA-Langley, 1972 —— 2 L-8193

1. Report No.	2. Government Accession No.	3. Recipient's Catalog No.
NASA TN D-6826		

4. Title and Subtitle	5. Report Date
WIND-TUNNEL INVESTIGATION AT LOW SPEEDS OF A MODEL OF THE KESTREL (XV-6A) VECTORED-THRUST V/STOL AIRPLANE	July 1972
	6. Performing Organization Code
7. Author(s)	8. Performing Organization Report No.
Richard J. Margason, Raymond D. Vogler, and Matthew M. Winston	L-8193
	10. Work Unit No.
9. Performing Organization Name and Address	760-72-01-08
NASA Langley Research Center Hampton, Va. 23365	11. Contract or Grant No.
	13. Type of Report and Period Covered
12. Sponsoring Agency Name and Address	Technical Note
National Aeronautics and Space Administration Washington, D.C. 20546	14. Sponsoring Agency Code

15. Supplementary Notes

16. Abstract

Longitudinal and lateral stability data were obtained with the model out of and in ground effect over a moving ground plane for a range of model angles of attack and sideslip at various thrust coefficients. These data were taken primarily at thrust coefficients which simulate transition speeds on the airplane between hover and 200 knots. Some data, however, represent the effect of thrust deflection at speeds up to 350 knots. Also presented are the effects of control-surface deflections and interference between the jets and free stream.

17. Key Words (Suggested by Author(s))	18. Distribution Statement
Kestrel (XV-6A) airplane V/STOL model Ground effects Interference effects	Unclassified – Unlimited

19. Security Classif. (of this report)	20. Security Classif. (of this page)	21. No. of Pages	22. Price*
Unclassified	Unclassified	176	$3.00

*For sale by the National Technical Information Service, Springfield, Virginia 22151

"The aeronautical and space activities of the United States shall be conducted so as to contribute . . . to the expansion of human knowledge of phenomena in the atmosphere and space. The Administration shall provide for the widest practicable and appropriate dissemination of information concerning its activities and the results thereof."

—NATIONAL AERONAUTICS AND SPACE ACT OF 1958

NASA SCIENTIFIC AND TECHNICAL PUBLICATIONS

TECHNICAL REPORTS: Scientific and technical information considered important, complete, and a lasting contribution to existing knowledge.

TECHNICAL NOTES: Information less broad in scope but nevertheless of importance as a contribution to existing knowledge.

TECHNICAL MEMORANDUMS: Information receiving limited distribution because of preliminary data, security classification, or other reasons. Also includes conference proceedings with either limited or unlimited distribution.

CONTRACTOR REPORTS: Scientific and technical information generated under a NASA contract or grant and considered an important contribution to existing knowledge.

TECHNICAL TRANSLATIONS: Information published in a foreign language considered to merit NASA distribution in English.

SPECIAL PUBLICATIONS: Information derived from or of value to NASA activities. Publications include final reports of major projects, monographs, data compilations, handbooks, sourcebooks, and special bibliographies.

TECHNOLOGY UTILIZATION PUBLICATIONS: Information on technology used by NASA that may be of particular interest in commercial and other non-aerospace applications. Publications include Tech Briefs, Technology Utilization Reports and Technology Surveys.

Details on the availability of these publications may be obtained from:

SCIENTIFIC AND TECHNICAL INFORMATION OFFICE

NATIONAL AERONAUTICS AND SPACE ADMINISTRATION

Washington, D.C. 20546